



2014

**EXPLORING THE ASYMMETRIC ENVIRONMENT OF VARIOUS  
CHIRAL CATALYSTS USING A MODIFIED ION-TRAP MASS  
SPECTROMETER: TOWARDS THE DEVELOPMENT OF A RAPID  
CHIRAL CATALYST SCREENING METHOD**

Cary M. Davis

Follow this and additional works at: <https://scholarscompass.vcu.edu/etd>

 Part of the [Analytical Chemistry Commons](#)

© The Author

---

Downloaded from

<https://scholarscompass.vcu.edu/etd/3646>

This Thesis is brought to you for free and open access by the Graduate School at VCU Scholars Compass. It has been accepted for inclusion in Theses and Dissertations by an authorized administrator of VCU Scholars Compass. For more information, please contact [libcompass@vcu.edu](mailto:libcompass@vcu.edu).

© Cary Mark Davis 2014

All Rights Reserved

**EXPLORING THE ASYMMETRIC ENVIRONMENT OF VARIOUS CHIRAL  
CATALYSTS USING A MODIFIED ION-TRAP MASS SPECTROMETER:  
TOWARDS THE DEVELOPMENT OF A RAPID CHIRAL CATALYST  
SCREENING METHOD**

A dissertation submitted in partial fulfillment of the requirements for the degree of Doctor  
of Philosophy at Virginia Commonwealth University

By

Cary Mark Davis  
B.S., Heidelberg College, 1998

Director: Scott Gronert  
Professor Department of Chemistry

Virginia Commonwealth University  
Richmond VA,  
December 2014

Acknowledgements and Dedication

## **Acknowledgements**

My journey to this point in life has been, to paraphrase Robert Frost, “the road less traveled, and that has made all the difference.” The non-traditional route to this point has led to a great job, at a great company, albeit far from the comforts of home, but is proof positive that the years of sacrifice and hard work have come to bear fruit. That being said, I would like to thank my wife, Kristi, for her love and support through these very trying times. It is fitting that my studies relied significantly on equilibrium measurements, as my life during this endeavor has been a delicate balancing act between work, school, and family. At a given point in time, any one or two of these were significantly out of balance and far from ideal.

It is my sincere hope my daughter, Kateland-Marie, will read this someday (the acknowledgements, not the thesis, that would be cruel) and will be inspired to do the same; to set her goals high and work hard to achieve them, knowing her own path will be fraught with many obstacles, but through hard work, perseverance, and vision these may be overcome. I therefore dedicate this to her, as she was the driving force for me to finish and complete this degree.

My profound thanks and gratitude goes to my advisor Dr. Gronert, who suffered through years of my ADD and obsessive/compulsive, neurotic behavior. I would also like to thank my committee for their guidance over the years. This also would not have been possible if not for many colleagues at my former employer that supported my decision for graduate school, including the following: Dr. Frank Gupton, Dr. Matt Payne,



Dr. Kai Donsbach, Dr. Jack Brown, Dr. Bryan Wicks, Dr. Joe Pompano, Dr. Saeed Ahmad, and Dr. Ahmad Khodabocus all of whom have provided incalculable wisdom, support, and friendship over the years.

I'd also like to thank all my lab mates at VCU, Chelsea Coffey, Dr. Surresh Narayanasamy, Dr. Qingyuan Liu, Keyanna Conner, Chris Swift, Dr. Jamal Aldajaei, and Dr. Zafer Uger, as well as Dr. Dave Simpson, Dr. Hope Bailey, and Dr. Daniela Hawkins for all the insightful scientific (and non-scientific) discussions and debate.

And finally, I need to acknowledge and thank my father who provided a positive role model for me over the years. Only one that has traveled a similar path can truly understand the journey. I will end with one of his favorite quotes by John Lennon, "Life is what happens to you when you are busy making other plans."

## Table of Contents

Acknowledgements .....	ii
Table of Contents .....	iv
List of Figures.....	xi
List of Tables.....	xxiv
List of Schemes.....	xxvi
List of Abbreviations .....	xxviii
Abstract.....	xxxi
Chapter 1 – Chirality and Asymmetric Catalysis .....	1
1.1 – Chirality .....	1
1.2 – Methods for Achieving Enantiopurity .....	6
1.2.1 – Resolution .....	8
1.2.2 – Kinetic Resolution .....	9
1.2.3 – Chromatography and Direct Crystallization .....	11
1.2.4 – Chiral Pool.....	14
1.2.5 – Chiral Auxiliary .....	17
1.3 – Catalysis .....	19
1.3.1 – Organometallic Catalysis.....	20
1.3.2 – Biocatalysis .....	21
1.3.3 – Enantioselective Catalysis.....	23
1.3.3.1 – Metal.....	26

1.3.3.2 – Ligands .....	27
1.4 – C <sub>2</sub> -Symmetric Ligands .....	29
1.4.1 – Bis-Oxazolines (BOX) .....	31
1.4.2 – C <sub>2</sub> -Symmetric Di-Imines .....	34
1.5 – Enantioselective Catalysis and the Transition State .....	37
1.5.1 – Gibbs Free Energy .....	37
1.5.2 – Temperature and Background Effects on Stereoselectivity .....	41
1.6 – Conclusions .....	45
Chapter 2 – Mass Spectrometry .....	47
2.1 – Mass Spectrometers .....	47
2.2 – Ion Sources .....	47
2.3 – Electrospray Ionization (ESI) .....	48
2.3.1 – Charged Droplet Formation .....	48
2.3.2 – Charged Residue Model .....	50
2.3.3 – Ion Evaporation Model .....	51
2.4 – Mass Analyzers .....	53
2.4.1 – Quadrupole Ion Trap (QIT) Mass Analyzers .....	54
2.4.1.1 – Mass Selection Detection and Storage .....	54
2.4.1.2 – Mass Selective Ejection .....	55
2.5 – Ion Trap Theory .....	56
2.5.1 – Ion Trap Construction .....	56
2.5.2 – Motion of Ions in a Quadrupole Field .....	57
2.6 – Ion Ejection .....	60

2.6.1 – Mass-Selective Instability .....	61
2.6.2 – Resonance Ejection .....	63
2.7 – Resonance Excitation .....	64
2.7.1 – Collision Induced Dissociation (CID) .....	65
2.8 – Scan Speed .....	67
2.9 – Conclusion .....	69
Chapter 3 – Gas-Phase Ion-Molecule (IM) Reactions and Enantioselectivity in Mass Spectrometry .....	
3.1 – Gas-Phase Reactions and Mass Spectrometry .....	71
3.1.1 – History and Instrumentation .....	72
3.1.2 – ESI and Organometallic Chemistry .....	73
3.2 – Trapping Instruments for Gas-Phase Chemistry .....	75
3.3 – Neutral Reagent Introduction .....	77
3.3.1 – Introduction of Neutral Reagent via Solution Phase .....	77
3.2.2 – Introduction of Neutral Reagent via Gas-Phase .....	80
3.2.2.1 – Introduction via a Valve .....	80
3.2.2.2 – Introduction via Gas-Phase .....	82
3.2.2.3 – Laser Desorption .....	85
4 – Mass Spectrometry for Rapid Chiral Recognition .....	86
4.3.1 – Kinetic Resolutions .....	86
4.3.2 – Cook’s Kinetic Method .....	90
4.3.3 – Direct Catalyst Screening .....	92
4.3.3.1 – Pd-Catalyzed Allylic Substitutions .....	92

4.4 – Precedence.....	97
4.6 – Conclusion.....	100
5 – Bis-oxazolines and Cyclopropanation .....	102
5.1 – Cyclopropanation.....	102
5.2 – Copper Background.....	103
5.2.1 – Physical Properties .....	104
5.3.1 – Copper in Organometallic Synthesis .....	105
5.4 – BOX Cu-Catalyzed Cyclopropanation Mechanism .....	106
5.4.1 – Mechanism of Enantioselectivity .....	107
5.5 – Bis-oxazolines Experimental.....	110
5.5.1 – ESI .....	110
5.5.2 – Chiral Probe Introduction.....	111
5.5.3 – Mass Spectrometer Settings .....	113
5.5.3.1 – Mass Selection .....	114
5.5.3.2 – Scan Activation.....	114
5.5.3.3 – Data Collection and Analysis .....	116
5.6 – Synthesis of Ethers.....	121
5.7 – Results.....	122
5.7.1 – General Results .....	122
5.7.1.1 – Diastereomeric Excess .....	125
5.7.1.2 – Average Selectivity for Groups .....	130
5.7.1.3 – Distal Modifications.....	133
5.7.1.4 – Gibbs Free Energy.....	134

5.8 – System Checks and Variability .....	135
5.8.1 – RSD .....	136
5.8.2 – System Checks (ESI) .....	140
5.8.3 – Chiral and Achiral Controls.....	143
5.8.3.1 – Instrument Variability and Accuracy .....	143
5.8.3.2 – Neutral Reagent Preparation .....	145
5.8.3.3 – Propylene Oxide and Sample Preparation Variation .....	149
5.8.4 – Helium Pressure and Variability .....	150
5.8.5 – Chiral Check.....	151
5.8.6 – Different Instruments .....	153
5.9 – Chiral Amines .....	154
5.10 – Combinatorial Approach .....	156
5.11 – Catalyst E Investigation .....	157
5.11.1 – Ligand E Investigation.....	158
5.11.2 – Ligand E with Na .....	161
5.11.3 – Fenton Chemistry .....	161
5.11.3.1 – Fragmentation of Catalyst E .....	162
5.11.3.2 – Stability of Catalyst E.....	163
5.11.4 – Minimizing Degradation and Fenton Chemistry.....	164
5.12 – Integration Methods .....	165
5.13 – Conclusion.....	171
Chapter 6 – Di-Imines and the Combinatorial Approach .....	173
6.1 – Synthesis of Di-imines .....	175

6.1.1 – General Synthesis Procedure .....	177
6.2 – Combinatorial Approach .....	178
6.3 – <i>Trans</i> -1,2-diaminocyclohexane-based Di-Imine Cu Catalysts .....	183
6.3.1 – General Discussion .....	188
6.3.2 – Chiral Cross Check .....	192
6.3.3 – Combinatorial versus Single Runs .....	193
6.3.4 – RSD .....	195
6.4 – BINAM Di-Imine Catalysts .....	198
6.4.1 – General Discussion .....	199
6.4.2 – Gibbs Free Energy .....	204
6.4.3 – Chiral Cross Check .....	206
6.4.4 – Combinatorial versus Single Runs .....	208
6.4.5 – RSD .....	209
6.4.6 – System Checks .....	213
6.4.6.1 – Linearity .....	213
6.5 – Mixed 2,2'-Diaminobinaphthyl System .....	215
6.5.1 – General Discussion .....	216
6.5.2 – Gibbs Free Energy .....	226
6.5.3 – RSD .....	228
6.6 – <i>Meso</i> -1,2-Diphenylethylenediamine-based Di-Imines .....	230
6.7 – Conclusion .....	232
Chapter 7 – Conclusions .....	252
List of References .....	257

List of References .....	258
Appendix .....	274
8.1 – (1 <i>S</i> , 2 <i>S</i> )-diaminocyclohexane-based di-imines.....	274
8.2 – BINAM-based Di-imines .....	282
8.2 – 1,1'-binaphthyl-2,2'-diamine (BINAM) .....	283
8.3 – Diphenylethylene-based di-imines .....	287
8.4 – Bis-Oxazolines.....	288
8.5 – NMR .....	289
8.6 – Synthesis of catalysts .....	307
8.6.1 – <i>Meso</i> -1,2-diphenylethylenediamine.....	307
8.6.2 – BINAM-based Di-imines.....	310
8.6.3 – 1,2-diaminocyclohexane-based Ligands .....	314
8.6.3.1 – <i>trans</i> -(1 <i>S</i> , 2 <i>S</i> )-diaminocyclohexane di-imines .....	314
8.7 – Synthesis of Ethers.....	317
8.6 - Chiral GC Analysis of Ethers .....	320
Vita .....	328



## List of Figures

Figure 1. Examples of chiral molecules. (a) displays a pair of enantiomers (2-butanol). (b) displays an example of axial chirality (axis in red). (c) example of axial chirality in DNA (taken from Dickerson et al.) <sup>6</sup> (d) diastereomers (tartaric acid).....	2
Figure 2. R/S-limonene. ....	2
Figure 3. Thalidomide enantiomers. ....	3
Figure 4. Enantiomeric composition of drugs approved by the FDA by year. <sup>11</sup> .....	4
Figure 5. Example of drugs that have undergone the chiral switch. ....	5
Figure 6. Different routes to enantiopurity. ....	7
Figure 7. Method of chiral induction for single-enantiomer drugs released from 1992 – 2003. Adapted from. <sup>13</sup> .....	8
Figure 8. Free energy diagram of the dynamic kinetic resolution of the stereoselective hydrogenation of a $\beta$ -keto-ester. <sup>27</sup> .....	11
Figure 9. Three-point model of chiral separation. Note the S enantiomer (left) has three points of contact, while the R enantiomer (right) only has one point of contact.....	12
Figure 10. SMB set-up for industrial chiral chromatographic separation of the intermediate tetralone, which is processed to the antidepressant Sertraline. Adapted from US patent 6,444,854 and Hawkins et al. <sup>31</sup> .....	13
Figure 11. Selection of chiral molecules comprising the chiral pool. ....	16
Figure 12. Chiral induction via blockage from the bottom.....	19
Figure 13. Free energy diagram for a catalyst vs. non-catalyst reaction. Taken from <a href="http://www.uic.edu/classes/bios/bios100/lectures/energyhump01.jpg">http://www.uic.edu/classes/bios/bios100/lectures/energyhump01.jpg</a> .....	20
Figure 14. Historically significant chiral catalysts. ....	23

Figure 15. Price of Pd (\$US/gram) since 1986. Taken from infomine.com.....	27
Figure 16. Common C <sub>1</sub> -symmetric catalysts. ....	28
Figure 17. Examples C <sub>2</sub> -Symmetric Ligands.....	30
Figure 18. Left – Generic C <sub>2</sub> -symmetric catalyst with quadrants. Right - Schematic of a C <sub>2</sub> -symmetric quadrant and the chiral fence produced by the substituents. Modified from Nishiyama et al. <sup>77</sup> .....	31
Figure 19. The range of enantioselective reactions catalyzed by 1 and 1a yielding at least 50% ee (left). Different metals used with 1 and 1a as a percentage of transformations with at least 50% ee (right). <sup>36</sup> .....	32
Figure 20. Top left (a) – generic reaction upon a prochiral substrate with out a chiral catalyst. Bottom left (c) – resultant Gibbs free energy diagram with equal transition states. Top right (b) – same reaction with a chiral catalyst. Bottom right (d) – resultant Gibbs free energy diagram with unequal transition states. The transition state with the lowest E <sub>A</sub> (left) will be the dominant product. ....	38
Figure 21. DAIB catalyzed alkylation of benzaldehyde producing (S)-phenyl-propanol in 98% ee. The $\Delta\Delta G^\ddagger$ ( $\Delta G_{TSR} - \Delta G_{TSS}$ ) for the reaction only ~ 2.7 kcal mol <sup>-1</sup> . <sup>104</sup> .....	39
Figure 22. The A value for a methyl ring ~ 1.7 kcal mol <sup>-1</sup> . <sup>105</sup> .....	40
Figure 23. Differences in free energy of the TS and corresponding selectivities at 25 °C. ....	40
Figure 24. Reactions under kinetic control (a) and thermodynamic control (b). ....	41
Figure 25. Top - Table of %ee (and er) at different temperatures. Taken from Koskinen. <sup>106</sup> Bottom – Temperature and effect on ee. ....	42

Figure 26. Box-catalyzed Mukaiyama aldol reaction displaying ideal temperature dependence. ....	43
Figure 27. Multiple diastereomeric transition states, accessible at different temperatures. ....	44
Figure 28. Asymmetric Michael addition with deviations from expected ee due to cesium carbonate and bicarbonate background reactions. ....	44
Figure 29. Schematic of the ESI source. <sup>119</sup> .....	49
Figure 30. The process from large, parent ion, to the smaller charged droplets, which are precursors to the gas-phase ions. Only the first three fissions are shown. The time between fissions, droplet radii, and the number of estimated charge ions are given. The onset displays the shape of the droplet as fission occurs. <sup>119</sup> .....	50
Figure 31. Schematic of the Charged Residue Model. <sup>125</sup> .....	51
Figure 32. Ion Evaporation Model. <sup>125</sup> .....	52
Figure 33. Effect of He on resolution and sensitivity. <sup>143</sup> .....	55
Figure 34. Ion trap with ring and end cap electrodes <sup>148</sup> .....	56
Figure 35. Cross section ideal trap <sup>150</sup> .....	57
Figure 36. Example of a pure quadrupole field. <sup>150</sup> .....	57
Figure 37. Stability diagram with $a_z$ as the y-axis and $q_z$ as the x-axis. <sup>143</sup> .....	59
Figure 38. Simulated ion motion in an ion trap (left), <sup>140</sup> photomicrograph of single charged ion of Al. <sup>140</sup> .....	60
Figure 39. Effect of increasing the amplitude of the rf on three ions of different m/z. <sup>149</sup> .....	62
Figure 40. Effect of resonance ejection to access higher mass range. <sup>149</sup> .....	64

Figure 41. Schematic of an ion trap MS, displaying the tube lens region where ion fragmentation may occur. <sup>119</sup>	65
Figure 42. First electrosprayed transition metal organometallic compound, Ru(II)(bpy) <sub>3</sub> Cl <sub>2</sub> . <sup>181</sup>	74
Figure 43. Catalytic cycle of the Suzuki mechanism with the pyridine-substituted aryl halide.	75
Figure 44. First ion-molecule reaction recorded in an ion trap. From March and Todd. <sup>189</sup>	76
Figure 45. Modified ion trap with pulse valve. Taken from Ryzhov. <sup>233</sup>	81
Figure 46. Schematics for introduction of neutral reagent via leaks valves. Left (a) <sup>236</sup> Right (b) <sup>210</sup>	82
Figure 47. Diagram of the modified LCQ ion-trap to allow introduction of a neutral reagent.	84
Figure 48. MUX ESI Spray system with eight-channels by Micromass. <sup>241</sup>	87
Figure 49. Setup by Thurow for rapid MS analysis. <sup>243</sup>	90
Figure 50. Comparing results from MS via the back reaction, and reaction products via condensed phase and chiral HPLC. <sup>247</sup>	96
Figure 51. DFT results comparing the lowest energy conformers for the Mn-salen catalyst complexed to (a) •CH <sub>2</sub> CH <sub>2</sub> O• and (b) CH <sub>3</sub> CH <sub>2</sub> OH. <sup>251</sup>	98
Figure 52. Example spectra for the Mn-salen catalyst with the 1-phenylethanol system. (a) ( <i>R,R</i> ) I (Z = <i>t</i> -Bu) and ( <i>R</i> ) 1-phenylethanol and <i>d-ring</i> 1-phenylethanol as the internal standard in a 1:1 ratio. (b) ( <i>R,R</i> ) I (Z = <i>t</i> -Bu) and ( <i>S</i> ) 1-phenylethanol and	

<i>d</i> -ring 1-phenylethanol in a 1:1 ratio. Of note is the larger peak intensity for the <i>S</i> enantiomer. <sup>251</sup>	100
Figure 53. C <sub>2</sub> -symmetry and resultant reduction of possible paths and transition states. <sup>285</sup>	108
Figure 54. Proposed transition states for the simplified methyl BOX ligand in the cyclopropanation step for ethylene attack for the (a) <i>Re</i> attack with a dihedral angle of 69.8 and 9b) <i>Si</i> approach; dihedral angle 87. <sup>281</sup>	108
Figure 55. Copper carbenoid with alkene attack. <sup>281</sup>	109
Figure 56. The four transition state structures for the propylene addition to bis-oxazoline carbenoid. The two <i>cis</i> approaches, (b) and (d), have unfavorable interactions between the oxygen of the carbonyl and <i>t</i> -Bu group of the bis-oxazoline. The <i>Re-trans</i> (c) is favored over the <i>Re-cis</i> (a) approach by 0.2 kcal mol <sup>-1</sup> . <sup>281</sup>	110
Figure 57. Scan activation time with catalysts C and G (enantiomers) and 1-phenyl-2-propanol. The homo-couplings are identical, as are the hetero-couplings.	115
Figure 58. Bis-oxazoline catalyst B before isolation.	116
Figure 59. Catalyst B after ion isolation.	117
Figure 60. Catalyst B after equilibrium with the chiral probe ( <i>R</i> )-1-phenylethanol and the internal standard, <i>d</i> -ring 1-phenylethanol.	118
Figure 61. Catalyst B after isolating the <sup>65</sup> Cu isotope and allowing equilibrium with the chiral probe ( <i>R</i> )-1-phenylethanol and the internal standard, <i>d</i> <sub>5</sub> -ring 1-phenylethanol.	119

Figure 62. Catalyst B after isolating the $^{65}\text{Cu}$ isotope and allowing equilibrium with the chiral probe ( <i>S</i> )-1-phenylethanol) and the internal standard, <i>d</i> -ring 1-phenylethanol. .....	120
Figure 63. Summary of results for the bis-oxazolines. Grouped by chiral probe. The line in black represents no selectivity.....	123
Figure 64. Summary of results, grouped by catalysts. The black line represents no selectivity. ....	124
Figure 65. Results presented as diastereomeric excess, grouped by catalyst.....	126
Figure 66. Results as percent DE, grouped by chiral probe.....	127
Figure 67. Orientation of ( <i>R</i> )-1-phenylethanol and ( <i>S</i> )-styrene oxide.....	128
Figure 68. Catalysts G and C with 1-phenylethanol. The homo-couplings are similar as are the hetero-couplings. ....	129
Figure 69. Structure of catalyst A.....	130
Figure 70. Average selectivity factor for each chiral probe.....	131
Figure 71. Average selectivity factor for catalysts. ....	132
Figure 72. Distal modification to the bis-oxazoline scaffold and resultant effect on the selectivity. Only two results displayed significant differences, circled in red. ....	133
Figure 73. Plot of Gibbs free energy versus chiral probe molecular weight.....	135
Figure 74. RSD grouped by probe. ....	136
Figure 75. RSD grouped by catalyst.....	137
Figure 76. Mass Spectrum of catalyst C and 1,2-epoxybutane with EtOH as the internal standard. ....	138
Figure 77. Box plots of all results for the bis-oxazolines.....	139

Figure 78. (a) Stability of the ESI spray before regular trimmings of the capillary tubing. Also shown a picture of the tubing. Black solid was observed at the entrance to the ground junction of the instrument. (b) and (c) examples of the stability after clipping of capillary tubing. ....	141
Figure 79. Time to equilibrate the manifold and ion-trap with the chiral probe. ....	142
Figure 80. Fe(III) tetraphenyl porphyrin achiral catalyst. ....	143
Figure 81. Achiral catalyst with 2-Octanol run over 5 days.....	144
Figure 82. Catalyst B with 2-Octanol run over 5 days. ....	145
Figure 83. Spectrum of the <i>t</i> -Bu catalyst with propylene oxide and 1-octanol as the internal standard. ....	149
Figure 84. Chiral cross check with catalysts C and G. ....	152
Figure 85. Scan activation of catalyst B and phenylethanol on two different instruments. .....	153
Figure 86. Catalyst B and <i>sec</i> -butyl amine with <i>i</i> -pro amine.....	155
Figure 87. Scan activation time study of butyl amine with octanol as the internal standard. The amine never reaches equilibrium. Inset – normalized ratio of the butylamine and octanol. ....	155
Figure 88. Results of the single run versus combinatorial approach. ....	157
Figure 89. (a) Catalyst E with the expected isotopic abundances. (b) Mass Spectrum of catalyst E. The major peak is minus one from expected. ....	157
Figure 90. (a) Fresh prep of catalyst E. (b) Prep after nine days.....	158
Figure 91. (a) Ligand only of catalyst E. (b) Fragmentation pattern for ligand E . ....	158
Figure 92. Ligand of catalyst E proposed fragmentation mechanisms. ....	160

Figure 93. Ligand E with Na. ....	161
Figure 94. Fenton chemistry and the catalyst E. ....	162
Figure 95. (a) Peak before fragmentation. (b) Peak with 15% collision energy applied, 271m/z appears, with 329m/z, still intact. (c) Increase to 30% energy. 247m/z now evident, with no evidence of 329m/z (d) .....	163
Figure 96. The effect of time on the coordination of catalyst E and 2-octanol. ....	164
Figure 97. Design of the dual syringe and tees to minimize the ligand exposure to copper. ....	165
Figure 98. Method 1 for integrating all peaks over isotopic range (black line – non- deuterated analyte, red line – deuterated internal standard).....	166
Figure 99. Method 2, isolating all peaks, but integrating only the $^{63}\text{Cu}$ and $^{65}\text{Cu}$ peaks. .....	167
Figure 100. Isolation and fragmentation of 357m/z at 30% energy and 30 msec activation time. ....	169
Figure 101. Isolation of 356 m/z, followed by fragmentation at 30% energy and 30 msec activation time. ....	170
Figure 102. Proposed mechanism of the formation of the 356 m/z ion, followed by fragmentation, leading to 300m/z. ....	170
Figure 103. Catalyst Screening Process .....	174
Figure 104. Mix of catalysts with CuI:CuCl in approximately 1:1 ratio, with the structures and assignments. ....	180
Figure 105. Ligand mix with CuI. No coordination evident. ....	181



Figure 106. (a) – Catalyst mix with good ratio (1:1) of CuI:CuCl. (b) - Same ligand mix with a 2:1 ratio CuI:CuCl. ....	182
Figure 107. Results of the (1 <i>S</i> ,2 <i>S</i> ) cyclohexane di-imine catalysts. ....	184
Figure 108. Results grouped by catalyst. ....	185
Figure 109. Results converting equilibrium ratios to diastereomeric excess. ....	186
Figure 110. Results presented as box plots. ....	187
Figure 111. Plot of delta G versus selectivity factor. ....	190
Figure 112. Gibbs Free Energy of binding versus chiral probes molecular weight. ....	191
Figure 113. Comparison of di-imine catalysts enantiomers. ....	192
Figure 114. Chiral cross check of the di-imines. ....	193
Figure 115. Single versus combinatorial runs. ....	194
Figure 116. Fragmentation of the benzaldehyde catalyst (3a) isolated from a mixture (left) and from a pure solution (right). ....	194
Figure 117. RSD of the trans cyclohexane di-imine results. Top – grouped by chiral probe. Bottom – grouped by catalyst. ....	196
Figure 118. ( <i>S</i> ) Styrene oxide with internal standard and catalyst 3c. ....	197
Figure 119. 1-phenyl-2-propanol spectra. ( <i>S</i> ) enantiomer on the left and ( <i>R</i> ) enantiomer of the right. ....	198
Figure 120. Nucleophilic attack by alcohol on catalyst 3b. ....	198
Figure 121. Results for the BINAM-based catalysts. ....	200
Figure 122. BINAM-based catalysts results as DE. ....	201
Figure 123. Averages for the chiral probes. ....	203
Figure 124. Average selectivity for the catalysts. ....	204

Figure 125. Plot of Gibbs binding energy versus the chiral probe molecular weight. ..	206
Figure 126. Selectivity factors for both enantiomers of the BINAM-based catalysts. ..	207
Figure 127. Chiral cross check for the BINAM-based di-imines. ....	208
Figure 128. The combinatorial approach versus single-run catalysts.....	209
Figure 129. Box plot of the results for the (S) BINAM-based di-imines. ....	211
Figure 130. RSD for the (S) BINAM-based systems grouped by catalysts (top) and by chiral probe (bottom). ....	212
Figure 131. Linearity of the method with racemic benzaldehyde-BINAM and d <sub>5</sub> -ring 1- phenylethanol and 1-phenylethanol. ....	214
Figure 132. Representative spectra of the crude mixed BINAM catalysts.....	216
Figure 133. Results of the crude mixed catalyst system. ....	217
Figure 134. Diastereomeric excess grouped by chiral probes.....	218
Figure 135. Diastereomeric excess grouped by catalyst. ....	219
Figure 136. Comparison of the mixed catalyst 6d (Benz & DiF) with the C <sub>2</sub> counterparts 5a (benzaldehyde) and 5b (3,5-diF). ....	220
Figure 137. Mixed catalyst 6b (Benz and Mesital) versus the C <sub>2</sub> -symmetric catalyts..	221
Figure 138. Mixed catalyst 6a (DiF and mesitaldehyde) versus 5b (benzaldehyde) and 5c (mesitaldehyde).....	223
Figure 139. Mixed catalyst 6c compared to the C <sub>2</sub> -symmetric catalysts.....	224
Figure 140. Average selectivity for the chiral probes with the mixed catalysts. ....	225
Figure 141. Average selectivity factor for the catalysts. ....	226
Figure 142. Binding energy versus molecular weight of chiral probe. ....	228
Figure 143. Box plot of the results for the crude mixed catalyst system.....	229

Figure 144. RSD values for the mixed system. Grouped by chiral probe (top) and catalyst (bottom).....	230
Figure 145. Selectivity for the <i>meso</i> -1,2-diphenylethylenediamine-based di-imines. ...	232
Figure 146. Catalyst 3a in mixture of catalysts 3 b-d-g (top) and as single solution (bottom).....	275
Figure 147. Catalyst 3b in mixture of catalysts 3 a, c, & d-g (top) and as single solution (bottom).....	276
Figure 148. Catalyst 3c in mixture of catalysts 3 a, b, & d-g (top) and as single solution (bottom).....	277
Figure 149. Catalyst 3d in mixture of catalysts 3 a – c, and e-g (top) and as single solution (bottom). ....	278
Figure 150. Catalyst 3e in mixture of catalysts 3 a – d, f, and g (top) and as single solution (bottom). ....	279
Figure 151. Catalyst 3f in mixture of catalysts 3 a – e, and g (top) and as single solution (bottom).....	280
Figure 152. Catalyst 3g in mixture of catalysts 3 a – f (top) and as single solution (bottom).....	281
Figure 153. Catalyst 5a in a mixture of catalysts 5b-d (top) and single solution (bottom). ....	283
Figure 154. Catalyst 5b in a mixture of catalysts 5a, c, and d (top) and single solution (bottom).....	284
Figure 155. Catalyst 5c in a mixture of catalysts 5a, b, and d (top) and single solution (bottom).....	285

Figure 156. Catalyst 3d in mixture of catalysts a-c. No spectra was recorded for the single catalyst solution. ....	286
Figure 157. Proton NMR Catalyst 3a.....	289
Figure 158. Proton NMR of catalyst 3e. ....	290
Figure 159. Proton NMR of catalyst 3b. ....	291
Figure 160. Proton NMR catalyst 3g. ....	292
Figure 161. Proton NMR catalyst 3c.....	293
Figure 162. Proton NMR of Catalyst 3e with Cu(I) trifluormethanesulfonate. Indicates oxidation of Cu (I) to Cu(II) which is paramagnetic and hence the lack /broadness of NMR peaks. ....	295
Figure 163. Proton NMR of catalyst 5i.....	296
Figure 164. Proton NMR of catalyst 5a. ....	297
Figure 165. Expanded proton NMR of (R) 2-methoxyoctane. ....	298
Figure 166. Expanded proton NMR of (S) 2-methoxyoctane.....	299
Figure 167. Proton NMR of (S)-2-methoxyethylbenzene.....	300
Figure 168. Expanded proton NMR (R)-2-methoxyethylbenzene.....	302
Figure 169. Proton NMR of catalyst 5b. ....	303
Figure 170. Extracted mineral oil from NaH. ....	304
Figure 171. Proton NMR of racemic [1-(Benzyloxy)ethyl]benzene (too big to coordinate). ....	306
Figure 172. (R)-1-methoxyethylbenzene chiral GC analysis. ....	321
Figure 173. (S)-1-methoxyethylbenzene chiral GC analysis. ....	322
Figure 174. Racemic phenylethanol GC analysis.....	323

Figure 175. (S)-2-methoxyocatne chiral GC analysis.....	324
Figure 176. (R)-2-methoxyoctane chiral GC analysis.....	325
Figure 177. (R)-2-octanol chiral GC analysis. ....	326
Figure 178. (S)-2-2octanol chiral GC analysis.....	327

## List of Tables

Table 1. Metal coordinated chiral catalyst in industrial use. <sup>64</sup> .....	26
Table 2. Mass spectrometer types. <sup>131, 132</sup> .....	53
Table 3. Results of ESI-MS screening of BOX Cu(II) catalysts. <sup>249</sup> .....	97
Table 4. Results for various Mn-Salen catalysts and their stereoselective preferences for 1-phenylethanol in the gas-phase. ....	99
Table 5. Bis-oxazolines utilized in study.....	111
Table 6. List of chiral reagents and corresponding internal standards and ratios used during testing of the bis-oxazolines. ....	111
Table 7. Table of chiral probes utilized in the bis-oxazoline study.....	112
Table 8. Gibbs free energy of binding for the complexes (kcal/mol).....	134
Table 9. Result of ANOVA for sample preparation variability. ....	146
Table 10. ANOVA results comparing data obtained on 8/16/12 to the previously obtained results. No statistical different was apparent. ....	147
Table 11. Variability in sample prep and run-to-run with catalyst B and 2-octanol. ....	148
Table 12. Effect of pressure on results.....	150
Table 13. ANOVA comparing the results of catalyst B and phenylethanol on two different instruments.....	154
Table 14. Table of the single runs versus combinatorial mixes. ....	156
Table 15. Starting materials and products used in the di-imine study. ....	176
Table 16. Averages for the chiral probes with the (1S,2S) cyclohexane di-imines. ....	188
Table 17. Free energy of binding for the trans cyclohexane di-imines (kcal/mol).....	189
Table 18. Binding energies of the BINAM-based complexes (kcal/mol). ....	205

Table 19. Selectivity factors obtained with select chiral probes and a racemic BINAM- based catalyst (5a).....	213
Table 20. Regression analysis results.....	215
Table 21. Gibbs free energy for the mixed system (kcal/mol). ....	226

## List of Schemes

Scheme 1. Classical resolution of tartaric acid via enantiopure (d)-quinotoxine.....	9
Scheme 2. First example of kinetic resolution by Marckwald & MaKenzie. <sup>25</sup> .....	10
Scheme 3. Synthesis of bis-oxazoline (tBOX) via the chiral pool method. ....	15
Scheme 4. Oxazolidinone and common oxazolidinones used as chiral auxiliaries (top). Example of Evan's oxazolidinone for use as a chiral auxiliary in an aldol addition. <sup>38</sup> .....	17
Scheme 5. First enantioselective synthesis of Methlphenidate via Evan's oxazolidinone and a chiral auxiliary. ....	18
Scheme 6. General Catalytic Cycle.....	21
Scheme 7. Enzymatic synthesis of L-DOPA. ....	22
Scheme 8. Enantioselective decarboxylation with brucine. ....	23
Scheme 9. First enantioselective cyclopropanation by Noyori in 1966. <sup>54</sup> .....	24
Scheme 10. First commercial use of an asymmetric catalyst.....	24
Scheme 11. Asymmetric hydrogenation using BINAP and Rh.....	25
Scheme 12. Sharpless epoxidation.....	25
Scheme 13. Different synthetic routes to BOX ligands. <sup>36</sup> .....	32
Scheme 14. Alternate synthesis of BOX ligand.....	33
Scheme 15. Synthesis of a salen ligand.....	34
Scheme 16. Generic synthesis of di-imine ligands.....	35
Scheme 17. Epoxidation using Jacobsen or Katsuki catalyst.....	36
Scheme 18. Di-imine used as a chiral activator in the synthesis of (S)-phenyl-1- propanol. ....	37



Scheme 19. Isotopic labeling of 1-phenylethyl acetate for kinetic resolution in MS.....	86
Scheme 20. Kinetic resolution of 1-phenylethanol via the Stiglech reaction utilizing two acids differing in mass of 15 (CH <sub>3</sub> ).....	88
Scheme 21. Allylic ester used in the Pd-catalyzed screening. ....	93
Scheme 22. Tsuji-Trost Pd-catalyzed allylic substitution.....	93
Scheme 23. Mix of ligands to screen Pd catalysts with 16a and 16b, with resultant mass spectrum. <sup>247</sup> .....	94
Scheme 24. Substrates used in the Pd-catalyzed back-reaction study. ....	95
Scheme 25. Retro-Diels-Alder with the quasi-enantiomers (24a) and (24b). ....	96
Scheme 26. Radical mechanism for the formation of enantioselective epoxide from olefins.....	98
Scheme 27. Simmons Smith reaction. ....	103
Scheme 28. General cyclopropanation via diazoalkanes. ....	103
Scheme 29. Ligands used in enantioselective cyclopropanations.....	103
Scheme 30. Nucleophilic organocopper reactions. <sup>270</sup> .....	105
Scheme 31. Copper used in cross coupling before Pd.....	105
Scheme 32. Formation of a copper carbenoid. ....	106
Scheme 33. Proposed mechanism Cu-catalyzed cyclopropanation. <sup>259</sup> .....	107
Scheme 34. Synthesis of the chiral ethers. ....	121
Scheme 35. Synthesis of di-imines. ....	176

## List of Abbreviations

ACN	Acetonitrile
ADHD	Attention deficient hyperactive disorder
AMU	Atomic mass unit
BINAM	1,1'-binaphthyl-2-2'-diamine
BINAP	2,2'-bis(diphenylphosphino)-1,1'-binaphthyl
BINOL	1,1'-bi-2-naphthol
BOX	Bis-oxazoline
CAD	Collision activated dissociation
CD	Circular dichroism
CE	Capillary electrophoresis
CEC	Capillary electrochromatography
CI	Chemical ionization
CID	Collision induced dissociation
CRM	Charge residue model
DAIB	(2 <i>S</i> )-(-)- <i>exo</i> -(dimethylamino)isoborneol
DC	Direct Current
DE	Diastereomeric excess
DFT	Density functional theory
EE	Enantiomeric excess
EI	Electron ionization
ESI	Electrospray ionization

FAB	Fats atom bombardment
FDA	Food and Drug Administration
FT-ICR	Fourier Transform Ion Cyclotron Resonance
FWHM	Full width half-maximum
GC	Gas chromatography
HPLC	High performance liquid chromatography
HSS	High-speed screening
HST	High-throughput screening technology
I	Ion-Trap
IEM	Ion evaporation model
IM	Ion-molecule
IR	Infra-red
LMCO	Low Mass Cut-Off
m/z	mass-to-charge
MS	molecular sieves
MS	Mass spectrometer
NMR	Nuclear magnetic resonance
OMC	Organometallic catalysts
PDA	photo diode array
PhBOX	phenyl bis-oxazoline
QIT	Quadruple ion trap
QSAR	Quantitative structure-activity relationship
QSSR	Quantitative structure selectivity relationships

RF	Radio Frequency
RF	response factor
RRF	relative response factor
RSD	relative standard deviation
SFC	supercritical fluid chromatography
SIFT	selected ion flow tube
SLM	standard liter minutes
SMB	simulated moving bed
<i>t</i> -Bu	<i>tert</i> -butyl
TBF	round bottom flask
tBOX	<i>tert</i> -butyl bis-oxazoline
TOF	turnover frequency
TOF	Time-of-flight
TON	turnover number
TQ	triple quad
TS	transition state
UPLC	ultra performance liquid chromatography
UV	ultra violet

## **Abstract**

EXPLORING THE ASYMMETRIC ENVIRONMENT OF VARIOUS CHIRAL CATALYSTS USING A MODIFIED ION-TRAP MASS SPECTROMETER: TOWARDS THE DEVELOPMENT OF A RAPID CHIRAL CATALYST SCREENING METHOD

By Cary Mark Davis

A dissertation submitted in partial fulfillment of the requirements for the degree of Doctor of Philosophy at Virginia Commonwealth University

Virginia Commonwealth University, 2014

Director: Scott Gronert, Professor, Department of Chemistry

Since the tragedy of the drug Thalidomide® in the late 1950 to early 1960's, chirality has been recognized as an important aspect that must be controlled in the drug development process in the pharmaceutical industry. Since then, there has been a considerable movement towards single enantiomer drugs. This demand has presented many challenges for the synthetic organic chemist. Chiral catalysts offer one solution to this problem, as they afford the unique ability to preferentially synthesize one enantiomer. Unfortunately, the design of new chiral catalysts is often empirical, with luck and trial and error necessary due to factors that govern enantioselectivity. *Therefore, it would be highly beneficial to develop a method that is capable of screening multiple chiral catalysts early in the catalyst development cycle.*

Using a modified ion-trap mass spectrometer, the chiral environment of various chiral catalysts may be examined, free from solvent and ion-pairing affects. Thus, the catalyst's inherent asymmetric environment (enantioselectivity) may be probed using simple chiral molecules, including alcohols, ethers, and epoxides of various steric demands. Using these probes, various  $C_2$ -symmetric bis-oxazolines and di-imines catalysts were examined. Use of the binaphthyl-based diamine, BINAM, condensed with various 3,5-disubstituted benzaldehydes, provided selectivity close to the privileged catalyst, bis-oxazoline. In general, the chiral probes 1-phenyl-2-propanol, 1-methoxyethylbenzene, and styrene oxide offer the best look at the catalyst's enantioselectivity potential. With the use of the ion-trap mass spectrometer as a mass filter, the purity of the catalyst is not paramount, thus, multiple catalysts may be screened simultaneously, with the constraint that the catalysts must be of different  $m/z$ . This thesis presents results found during the exploration of various  $C_2$  and  $C_1$ -symmetric chiral catalysts, in the development of the new chiral screening method utilizing various chiral probes.

## Chapter 1 – Chirality and Asymmetric Catalysis

### 1.1 – Chirality

Chirality, or the spatial arrangement of atoms in space, prompted Louis Pasteur, the father of modern stereochemistry due to his pioneering work with tartaric acid, to write: “*L’ univers est dissymétrique.*”<sup>1</sup> His separation of tartaric acid salts in 1848, with a pair of tweezers and a microscope, gave birth to the field of stereochemistry,<sup>2</sup> and is a landmark in the history of organic chemistry. His keen insight into the three-dimensional aspects of Nature served him well later in life, when, in 1857, he discovered the enantioselective fermentation of tartaric acid.<sup>3</sup> He thus discovered the significance chirality imparts in biological systems, as many of the molecules necessary for life, carbohydrates, amino acids, DNA, etc., are inherently *dissymétrique*, the origin of which is an interesting and much debated topic (homochirality).<sup>4,5</sup>

A chiral molecule may be defined by a stereocenter, usually an asymmetric carbon with four different atoms attached. A molecule with an asymmetric carbon forms non-superimposable mirror images, which form a pair of enantiomers, **(a)** in Figure 1. Axial chirality also exists in Nature and is unique in that an asymmetric carbon is absent, instead replaced by an axis of chirality. Examples include allenes and biphenyl or binaphthyl-based molecules such as BINOL, BINAP, and BINAM see **(b)** in Figure 1,

and the right-hand turn of a DNA helix (c).<sup>6</sup> Enantiomers have the same physical properties, such as melting/boiling points, molecular weight, etc., differing only in the atom's 3D arrangement in space. Diastereomers are stereoisomers that are not mirror images of one another, possessing at least two stereocenters, at least one of which differs from the other (Figure 1).

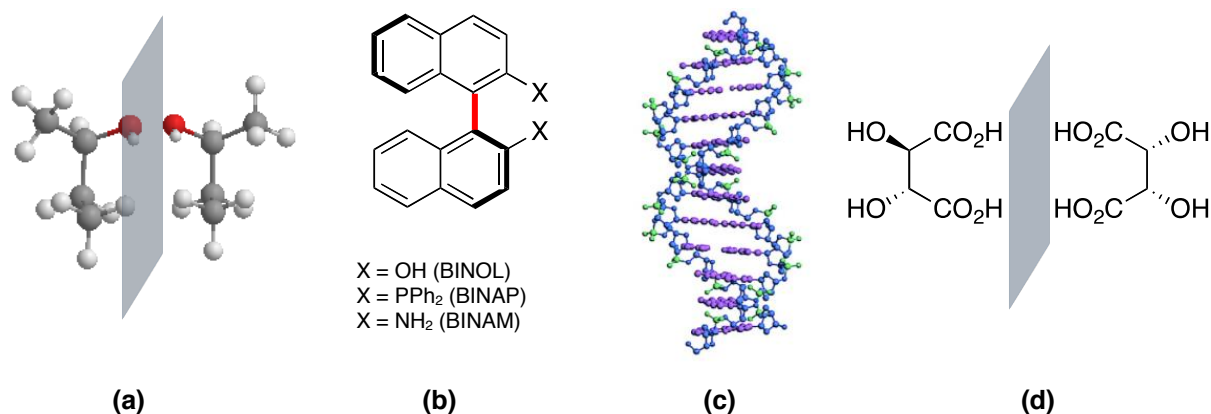


**Figure 1.** Examples of chiral molecules. (a) displays a pair of enantiomers (2-butanol). (b) displays an example of axial chirality (axis in red). (c) example of axial chirality in DNA (taken from Dickerson et al.)<sup>6</sup> (d) diastereomers (tartaric acid).

The pervasiveness of chirality in biological systems imparts significant importance to its control in the synthesis of pharmaceutical-based medicines, as

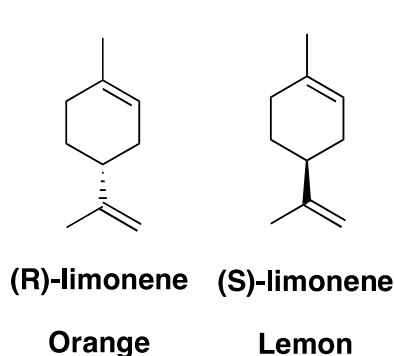


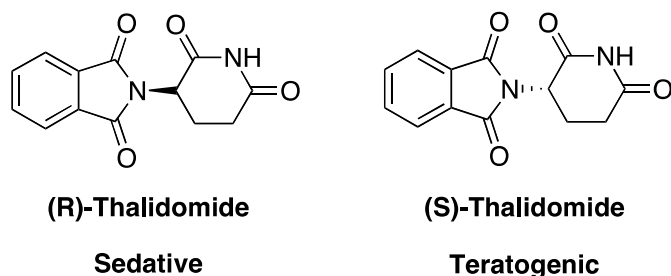
**Figure 2.** R/S-limonene.

individual enantiomers may exhibit stark differences in pharmacological, and toxicological activities/effects, as well as differences in efficacy/potency (i.e., pharmacodynamics and pharmacokinetics). The pharmacodynamics may be innocuous, as is the case for limonene, where (S)-limonene invokes the smell of lemon, while the (R) enantiomer triggers the smell of orange



(Figure 2).<sup>7</sup> Unfortunately, the pharmacological differences may also be tragic, as was the case for the drug thalidomide.

Thalidomide was prescribed for pregnancy-related nausea in the late 1950s and early 1960s in Europe, Australia, Japan, and Canada. Sold in its racemic form, it was



later found to cause severe birth defects. Specifically, it was found the S enantiomer was responsible for the teratogenicity, while the R enantiomer conferred the desired sedative effect

**Figure 3.** Thalidomide enantiomers.

(Figure 3). It was also later found to

racemize *in vivo*, thus, preventing the sale of the desired pure enantiomer, and muting the argument whether the single-enantiomer form would have prevented the tragedy.

Prior to this, enantiomeric forms were not a consideration in drug formulation, due in part to the difficulty in separation,<sup>8</sup> and synthesis.<sup>9</sup> Since thalidomide, however, the industry has become aware the need to consider enantiomers as separate drug candidates. This became mandated in 1992, when the FDA issued guidelines on drug development and stereoisomeric drugs, changing the landscape of drug discovery and development for the industry.<sup>10</sup> Figure 4 displays the percentage of drugs approved by the FDA from 1999-2008 by enantiomeric formulation. The trend towards single-enantiomer drugs over the racemic version is discernible and unequivocal,<sup>11</sup> especially when considering the fact in the early 1990s, 90% of chiral drugs were still racemic.<sup>9</sup>

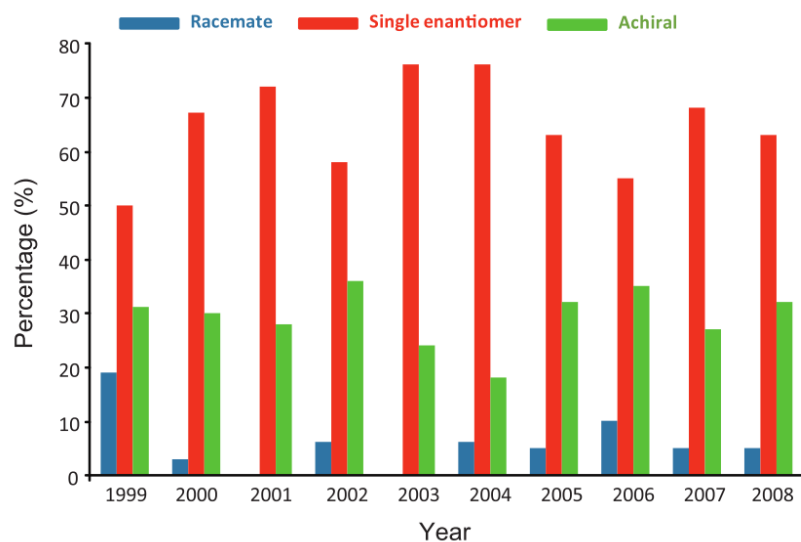


**Figure 4.** Enantiomeric composition of drugs approved by the FDA by year.<sup>11</sup>

The reasons for the shift are two-fold: therapeutic and financial. The therapeutic benefits of single-enantiomer drug formulations, according to Hutt & Valentová, include the following:

- increased efficacy (potentially);
- less complex, more selective pharmacodynamics profile;
- less complex pharmacokinetic profile;
- less complex relationship between plasma concentration and effect; and
- less potential for complex drug interactions.<sup>12</sup>

The financial impacts are also large and palatable. From a drug development perspective, it is usually much cheaper to develop an asymmetric process (via synthesis or separation), than spend money on characterizing the toxicological and pharmacokinetic profile of the undesired enantiomer and racemate.<sup>13</sup>

Patent protection/extension, however, is the main driver for single-enantiomer drugs. It is estimated a new drug costs between \$92-883 million to bring to market.<sup>14</sup> Couple this to the low percentage of drugs passing clinical trials, 32% for large molecule and 13% for small molecules,<sup>15</sup> and it becomes clear – companies must protect their investment and extend patent life as long as possible. Developing the single-enantiomer form increases the complexity and associated costs, increasing capital requirements, both monetary and human, required for generic companies to enter the market. Since they run on razor-thin margins, this is seen as a competitive advantage.

A racemic version may also allow a competitor to skirt patent laws and gain access to the market. If one of the enantiomers is inactive, a competitor may synthesize the enantio-active form, patent it as a new chemical entity, and market it. This “chiral switch” also allows patent holders the ability to extend the life of their patents and is actively pursued by patent holders, and smaller companies, as an alternative strategy to the time-consuming and expensive drug discovery process (for example, the company Sepracor who’s business model is built around the chiral switch).<sup>16</sup> Figure 5 displays three examples of common drugs that have undergone the chiral switch strategy.<sup>12</sup>

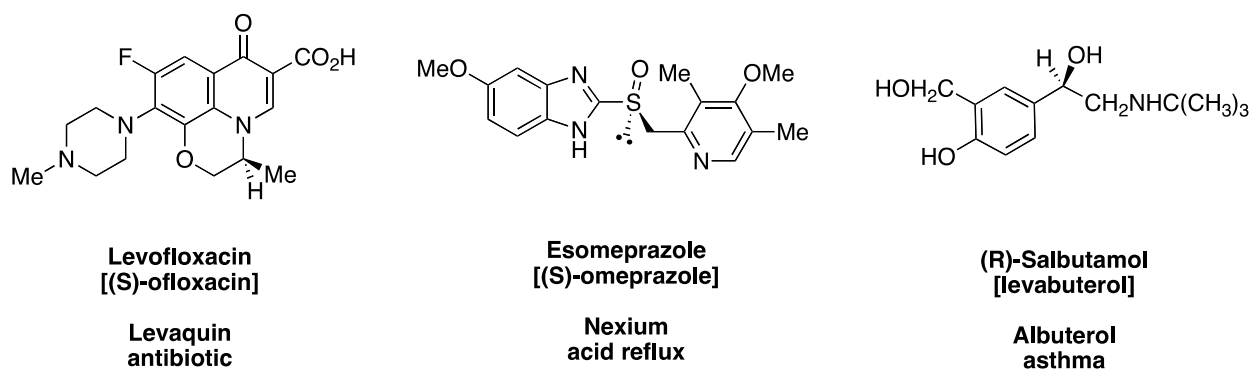


**Figure 5.** Example of drugs that have undergone the chiral switch.

Chiral molecules are a multi-billion dollar-a-year business. The market for single-enantiomer fine chemicals (agricultural, flavor, fragrances, etc.) was expected to be \$16 billion in 2007, a 13.2% growth rate.<sup>17</sup> In 2011, seven of the top-ten best-selling drugs were single enantiomers,<sup>18</sup> with sales of pharmaceutical-based single enantiomers at \$225 billion in 2005,<sup>19</sup> with projected sales of \$5.1 billion for chiral technologies (methodology, separations etc.) by 2017.<sup>20</sup> This huge market for chiral molecules has presented many challenges for chemists. The cost, and more so the speed of drug development, with the need to get to market as fast as possible, places enormous pressure on the synthetic organic chemist to derive fast, efficient asymmetric methodologies, as well as the analytical chemist to develop methodologies to separate and quantitate chiral molecules.

From an atom economy point of view, asymmetric catalysis affords an excellent opportunity to introduce asymmetry into the molecule. Unfortunately, this is complicated due to the fact that many chiral catalysts are patented, requiring royalties and freedom to operate agreements, limiting industrial use.<sup>21</sup> Rather, other methods and/or in-house development of catalysts/ligands are pursued. *It would therefore be highly beneficial to develop a rapid chiral catalyst screening method to aid in the discovery of new catalyst systems in pursuit of cheaper, faster, and more efficient asymmetric synthetic routes/methodologies.*

## **1.2 – Methods for Achieving Enantiopurity**

Enantiopurity may be attained through numerous methods, (Figure 6). Each method has its merits and faults, discussed briefly in the proceeding paragraphs; thus, the method selected depends on many factors, such as chemistry, time, money, commercial availability, “elegance”, and simplicity.

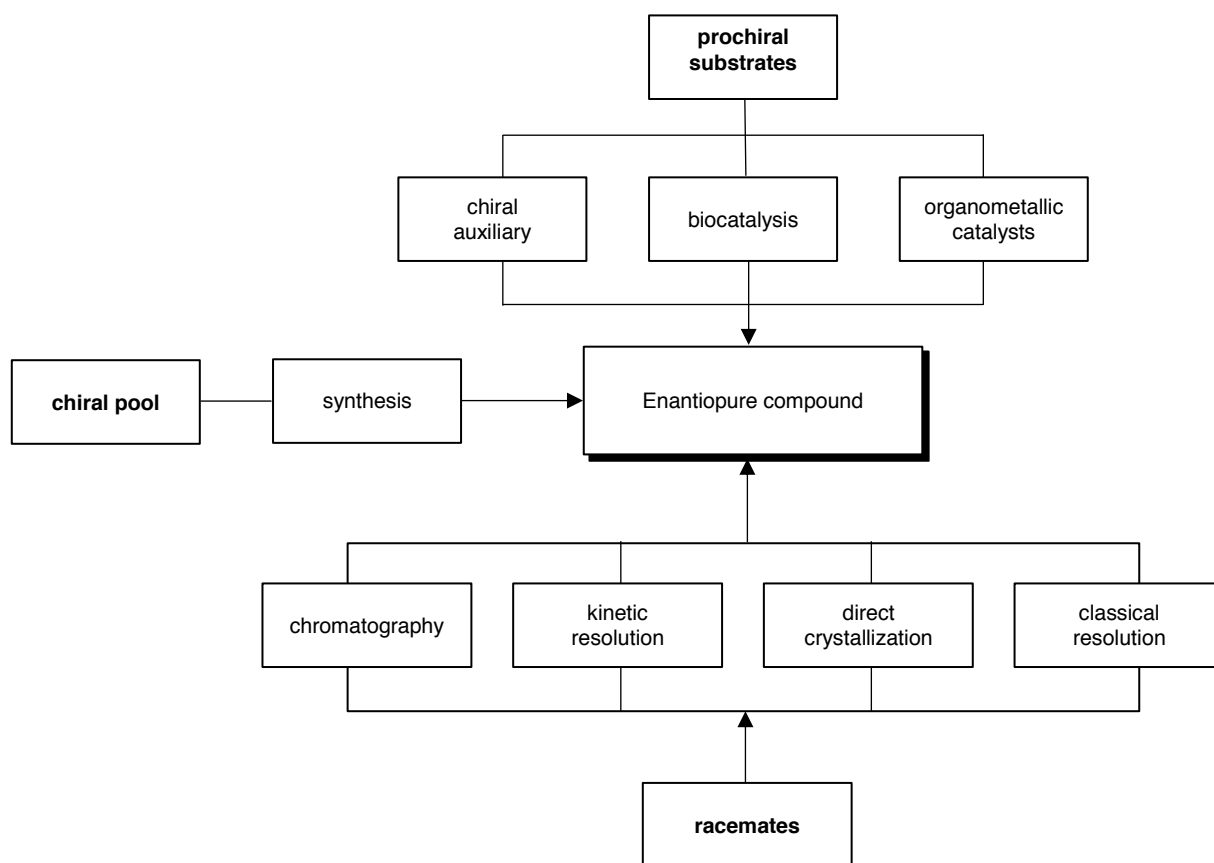


**Figure 6.** Different routes to enantiopurity.

Farina et al. performed a brief survey of single-enantiomer drugs released from 1992 – 2003 and deduced the chiral method of induction through patents.<sup>13</sup> Based on the data in Figure 7 the chiral pool method was by far the most popular method used in industry to induce chirality.

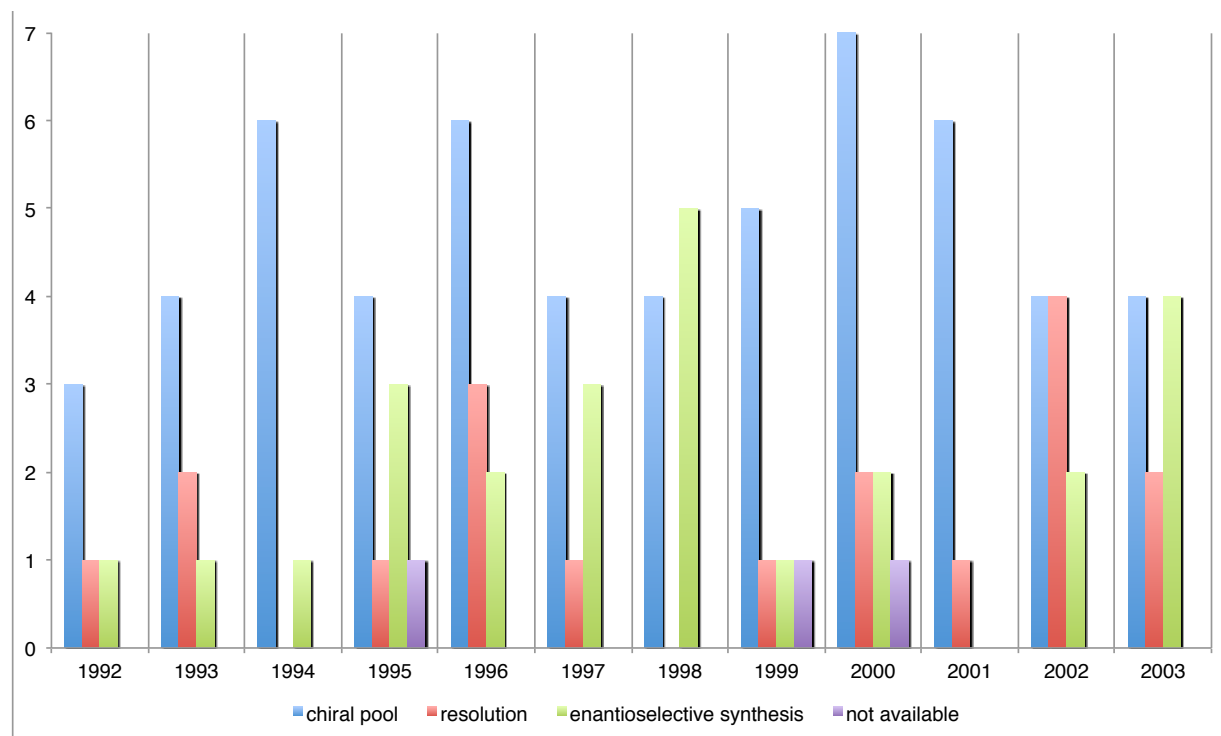
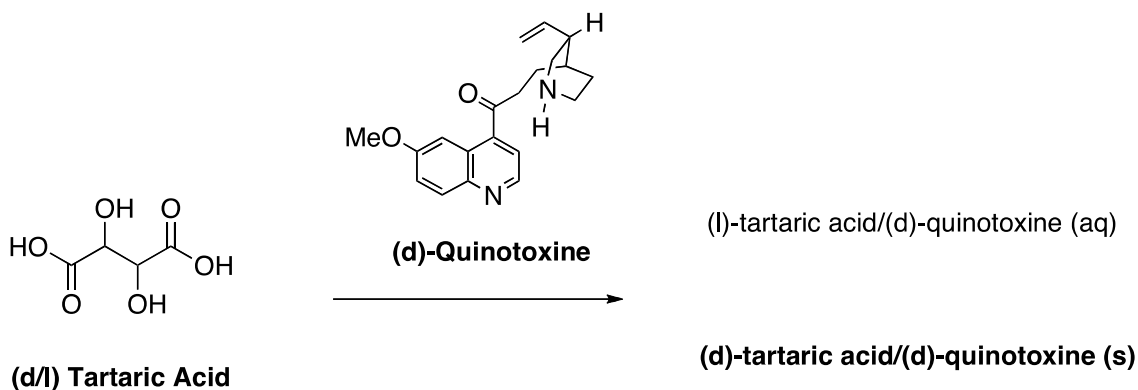


**Figure 7.** Method of chiral induction for single-enantiomer drugs released from 1992 – 2003.<sup>13</sup>

### 1.2.1 – Resolution

Resolution requires the use of a stoichiometric quantity of an enantiomerically pure resolving agent with a racemic mixture to form a diastereomer, where differences in physical properties of the two may be exploited, such as solubility (crystallization), boiling points (distillation), and polarity (chromatography), etc. A requirement of the diastereomer is reversibility; hence, acid-base chemistry is preferred. In 1853, Pasteur first reported the first classical resolution, via formation of a diastereomeric salt with subsequent crystallization. He found a racemic mixture of tartaric acid mixed with the basic resolving agent, (+)-quinotoxine, precipitated the enriched (d)-tartaric acid/(d)-quinotoxine, shown in Scheme 1.<sup>22,23</sup> This method remains popular today, with little

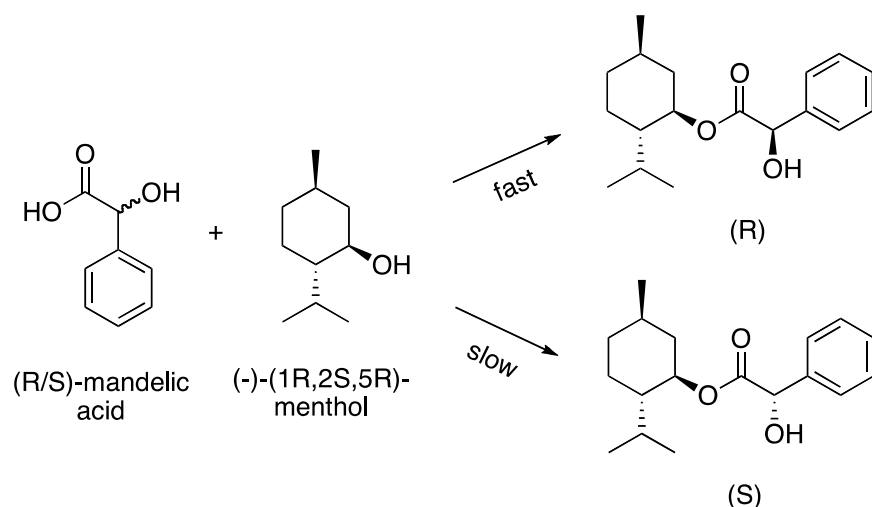


**Scheme 1.** Classical resolution of tartaric acid via enantiopure (d)-quinotoxine.

modification, due to the scalability, ranging from mg to kg, reproducibility, ease of implementation (i.e., no equipment modifications), and historical knowledge. However, not every compound forms a salt and the maximum yield is 50%, with the other enantiomer a waste product, if there is no commercial application/market.<sup>24</sup>

### 1.2.2 – Kinetic Resolution

Kinetic resolutions are based upon differential rates of reaction between the two enantiomers. Marckwald and McKenzie first discovered the principle in 1899 with the preferential esterification for the R enantiomer when a racemic mix of mandelic acid was reacted with (-)-menthol (Scheme 2).<sup>25</sup> This method confers extremely high ee's, but usually at a cost of yield (driven by the  $\Delta\Delta G$  of the two transition states), which itself is limited to a maximum of 50%. This again produces waste from the other enantiomer and is thus viewed as inelegant.



**Scheme 2.** First example of kinetic resolution by Marckwald & MaKenzie.<sup>25</sup>

A variation on the kinetic method is found when the enantiomers are able to racemize on a time scale faster than the reaction, and is called a dynamic kinetic resolution. It was first reported by Noyori in 1989, with the stereoselective hydrogenation of  $\beta$ -ketoesters.<sup>26</sup> Figure 8 displays the free energy diagram of the reaction, clearly demonstrating the thermodynamic preference for the faster-forming anti-epimer. Since the enantiomers racemize, the theoretical yield can be 100%, however, for good ee, the  $k_A/k_B$  should be at least 20 and  $k_{inv}$  should be faster than  $k_A$ , hence  $k_{inv} > k_A \gg k_B$ .<sup>27</sup>



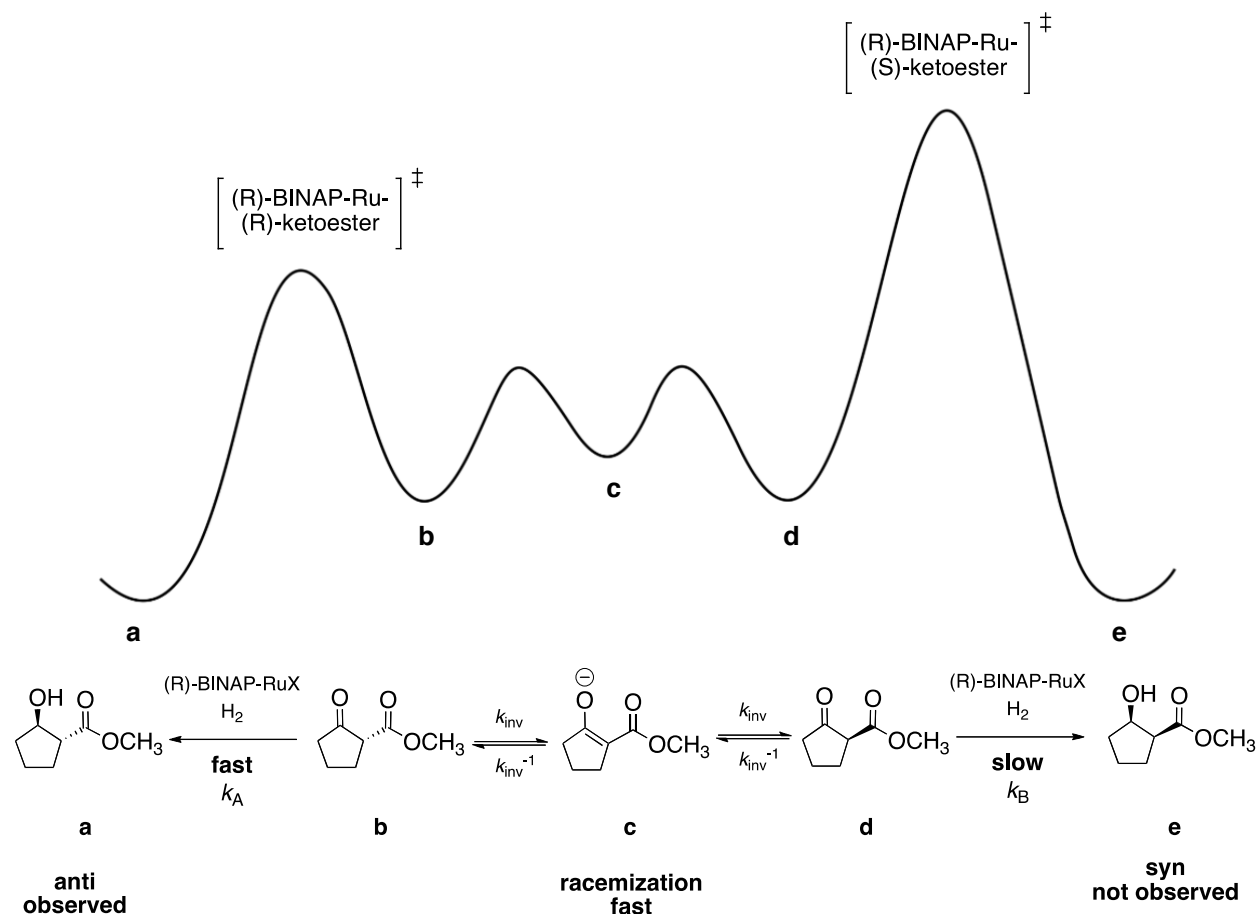


**Figure 8.** Free energy diagram of the dynamic kinetic resolution of the stereoselective hydrogenation of a  $\beta$ -keto-ester.<sup>27</sup>

### 1.2.3 – Chromatography and Direct Crystallization

Two other methods for separation of racemates include chromatography and direct crystallization. Separation of racemates utilizing a column requires conversion to diastereomers either directly by derivatization, or through interaction with a chiral stationary phase, forming a “transient” diastereomer. In 1952, Dalgliesh introduced the three-point model of interaction to explain the separation of enantiomers, an extension of the biological enzyme-substrate mechanism of Easson and Stedman.<sup>28,29</sup> The three-

point model postulates three points of contact are necessary for enantiomeric separation. This can only be met in an asymmetric environment with only one of the enantiomers in the correct 3D configuration (Figure 9).

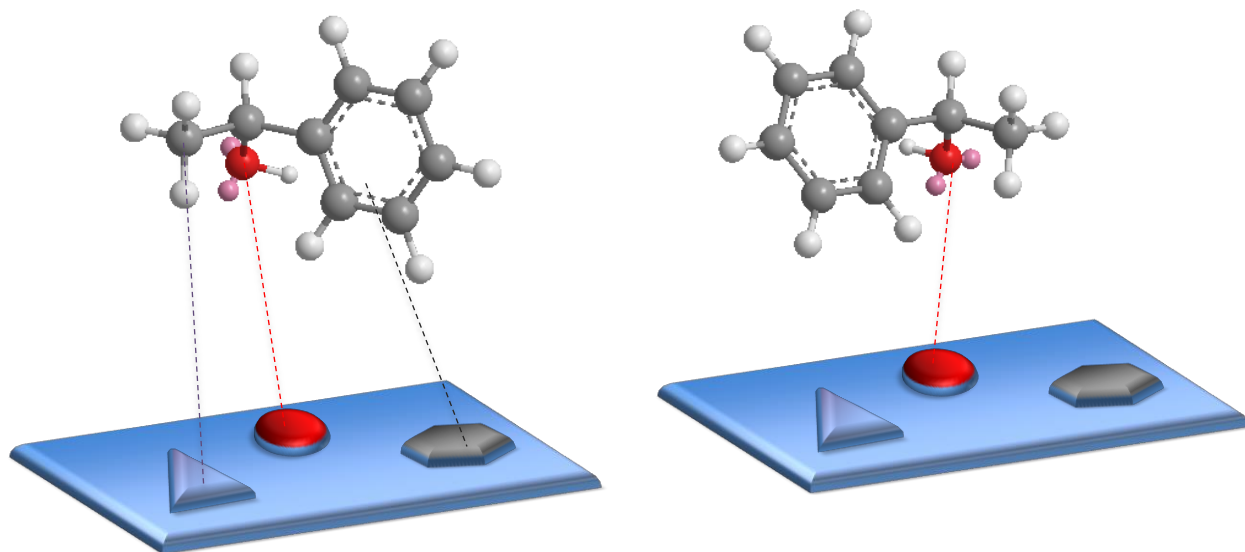


**Figure 9.** Three-point model of chiral separation. Note the S enantiomer (left) has three points of contact, while the R enantiomer (right) only has one point of contact.

Chromatography is inherently difficult to translate to larger scales, and is therefore regulated more towards the smaller scales of academia. However, newer technology, designated simulated moving bed (SMB), has been used to resolve the intermediate tetralone in the synthesis of sertraline, an antidepressant, by Pfizer.<sup>30</sup> The SMB is a series of valves and switches that allow for multiple columns to be placed in series with appropriate inlets and outlets. This set-up also (Figure 10)<sup>31</sup> allows for the undesired enantiomer to be racemized with NaOH and acetonitrile, and recycled through the process, increasing yield to theoretically 100%, but requiring significant capital investment, and most likely a dedicated reactor train.

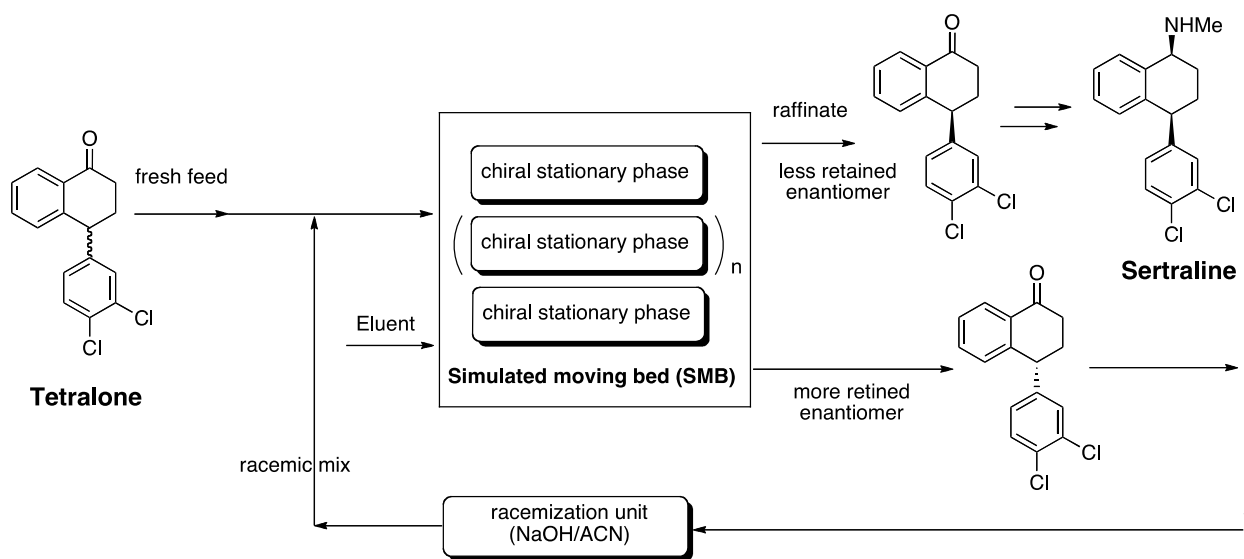


**Figure 10.** SMB set-up for industrial chiral chromatographic separation of the intermediate tetralone, which is processed to the antidepressant Sertraline. Adapted from US patent 6,444,854 and Hawkins et al.<sup>31</sup>

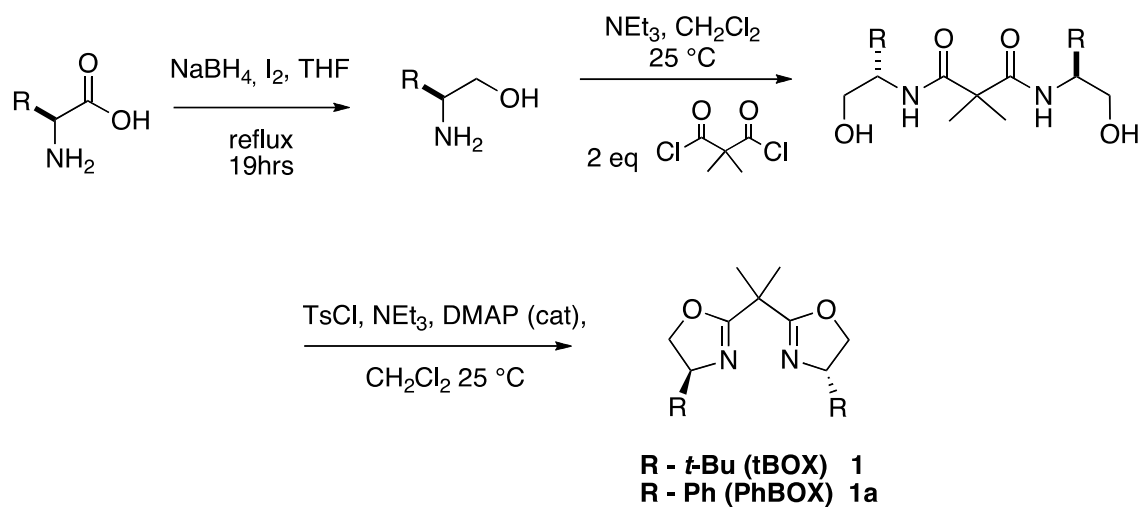
Direct crystallizations are much less common due to the fact the enantiomers must crystallize as two separate mirror image (enantiomorphous) crystals or conglomerates. The number of racemates that meet this criteria was estimated to be between 5-10%.<sup>32</sup> Fortuitously, the tartaric acid crystals Pasteur separated manually meet this definition. In 1882, Jungfleisch seeded a supersaturated solution of sodium ammonium tartrate with one enantiomer on one side of a vessel, and the other enantiomer on the other side. He found each enantiomer to selectively crystallize on the respective side on the vessel in which it was seeded.<sup>33</sup> This method was successfully used to separate a racemic mixture of *d/l*-Methadone,<sup>34</sup> but again, a maximum of 50% yield is achieved.

A second method of crystallization is called resolution by entrainment, or preferential crystallization. This technique seeds a racemic mix with one of the

enantiomers and is heated to dissolve. Upon cooling to the supersaturation point, the enriched enantiomer will start to crystallize, after which it is filtered, leaving the other enantiomer enriched in the mother liquor. Afterwards, additional racemate is added to adjust to the starting point concentration. The contents are heated, allowed to cool, and the other enantiomer will preferentially crystallize. After filtration, more of the racemic mix is added and the process is repeated. The purity attained for this method can be quite high, for example, after 15 cycles, a 97% optical purity was obtained for the preferential crystallization of the (-)-hydrobenzoin enantiomer.<sup>35</sup> However, impurities that become enriched after each cycle may begin to interfere with the crystallization process.

#### 1.2.4 – Chiral Pool

The simplest method for introducing chirality into a target molecule is to start with enantiopure starting material that may be transformed to the target molecule with the chirality preserved during the course of the synthetic process. This method is called chiral pool synthesis and was used in the synthesis of the *t*-Bu bis-oxazoline (**1**, **1a**) used in this work (Scheme 3).<sup>36</sup> Upon inspection of Figure 7, it becomes obvious most process chemists' prefer to draw from the chiral pool when introducing chirality into a desired molecule. This is most likely a matter of convenience, as time is critical in the drug discovery/development stage. Nature serves as the provider of the pool, as the



**Scheme 3.** Synthesis of bis-oxazoline (tBOX) via the chiral pool method.

majorities of synthons are of natural origin, and as such, are relatively cheap. These include alkaloids, amino acids, carbohydrates, hydroxy acids, and terpenes (Figure 11).

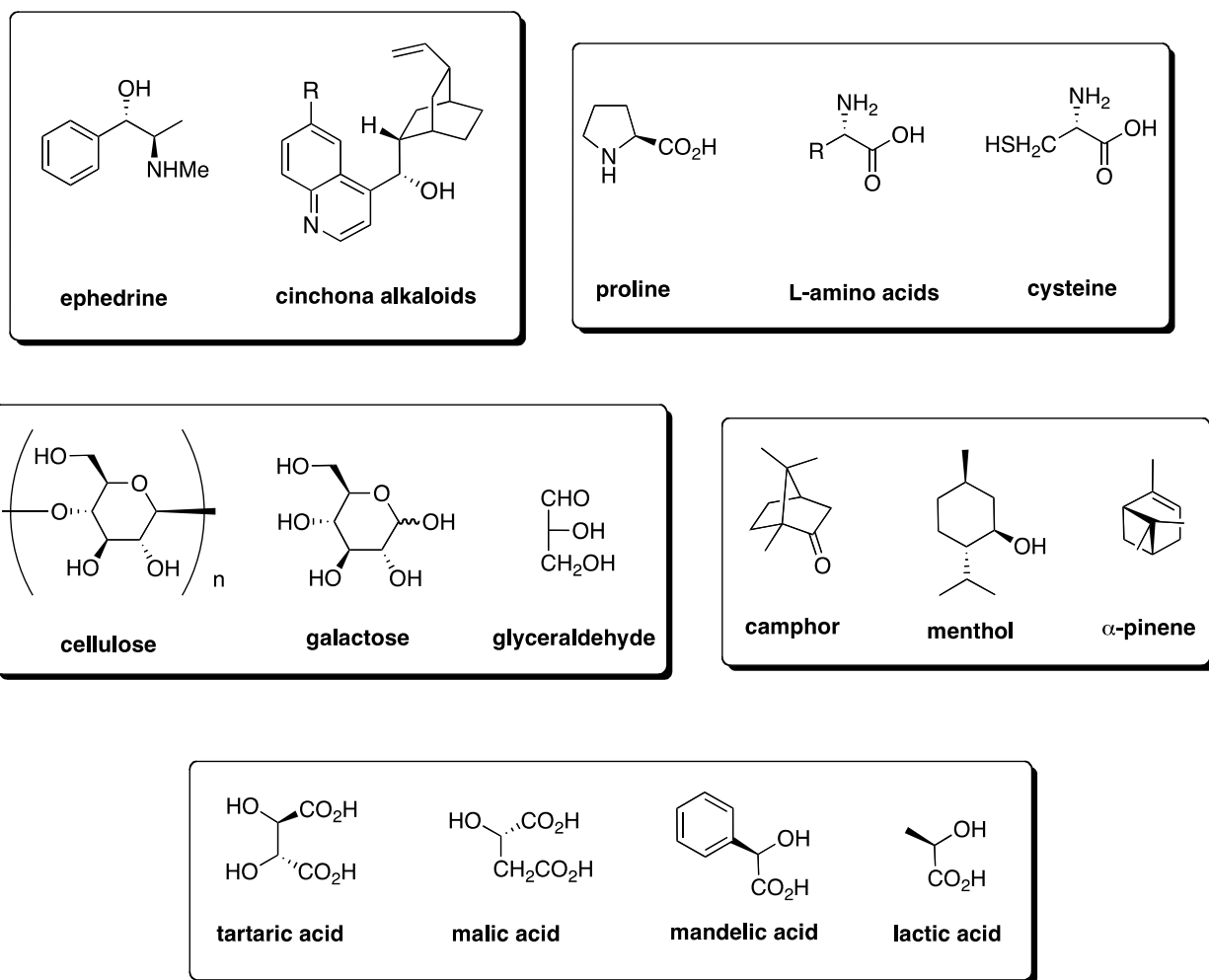
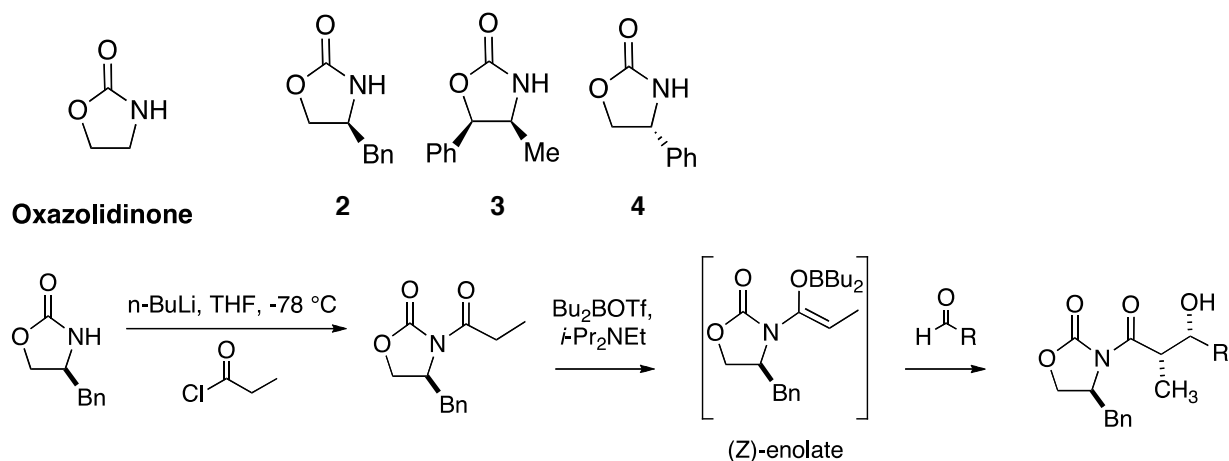


**Figure 11.** Selection of chiral molecules comprising the chiral pool.

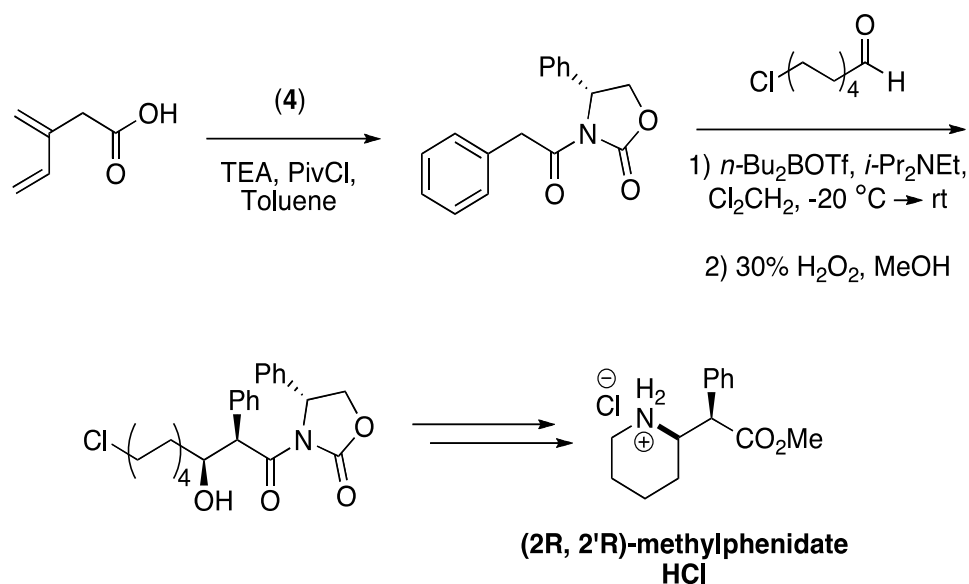
The chiral pool method has represented the only source of chiral materials for years; therefore, the methodology has been proven through time. The disadvantage of the chiral pool method is the limited availability of both natural enantiomers, and the potential extra steps in the synthesis, assuming the starting material can even be transformed to the desired product.

### 1.2.5 – Chiral Auxiliary

Alternatively, the chiral center(s) may be introduced during the synthesis by introducing a chiral auxiliary (which itself is derived from the chiral pool) that directs enantioselectivity via intramolecular asymmetric induction. The auxiliary is then removed afterwards and potentially recycled.<sup>37</sup> Oxazolidinones are common chiral auxiliaries, and were pioneered by David Evans in enantioselective aldol condensations via a boron enolates (Scheme 4).<sup>38</sup> The oxazolidinone (**4**) was used in the first enantioselective synthesis of methylphenidate (Ritalin), used for the treatment of attention deficient hyperactive disorder (ADHD) (Scheme 5).<sup>39</sup>



**Scheme 4.** Oxazolidinone and common oxazolidinones used as chiral auxiliaries (top). Example of Evan's oxazolidinone for use as a chiral auxiliary in an aldol addition.<sup>38</sup>



**Scheme 5.** First enantioselective synthesis of Methylphenidate via Evan's oxazolidinone and a chiral auxiliary.

The method of removing the oxazolidinone allows for the generation of different functionalities for the new aldol. For example, reductive conditions yield a primary alcohol<sup>40</sup> while oxidative conditions yield a carboxylic acid.<sup>41</sup> Weinreb amides may even be synthesized for later use as ketones by employing *N,O*-dimethylhydroxylamine.<sup>42</sup> The Evan's oxazolidinone, as well as others, direct asymmetry in other transformations including alkylations, conjugate additions, cycloadditions, and nucleophilic addition reactions.<sup>13</sup>

In the case of alkylations, the chiral auxiliary directs chiral induction due to the resulting 3D conformation of the molecule. Due to metal chelation to the carbonyl and enolate, the conformation is more rigid, forming a six membered ring between the N-C-CO portion of the oxazolidinone and the enolate. The chiral moiety at the 4-position of



the oxazolidinone directs the incoming electrophile, effectively blocking its path from the bottom, and forcing attack from the top, as shown in Figure 12.<sup>43</sup>

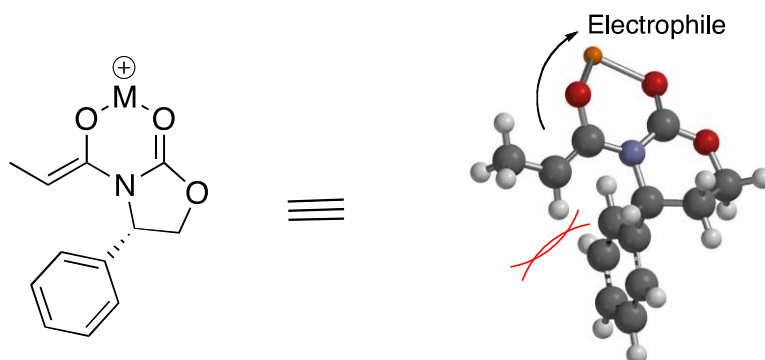


**Figure 12.** Chiral induction via blockage from the bottom.

The disadvantage of using chiral auxiliaries is the stoichiometric amount of material that is required to induce chirality. The fact that the auxiliaries are usually cheap somewhat negates this fact; however, the method requires two extra steps in the synthesis, introduction and cleavage of the auxiliary, thereby reducing atom economy and cycle time.<sup>44</sup> There may also be complications removing the product from the stoichiometric amount of auxiliary, which itself is a highly desired commodity, to be isolated and reused later, reducing costs and waste, and increasing efficiency.

### 1.3 – Catalysis

Due to the inefficiencies or limitations of the previous methods, it would be ideal to develop methodologies that incorporate sub-stoichiometric amounts of chiral material, i.e. catalysis, into the synthesis. In 1835, Baron J. J. Berzelius defined a catalyst as any substance that facilitates chemical reactions without being consumed in the process.<sup>45</sup>

Catalysts “facilitate” reactions by reducing the energy of activation required for a

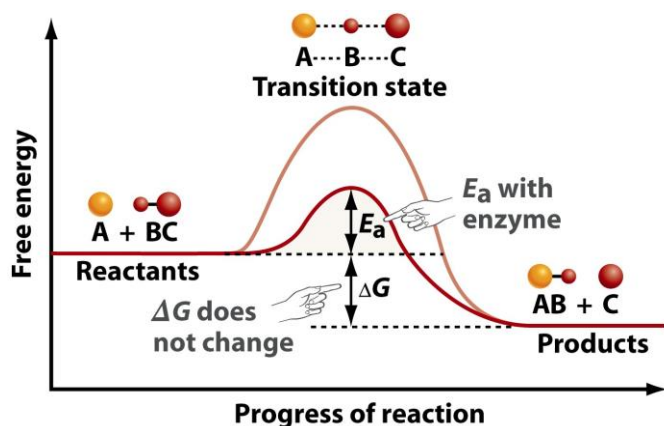


**Figure 13.** Free energy diagram for a catalyst vs. non-catalyst reaction. Taken from [http://www.uic.edu/classes/bios/bios100/lectures/energy\\_hump01.jpg](http://www.uic.edu/classes/bios/bios100/lectures/energy_hump01.jpg)

reaction to take place. Figure 13 displays the free energy diagram for a generic reaction with and without a catalyst. Many of the biochemical processes required for life are catalyst-driven via enzymes. It is also crucial for our economy and our way-of-life, as an estimated 90% of all chemical processes currently in use are catalytic

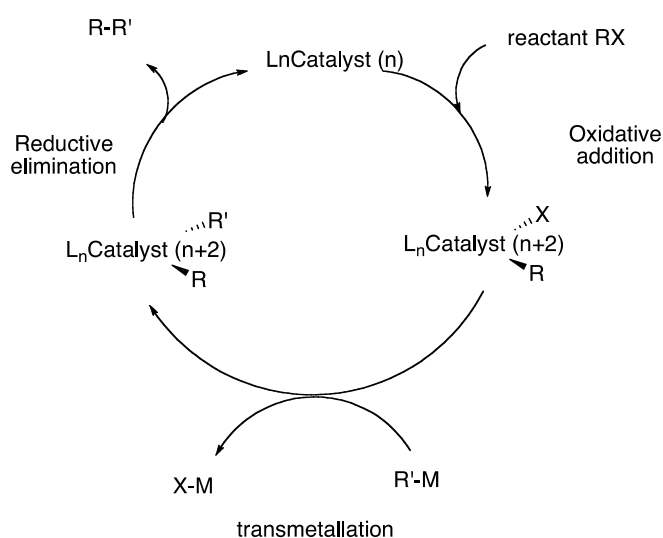
in nature.<sup>46</sup> Catalysts are divided into three categories, homogeneous (same phase), heterogeneous (different phase), and enzymatic (biocatalysis). Heterogeneous catalysis is by far the most prevalent in use today, with an estimated 80% of the global market share, followed by 17% for homogeneous, and 3% for enzymatic.<sup>46</sup>

### 1.3.1 – Organometallic Catalysis

Organometallic catalysts (OMC) bridge the fields of organic and inorganic chemistry, and have become an indispensable tool for the modern synthetic chemist, as they provide unique solutions to enantioselectivity and CH bond activation. The d-orbitals of metals allow access to energetically favorable alternative pathways to CH bond activation. This lower energy of activation allows for much greater selectivity, because alternate higher energy pathways are not accessible. In recognition of the

importance of OMC to chemistry, The Royal Swedish Academy of Sciences has awarded ten Nobel Prizes to Chemists whose work pioneered/advanced the field of OMC,<sup>47</sup> with the most recent (2010) recipients, Akira Suzuki, Ei-ichi Negishi, and Richard Heck, for their contributions in the field of Pd cross-couplings.<sup>48</sup>

The mechanisms of a transformation utilizing OMC can range from complex to nuanced, but they all generally go through some oxidative addition to the metal,



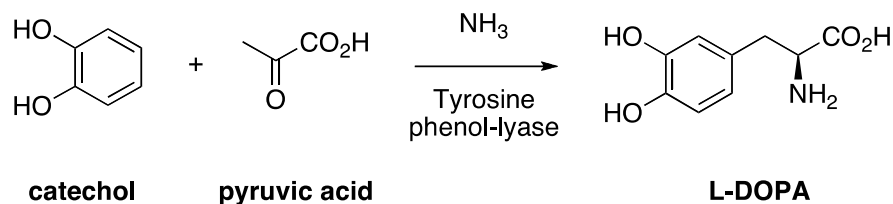
**Scheme 6.** General Catalytic Cycle.

transmetalation, followed by reductive elimination leading to the product and the regenerated catalyst, shown in Scheme 6. OMC have also found use in asymmetric synthesis, where the ligand coordinates to the catalyst, forming a rigid, three-dimensional template, necessary to differentiate the enantiomers or direct a group to the

prochiral face. Due to the regeneration of the catalyst, catalysis is ideally suited for asymmetric synthesis, since the chiral portion is usually the most expensive and hardest molecule to obtain.

### 1.3.2 – Biocatalysis

Biocatalysis utilizes enzymes to transfer chirality, yielding an extremely selective (chemo, regio, and enantio) process, due in part to the very specific nature of the enzyme-substrate complex.<sup>49</sup> The enzyme, tyrosine phenol-lyase (Tpl), is used to produce L-DOPA, the precursor of the neurotransmitter dopamine, norepinephrine, and epinephrine (adrenaline). *Erwinia herbicola* cells, previously treated in L-tyrosine medium to induce Tpl and subsequently isolated by centrifugation, were added to catechol, pyruvic acid, and ammonia to produce (S)-3,4-dihydroxyphenylalanine, or L-DOPA, shown in Scheme 7.<sup>50</sup> Of note is the high regioselectivity of the new aryl-C bond

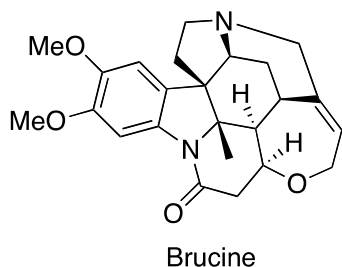


**Scheme 7.** Enzymatic synthesis of L-DOPA.

formation, in addition to the high enantioselectivity of the hydrogenation. The only impurities observed were from the L-tyrosine, a product of the medium used to cultivate the cells, and a natural byproduct of the Tpl. This process is used to produce approximately half of the 250 tons of L-DOPA produced annually (as of 2005).<sup>50</sup>

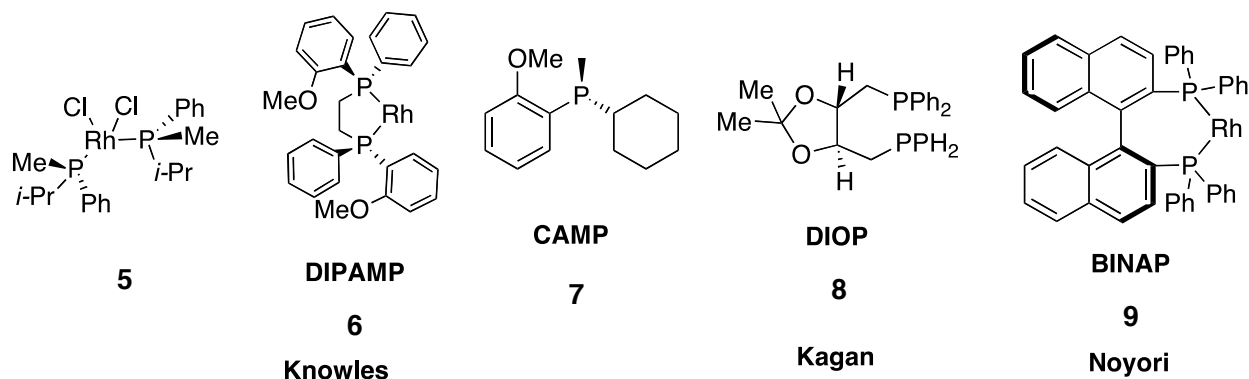
The previous example highlighted the advantages conferred by biocatalysis – the high selectivity. However, this is tempered by the limited reaction conditions that enzymes can tolerate, such as aqueous solvents, and limited pH and temperature ranges, oxidation, as well as substrate and product inhibition.<sup>51</sup> In addition, some people may suffer from allergic reactions to proteins, particularly if they manage to get into the

### 1.3.3 – Enantioselective Catalysis

CCC(C)(O)C(=O)O>Brucine>CCC(C)C(=O)O

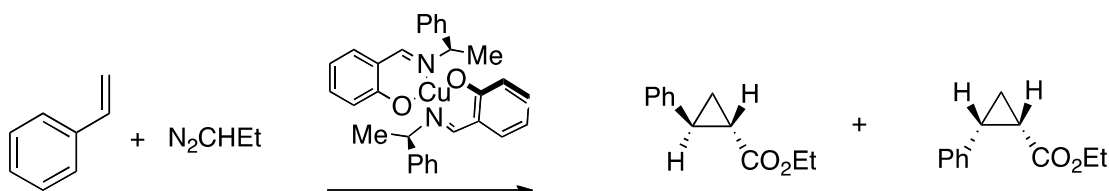
ligands, as with Cu bis-oxazolines, or consist solely of a chiral molecule, usually derived from nature, for example, proline. One of the first examples of an asymmetric synthesis was reported in 1904 by Willy Marckwald when he enantioselectively (10% ee) decarboxylated 2-ethyl-2-methylmalonic acid with the alkaloid brucine (Scheme 8).<sup>53</sup> Since

then, numerous chiral ligands have been developed for enantioselective synthesis, particularly for asymmetric hydrogenations, due to historical reasons (Figure 14).



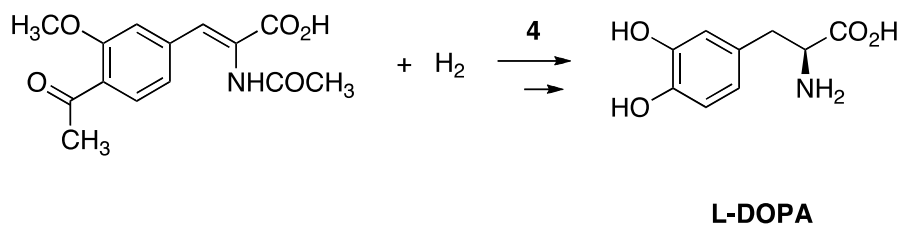
23

The first asymmetric organometallic procedures were developed by Noyori in 1966 for the cyclopropanation of styrene with ethyldiazoacetate and a (salicyladiminato)-copper complex (Scheme 9).<sup>54</sup> This was followed by the rise of phosphines for use in asymmetric hydrogenation, where much of the early work was concentrated. In 1986, Knowles and Horner modified Wilkinson's catalyst,  $\text{RhCl}(\text{PPh})_3$ , used in hydrogenation of alkenes, with a chiral bisphosphine (**5**) to produce an asymmetric hydrogenation, albeit at low optical purity (**15**).<sup>55,56</sup>



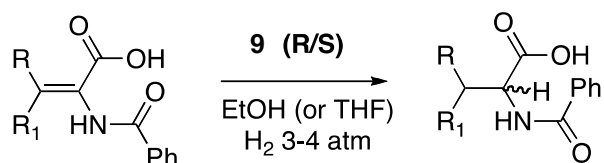
**Scheme 9.** First enantioselective cyclopropanation by Noyori in 1966.<sup>54</sup>

A few years later, Kagan reported the highest optical yields, 72%, to date (1971) for an asymmetric homogeneous catalyst using the  $\text{C}_2$ -symmetric DIOP (**8**) for an alkene hydrogenation.<sup>57</sup> Knowles also continued to make progress, increasing ee to 87% with the CAMP ligand (**7**) and Rh in 1972.<sup>58</sup> By 1974, the ee's were high enough for commercial viability. Knowles, while working with Monsanto, was the first to develop an industrial-scale enantioselective hydrogenation process for the production of L-DOPA using DIPAMP (**6**), shown below in Scheme 10.<sup>59</sup>



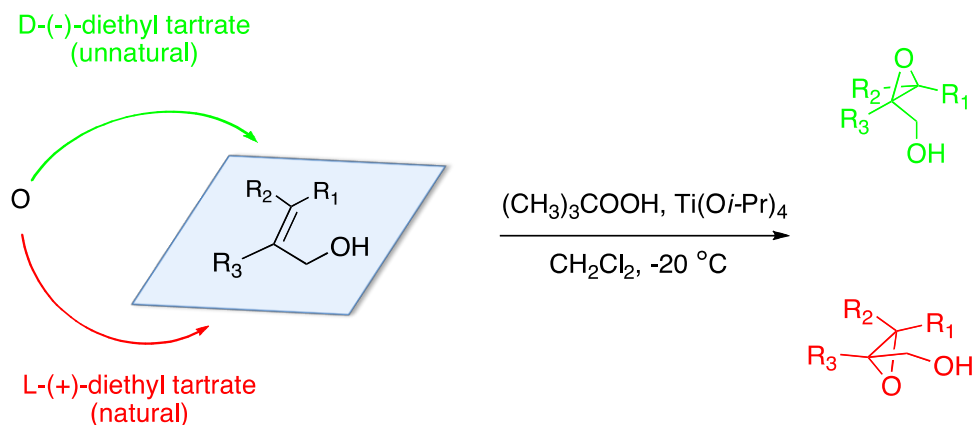
**Scheme 10.** First commercial use of an asymmetric catalyst.

By 1980, Noyori and Takaya discovered the usefulness of atropisomerism in asymmetric synthesis and used the Rh(I)-based BINAP (**9**) for an asymmetric hydrogenation of  $\alpha$ -(acylamino)acrylic acids (Scheme 11).<sup>60</sup> In 1986, Noyori used Ru(II) with BINAP in the asymmetric hydrogenation of isoquinoline alkaloids,<sup>61</sup> and in the process significantly increased the scope of the catalyst.



**Scheme 11.** Asymmetric hydrogenation using BINAP and Rh.

In 1980, Sharpless introduced the first asymmetric epoxidation shown in Scheme 12.<sup>62</sup> For their pioneering efforts into asymmetric catalysis, Knowles, Noyori and



**Scheme 12.** Sharpless epoxidation.

Sharpless, shared the 2003 Nobel Prize in Chemistry.<sup>63,9,59</sup> Since then, numerous enantioselective catalysis have been employed on an industrial scale (Table 1).<sup>64</sup>

**Table 1.** Metal coordinated chiral catalyst in industrial use.<sup>64</sup>

Company	Metal	Reaction Type	Final Product
Monsanto	Rh	Hydrogenation	L-Dopa
Sumitomo	Cu	Cyclopropanation	Cilastatin
Anic. Enichem	Rh	Hydrogenation	L-Phenylalanine
J. T. Baker	Ti	Epoxidation	Disparture
ARCO	Ti	Epoxidation	Glycidols
Takasago	Rh	Rearrangement	L-Menthol
Merck	B	C=O reduction	MK-417 (ophthalmic)*
E. Merck	Mn	Epoxidation	Antihypertensive*
Takasago	Ru	Hydrogenation	Carbapenem

\*Developmental quantities for safety assessment and clinical trials

There are many factors that one must consider when selecting an asymmetric catalyst, such as the turnover number (TON = mol product/mol catalyst), turnover frequency (TOF = TON hr<sup>-1</sup>), catalyst loading, and patents and associated legalities; however, these are subsumed by the choice of the metal and ligand.

#### 1.3.3.1 – Metal

The choice of metal is an important aspect to consider for asymmetric induction, with the noble and transition-based metals by far the most popular.<sup>65</sup> Different metals possess different coordination spheres, which affect geometry and steric crowding, a major driving force for enantioselectivity. Additionally, the ability to adopt multiple oxidation states is crucial for catalytic activity.



While Pd is extremely popular on an industrial scale, due in no small part to the popularity of the C-C bond coupling reactions, such as the Suzuki, Negishi, Heck, Stille, Buchwald-Hartwig, etc.<sup>66</sup> For asymmetric catalysis, Ru, Rh, and Ti are the most prevalent.<sup>65</sup> This is no doubt related to the pioneering asymmetric work of Noyori, Knowles, and Sharpless. A final consideration is the price of the metal. Although it is

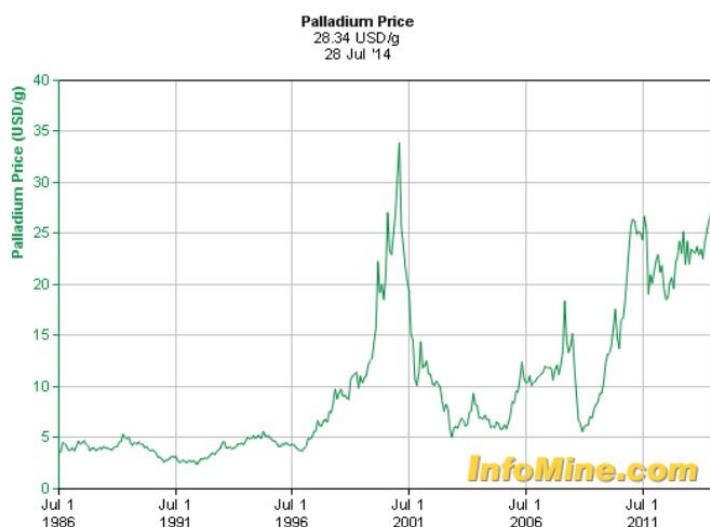


**Figure 15.** Price of Pd (\$US/gram) since 1986. Taken from infomine.com

used in catalytic amounts, the price may fluctuate drastically, as shown with Pd in Figure 15.<sup>67</sup> In some cases, the metal may be recycled, but most lose catalytic activity with each cycle and may need to be regenerated via an acid or base wash. Many are air and moisture sensitive as well, which

are other factors that must be considered.

### 1.3.3.2 – Ligands

The choice of ligand is the most important aspect of asymmetric synthesis since it forms the template that will dictate the direction of approach a reagent will take, and hence the enantioselectivity. Electronics of the ligand can affect the electron density on the metal and hence accelerate or decelerate the rate of the catalysis (ligand activation/deactivation).<sup>68</sup> The ideal class of ligand is stable in air and water,

inexpensive and easy to prepare in both enantiomeric forms.<sup>69</sup> The catalyst should also be highly tunable, offering the ability to easily modify the ligand with various functional groups. Even small differences in ligand structure can have a drastic effect on selectivity.<sup>70</sup> This has been termed a modular approach and is critical since performance of a new catalyst/ligand is more empirical than theoretical.

The diphosphines are the most widely used class of ligands on the industrial scale, again due to Noyori and historical precedence of the asymmetric hydrogenations.<sup>65</sup> C<sub>1</sub>-symmetric ligands, such as those shown in Figure 16 have been

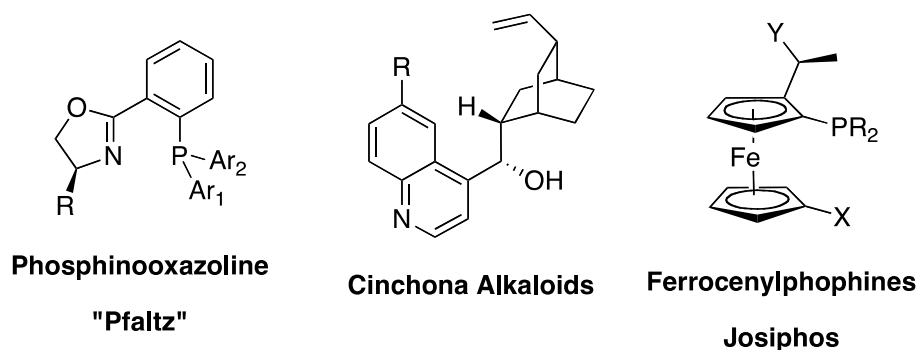


**Figure 16.** Common C<sub>1</sub>-symmetric catalysts.

shown to induce modest to excellent enantioselectivities.<sup>71</sup> Unsymmetrical, with two different substituents, or mono substituted ligands have also been employed, resulting in generally lower ee's than the corresponding C<sub>2</sub>-symmetric catalysts. Analog C<sub>2</sub>-symmetric catalysts have been synthesized bearing two different groups (unsymmetrical) substituents, as well as mono substituted catalyst, all displaying generally lower ee's than the corresponding C<sub>2</sub>-symmetric originals,<sup>72,73</sup> but in some cases offering better selectivity.<sup>71</sup>

Of all the ligands, a certain class has stood out and become common in asymmetric synthesis due to their high ee's and, perhaps more importantly, their success over a wide range of transformations. As such, they have been termed "privileged structures."<sup>74</sup> This generality hints at a common template inherent to all privileged structures. A common feature of this class, aside from the generality, is a C<sub>2</sub>-symmetric framework.

#### 1.4 – C<sub>2</sub>-Symmetric Ligands

C<sub>2</sub>-symmetry in catalysts was first developed by Kagan in the 70's with the introduction of the diop ligand (**5**).<sup>75</sup> These ligands contain an axis of symmetry, such that a 180° rotation will return the original molecule, i.e., it will be indistinguishable from the original upon a 180° rotation. Examples of this class are shown in Figure 17. Common transformations catalyzed by these ligands include the Diels-Alder reaction (**1**, **2**, **10**, **12**), the Mukaiyama aldol reaction (**1**, **2**, **11**), conjugate additions (**1**, **1a**, **2**), cyclopropanations and aziridinations (**1**, **1a**, **2**), and epoxidations (**2**), among others.<sup>36</sup>

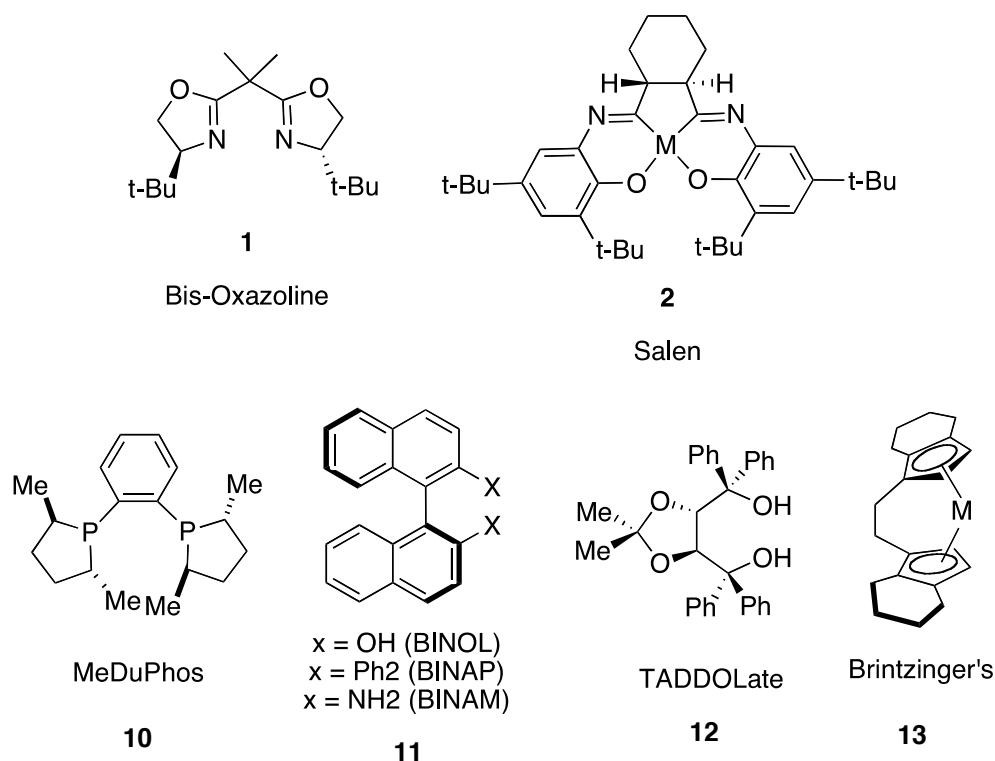


**Figure 17.** Examples  $C_2$ -Symmetric Ligands.

This generality is crucial since predicting the behavior/performance of a new catalyst based on mechanistic or electronic/steric nature is not always possible due to the potential complexities of the catalyst's mechanism (if known). A chemist may select one of these  $C_2$ -symmetric catalysts and, with a high degree of confidence, be assured a decent ee, regardless of functionalization or reaction/mechanism.

Inherent to all  $C_2$ -symmetric catalysts is a reduction in the number of competing transition states due to the intrinsic symmetry.<sup>76</sup> If one takes a generic  $C_2$ -symmetric ligand and divides it into four equal quadrants, it becomes clear: two quadrants are equal upon rotation. Figure 18 displays the equivalency of quadrants I and IV, and II and III. The framework provided by the symmetry provides a “fence” surrounding the

reaction site (metal center) and effectively blocks one side of the molecule for reaction.<sup>77</sup>

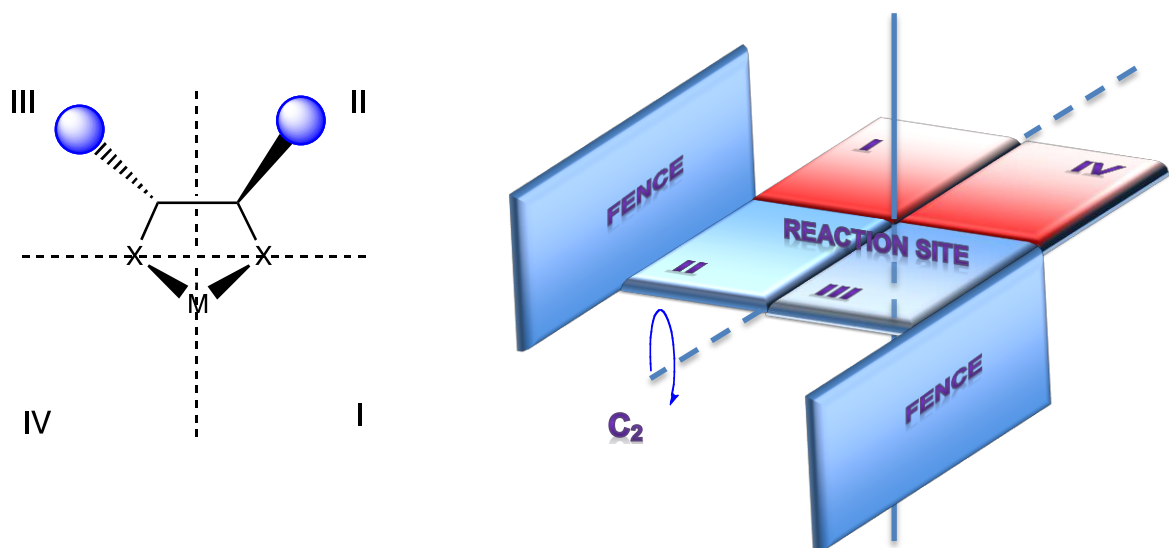


**Figure 18.** Left – Generic  $C_2$ -symmetric catalyst with quadrants. Right - Schematic of a  $C_2$ -symmetric quadrant and the chiral fence produced by the substituents. Modified from Nishiyama et al.<sup>77</sup>

#### 1.4.1 – Bis-Oxazolines (BOX)

The bis-oxazoline class of ligands has become popular due to their synthetic ease, being derived from the chiral pool (chiral amino alcohols), and excellent ee over a wide range of transformations. Figure 19 displays some of the transformations yielding over 50% ee, with copper proving to be the best metal.

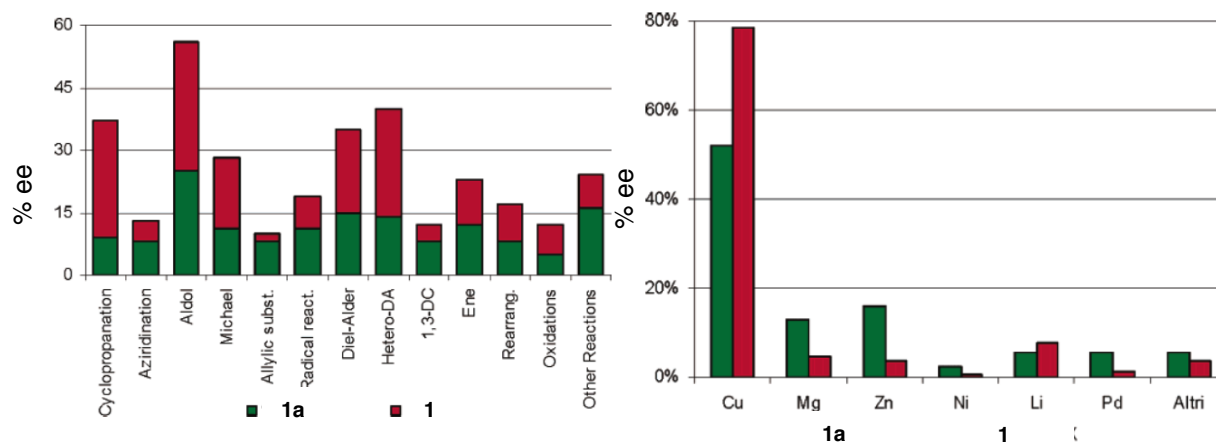
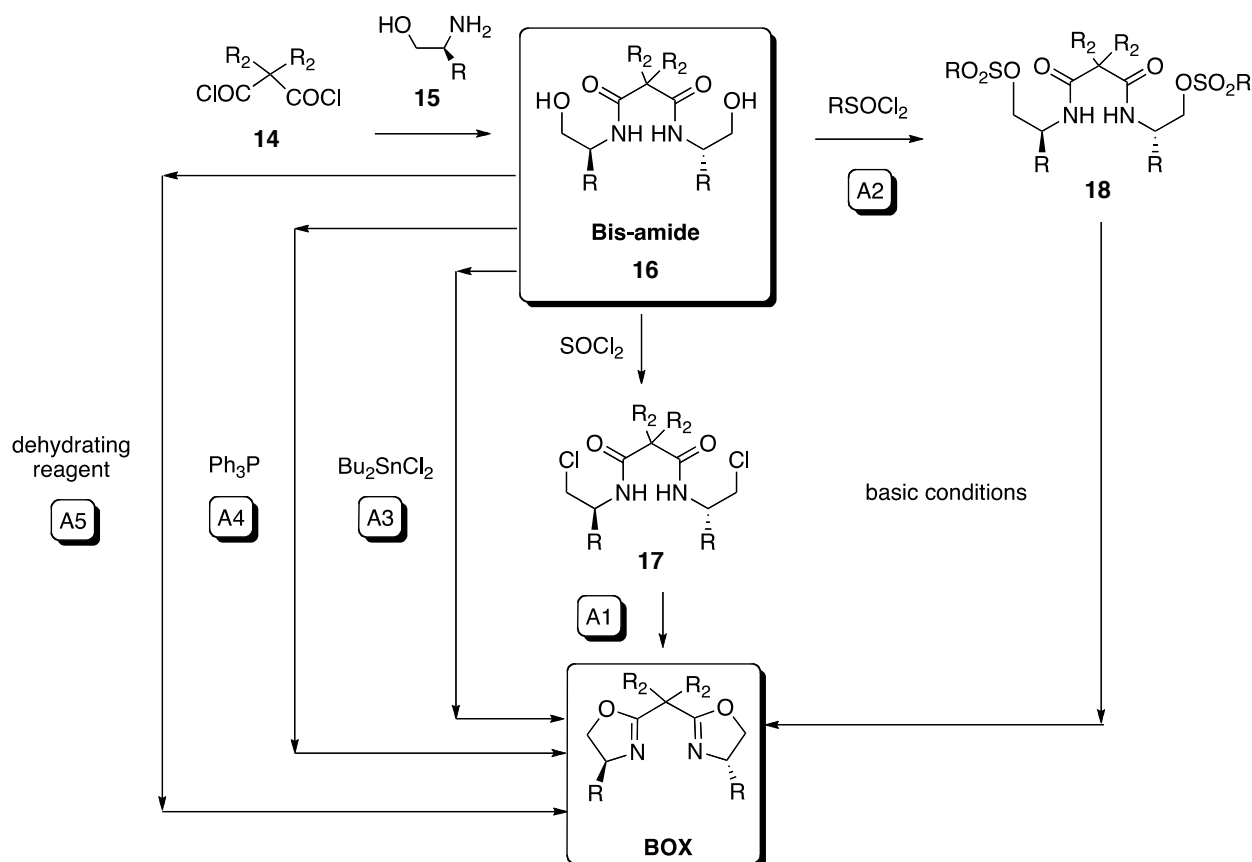


**Figure 19.** The range of enantioselective reactions catalyzed by 1 and 1a yielding at least 50% ee (left). Different metals used with 1 and 1a as a percentage of transformations with at least 50% ee (right).<sup>36</sup>

BOX ligands are derived from the chiral pool, retaining the natural chirality derived from nature. Scheme 13 displays the common routes to the synthesis of the

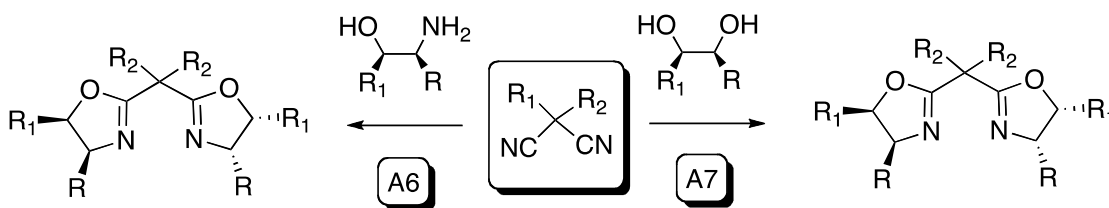


**Scheme 13.** Different synthetic routes to BOX ligands.<sup>36</sup>

BOX ligand. The bridge of the molecule is provided by a symmetrical di-substituted malonic acid derivative (**14**), while two equivalents a chiral  $\beta$ -amino alcohol (**16**) provides the asymmetric inducer. This  $\beta$ -amino alcohol is usually prepared as in Scheme 3, page 15, from a chiral amino acid, which is subsequently reduced to the alcohol. Coupling of the  $\beta$ -amino alcohol and malonic acid produces the bis-amide (**16**), with the final cyclization step a matter of converting the alcohol to a better leaving group.

Method A1 in Scheme 13, used by Corey et al.<sup>78</sup> converted the alcohol to an acid chloride via thionyl chloride, followed by basic conditions for cyclization. Conversion to a tosylate (or mesylate) followed by basic conditions was also utilized to produce BOX ligands (A2).<sup>79</sup> Less conventional methods have been used to cyclize bis-amides with  $\text{Bu}_2\text{SnCl}_2$  (A3),<sup>80</sup>  $\text{Ph}_3\text{P}$  (A4),<sup>81</sup> and with dehydrating conditions/reagents (A5).<sup>36</sup>

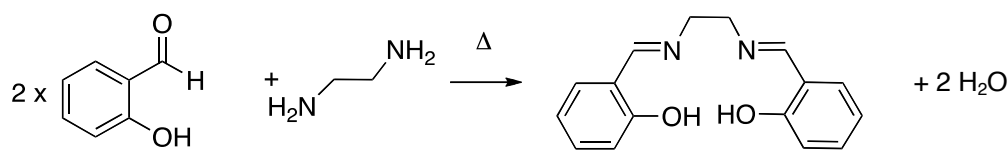
Alternatively, a di-substituted malononitrile may also be used to couple two equivalents of a  $\beta$ -amino alcohol (A6), or a 1,2-diol (A7). Other routes have been developed to synthesize more exotic BOX-like ligand. As of 2006 there were over 140 different BOX ligands synthesized.<sup>36</sup>



**Scheme 14.** Alternate synthesis of BOX ligand.

### 1.4.2 – C<sub>2</sub>-Symmetric Di-Imines

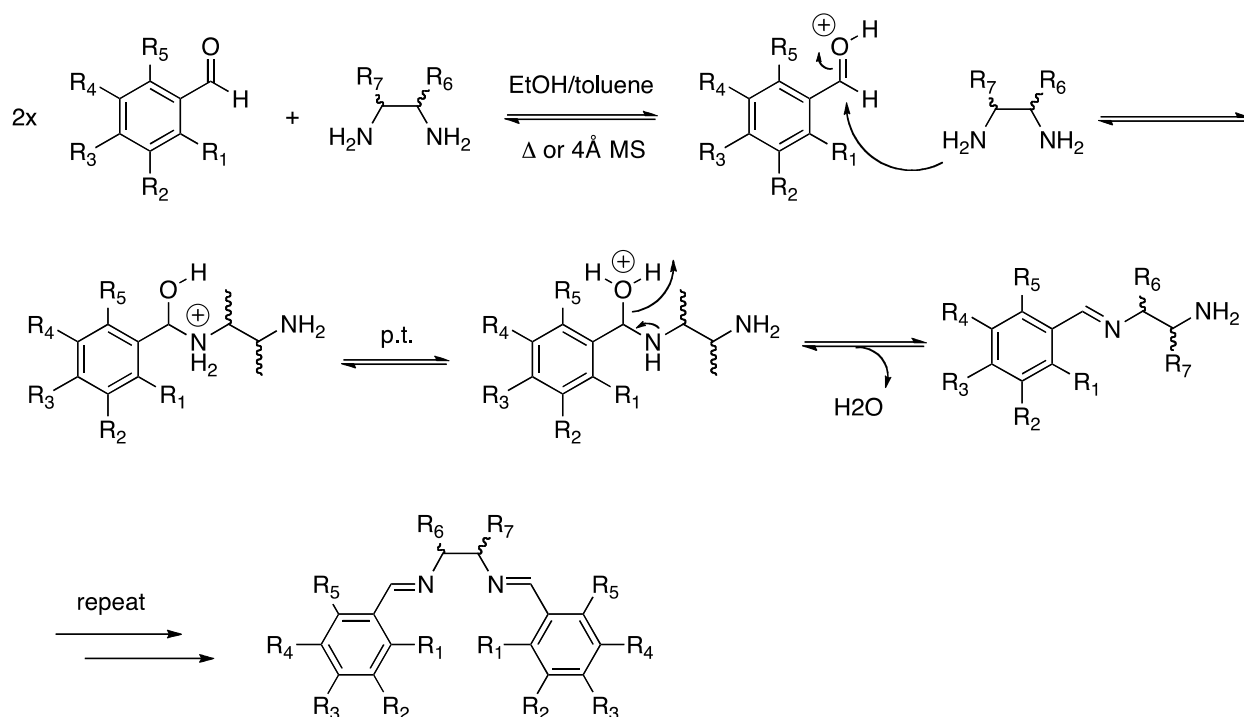
Di-imines, or Schiff bases,<sup>82</sup> are also excellent ligands for enantioselective transformations, such as epoxidations,<sup>83,84,85</sup> enantioselective epoxide ring openings,<sup>86,</sup><sup>87</sup> aziridinations,<sup>84</sup> cyclopropanations,<sup>88</sup> and Diels-Alder reactions.<sup>89,90,71</sup> Among di-imines, the salen ligand is frequently involved in the most popular and well-studied reactions. Salen's derive their name from the starting materials used in the synthesis, salicylaldehyde and ethylenediamine (Scheme 15).<sup>91</sup>



**Scheme 15.** Synthesis of a salen ligand.

The synthesis of di-imines is straightforward – a condensation between a chiral diamine and an aromatic aldehyde to produce the mono-imine and loss of water. The process is repeated for the second amine. As the reaction is in equilibrium, any method that removes the water will drive the reaction forward (Scheme 16). Heating to reflux or 4Å molecule sieves (sometimes with ZnCl<sub>2</sub>, or MgSO<sub>4</sub>)<sup>92</sup> are the two most popular additives for removing water; alternatively, a Dean-Stark apparatus may be used.<sup>93</sup> Reaction times vary greatly from hours to days, depending on the dehydrating method and temperature.<sup>94,95,96</sup>





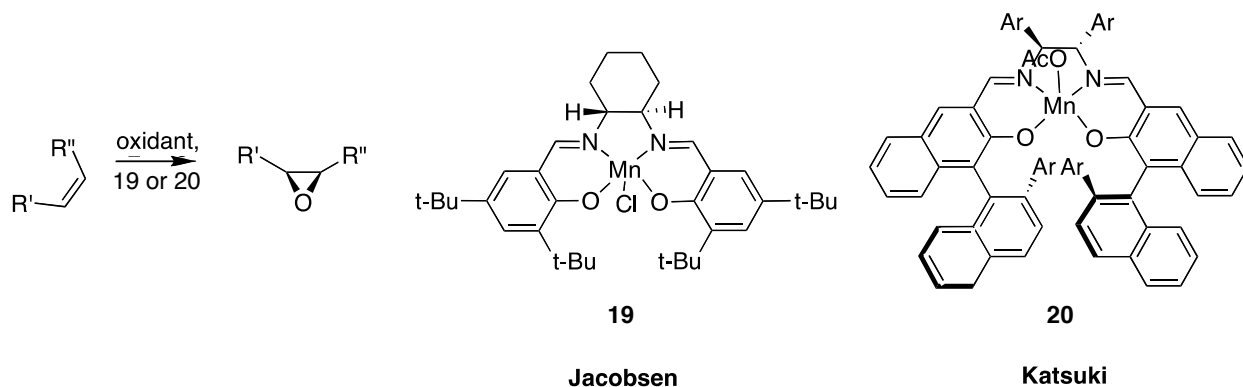
**Scheme 16.** Generic synthesis of di-imine ligands.

A variety of aromatic aldehydes are readily available from commercial sources. Chiral di-imines are less prevalent, with 1,2-cyclohexanediamine and 1,2-diphenylethylenediamine, used for the Jacobsen and Katsuki catalysts, commercially available. Di-imines may also be engineered to take advantage of the axial chirality that has proven successful with the BINAP catalysts, via BINAM (b) in Figure 1. The ease in which they are synthesized, and the breadth of commercially-available sources for the aromatic aldehyde, makes them an attractive target for combinatorial synthesis.<sup>97</sup>

Noyori utilized a salen ligand in the first enantioselective synthesis of a cyclopropane (Scheme 9, page 24). Salen ligands further gained popularity due to their use in enantioselective epoxidations with  $\text{Mn(III)}$  as described by Jacobsen et al, and

Katsuki et al in 1990, who modified the ligand to achieve high ee's in excess of 90%.<sup>98,99</sup>

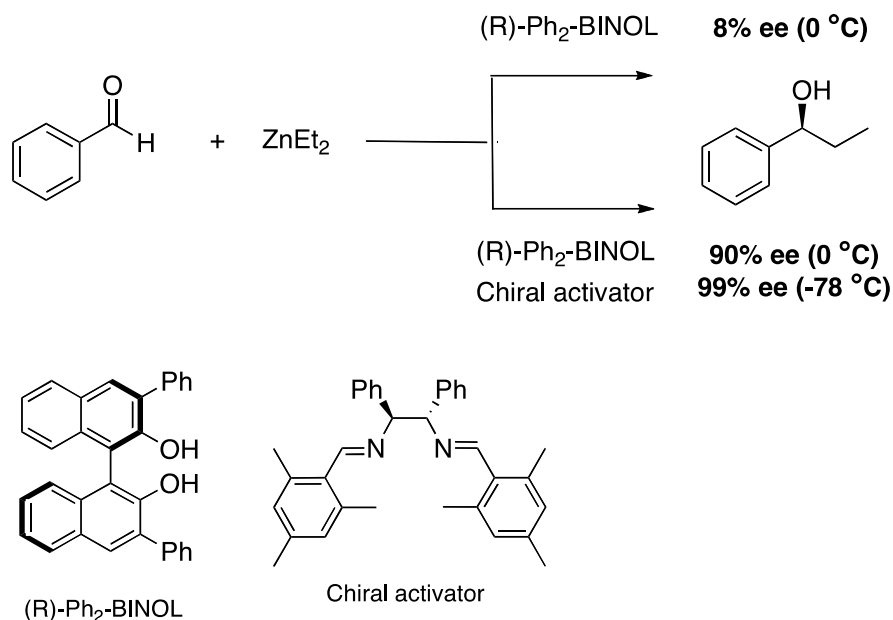
Scheme 17 displays the Jacobsen and Katsuki catalysts. Both ligands, as well as BINAM-based ligands have been used in cyclopropanations and aziridinations, utilizing



**Scheme 17.** Epoxidation using Jacobsen or Katsuki catalyst.

wide variety of metals, Cr, Mn, Ru, Co, and Cu, and generally gave ee lower than the bis-oxazolines.<sup>100</sup> Di-imine use with copper is predominately salen-based, as the oxygens provide a tetra-coordinate chelation sphere, favorable conditions for stabilizing the catalyst. Thus, 2,6 diCl substitution of the aryl ring is the next most popular di-imine. It was used with Cu(II) producing ee's >86% for asymmetric aldol reactions of pyruvate esters.<sup>101</sup>

A secondary use for these ligands is as chiral activators; ligands that are added to a catalyst to further enhance selectivity, particularly with diethyl zinc. For example, when (R)-Ph<sub>2</sub>-BINOL only was used in the production of (S)-phenyl-1-propanol from benzaldehyde and diethylzinc, the ee was only 8%; however, when a chiral activator was added, ee up to 99% were obtained (Scheme 18).<sup>102</sup>



**Scheme 18.** Di-imine used as a chiral activator in the synthesis of  $(S)$ -phenyl-1-propanol.

## 1.5 – Enantioselective Catalysis and the Transition State

In the simplest case, forming diastereomers, either real or transient, creates enantioselectivity. This creates small energy differences between the two transition states (TS). Understanding the TS is crucial for chiral catalysis: to quote Ian Williams, “catalysis is a transition-state molecular recognition event.”<sup>103</sup> The following sections will explore this quote in more detail.

### 1.5.1 – Gibbs Free Energy

In the absence of a chiral catalyst, a simple,  $\text{sp}^2$ -hybridized prochiral substrate will produce a racemic mix upon addition of a fourth group. If, however, a chiral catalyst is utilized, an excess of one enantiomer will be represented in the product mix (ideally).

This is represented in the illustration in Figure 20. At the top left (a), in the absence of a chiral catalyst, the incoming reactant may approach from either side. Alternatively, if a chiral catalyst is used (b), it blocks access to one side of the prochiral substrate, hence, preferentially forming one enantiomer.

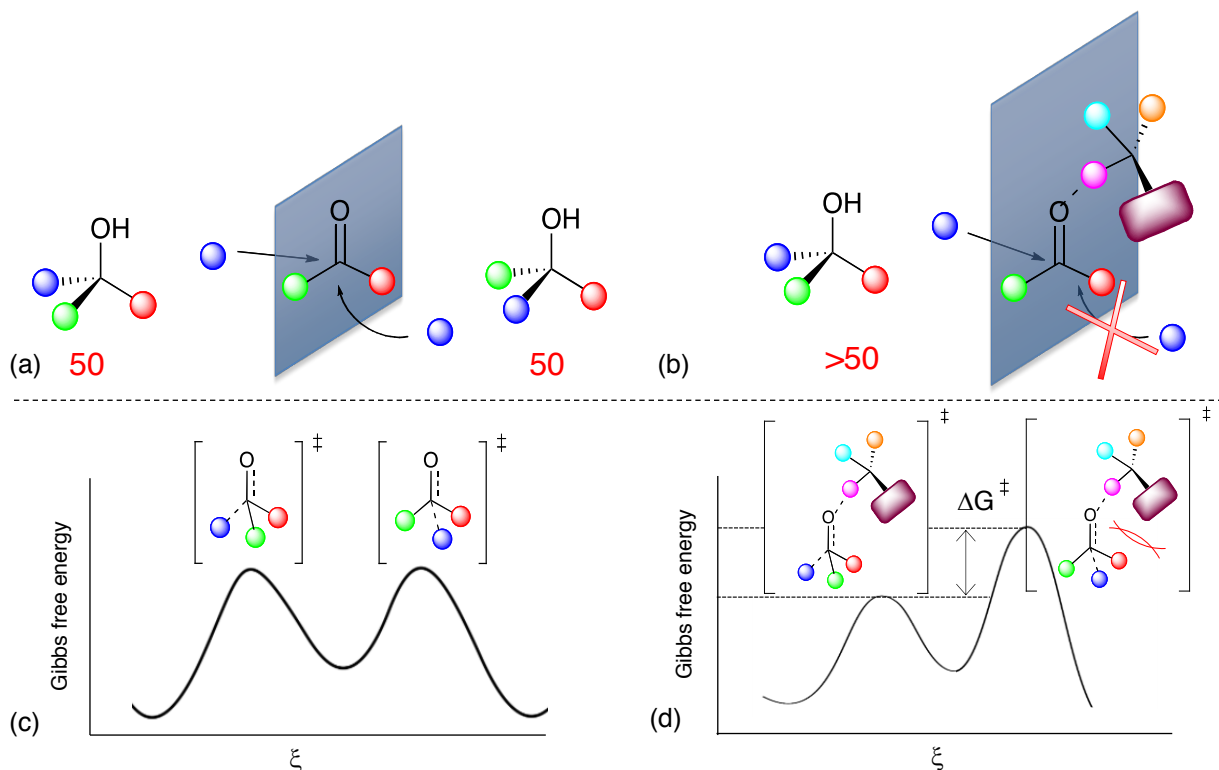


**Figure 20.** Top left (a) – generic reaction upon a prochiral substrate with out a chiral catalyst. Bottom left (c) – resultant Gibbs free energy diagram with equal transition states. Top right (b) – same reaction with a chiral catalyst. Bottom right (d) – resultant Gibbs free energy diagram with unequal transition states. The transition state with the lowest  $E_A$  (left) will be the dominant product.

The corresponding free energy diagrams for these cases are represented in (c) and (d). In the absence of a chiral influence, as in (c), there is no difference in TS energy between the enantiomers,  $\Delta G$  equals zero, and hence no difference in the enantiomer ratio. However, when a chiral catalyst is used, as in (d), the chiral catalyst increases the transition state energy for one of the enantiomers. This in turn favors

formation of the enantiomer with the lowest TS energy, and is manifested in the product distribution with an excess of one enantiomer.

An alternative synthesis to Scheme 18, developed by Noyori, et al.,<sup>104</sup> is given below (Figure 21) for the asymmetric alkylation of benzaldehyde, and serves as an excellent example of the TS energies driving selectivity, albeit greatly simplified. Benzaldehyde, when subjected to DAIB, (2*S*)-(-)-*exo*-(dimethylamino)isoborneol, and diethyl zinc, produces the (*S*) enantiomer in 98% ee. The (*S*) enantiomer is favored due to the lower energy of activation, i.e., the TS is stabilized by 2.7 kcal mol<sup>-1</sup> relative to the (*R*) enantiomer (Figure 19).

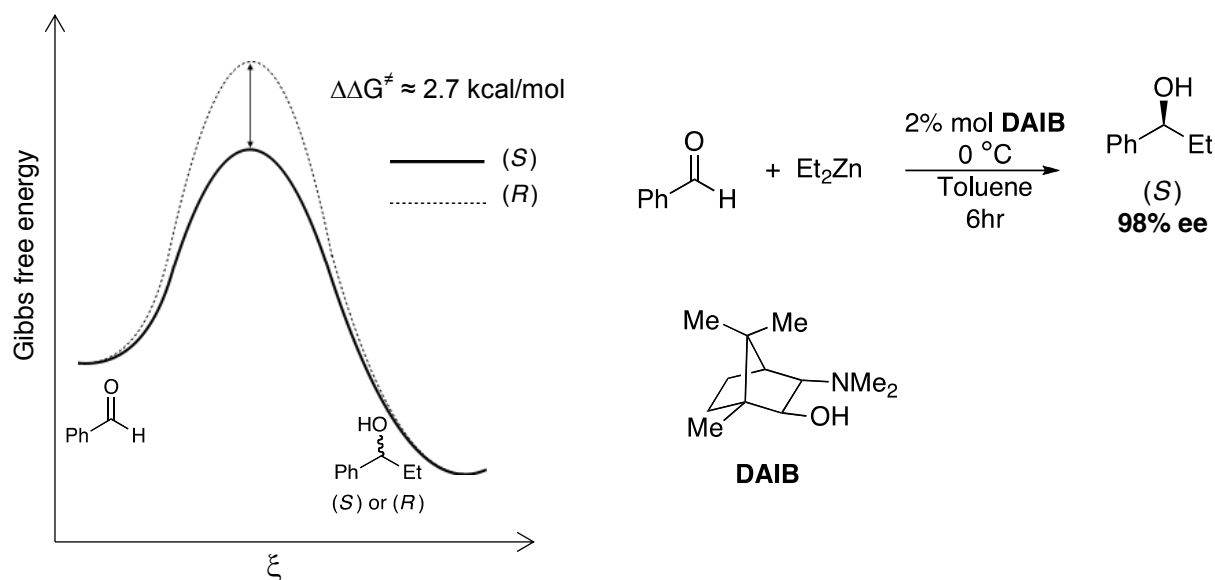


**Figure 21.** DAIB catalyzed alkylation of benzaldehyde producing (*S*)-phenyl-propanol in 98% ee. The  $\Delta\Delta G^\ddagger$  ( $\Delta G_{\text{TSR}} - \Delta G_{\text{TSS}}$ ) for the reaction only  $\sim 2.7 \text{ kcal mol}^{-1}$ .<sup>104</sup>

As a point of reference, the energy for a ring flip from equatorial to axial for methylcyclohexane is  $\sim 1.7 \text{ kcal mol}^{-1}$ , shown in Figure 22.<sup>105</sup> Therefore, small

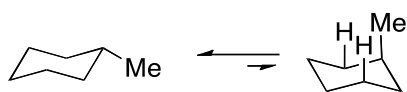


**Figure 22.** The A value for a methyl ring  $\sim 1.7 \text{ kcal mol}^{-1}$ .<sup>105</sup>

differences in energy are the crux of enantioselectivity – any interaction that stabilizes (or destabilizes) a transition state relative to the other, can result in large

differences in product distribution (ee). This relationship is shown in the graph in Figure 23. The Gibbs free energy was calculated from the following equation:

$$\Delta G^\ddagger = -RT \ln k_1/k_2 \quad (1)$$

when  $k_1/k_2$  is the ratio of rates of forming the enantiomeric products.

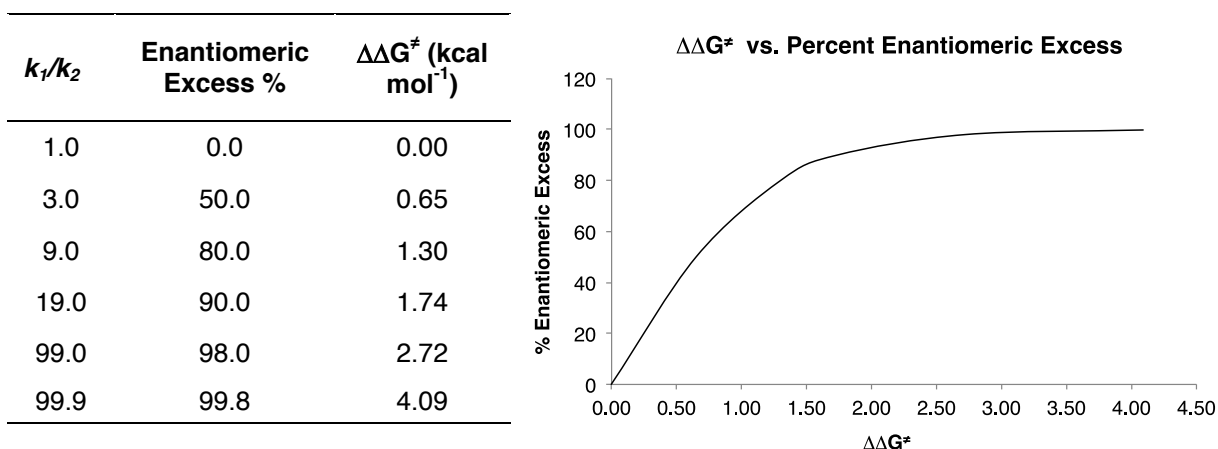


**Figure 23.** Differences in free energy of the TS and corresponding selectivities at 25 °C.

The preceding examples displayed reactions under kinetic control, the category in which the majority of all reactions fall.<sup>24</sup> The alternative is thermodynamic control, where the products are in equilibrium. Figure 24 displays free energy diagrams for reactions under kinetic and thermodynamic control. For a newly formed pair of enantiomers, the isoenergetic nature of the two excludes thermodynamic control, i.e.,

they occur under kinetic control only. New stereocenters around a diastereotopic face may occur by either thermodynamic or kinetic control.

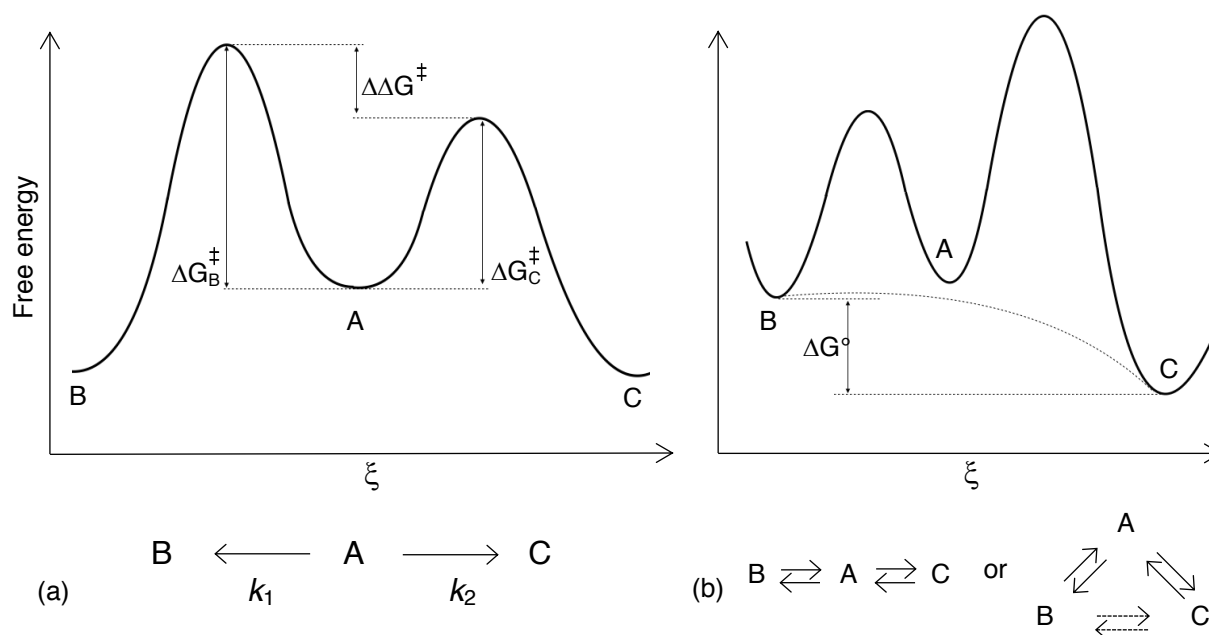


**Figure 24.** Reactions under kinetic control (a) and thermodynamic control (b).

### 1.5.2 – Temperature and Background Effects on Stereoselectivity

Explicit in the Gibbs free energy equation (1) is the dependence of selectivity upon temperature. Lower temperatures allow less energy for competing pathways; More importantly, the lower the energy, the less conformational freedom for a molecule in the TS and hence, a much more rigid TS – of paramount importance for enantioselectivity.<sup>71</sup> This relationship is illustrated below in tabular<sup>106</sup> and graphical form in Figure 25.

	$\Delta G$ in $\text{kJ mol}^{-1}$ .		Temperature ( $^{\circ}\text{C}$ )				
% ee	-100	-78	-40	-23	0	23	er
99.9	10.9	12.4	14.7	15.8	17.3	17.7	99.95:0.05
99.5	8.63	9.72	11.6	12.5	13.6	14.7	99.75:0.25
99	7.63	8.59	9.39	11.0	12.0	13.0	99.5:0.5
98	6.62	7.46	8.92	9.55	10.4	11.3	99:1
95	5.28	5.95	7.12	7.63	8.34	9.05	97.5:2.5
90	4.23	4.78	5.70	6.12	6.70	7.25	95:5
80	3.18	3.56	4.27	4.57	4.99	5.41	90:10
70	2.51	2.81	3.35	3.60	3.94	4.27	85:15
60	2.01	2.26	2.68	2.93	3.14	3.39	80:20
50	1.59	1.80	2.14	2.30	2.51	2.72	75:25
40	1.22	1.38	1.63	1.76	1.93	2.10	70:30
30	0.88	1.01	1.22	1.30	1.42	1.51	65:35
20	0.59	0.67	0.80	0.84	0.92	1.01	60:40
10	0.29	0.34	0.38	0.42	0.46	0.50	55:45

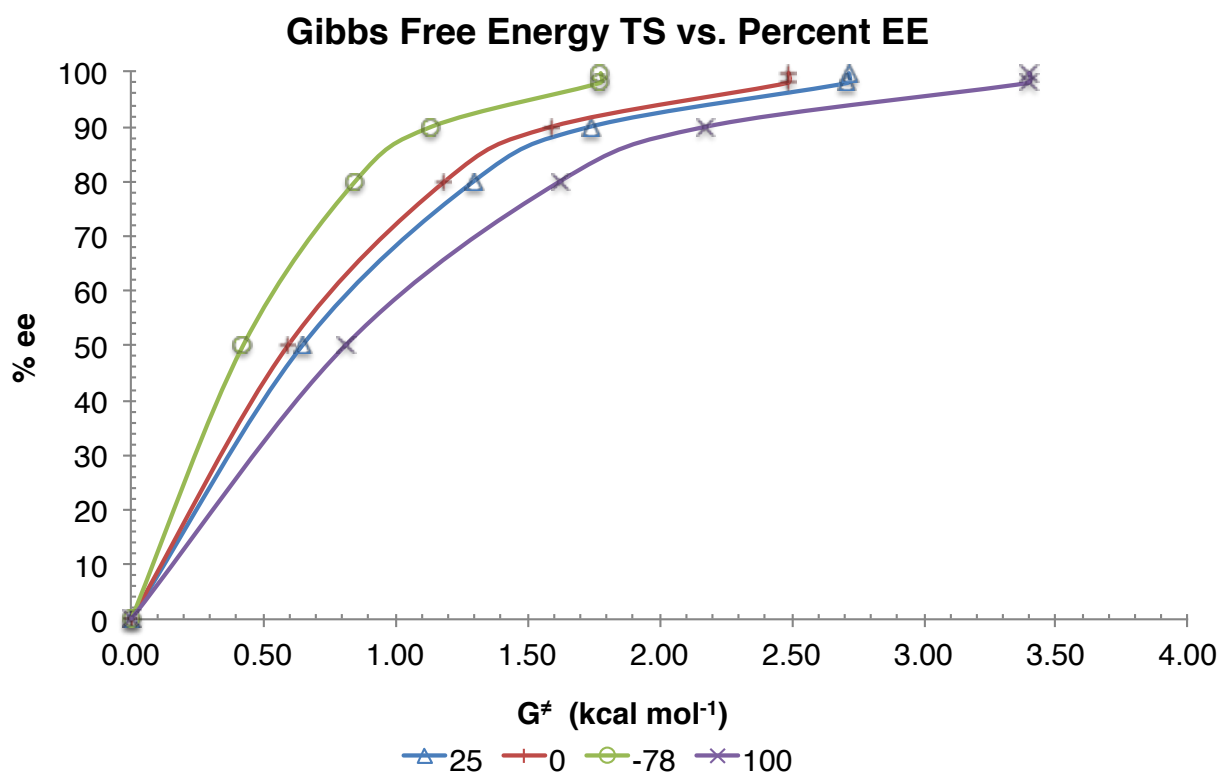


**Figure 25.** Top - Table of %ee (and er) at different temperatures. Taken from Koskinen.<sup>106</sup> Bottom – Temperature and effect on ee.

These data are a generalized/simplified application of equation (1) and assume only two diastereomeric pathways, and no shift in the rate-determining step or



mechanism.<sup>107</sup> An ideal example of ee and temperature dependence is illustrated in Figure 26 with a Mukaiyama aldol reaction catalyzed with BOX (1).<sup>101</sup> The slight deviation is thought to be a result of free CuOTf<sub>2</sub> acting as a Lewis acid.

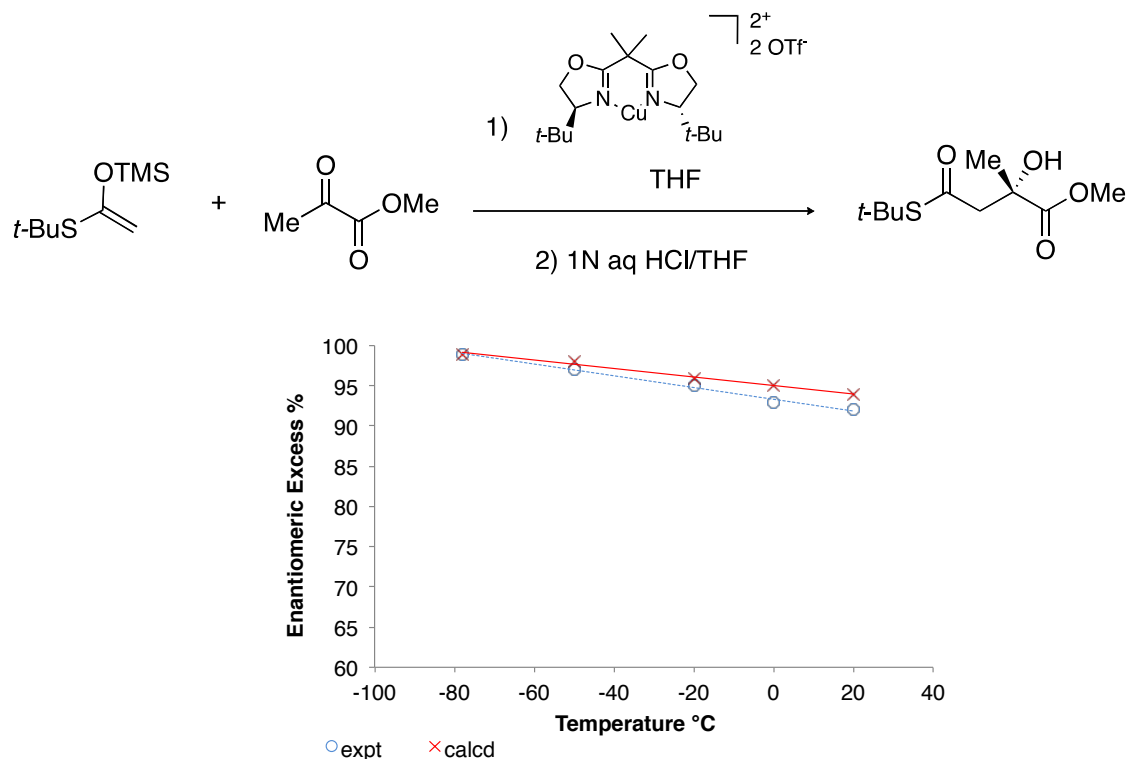


**Figure 26.** Box-catalyzed Mukaiyama aldol reaction displaying ideal temperature dependence.

In other cases, there may be multiple diastereomeric transition states. For example, in the DAIB catalyzed enantioselective alkylation of benzaldehyde in Figure 21, there are actually eight possible transition states shown in Figure 27. At higher temperatures, all are accessible and are represented in the product distribution by the relative Gibbs free energies of the transition state.

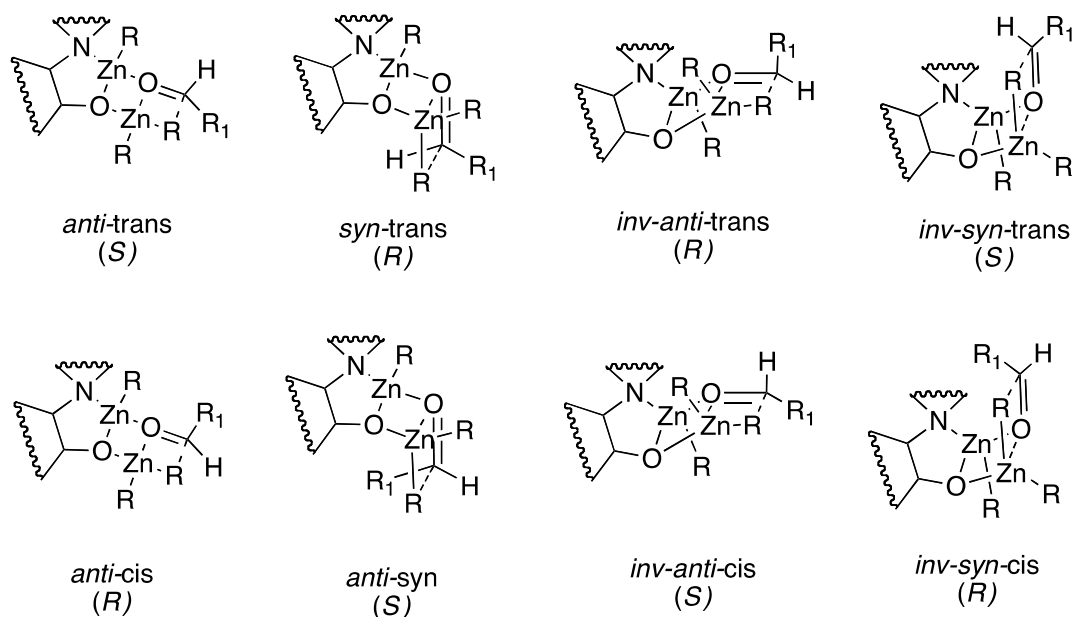


**Figure 27.** Multiple diastereomeric transition states, accessible at different temperatures.

An example of competing reactions accessible at higher temperatures is found in the asymmetric Michael addition of cyclohexenone and benzyl malonate, catalyzed by a BINOL-salen Ni catalyst (**21**) shown in Figure 28. The deviation from theoretical is due to the non-selective background reactions from  $\text{CsHCO}_3$  and  $\text{Cs}_2\text{CO}_3$ , accessible at

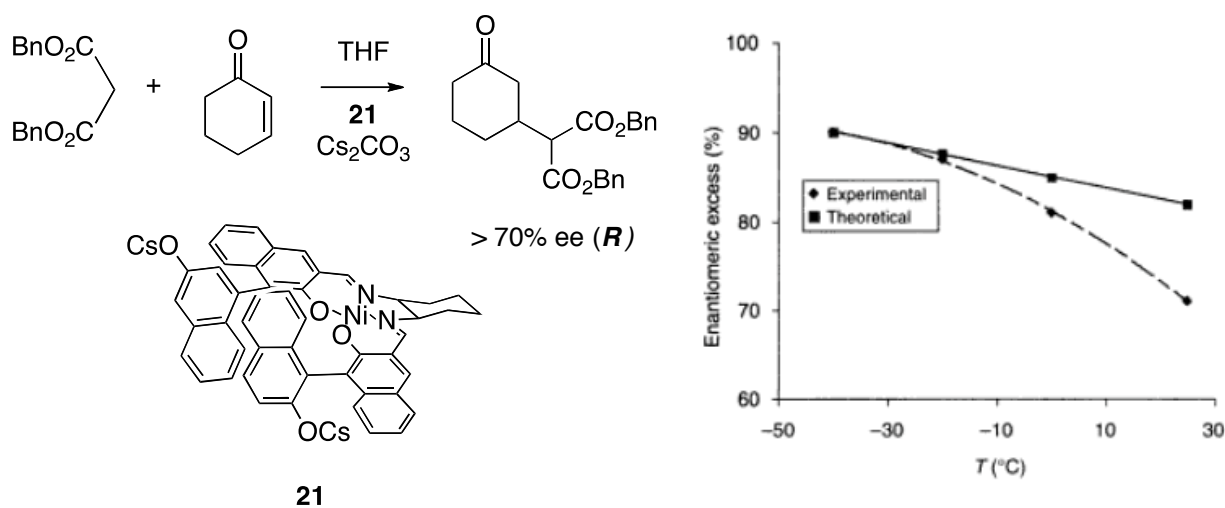


**Figure 28.** Asymmetric Michael addition with deviations from expected ee due to cesium carbonate and bicarbonate background reactions.

higher temperatures.<sup>108</sup> These background reactions can have a drastic effect on enantioselectivity. The metals themselves may act as Lewis acids (non-selectively), or may coordinate to solvent, product, or counter ions resulting in ligand decelerated catalysis.<sup>107</sup>

## 1.6 – Conclusions

Chirality is ubiquitous in nature and affects our everyday lives in various and subtle ways, for example smell and taste. The inherent chirality in living systems imparts important consequences if it is not taken into consideration, as the thalidomide case demonstrated. It has brought about significant changes to industries, mainly in the pharmaceutical arena, with the need to recognize and control chirality. The result is a shift towards producing and marketing single enantiomer drugs, and in the process, creating of a market worth billions of dollars annually.

This in turn has catalyzed a movement to improve methodologies for transferring the native chirality found in nature to synthetically made molecules. While many methods exist, asymmetric synthesis via chiral catalyst is an attractive option due to the small amount of expensive chiral material needed to produce achiral products. The ideal chiral catalyst is extremely sensitive to small energy differences in the TS of the diastereomeric complexes. The exploitation of these differences results in ee's of 90% with differences in the transition state energies as low  $1.7 \text{ kcal mol}^{-1}$ , the same amount of energy required for a ring flip in methylcyclohexane. Lowering of the reaction

temperature may also further increase selectivity; however, solvent, counter-ions, and multiple diastereomeric TS can complicate extrapolation of the results.

Among chiral catalysts, the “privileged ligand” class, comprising many  $C_2$ -symmetric ligands, offers excellent enantioselectivity over a wide range of transformations and substrates. This suggests a common template inherent within the class. Unfortunately, current methodologies for evaluating this template are done in the condensed phase, measuring ee's from isolated reaction products where various substrates and catalyst were varied. This is a time-consuming and inefficient process for accessing a catalyst's performance. *It would be highly advantageous to develop a method that could rapidly determine the chiral environment induced by a metal and ligand, explicitly measuring the catalyst's intrinsic discriminatory potential, unencumbered by solvent and counter-ion/aggregate phenomena.* The next chapter will present a brief survey of current methods for evaluating chiral catalysis performance.

## Chapter 2 – Mass Spectrometry

### 2.1 – Mass Spectrometers

Mass spectrometry is an analytical technique that determines a gas-phase ion's mass-to-charge ratio ( $m/z$ ) via a mass spectrometer (MS) instrument. In 1913, J.J. Thompson separated the isotopes  $^{20}\text{Ne}$  and  $^{22}\text{Ne}$  of neon, and is considered the inventor of the technique.<sup>109</sup> The historical impact of MS cannot be over-stated; its underlying principles played a crucial role in World War II and the invention of the atomic bomb, as it was used to separate the isotopes  $^{235}\text{U}$  and  $^{238}\text{U}$  of uranium.<sup>110</sup> It has recently crept into popular culture via popular television shows such as CSI and the Big Bang Theory. Its utility is recognized from the fact that it is in use today on the MARS Curiosity rover for analyzing gas and solid samples for evidence of life.<sup>111</sup>

### 2.2 – Ion Sources

Since the MS measures a mass per charge ratio, the molecule must be ionized in order to be detected. Therefore, ion sources are *sine qua non* to mass spectrometry. Electron impact or ionization (EI), invented by Dempster in 1918, is the oldest method still in use today, most often coupled to a GC.<sup>112</sup> The 70eV electron energy used in EI produces a de Broglie wavelength close to that of an organic bond (0.14nm). This

causes many fragmentations and is thus referred to as a “hard” ionization technique. Alternatively, chemical ionization is a soft ionization technique and was created in 1966 by Munson and Field as an alternative to EI.<sup>113</sup> It is an ion molecule reaction, a result of high impact electrons ionizing a reagent gas, typically methane, ammonia, or isobutene, ultimately forming a plasma medium conducive for proton transfer to the neutral molecule. As a soft ionization technique, the parent ion peaks are usually visible.

## **2.3 – Electrospray Ionization (ESI)**

The technique, electrospray ionization (ESI), was invented by Fenn in 1984 and subsequently won him the Nobel Prize in Chemistry in 2002.<sup>114,115</sup> It is the most common and popular ionization technique due its ease of coupling with other techniques (such as LC-MS), its “soft” ionization nature, high sensitivity, and access to multiple charge states, effectively extending the mass range of the instrument.<sup>116,117,118</sup>

### **2.3.1 – Charged Droplet Formation**

In essence, ESI transfers ions formed in solution to the gas-phase, intact. The exact mechanism of how it achieves this remains controversial.<sup>117</sup> The first step is production of charged droplets (with the use of nitrogen to aid in the nebulization) by applying a potential difference of 2-6 kV between the capillary and a counter electrode to produce an electric field. The field, when in positive mode, induces the positive charges to migrate towards the tip of the needle and meniscus of the droplet, while the

negative charges drift away from the surface. The Coulombic repulsion eventually overcomes the surface tension of the liquid, forming the Taylor cone and a fine mist of small, charged droplets.<sup>114</sup> The droplet continues evaporation via the sheath gas (nitrogen) and a heated capillary, shown in Figure 29, until the gas-phase ion exists.

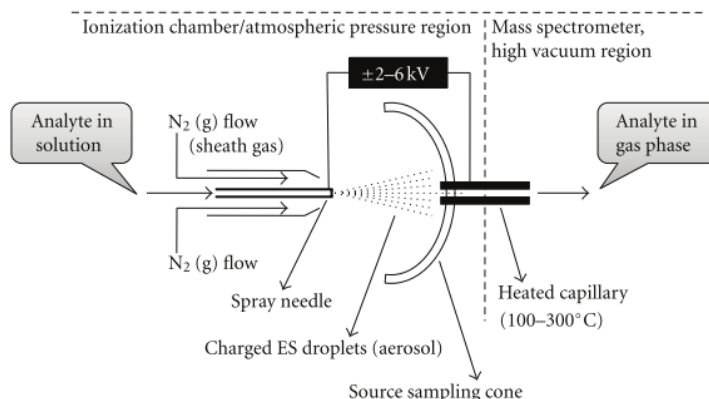
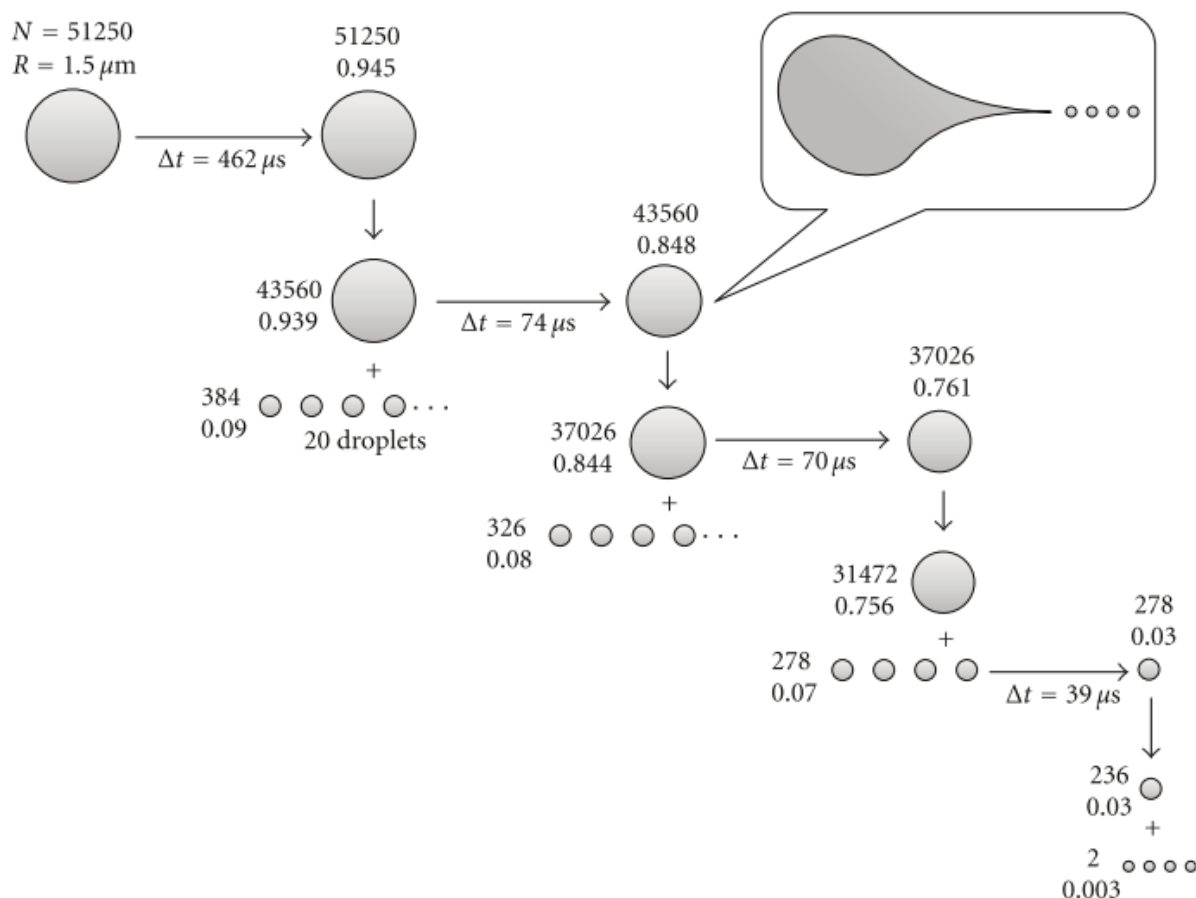


FIGURE 3: A schematic representation of the ESI-ion source.

**Figure 29.** Schematic of the ESI source.<sup>119</sup>

The process from parent droplet produced from the Taylor cone to the precursor of the gas-phase ion including the time between fissions, droplet size, and number of charges is shown in Figure 30. The parent droplets, when produced at low flow rates ( $<5\mu\text{L}/\text{min}$ ), yield an average droplet size of  $1.5\text{ }\mu\text{m}$ , with approximately 60,000 singly charged ions.<sup>119</sup> The Coulombic repulsion of the charged particles, trying to maximize the distance between charges, is countered by the attractive force of the solvent surface tension. As evaporation continues, the charge density becomes greater, until a Coulombic explosion/fission occurs, producing smaller droplets. These daughter droplets contain 2% of the mass and 15% of the charge of the original parent droplet, hence they have much more charge density than before fission.<sup>120</sup> This process is

repeated until a small charged droplet is left, i.e., the precursor of the gas-phase ion (Figure 30).<sup>119</sup>



**Figure 30.** The process from large, parent ion, to the smaller charged droplets, which are precursors to the gas-phase ions. Only the first three fissions are shown. The time between fissions, droplet radii, and the number of estimated charge ions are given. The onset displays the shape of the droplet as fission occurs.<sup>119</sup>

### 2.3.2 – Charged Residue Model

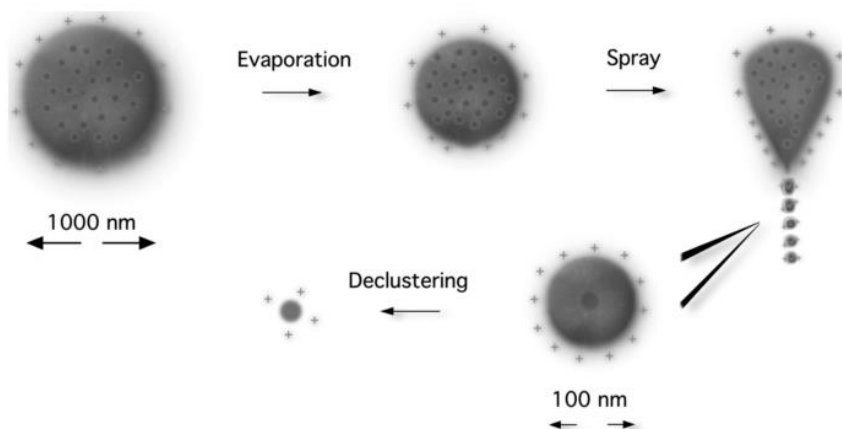
The exact mechanism of how the charged droplets ultimately become gas-phase molecules is a matter of controversy.<sup>121</sup> Dole proposed the charged residue model



(CRM) where Coulombic repulsions and Rayleigh instabilities are the dominating force producing gas-phase ions.<sup>122</sup> As the parent droplet forms and is released from the Taylor cone, solvent evaporation, continues, decreasing the radius of the droplet in the process. At some radius, the Coulombic repulsions of the surface charges will equal the force from the surface tension of the liquid. This is termed the Rayleigh limit and may be calculated from equation (2).

$$q = 8\pi(\epsilon_0\gamma R^3)^{1/2} \quad (1)$$

where  $\epsilon_0$  is the permittivity of vacuum, R is the radius of the droplet, and  $\gamma$  is the surface tension of the liquid.<sup>123</sup> These daughter droplets then repeat the process and decluster



until a charged droplet with a single analyte is left. Final desolvation transfers the charge to the analyte.<sup>124</sup> Figure 31 illustrates the CRM schematically.<sup>125</sup>

**Figure 31.** Schematic of the Charged Residue Model.<sup>125</sup>

CRM dominates with larger molecules.<sup>126,124</sup>

Evidence suggests the

### 2.3.3 – Ion Evaporation Model

The second theory was developed by Iribarne and Thompson and is called the ion evaporation method (IEM).<sup>127,128</sup> The authors theorize after a number of Coulombic fissions, droplets of the correct radii (10-20 nm) possess enough energy to overcome the surface tension and are ejected from the droplet. Thus, unlike the CRM, the droplets do not reach a point where containment of a single ion is necessary. The authors suggest a rate constant for ion emission may be calculated from the following formula:

$$k_1 = \frac{k_b T}{h} e \left( -\frac{\Delta G^\ddagger}{RT} \right) \quad (2)$$

where  $k_b$  is the Boltzmann constant,  $T$  is the temperature of the droplet,  $h$  is Planck's constant, and  $\Delta G^\ddagger$  is free energy of activation. Figure 32 displays the IEM schematically.<sup>125</sup> Evidence suggests that the ionization of small molecules are dominated by the IEM process.<sup>129,130</sup>

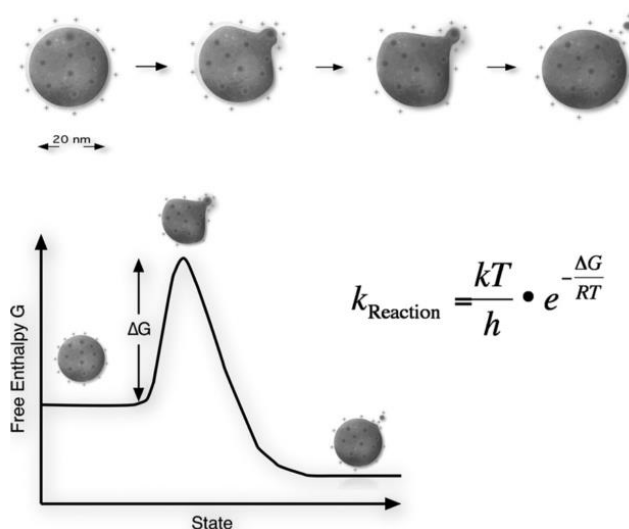


**Figure 32.** Ion Evaporation Model.<sup>125</sup>

## 2.4 – Mass Analyzers

The mass analyzer is the heart of the MS, as it separates the ions based on the  $m/z$ . There are a number of methods to separate the ions and various instruments have been built to do so, each with its advantages and disadvantages, as shown in Table 2.<sup>131,132</sup>

**Table 2.** Mass spectrometer types.<sup>131, 132</sup>

Method	Quantity Measured	Mass/charge ( $m/z$ ) range	Resolution at $m/z = 1,000$	Dynamic Range
Sector Magnet	momentum/charge	$10^4$	$10^5$	$10^7$
Time of Flight	flight time	$10^6$	$10^3 - 10^4$	$10^4$
Ion Cyclotron Resonance	cyclotron frequency	$10^5$	$10^6$	$10^4$
Ion Trap	frequency	$10^4$	$10^4$	$10^4$
Quadrupole mass filter	filters for $m/z$	$10^3 - 10^4$	$10^3 - 10^4$	$10^5$

Of all the analyzers, the quadrupole MS is the most popular due to the small footprint, low maintenance, general robustness, and low cost.<sup>133</sup> Many of the analyzers are combined for enhanced functionality. For example, coupling of two quadrupoles and an RF quadrupole only forms a triple quad (TQ), and allows for MS/MS and specialized experiments, such as neutral ion loss, and product and precursor ion scan, as well as increased sensitivity with selected (single) ion monitoring.<sup>134,133</sup> More recently, the TQ has in turn been coupled to a 2D linear ion trap, which itself has been coupled to time-of-flight (TOF), and an Fourier transform ion cyclotron resonance (FT-ICR),<sup>135</sup> each of which can access different features of the technique. For gas-phase ion-molecule

reactions, however, ion-trap MS analyzers is the instrument of choice since they can trap an ion for enough time to allow reactions to occur.

#### **2.4.1 – Quadrupole Ion Trap (QIT) Mass Analyzers**

The quadrupole ion trap (QIT), also known as a 3D ion trap, was first conceived by Wolfgang Paul and H. Steinwedel in the 1950s,<sup>136,137</sup> a conception that won Paul the Nobel Prize for Physics in 1989, along with Hans Dehmelt.<sup>138</sup> Its advantages, aside from the ability to monitor ion-molecule reactions, include a small footprint, high sensitivity, high resolution (at slow scan speeds), and perhaps most popular, the ability to perform multiple stages of MS ( $MS^n$ ).<sup>132</sup>

##### **2.4.1.1 – Mass Selection Detection and Storage**

The initial use of the trap was rather limited, mainly as an ion storage device, using the mass-selective mode of detection, where the ions of stable trajectory increase the inductive load of the system. The ions may then be detected by monitoring the power requirements. Fischer used the instrument as a mass spectrometer to obtain a crude mass spectra of krypton,<sup>139</sup> while Dehmelt and Major used the instrument as an ion storage device for spectroscopy.<sup>140</sup>

In the late 1960s, the mass-selective storage mode was invented by Dawson and Whetten.<sup>141</sup> This mode operates similar to a quadrupole MS, operating in a stability region where single ions only are stable, with all other falling into the sides of the ion trap. The ion may be ejected and detected by an external detector, greatly enhancing the performance of the instrument.

#### 2.4.1.2 – Mass Selective Ejection

In the early 1980s, two watershed moments in the history of ion traps occurred that brought them out of the niche market of academia and into the mainstream. The first was invention of the mass-selective ejection mode by Stafford and others at Finnigan.<sup>142</sup> This allowed the instrument to act as an ion trap and trap a large range of ions then sequentially eject them out of the trap to an external detector. The second was the serendipitous discovery that He gas at approximately 1 mtorr increases instrument performance (resolution and sensitivity).<sup>143</sup> This was discovered when trying to interface an ion trap to a GC. Figure 33 displays the effect of helium on the resolution

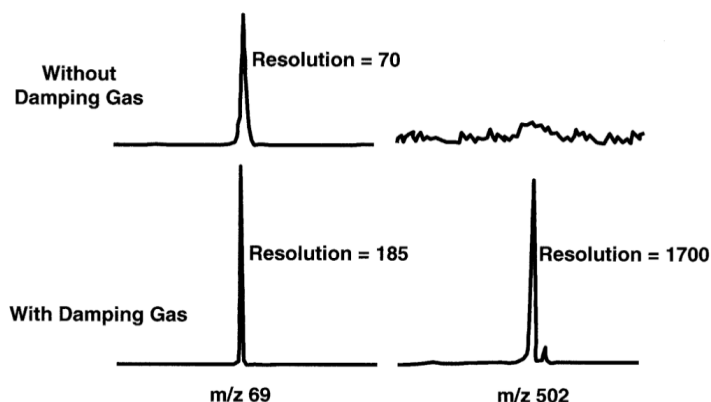


**Figure 33.** Effect of He on resolution and sensitivity.<sup>143</sup>

and sensitivity. Since then, many advances have been made in the field, including extension of the mass range via axial modulation,<sup>144</sup> high resolution (30,000 FWHM) by decreasing the scan speed,<sup>145</sup> and multi-

stage MS<sup>n</sup>.<sup>146</sup> A new linear ion-trap has also recently been developed that increases the ion capacity and trapping efficiency relative to the 3D ion trap.<sup>147</sup>

## 2.5 – Ion Trap Theory

QIT are dynamic mass analyzers as opposed to static analyzers such as the sectors. QITs use dynamic fields via radio frequency (RF) and direct current (DC) potentials to create a quadrupole field and a potential well to trap ions. The following sections briefly describe the theory of operation.

### 2.5.1 – Ion Trap Construction

An ion trap mass analyzer consists of a hyperboloidal ring electrode surrounded by two hyperboloidal-shaped end caps (Figure 34), and is roughly the size of a tennis ball.<sup>148,149</sup> One of the end caps contains a hole that allows ions to pass through, while the other end cap contains multiple holes forming a circle to allow the ions to pass out of the trap and to the detector. This axis is defined as z-axis. Application of an rf voltage to the ring electrode, called the fundamental rf, usually in the MHz range, produces a quadrupole field, which confines the ions inside the

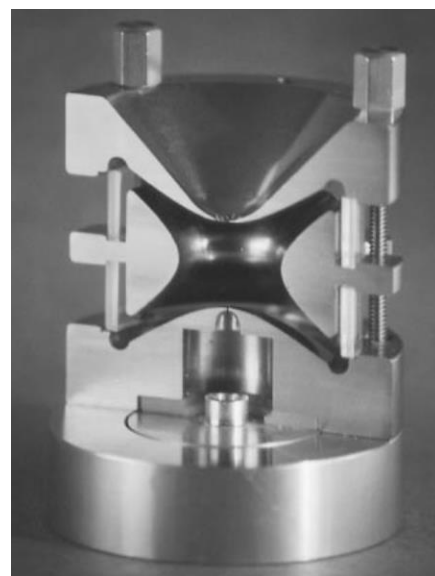


**Figure 34.** Ion trap with ring and end cap electrodes<sup>148</sup>

trap.

## 2.5.2 – Motion of Ions in a Quadrupole Field

The quadrupole field is defined by the geometry of the trap, specifically the ratio of  $r_0$  to  $z_0$  as shown in Figure 35. The ideal ratio is given by the following formula:

$$r_0^2 = 2z_0^2 \quad (4)$$

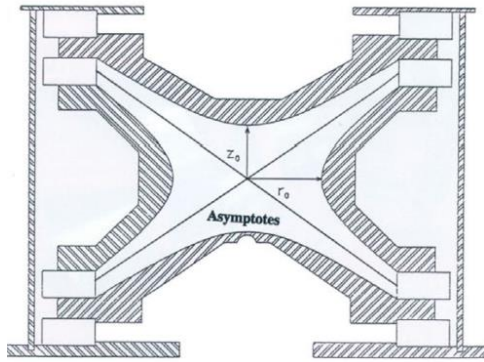


**Figure 35.** Cross section ideal trap<sup>150</sup>

where  $r_0$  to  $z_0$  are defined in Figure 35. The majority of ion traps on the market employ a  $r_0$  of 1.00 or 0.707 cm.<sup>150</sup> Knight suggested that the ideal ratio did not have to be 2,<sup>151</sup> and in fact, manufacturers have been utilizing a “stretch” design. The Thermo LCQ used in this work is built with  $r_0 = 0.707$  cm and  $z_0 = 0.785$  cm, a 57% increase.<sup>150</sup>

Ions in a quadrupole field are guided to the center of the trap due to a strong,

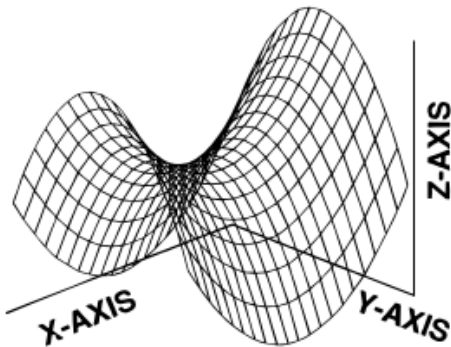


**Figure 36.** Example of a pure quadrupole field.<sup>150</sup>

linear restoring force as the ions deviate from the center. Application of an rf potential to the ring electrode and a dc potential applied to the endcaps produces the quadrupole field, shown in Figure 36. An ion will be focused to the center of

the trap where it will fall towards the y-axis. Rotation of the field about the z-axis at the correct frequency will refocus the ion to the center. Helium gas acts as a buffer gas to focus the ions towards the center of the trap and helps to thermalize the ions. The equation for the strength of the field is given by the following formula:

$$\Phi(r, z) = \frac{U - V \cos \omega t}{2} \left( \frac{r^2 - 2z^2}{r_0^2} \right) + \frac{U - V \cos \omega t}{2} \quad (5)$$

where  $U$  is the amplitude of the dc potential,  $V$  is the amplitude of the rf,  $\omega$  is the angular frequency of the rf potential, and  $r_0$  is the radius of the ring electrode.<sup>149</sup> The quadrupole field creates a pseudo-potential well in which the ions are trapped. The deeper the depth of the well, the more efficient the trapping and the more kinetic energy required to force an ion out of the well. Ions with the lowest  $m/z$  are trapped deeper in the well.

Accounting for the stretched geometry, the motion of the ions in a quadrupole field are governed by solutions to the Mathieu equations:

$$a_z = \frac{-16eU}{m(r_0^2 + 2z_0^2)\Omega^2}; \quad q_z = \frac{8eV}{m(r_0^2 + 2z_0^2)\Omega^2} \quad (6)$$

where  $a_z$  and  $q_z$  are stability parameters,  $\Omega$  is the angular frequency in  $\text{rad s}^{-1}$ ,  $e$  is the electric charge, and  $m$  is the mass of the ion.<sup>150</sup> Plotting solutions to the Mathieu equations, one obtains a stability diagram shown in Figure 37.



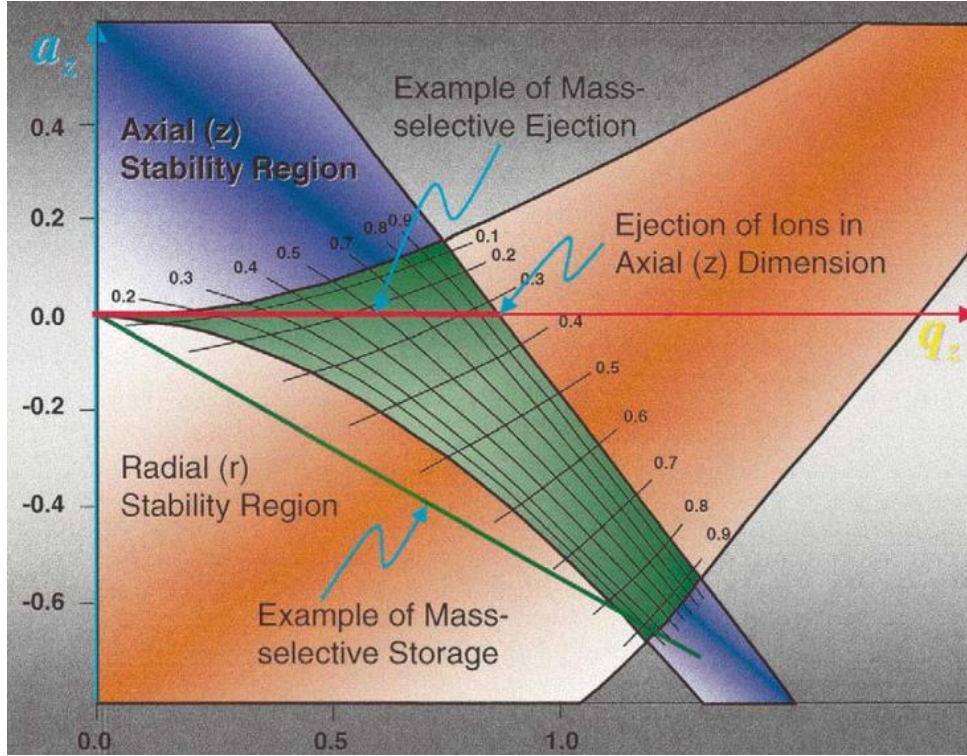


**Figure 37.** Stability diagram with  $a_z$  as the y-axis and  $q_z$  as the x-axis.<sup>143</sup>

The portion in blue represents the region where the ions are stable in the axial (z) direction (the axis in which the ions are injected and ejected). The portion in orange represents the stable region in the radial (r) direction. Where the regions overlap, the portion in green, is where ions are stable in the trap. There are other stability regions not displayed in Figure 37, which is an area of on-going research.<sup>152</sup>

The trapped ions oscillate at a characteristic frequency for each ion of a given  $m/z$ , known as the secular frequency, in both the axial and radial direction. The frequencies are given by<sup>140</sup>

$$\omega_r = \beta_r \Omega / 2 \quad \omega_z = \beta_z \Omega / 2 \quad (7)$$

where  $\beta$  is:

$$\beta \approx \sqrt{a_z + \frac{q_z^2}{2}} \quad (8)$$

Simulations were run on ion trajectories and graphed with the results shown in Figure 38, along with a photomicrograph of an aluminum ion in orbit of an ion trap. The ion

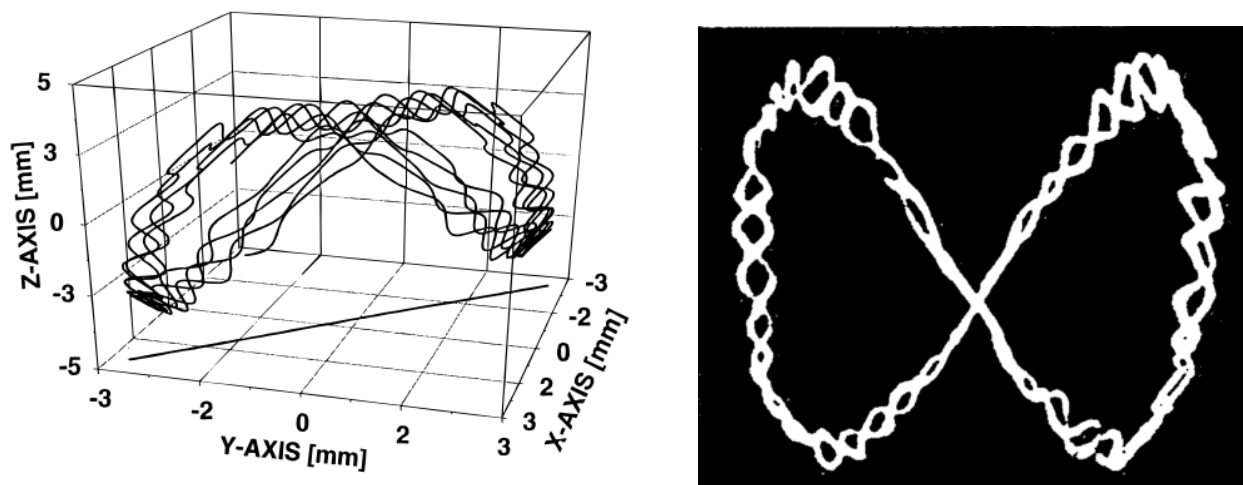


**Figure 38.** Simulated ion motion in an ion trap (left), <sup>140</sup> photomicrograph of single charged ion of Al. <sup>140</sup>

motion is typically described as/by a Lissajous curve. It has similar topology to the quadrupole field. Ions with a smaller m/z are more focused towards the center of the trap, followed by successively larger ions of m/z, much like a layer of onions.

## 2.6 – Ion Ejection

The mass-selection ejection mode was an important discovery in the history of the ion trap, second only to its discovery. It allowed a wide range of ions to be trapped, then ejected sequentially and detected. In essence, it allowed an ion trap to function as its namesake.

### 2.6.1 – Mass-Selective Instability

Most modern spectrometers operate with an rf potential applied to the ring electrode only and no dc potential applied to the electrodes, which reduces the  $a_z$  term to 0. From Figure 37 it can be seen that stability in the axial direction is obtained only to where  $q_z$  equals 0.908. After this value, ions are not stable along the z-axis and are thus ejected from the trap through the holes in the endcap. This value is known as  $q_{\text{eject}}$ .

To obtain a mass spectrum of a range of ions, the amplitude of the rf potential is increased, which in turn, increases each ion's  $q_z$  value until it reaches 0.908, at which point the ion is ejected from the trap, with ions of smaller  $m/z$  ejected first, followed by the larger  $m/z$  ions. This technique is often referred to as the mass-selective instability mode (or scan). Figure 39 displays an example of three ions of different  $m/z$  and the effect of increasing the amplitude of the rf on the position on the stability line.

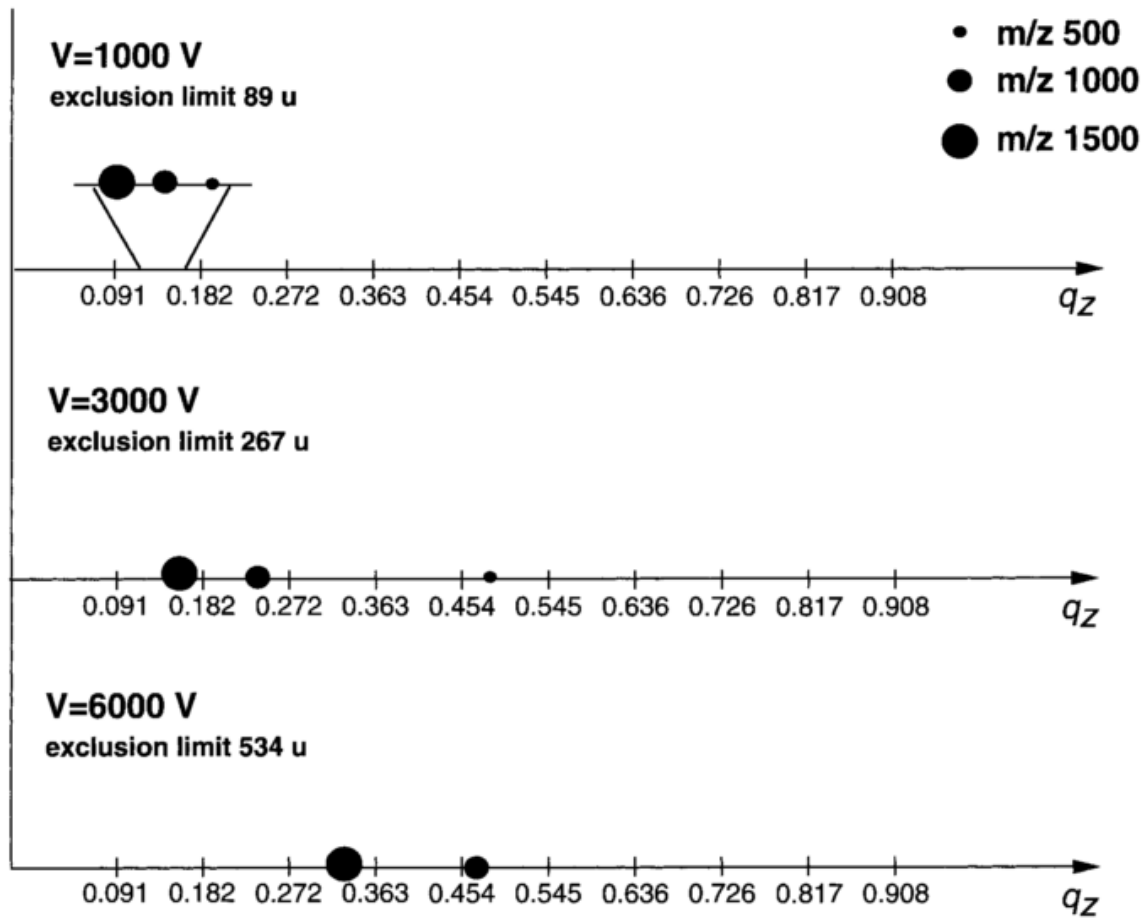


**Figure 39.** Effect of increasing the amplitude of the rf on three ions of different  $m/z$ .<sup>149</sup>

The exclusion limit in Figure 39 is a drawback of the trap technology as the ion trap has a low mass cut off (LMCO), below which no ions will be retained in the trap. The LMCO is given by the following formula:

$$m/z_{min} = 4.44V/(r_0^2\Omega^2) \quad (9)$$

where  $V$  is the amplitude of the rf potential applied to the ring electrode,  $\Omega$  is the angular frequency of the rf potential, and  $r_0$  is the inscribed radius of the ring electrode.<sup>153</sup>

## 2.6.2 – Resonance Ejection

Since ions possess a secular frequency in both the axial and radial dimensions, application of a “tickle voltage”, a small potential (hundreds mV) to the end caps can excite the ions and impart more kinetic energy to them. The helium reduces the ions kinetic energy to approximately 0.1eV. Excitation at an ion’s secular resonance frequency, aided by the trapping field, can increase the kinetic energy of an ion to tens of eV.<sup>150</sup> When this is applied to an ion’s axial secular frequency, in conjunction with an increase in the amplitude of the rf potential, ions may be ejected axially to the detector. This is referred to as resonance ejection or axial modulation, and has the added benefit of increasing the mass range of the ion trap. Figure 40 shows the same ions as in Figure 39 except with a resonance frequency applied. This creates a hole in the stability diagram so ions of higher  $m/z$  may be accessed since the  $q_{\text{eject}}$  is now 0.227, an increase of 4 for this mass range. Used in conjunction with other methods and modifications, the mass range may be extended by a factor of 960.<sup>144</sup> This method also greatly enhances the resolution of ions.<sup>148</sup>

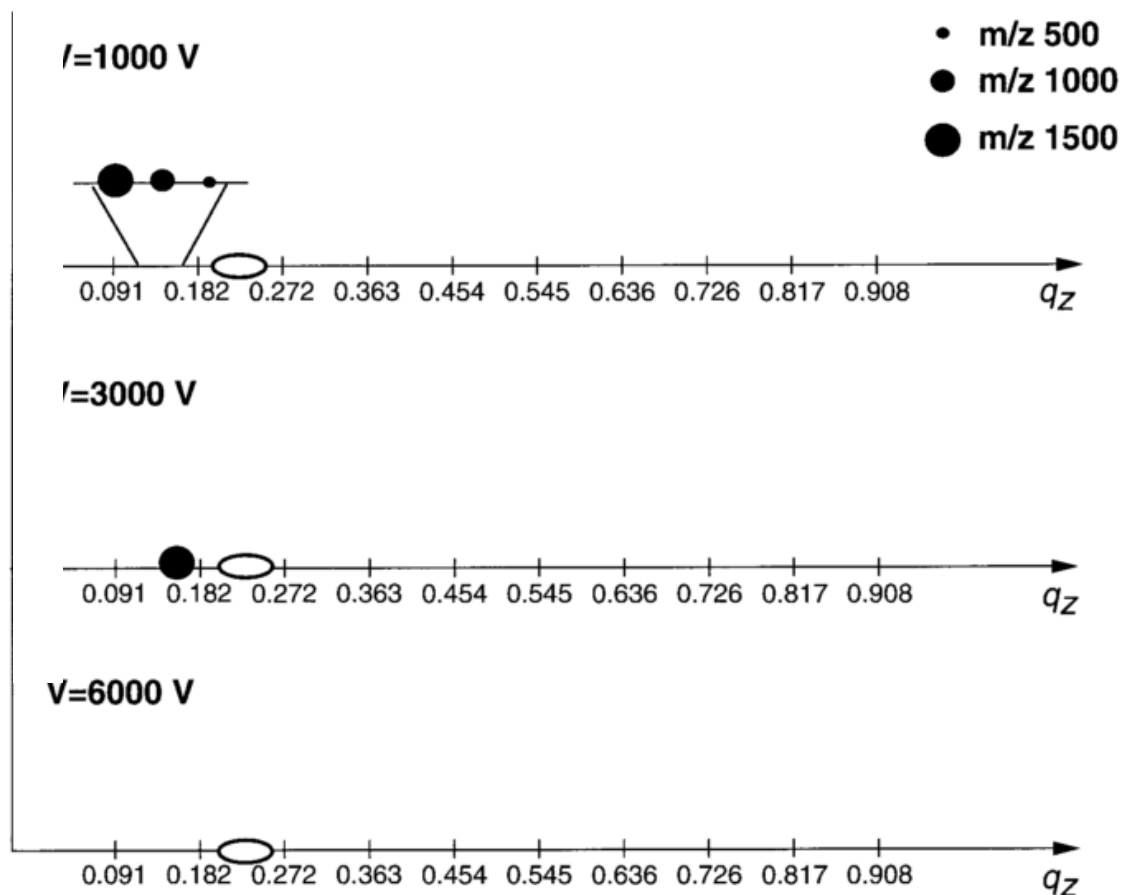


**Figure 40.** Effect of resonance ejection to access higher mass range.<sup>149</sup>

The previous technique of resonance excitation to impart kinetic energy may be utilized to perform a number of other useful applications. For example, ion isolation may occur by ejecting unwanted ions from the trap, isolating an ion or range of ions by way of applying a broadband set of frequencies;<sup>154</sup> the increase in kinetic energy may promote endothermic ion-molecule reactions, or bring the ion closer to a detector for an image current, thus allowing nondestructive measurements;<sup>150</sup> aside from ion ejection, the next most popular use of resonance ionization is to impart enough kinetic energy to activate the ion to high enough energies to cause fragmentation via collisional induced dissociation (CID).

### 2.7.1 – Collision Induced Dissociation (CID)

Ions may be resonantly activated and induced to fragment providing valuable structural information in the process. Different instruments activate ions differently and thus confer different advantages and disadvantages. One apparent requirement would be a trap or a tandem MS; however, a single quadrupole could be induced to fragment ions in-source, in the tube lens region, shown in Figure 41.<sup>119</sup> By increasing the capillary

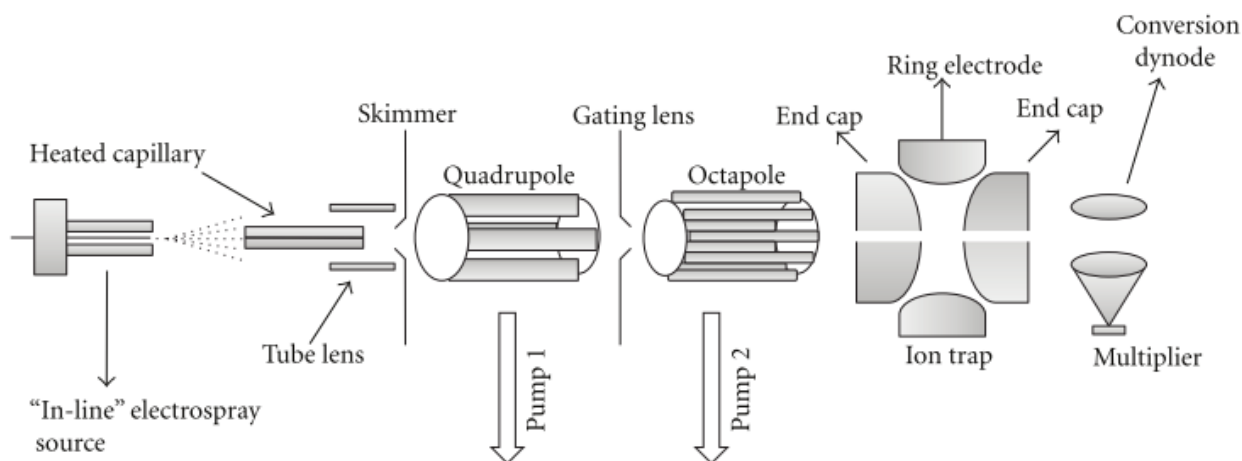


**Figure 41.** Schematic of an ion trap MS, displaying the tube lens region where ion fragmentation may occur.<sup>119</sup>

voltage, the ions will be accelerated through the high-pressure region where they will collide with atmospheric molecules and fragment. There is no separation, but coupling with an HPLC for the separation followed by in-source fragmentation could provide structural information; the caveat – the integrity of the MS data is reliant upon the separation of the LC method. Regardless, of the MS used, the ion source conditions need to be optimized to prevent in-source fragmentation.

Collision induced dissociation (CID), also referred to as collision activated dissociation (CAD), is the most popular method for ion activation and fragmentation.<sup>155</sup> TQMS and IT both use CID and via a neutral gas to induce fragmentation of an ion, usually argon for a TQMS and nitrogen for an IT. For a TQMS, fragmentation occurs in space; the “precursor” ions are isolated in the first quad and ejected into the second where the ions undergo collisions with the gas and fragment, producing “daughter” ions. The daughter ions are ejected and guided in the third quadrupole to the detector.

The disadvantage of this method is the lack of control for energy deposition. The ions enter the second quadrupole with a narrow range of energies, undergo inelastic collisions where some of the kinetic energy is transferred to internal energy (predominately vibrational, but others are possible if the energy is high enough)<sup>156</sup> and upon fragmentation, impart some energy to the fragmented ions where they can undergo further fragmentation. Therefore, it may be unclear as to the origin of the peaks in the mass spectra, whether they arise from the product peaks, or are fragments of the product peaks.

Alternatively, the method in which the IT induces CID imparts a significant advantage over activation using the TQMS – more control of the energy imparted to an ion, which may be calculated from the following formula:

$$E_{\text{int}} = E_{\text{kin}} m_{\text{target}} / (m_{\text{ion}} + m_{\text{target}}) \quad (10)$$



where  $m_{\text{ion}}$  is the mass of the ion and  $m_{\text{target}}$  is the mass of the neutral gas molecule. Ion activation in an IT takes advantage of the ion's secular frequency (axial). A small tickle voltage, is applied to the end caps. At the correct frequency, the ion's secular frequency, the ion gains enough kinetic energy to perturb the usual motion from the center of the trap. Recall, the restoring effect to an ion as it deviates from the center of the quadrupole field. This force imparts more kinetic energy to the ion whereupon it collides with the helium bath gas at 1 mtorr. Continued collision with the gas eventually leads to ion fragmentation, at which time the product ions are cooled via the helium gas, since the newly formed ions are out of resonance with the applied resonance frequency they cannot undergo further fragmentation.

The amount of kinetic energy imparted to the ion may be controlled by varying the voltage ( $< 1\text{V}$  zero-to-peak), or activation time (10-100ms).<sup>157</sup> The resonance frequency acts as a kick-start for the ion, with the quadrupole field and helium gas providing additional energy for fragmentation. The one negative aspect to trapped ion fragmentation is the lower limit of trapping, or the low mass cut-off (LMCO, equation 8). Adjusting the  $q_z$  value allows for some flexibility in moving this limit.<sup>158</sup>

## 2.8 – Scan Speed

Another unique feature of the trapping instruments is the use of variable scan speed to access higher resolutions. Mass resolution in trapping instruments is a function

of the time an ion spends interacting with the rf field. The resolution may be calculated from the following formula:

$$R = N^2/K_k \quad (11)$$

where  $R$  is the resolution,  $N$  is the number of rf cycles and  $K_1$  is 20 for the first stability region.<sup>159</sup> The theoretical basis for this was originally proposed by Fischer in 1959.<sup>160</sup> He argued to increase resolution, the amplitude of the auxiliary field should be minimized, thus maximizing the interaction time between the ions and the rf field; alternatively, the scan speed may be varied to achieve the same result.

Ions are ejected from the trap by ramping up the rf amplitude of the ring electrode until the ions have reached enough energy for ejection. If this rate is too fast, the next ion will be activated before the previous ion has been ejected, manifesting itself as a loss in resolution. Utilizing the techniques of resonance ejection and mass-selective instability modes, a slow scan speed ( $27.8 \text{ amu s}^{-1}$ ) and the minimization of the auxiliary field, a resolution in excess of 30,000 full width half max, (FWHM) was achieved for  $m/z$  of 502.<sup>145</sup> As a point of reference, the normal scan speed,  $5500 \text{ amu s}^{-1}$ , yields resolutions of 4000.<sup>118</sup>

When scanning at slow speeds ( $280 \text{ amu s}^{-1}$ ), referred to as zoom scan, a narrower range of masses must be scanned. Alternatively, the scan speed may be increased ( $55,000 \text{ amu s}^{-1}$ ), called turbo scan, at a loss of resolution. Normally, this is employed to increase the number of scans across a chromatographic peak, but it may

also be used to decrease the time from the ion trap to the detector, increasing signal of weakly coordinated ions.

## 2.9 – Conclusion

Mass spectrometry is a powerful tool that allows the one to study molecules in the gas-phase, deducing structure by the mass to charge ratio. The Nobel-Prize winning technique of ESI developed by Fenn, allows the transfer of ions in the solution phase to the gas-phase intact. Due to the work of many people, the ion trap mass spectrometer, previously a tool mainly for physicists has become indispensable for the modern scientist. The techniques of resonance excitation, mass-selective instability mode of ion ejection, CID, and many other methods, provide the chemist many tools from which to draw upon for their unique interests and research.

The QIT's ability to trap ions, offers the distinct ability to create and monitor chemical reactions. The ability to isolate an ion of a desired  $m/z$  in the presence of a complex matrix, could allow for screening of multiple catalysts present in a crude mixture. In addition, the helium gas, necessary for optimal performance of the instrument and unique to QIT mass spectrometers, allows for the possibility of introducing a neutral reagent to the trap, where upon it may react with the ion introduced via ESI. This would allow for the possibility of a rapid, chiral screening method.

The nature of mass spectrometry, i.e., gas-phase, presents the unique opportunity to study inherently unstable or reactive intermediates not possible in the condensed phase. The lack of solvent, counter ions, and aggregation phenomena enable the catalyst's native potential to be probed. The true chiral environment of a catalyst may then be accessed and studied, potentially gaining insight into the common template that drives  $C_2$ -symmetric catalysts towards excellent ee's over a range of reactions. The next chapter will detail ion-molecule reactions in the gas-phase, modifications to the instruments to provide said facility, and methods for determining enantioselectivity.

## **Chapter 3 – Gas-Phase Ion-Molecule (IM) Reactions and Enantioselectivity in Mass Spectrometry**

### **3.1 – Gas-Phase Reactions and Mass Spectrometry**

MS offers unique abilities to aid in the study of ion-molecule (IM) reactions. Since MS operates in the gas phase, it can offer insight into structures, intermediates, and mechanisms that are not accessible via traditional condensed phase methods. The low pressures required for operation of an MS, desolvates most solvated-catalysts. Hence, the catalyst's intrinsic nature is accessible, free from solvent effects, as well as any ion-pairing/aggregation phenomena.

The low pressure also increases the time between collisions, allowing for the study of reactive species/intermediates, assuming a trapping MS is used. According to Ottens et al., with a trapping parameter  $q_z$  of 0.25 (the default), the average velocity of an ion is 7m/ms. At a pressure of  $7 \times 10^{-6}$  torr, this corresponds to a mean free path of 7m, resulting in a collision every ms, allowing for numerous, potential reactions within the instrument's time-frame.<sup>161</sup>

The soft nature of ESI, in conjunction with the pre-formed charge on the metal catalyst, allows for the successful transfer of the catalyst from solution to the gas-phase,

intact. With the introduction of the ion via ESI, the neutral molecule may be introduced into the instrument several of ways, discussed later, or may be present in the background. While MS operates at low pressure, there is typically a series of stages of differential pressures before the mass analyzer. Thus, the ions are still exposed to neutrals/excipients as they transverse through the instrument. This mainly occurs in the tube lens region, where the pressure is still relatively high, approximately 1 torr (1.3 torr for a Thermo Deca QIT), as ions are still undergoing desolvation on the way to the octapole ion guide, and ultimately the mass analyzer.

### 3.1.1 – History and Instrumentation

Thompson first proposed the idea of gas-phase reactions in a MS in 1913,<sup>109</sup> while Dempster confirmed the existence of ion-molecule (IM) reactions in 1916 involving  $\text{H}_2^+$  and  $\text{H}_2$ .<sup>162</sup> In 1966, Munson and Field utilized IM reactions in a magnetic deflection MS to develop chemical ionization (CI), representing an alternative to EI as a source ionization mechanism for molecules.<sup>113</sup> It represents the most common application to ion-molecule reactions and an area where much of the research was conducted, searching for more selective CI reagents.<sup>163</sup>

Since then, technology and instrumentation has allowed for more controlled and refined IM reactions that could be performed with the instruments of the time. With the advent of the triple quad (TQ) by Yost in 1978,<sup>134</sup> separation in-space was feasible, allowing for the study of structures of reactant and product ions,<sup>164,165,166,163</sup> and ion-

molecule reactions inside the collision cell.<sup>167,168,169</sup> The flowing-afterglow,<sup>170</sup> and its closely related sibling, the selected ion flow tube (SIFT),<sup>171,172</sup> allowed for the study of the rate constants of IM reactions,<sup>173,174</sup> bond strengths,<sup>175</sup> H/D exchange,<sup>176</sup> proton affinities,<sup>177,163</sup> gas-phase basicity, and clustering equilibria.<sup>178,179</sup> Flowing afterglow and high-pressure mass spectrometry were among the first instruments used for ion-molecule experiments, along with the ICR. Newer techniques such as 2D separations with ion mobility, has further expanded the abilities of the IM as an analytical tool.<sup>180</sup> However, many of these techniques used direct insertion probes or EI/CI as a means for ionization, which are not favorable conditions for fragile organometallic complexes.

### 3.1.2 – ESI and Organometallic Chemistry

Due to John Fenn,<sup>114</sup> the ESI method was developed, and it opened up new areas of research for organometallic chemists, as the facile nature of transferring the metal ion from solution to gas phase by ESI is ideally suited for organometallic studies. Previous methods of ionization were not amenable to transition metal complexes due to the low volatility, thermal liability and redox nature of the metal complex.<sup>181,182</sup> ESI was a technique that addressed these obstacles. In 1990, Chait *et al*, successfully electrosprayed a solution of  $[\text{Ru(II)(bpy)}_3]\text{Cl}_2$ , and performed CID to remove the acetonitrile adducts from the complex, thus demonstrating the applicability of ESI and CID for studying organometallic complexes (Figure 42).<sup>181</sup>

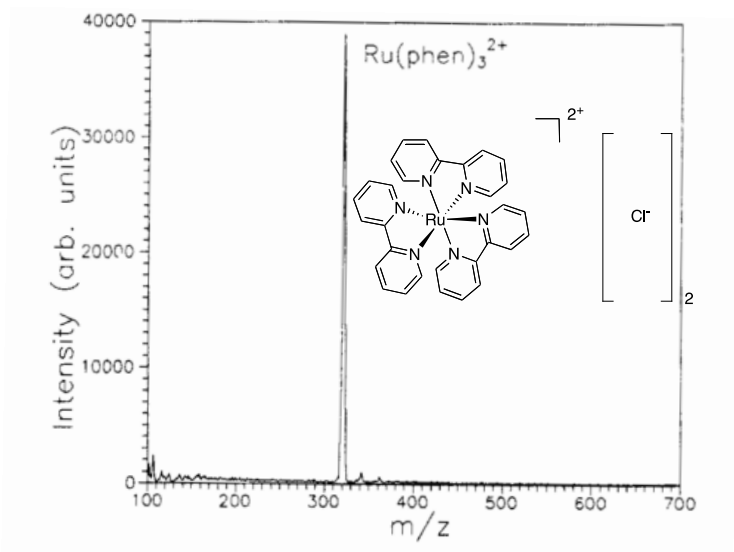


**Figure 42.** First electrosprayed transition metal organometallic compound,  $\text{Ru(II)(bpy)}_3\text{Cl}_2$ .<sup>181</sup>

In 1994, the first proof of an organometallic intermediate for the Suzuki reaction was obtained using a TQMS and ESI by Aliprantis and Canary. In order to detect the intermediates, pyridine was used in place of the aryl halide substituent, thus, providing a means for protonation and detection as the pyridinium salt,  $[(\text{pyH})\text{Pd}(\text{PhP}_3)_2\text{Br}]^+$  in the catalytic cycle. Intermediates I and II in Figure 43 were observed in the mass spectrum, providing proof of the Suzuki mechanism. Although these examples are not true gas-phase ion molecule reactions, they displayed the potential of ESI for elucidating organometallic mechanisms and intermediates, previously limited by ionization techniques.



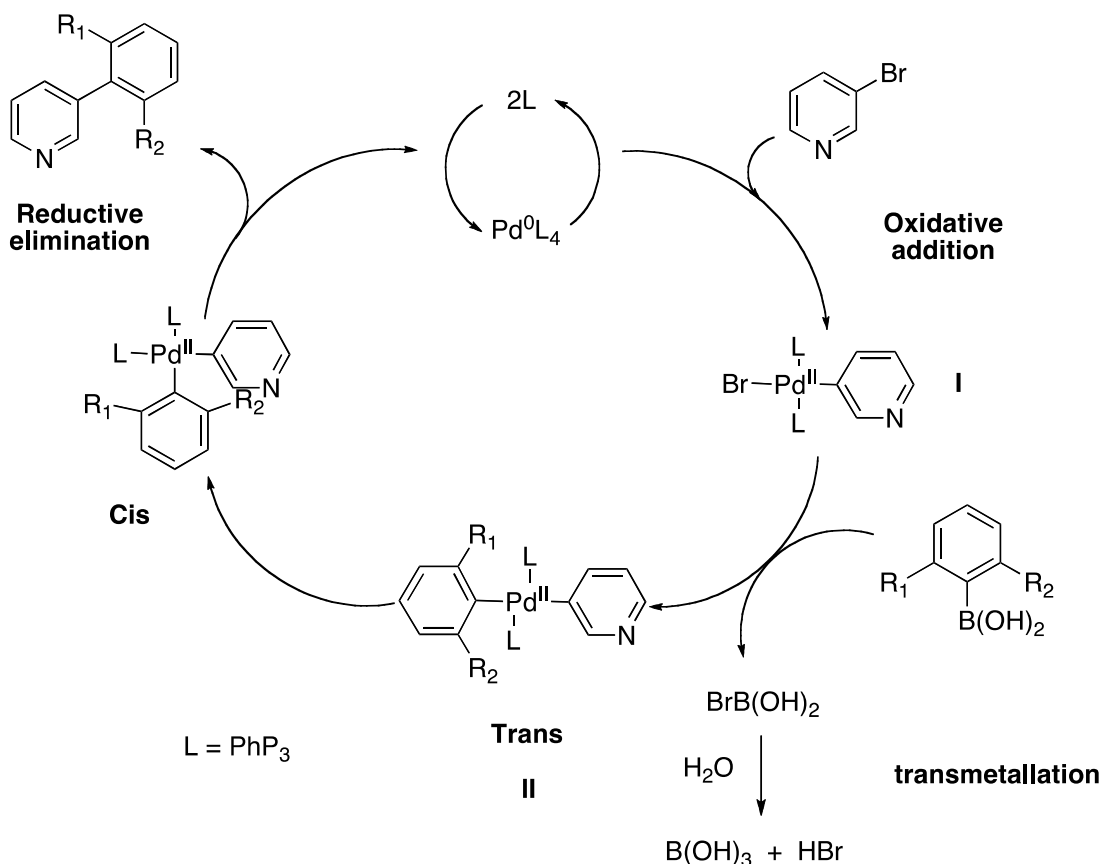


**Figure 43.** Catalytic cycle of the Suzuki mechanism with the pyridine-substituted aryl halide.

### 3.2 – Trapping Instruments for Gas-Phase Chemistry

Trapping instruments include the ICR (and FT variants) and the 3D and linear (2D) ion traps,<sup>147</sup> and the newest MS, the hybrid 2D-orbitrap (orbitrap).<sup>183</sup> ICRs were used to study kinetics<sup>184,185</sup> and were the first instruments used to study inorganic/organometallic compounds,  $\text{Fe}(\text{CO})_5$ .<sup>186</sup> More recently, the newer orbitraps have been modified using the Gronert method, discussed later, to study the Diels Alder,<sup>187</sup> and Heck reaction.<sup>188</sup>

The first recorded observation of a gas-phase reaction in an ion trap was by Rettinghaus in 1967, when he monitored the formation of  $\text{COH}^+$  from  $\text{CO}^+$  and

hydrocarbons present in the background (Figure 44).<sup>189</sup> Prior to commercialization

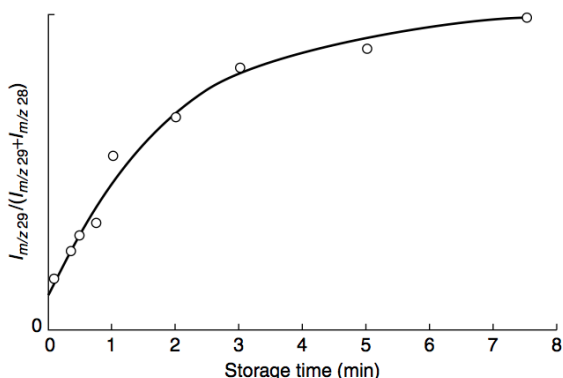


**Figure 44.** First ion-molecule reaction recorded in an ion trap. From March and Todd.<sup>189</sup>

around 1984, the field of ion traps was dominated by the labs of Todd and March, where their pioneering work in ion ejection methods,<sup>190,191,192</sup> ion injection,<sup>193</sup> and ion kinetic/energetics laid the groundwork for the ability to study ion-molecule reactions in the trap.<sup>194,195,196</sup>

Since the commercialization of ITMS instruments, they have been utilized in diverse fields of research, spanning disciplines of organic, inorganic, biochemistry, astrochemistry, and quantum mechanics. Typical applications range from ion structure elucidation,<sup>150,197</sup> mechanistic studies,<sup>198,199,200</sup> thermodynamic and kinetic studies,<sup>201,202,203,204</sup> to the common “omics” – proteomics,<sup>205,206,207</sup> metabolomics,<sup>208</sup> and lipidomics.<sup>209</sup> Recently, more exotic applications have been found. For example, NASA developed a portable QITMS for analysis of cryogenic leaks prior to space shuttle launches.<sup>210,161</sup> The ion-trap technology was used to develop an atomic clock accurate to the 17<sup>th</sup> decimal,<sup>211</sup> and is currently being investigated for use in quantum computers.<sup>212</sup>

Its popularity stems from its versatility, as it combines many attributes of separate mass analyzers into one instrument, i.e., no coupling of analyzers is needed. Together with ESI, the QIT has been described as a “complete gas-phase chemical

laboratory,”<sup>200</sup> by O’Hair, a modification of the title of Beynon’s book, *The Modern Mass Spectrometer – A Complete Chemical Laboratory*.<sup>213</sup> The “laboratory” offers the ability to control the time allowed for the reaction by modifying the trapping time. Similarly, using the secular frequency of the ion and resonance excitation, extra energy may be deposited to the ion for endothermic reactions,<sup>150,214</sup> or fragmentation of ions to access unique structures/chemistry.<sup>215,216,217</sup> QITs can also isolate an ion of single  $m/z$  or a range of  $m/z$ , alleviating the need for a pure sample, assuming the absence of isobaric species. Structure elucidation of resultant products are possible with  $MS^n$  capabilities, and if an FTICR is used, high-resolution is also available as a tool,<sup>163</sup> or alternatively, variable scan speeds, such as zoom scan, can increase resolution in a 3D trap.<sup>132</sup> Finally, the addition of helium as a bath gas thermalizes the ions, allowing for kinetic studies.<sup>218</sup>

### **3.3 – Neutral Reagent Introduction**

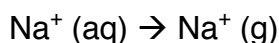
With the advent of ESI, a soft introduction of an organometallic compound, such as a catalyst, was possible. The ion trap allows a vessel for the reaction to occur, but a method is needed to introduce a substrate into the reaction.

#### **3.3.1 – Introduction of Neutral Reagent via Solution Phase**

Introduction of the neutral molecule to the mass analyzer may occur via solution or the gas-phase. Solution-phase introduction typically infuses a mix of the ion and

neutral molecule directly into the instrument, as was the case for the Suzuki example shown in Figure 43. Technically, this could also apply to a solid sample prepared in the appropriate matrix. The ion and neutral are then allowed to react *in-situ* and are transferred from the condensed phase to the gas-phase. This has the appeal of simplicity, as no instrument modifications are required, and near universal compatibility with the majority of ion sources. It may also potentially allow for the study of the ion-molecule complex as it exists in its native environment – that is, the mass spectrum should be representative of the solution-phase complex (assuming single stage MS),<sup>219</sup> although, this remains a controversial topic and an area of intense research.<sup>220</sup>

The solution introduction method assumes there is no change to the complex upon ionization/desolvation to the gas phase. Desolvation is a highly endothermic process. The endothermic nature of desolvation is evident in the feeling of a cooled flask, and the visual of a frosted receiving flask when rotovapping a solution. The free energy of desolvation for a sodium ion is shown below.<sup>221</sup>



$$-\Delta G^\circ_{\text{sol}} = 98 \text{ kcal/mol}$$

This is same amount of energy required to break a carbon-hydrogen bond and more than what is required to break a carbon-carbon bond (83-85 kcal/mol).<sup>222</sup> This fact is testimony to the “softness” of ESI as it delivers intact ions. Since many ion-molecule reactions involve weak intermolecular forces, such as  $\pi$ -cation ( $\Delta H = 19.3 \text{ kcal/mol}$  for  $\text{NH}_4^+$  - benzene),<sup>223</sup> or hydrogen bonds ( $\Delta G = 1.67 \text{ kcal/mol}$   $\text{S}-\text{H}\cdots\text{S}$ ,  $5.25 \text{ kcal/mol}$   $\text{O}-$

H $\cdots$ O),<sup>224</sup> this can call into question the effect of the ionization process on the ion-molecule complex.

Many studies have attempted to answer this question, with differing results. Wang and Agnes studied the labile equilibrium of strontium with EDTA ( $\text{Sr}^{2+} + \text{EDTA}^{4-} \rightleftharpoons \text{Sr-EDTA}^{2-}$ ) and found negligible differences between the measured equilibrium via the MS and the solution phase equilibrium.<sup>225</sup> Similarly, Leize et al. came to the same conclusion using metal alkali cations in competition with cryptate 222 and crown ether 18C6.<sup>226</sup>

However, Tureček and Gatlin, provided contradictory evidence when studying the dissociations of  $\text{Fe}^{2+}(\text{bpy})_3$  and  $\text{Ni}^{2+}(\text{bpy})_3$  complexes.<sup>227</sup> They found higher dissociation equilibrium constants in gas-phase ESI-MS than the expected solution-based calculations predicted. The authors attribute this to the ESI process, specifically the iterative droplet evaporations with concomitant increase of  $\text{H}_3\text{O}^+$  formation from the electrostatic field, localized near the surface of the liquid.<sup>228</sup> Thus, the gas-phase pH with the ion-complex of interest is different than the original bulk solution pH, shifting the equilibrium.<sup>227</sup>

This also highlights the precarious nature of solution-based methods for introduction of the complex. As each system is different, the acid/base nature of each system may dictate the accuracy of the data, and thus, not be reflective of the inherent characteristics of interest. As such, considerations must also be made for matrix

components and effects. Linder et al. found evidence of such matrix effects in the transfer to the gas-phase when studying diastereomers.<sup>229</sup> It is therefore desirable for an alternative method for introduction of a neutral molecule to the MS.

### **3.2.2 – Introduction of Neutral Reagent via Gas-Phase**

Introduction of the neutral reagent to the trap via gas-phase (after ion isolation) offers significant advantages over the solution-phase alternative. First, the question of the source's impact is immaterial (assuming the ion has not undergone transformation in the process). Second, ion-isolation followed by multi-stage MS allows for manipulation of the ion, allowing access to more possible reactive species (see next section). And third, ion-molecule chemistry may be allowed to occur under carefully controlled conditions. For example, time, temperature, and pressure, are all variables that may be controlled (to a point); however, permanent modification of the instrument is required, and trapping MS instruments are typically required.

#### **3.2.2.1 – Introduction via a Valve**

The neutral reagent may be pulsed into the trap or introduced at a constant, persistent rate. The pulsed introduction method via a pulse valve was first conceived of 1982,<sup>230</sup> and built in 1983 by Freiser and others at Purdue University for use in ICR,<sup>231</sup> and later adapted by Cooks et al. for use in ion traps in 1990.<sup>232</sup> Pulsing of the reagent utilizes a pulsed valve and necessitates drilling a small hole through the trap for

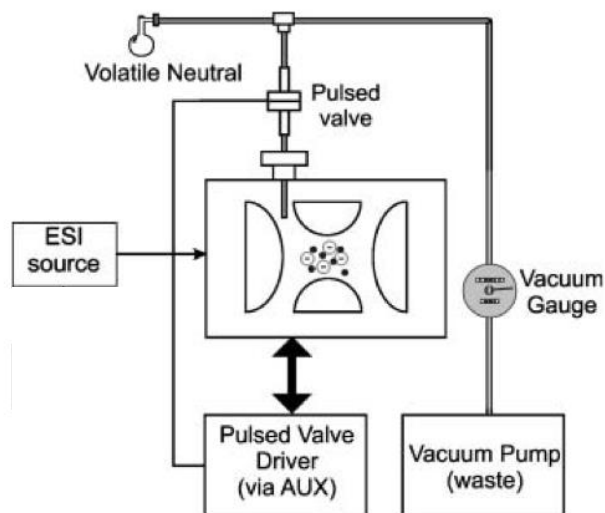


**Figure 45.** Modified ion trap with pulse valve. Taken from Ryzhov.<sup>233</sup>

introduction of the reagent. It also requires a pulse valve drive controller that synchronizes with the ion trap software. Figure 45 is a schematic of a Bruker Esquire 3000 modified with a pulse valve for introduction of a neutral reagent.<sup>233</sup> This set-up offers the advantage that the reagent gas is not persistent and thus minimizes contamination or interference

with subsequent operations, but the uncertainty in the pressure does not allow for the use in absolute kinetic measurements, although relative measurements of rates can be made.<sup>198</sup>

The alternative to the pulsed methodology is to introduce the reagent at a constant flow rate. The advantage over the pulsed methodology is the ability to obtain absolute kinetic data, assuming accurate measurements of the pressures are obtained. The downside is the constant, persistent presence of the neutral reagent during all stages of the experiment, which may introduce complications. For example, if the equilibrium between the neutral reagent and ion is on the same time-scale as the ion isolation scan, the ion and neutral reagent will coordinate and form a complex with a resultant larger  $m/z$  than the ion isolation window. Thus, it will be ejected from the trap and the signal of the ion of interest will be diminished.

Alternatively, delivery of the neutral reagent, at a constant flow rate, may utilize a leak valve, either directly to the trap,<sup>234,235</sup> similar to the pulsed valve set-up previously described, or to the ion trap vacuum manifold, with subsequent helium dilution.<sup>210,236</sup> Large errors were initially associated with the pressure determinations, as the pressure differential was determined via a manometer and visual inspection before and after the leak valve was closed to the trap (evacuated to a pressure of  $10^{-7}$  torr or less).<sup>185</sup> With the advent of ion pressure gauges and flow meters, the accuracy has greatly improved.<sup>237</sup> The use of a calibration reaction with a known rate constant (for example  $\text{CH}_3\text{I}$  with bromide anion)<sup>238</sup> allows for a compensatory factor to be made to allow for acquisition of the most accurate data. Figure 46 displays examples of systems utilizing leak valves for delivery of a reagent at a constant flow rate.<sup>236,210</sup>

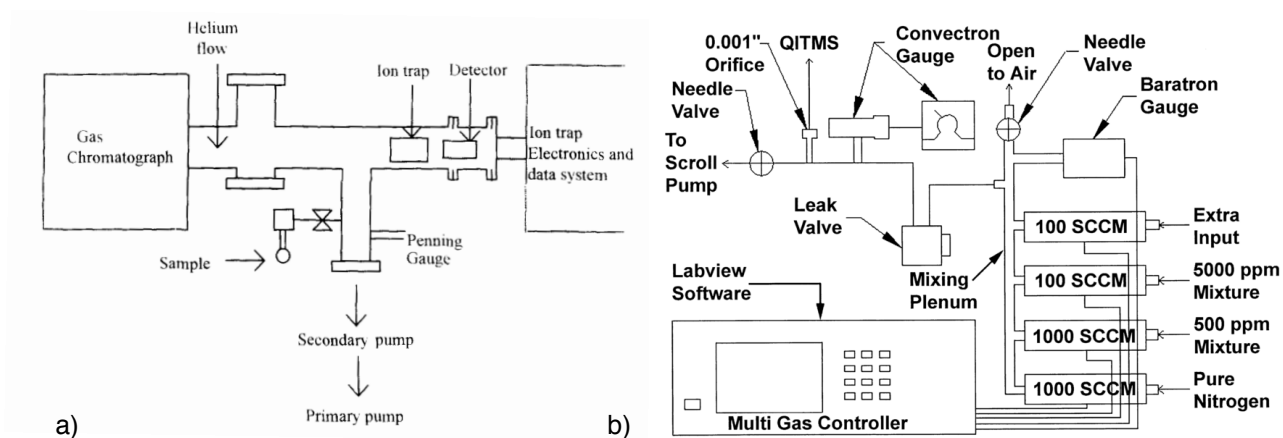


**Figure 46.** Schematics for introduction of neutral reagent via leak valves. Left (a)<sup>236</sup> Right (b)<sup>210</sup>

### 3.2.2.2 – Introduction via Gas-Phase



A mass spectrometer must be able to achieve a high vacuum ( $10^{-6} - 10^{-8}$  torr) with this method in order to obtain an accurate determination of the pressure.<sup>198</sup> While this is not a problem for ICRs that regularly operate at pressures of  $10^{-9}$ - $10^{-10}$  torr, ITs are not capable of meeting this low-pressure requirement. The precision of leak valves to deliver small increments of reagent may also bias some kinetic experiments.<sup>235</sup> In pursuit of addressing these concerns, Gronert developed a method for the constant infusion of a reagent to the trap via the *in-situ* helium line, with a slight modification to the internal plumbing.<sup>218</sup>

This method incorporates a syringe pump (30-300ul/hr) to infuse the neutral reagent via a septum port on a custom built manifold, into a helium stream, maintained at 1-2 L/min by a mass flow meter. The reagent may be diluted and/or the rate adjusted, as needed, to deliver reagent pressures from  $10^{-5} - 10^{-8}$  torr. A small portion of the flow is directed into the trap, while the majority is diverted to waste. This high dilution is necessary due to the low accuracy of the delivery of reagent from syringe pumps at lower flow rates.

In order to reduce the lag time of the reagent into the instrument, the internal pressure regulator of the instrument is removed. This regulator is used in conjunction with a restriction capillary to step the pressure down from the 40 lb/in<sup>2</sup> from the helium tank to the 3 lb/in<sup>2</sup> required of the ion trap. In the absence of the internal regulator, the 3 psi (above atmospheric pressure ~17.7 psi) is maintained manually via adjustment of

the helium tank regulator and a barometer (absolute pressure reader).<sup>198</sup> The illustration in Figure 47 represents the modified LCQ Deca ion trap.

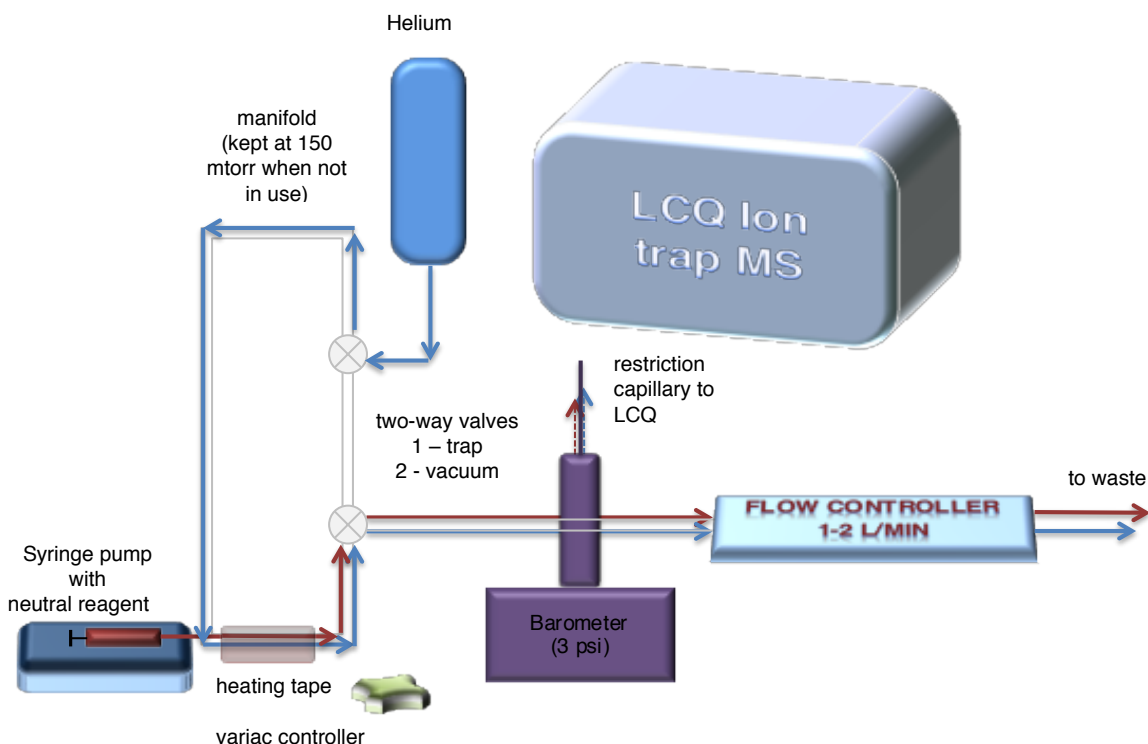


**Figure 47.** Diagram of the modified LCQ ion-trap to allow introduction of a neutral reagent.

Ejection of ions from the trap occurs through a series of small pinholes in the end cap detector side. These small holes, together with the fact that the mean free path is longer than the length of the ion trap, imparts a need to account for the differential effusion rates of the gases through the holes; otherwise, the results will be biased towards the heavier molecular weight compound. The following equation accounts for this differential effusion rate:<sup>198</sup>

(1)

$$P_R = 1.75 \times 10^{-3} \times \frac{F_R}{F_{He}} \times \frac{d_R}{MW_R} \times \frac{(MW_R)^{1/2}}{4}$$

where  $1.75 \times 10^{-3}$  is the pressure inside the trap when 3 psi of helium pressure is applied,  $F_R$ ,  $d_R$ , and  $MW_R$  are the flow rate, density, and molecular weight of the reagent, respectively, and  $F_{He}$ , is the flow rate of the helium (moles/min).

This method of introduction allows for much better control and quantification of the neutral reagent than with valve-type methods, offering precisions of  $\pm 5$ -10%, but uncertainties of  $\pm 20$ -30%.<sup>198</sup> This method eliminates the variability associated with ion sources and introduction of the neutral through the solution phase.

### 3.2.2.3 – Laser Desorption

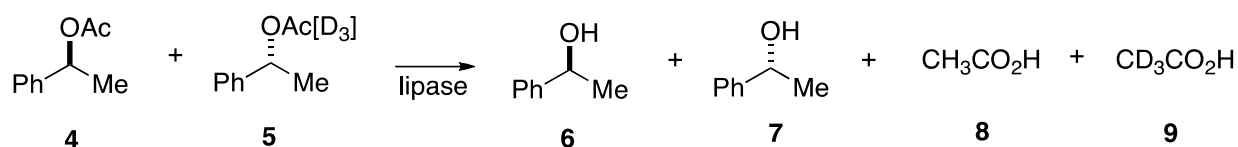
In some cases, laser desorption may be a suitable option for introduction of neutrals into the gas-phase for subsequent reactions. However, this method has not been routinely used due to the low yield of neutrals, and, if formed, a short lifetime before collisional loss or evacuation via vacuum system.<sup>163</sup>

## 4 – Mass Spectrometry for Rapid Chiral Recognition

The previous chapter discussed mass spectrometry and chiral recognition. This section will briefly discuss its use as a rapid chiral screening method.

### 4.3.1 – Kinetic Resolutions

The majority of rapid mass spectrometry-based methods employ kinetic resolution of *pseudo*-enantiomers, also referred to as quasi-enantiomers (as not to offend the crystallographers), to determine enantioselectivity. This method was originally developed by Horeau in 1990 to determine the absolute configuration of secondary alcohols<sup>239</sup>. This method incorporates isotopic labeling (Scheme 19).<sup>240,241</sup>



**Scheme 19.** Isotopic labeling of 1-phenylethyl acetate for kinetic resolution in MS.

The ee may be calculated by first taking the extent of conversion (c),

$$c = \frac{ee_s}{ee_s + ee_p} \quad (1)$$

where  $ee_s$  is the ee of the substrates and  $ee_p$  is the ee of the products (in this case,  $4/5$   $/ (4/5 + 8/9)$ ). The ee (E) may then be calculated.<sup>242</sup>

$$E = \frac{\ln[(1 - c)(1 - ee_s)]}{\ln[(1 - c)(1 - ee_p)]} \quad (2)$$

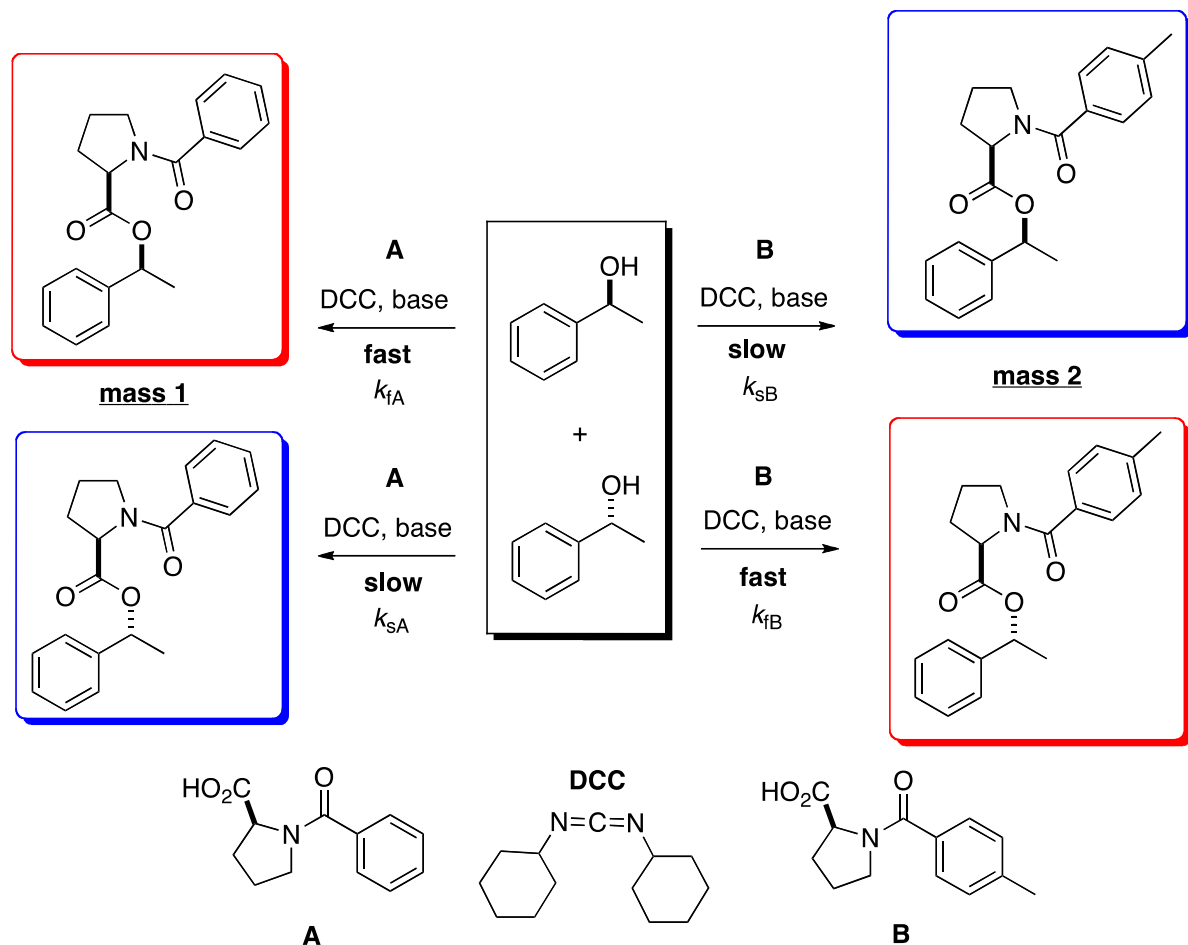
This method was been adapted to allow for rapid analysis by combining 96-well plates, a Water 600 pump, a Gilson 215/889 eight-channel liquid autosampler with a multi-



injector module (20 $\mu$ L loops), eight columns (C8 Waters Symmetry 2.1 x 20mm), and an eight-channel MUX ESI system (Figure 48) coupled to a Micromass TOF.<sup>241</sup> The ESI sprayer is control by a rotor, allowing a spectrum every 1.2 seconds. One cycle (eight samples) takes 70 seconds, thus, a 96-well plate can be run in 14 minutes.

**Figure 48.** MUX ESI Spray system with eight-channels by Micromass.<sup>241</sup>

As an alternative to isotopic labeling, two different, but closely related, mass-tagged auxiliaries may be used.<sup>243,244,245</sup> The rates of formation of the diastereomers (quasi-enantiomers) will be different and represented in the mass spectra. For example, in the Steglich esterification, shown in Scheme 20<sup>244</sup> the enantiomer of 1-phenylethanol reacts with the acid (**A** or **B**). A methyl group, far from the site of reaction, differentiates



**Scheme 20.** Kinetic resolution of 1-phenylethanol via the Stiglech reaction utilizing two acids differing in mass of 15 ( $\text{CH}_3$ ).

the acids. This allows for discrimination in the MS while not affecting the inherent reactivity. Calibrations must be performed to obtain the ionization efficiencies,  $q$ , and the selectivity factor,  $s$ , of the two acids. Preparation of a racemic mix yields the ionization efficiencies of the two acids:

$$q = I_{\text{mass 1}} / I_{\text{mass 2}} \quad (3)$$

Calibration with a known ee for each substrate yields  $k_{\text{fast}}$  and  $k_{\text{slow}}$ , from which  $s$  may be obtained:

$$s = k_{\text{fast}} / k_{\text{slow}} \quad (4)$$

Correcting for the intensity ratio from the formula:

$$y \cdot q = I_{\text{mass } 1} / I_{\text{mass } 2} \quad (5)$$

where q is derived from the racemic calibration and eq (3), the ee may be calculated from the equation:

$$\%ee = \left[ \frac{(y - 1)(s + 1)}{(y + 1)(s - 1)} \right] \times 100 \quad (6)$$

Thurrow *et al.*, adapted HTS, using a HTS-PAL from CTC Analytics AG for liquid-handling system for a dosing, diluting, injecting and transferring samples from a 96-well plate, which the authors state may be adapted to any major LC-MS system, shown in Figure 49.<sup>243</sup>

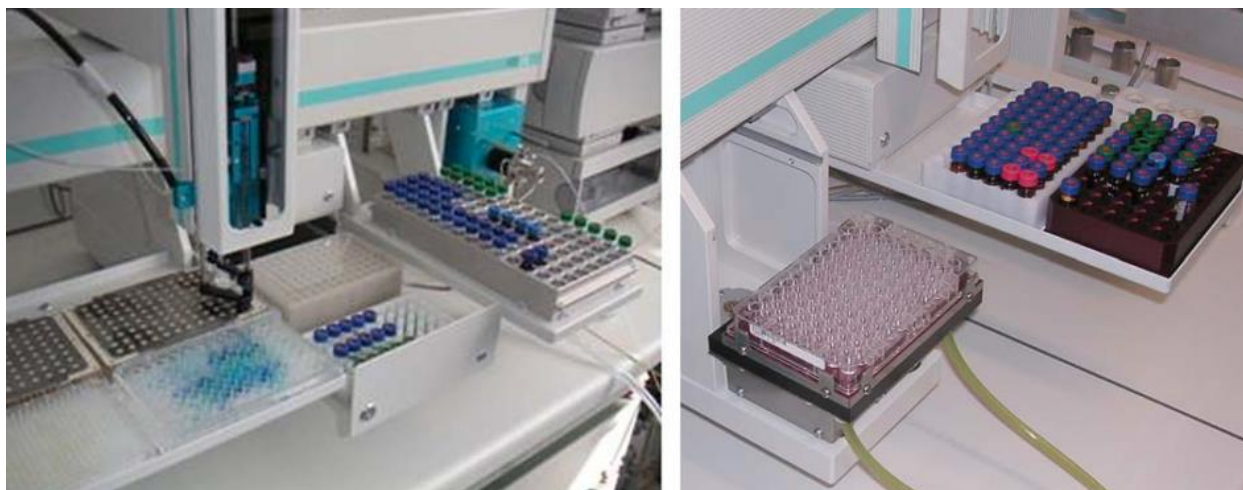


**Figure 49.** Setup by Thurow for rapid MS analysis.<sup>243</sup>

### 4.3.2 – Cook's Kinetic Method

The kinetic method has been used to determine a mixture of amino acids. Recalling from last chapter, the rates of the two competing dissociation channels can be measured by the fragment ion abundances, reflecting the stability and energy difference between the two. The branching ratio for the fragments may be written:

$$R = \frac{[M^{II}(A_x)(ref^*) - H^+]}{[M^{II}(ref^*)_2 - H^+]} \quad (7)$$

The degree of chiral recognition may then be written:

$$R_{chiral} = \frac{R_D}{R_L} = \frac{\frac{[M^{II}(A_D)(ref^*) - H^+]}{[M^{II}(ref^*)_2 - H^+]}}{\frac{[M^{II}(A_L)(ref^*) - H^+]}{[M^{II}(ref^*)_2 - H^+]}} \quad (8)$$



The energy difference may be obtained from the following equation:

$$\ln R = \frac{\Delta\Delta G}{RT_{eff}} \quad (9)$$

where **R** is the gas constant, and  $T_{eff}$  is the effective temperature. For a pure enantiomer, eq (9) may be used with eq (7) to calculate the energy difference for the individual enantiomeric complex:

$$\ln R_D = \frac{\Delta\Delta G_D}{RT_{eff}} \quad (10)$$

$$\ln R_L = \frac{\Delta\Delta G_L}{RT_{eff}} \quad (11)$$

For an enantiomeric mixture with an excess of D, the ee may be given as:

$$\begin{aligned} \Delta\Delta G &= \Delta\Delta G_D \frac{1+ee}{2} + \Delta\Delta G_L \frac{1-ee}{2} \\ &= \frac{[DDG_D + \Delta\Delta G_L]}{2} + \frac{[DDG_D - \Delta\Delta G_L]}{2} ee \end{aligned} \quad (12)$$

where D and L may be substituted for R and S. By combining equations (8), (9), (10), (11), and (12) the ee of the mixture may be delineated from the chiral recognition, R:

$$\ln R = \frac{[\ln(R_D) + \ln(R_L)]}{2} + \left[ \frac{\ln(R_{chiral})}{2} \right] ee \quad (13)$$

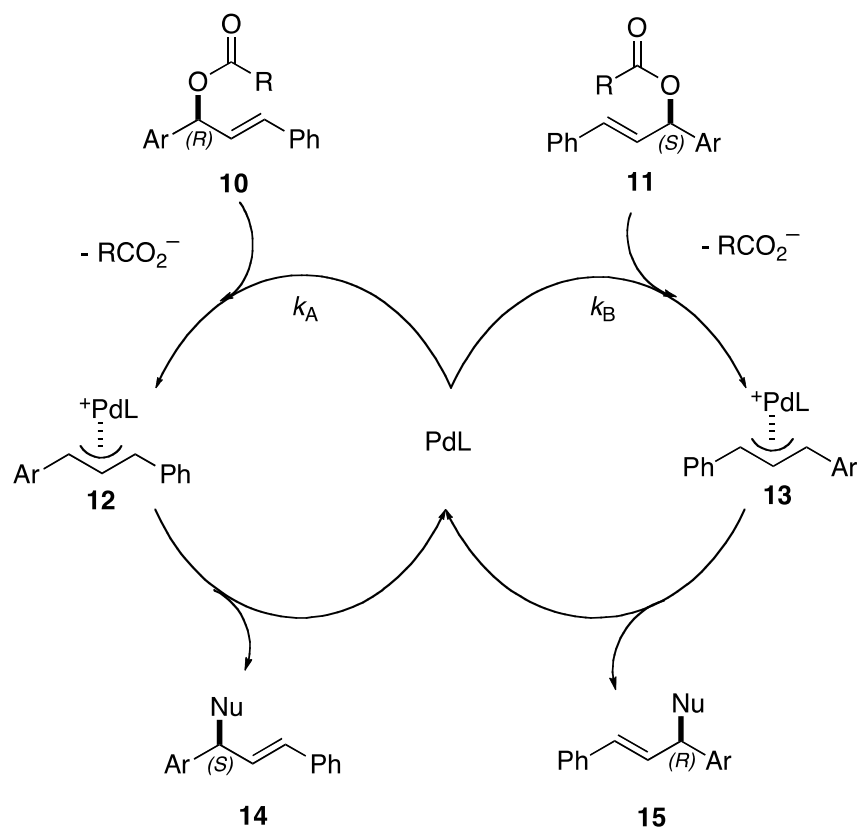
With a calibration curve, the ee of unknown samples may be determined. A mixture of three amino acids was performed, resulting in ee's that could be measured down to 2% ee with relative errors between 3.0-6.7%.<sup>246</sup> While the kinetic method cannot offer the HTS that the previous methods could, it does not require expensive specialized equipment. Instead, it affords the ability to study multiple samples in one prep (assuming equilibrium is achieved), on standard MS equipment.

#### **4.3.3 – Direct Catalyst Screening**

The group of Pfaltz has utilized the kinetic resolution method to screen intermediates in the Pd-catalyzed allylic substitution (Tsuji-Trost) and metal-catalyzed Diels-Alder reactions utilizing quasi-enantiomeric substrates. The method does not require any specialized equipment and is unique among the others methods in that it tests the catalysts, not the products.

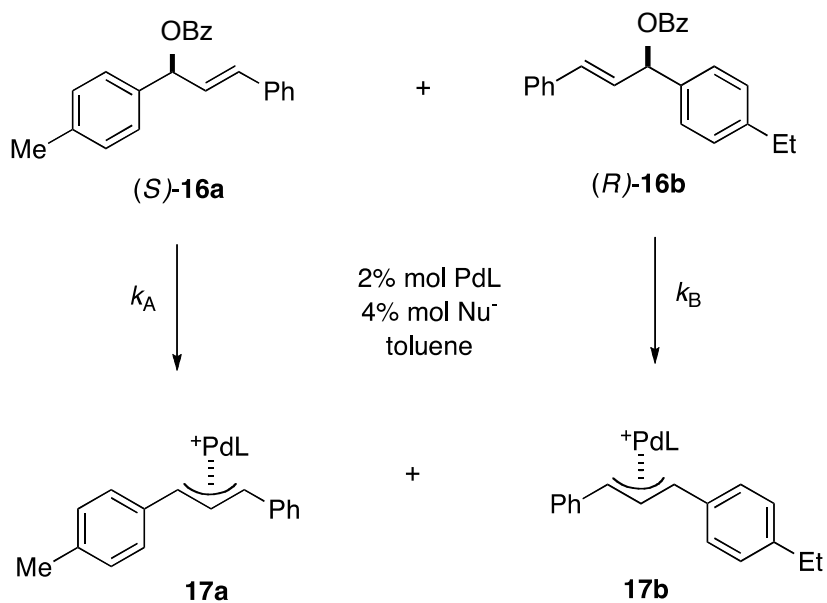
##### **4.3.3.1 – Pd-Catalyzed Allylic Substitutions**

The mechanism of Pd-catalyzed allylic substitution, the Tsuji-Trost, is shown in Scheme 21. Formation of the Pd-intermediate (**12** or **13**) is fast, while nucleophilic addition is rate-limiting, which allows access to the intermediates via MS. In this case, **16a** and **16b** (Scheme 22) were used to differentiate the two species in the MS.<sup>247</sup>



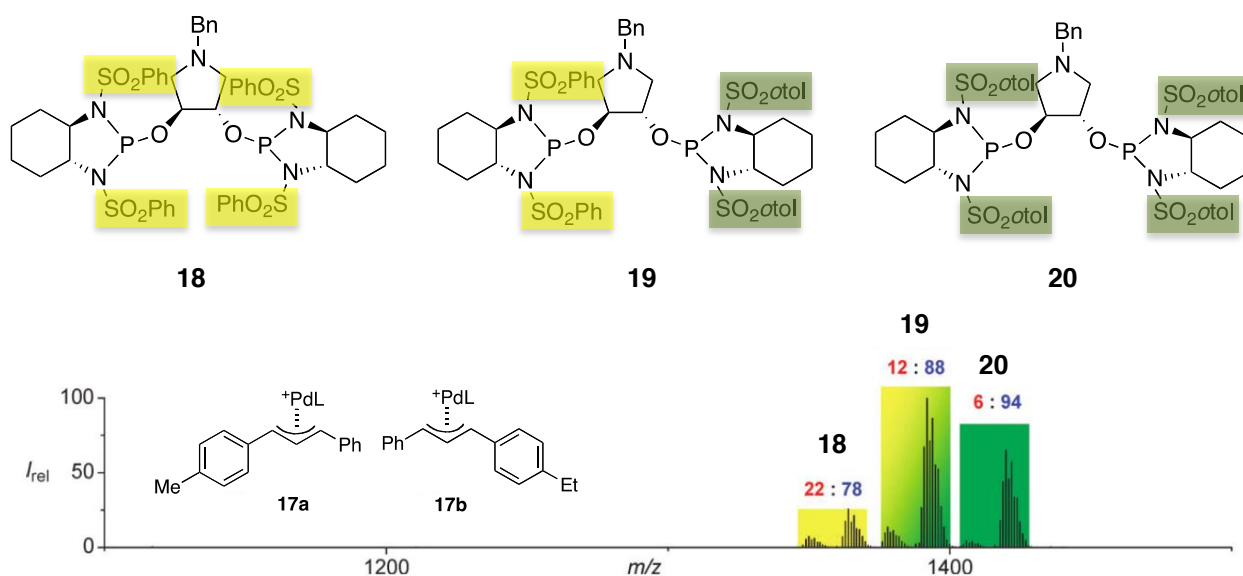
plus regioisomers

**Scheme 21.** Tsuji-Trost Pd-catalyzed allylic substitution.



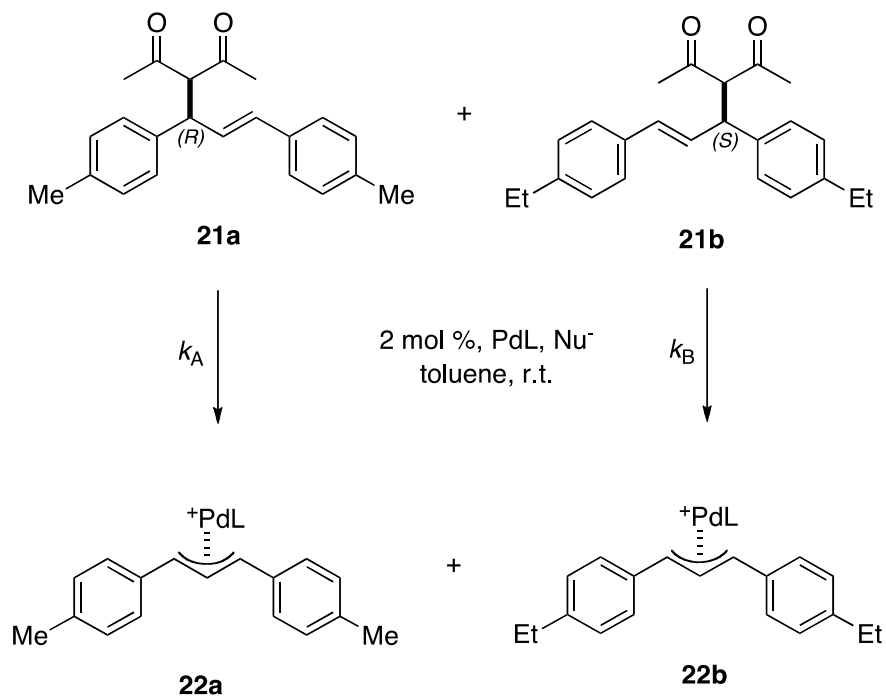
**Scheme 22.** Allylic ester used in the Pd-catalyzed screening.

The selectivity of the catalyst can be determined from the ratio of the rates  $k_A/k_B$ , which equals the ratio of the ion abundance **17a/17b**. Three catalysts were synthesized and screened with the MS. Ligand (**20**) was found to be the most enantioselective (Scheme 23).<sup>247</sup>



**Scheme 23.** Mix of ligands to screen Pd catalysts with **16a** and **16b**, with resultant mass spectrum.<sup>247</sup>

The previous methodology was also applied to studying retro-allylic substitution. According to the principle of microscopic reversibility, the transition states that govern enantioselectivity are the same for the forward and backward reaction. A suitable target was found in acetyl acetone, and (**21a**) and (**21b**) were used as the quasi-enantiomers for the Pd-catalyzed retro-allylic substitution (Scheme 24).



**Scheme 24.** Substrates used in the Pd-catalyzed back-reaction study.

A series of phosphinoxazoline ligands were screened via MS for enantioselectivity in the back-reaction. The corresponding condensed phase reactions were performed and compared via chiral HPLC; the results of the two “correlated very well,”<sup>248</sup> validating the methodology (Figure 50).<sup>247</sup>

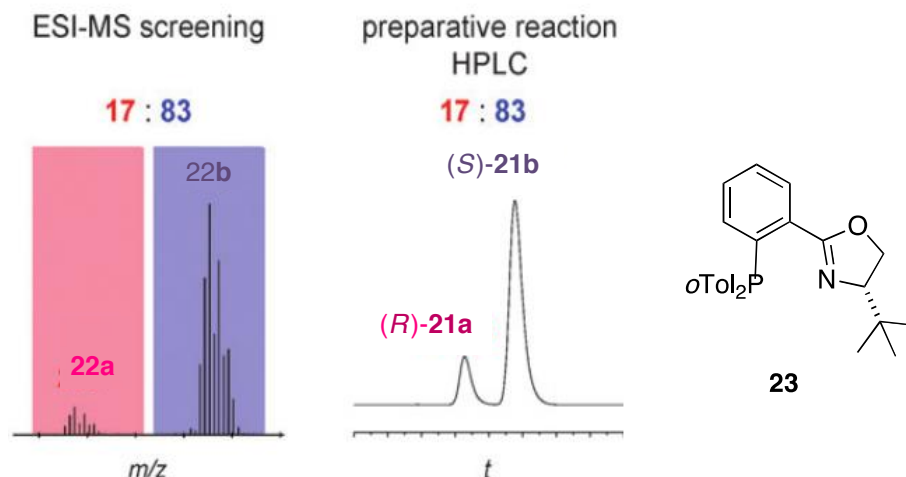
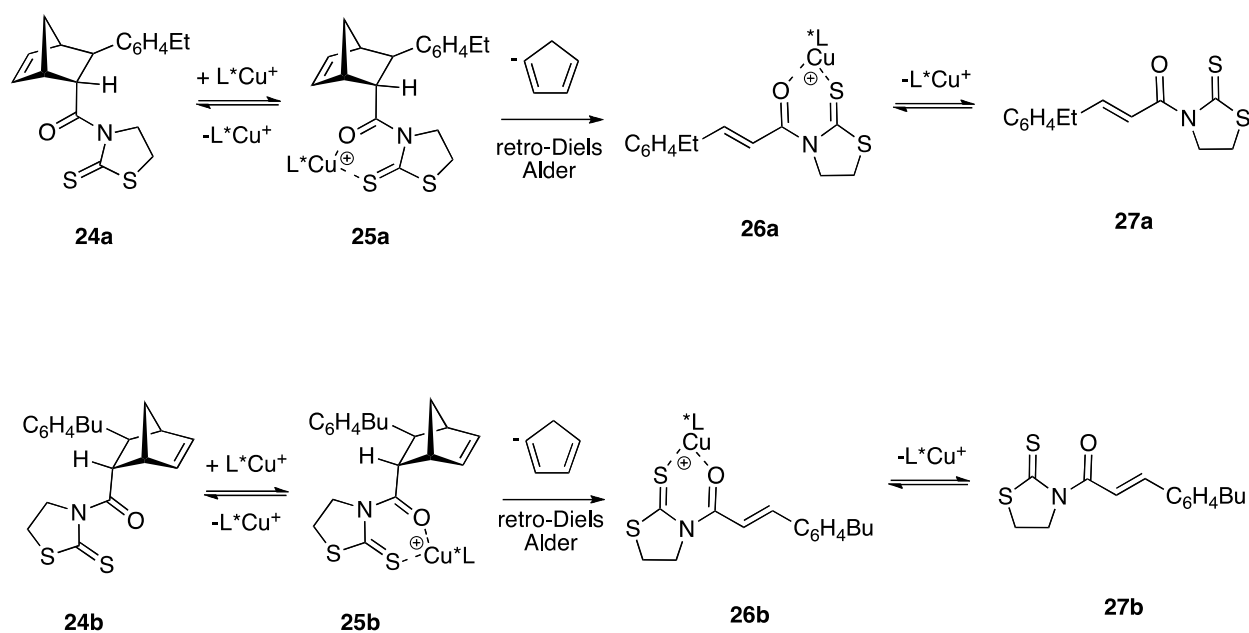


**Figure 50.** Comparing results from MS via the back reaction, and reaction products via condensed phase and chiral HPLC.<sup>247</sup>

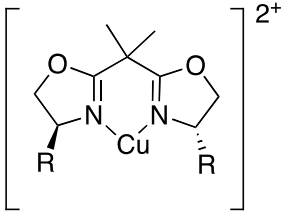
An attractive target to further research the back reaction would be the retro-Diels-Alder, which was pursued by the group of Pfaltz. The retro-Diels Alder reaction is shown below in Figure 25, with the quasi-enantiomers (**24a**) and (**24b**) chosen for discrimination in the MS. Utilizing Lewis acid, Cu(II) Box ligands, the reaction was



**Scheme 25.** Retro-Diels-Alder with the quasi-enantiomers (**24a**) and (**24b**).

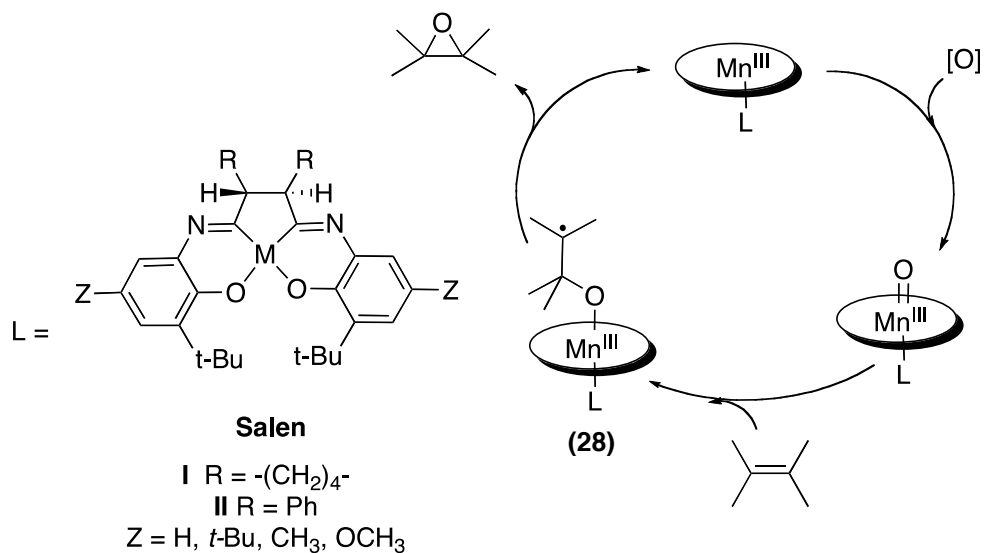
performed at 100 °C, the minimum temperature to induce the retro reaction. After 1 hour, samples were taken and subjected to MS. Again, excellent agreement was obtained between the MS results, and the condensed-phase results based on chiral HPLC (Table 3).<sup>249</sup>

**Table 3.** Results of ESI-MS screening of BOX Cu(II) catalysts.<sup>249</sup>

	ESI-MS <b>26a / 26b</b>	HPLC <b>27a / 27b</b>	Preparative reaction <i>endo</i> e.r.
2-naphthyl	86:14	90:10	88:12
Ph	80:20	85:15	86:14
<i>t</i> -Bu	68:32	69:31	64:36
<i>i</i> -Pro	61:39	58:42	56:44
benzyl	55:45	51:49	52:48

#### 4.4 – Precedence

The method briefly described above has precedence in the literature and is based upon the Gronert group's work with Mn Salen catalysts with various chiral alcohols. As mentioned in Chapter 1, Mn Salen catalysts (Jacobsen's catalyst) are excellent oxygen delivery catalysts, enantioselectivity forming epoxides with olefins. To account for the observed stereoselectivity in some conjugated olefins, a radical mechanism was theorized (Scheme 26).<sup>250</sup>



**Scheme 26.** Radical mechanism for the formation of enantioselective epoxide from olefins.

Due to difficulties activating the Mn catalyst in the gas-phase, the radical intermediate was not practical. However, using alcohols, the intermediate **(28)** could be mimicked, a hypothesis backed up by DFT calculations. Figure 51 displays the results comparing the proposed intermediate **(28)** in (a) to the ethanol complex.<sup>251</sup> The two

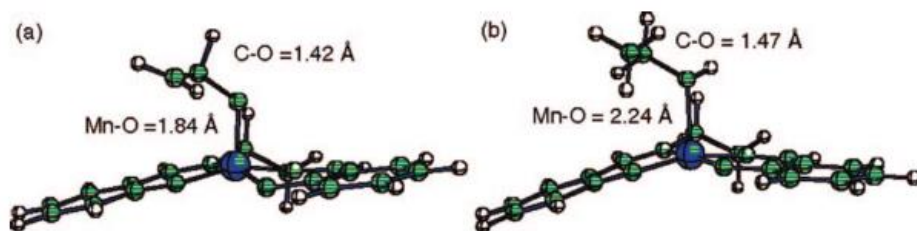


**Figure 51.** DFT results comparing the lowest energy conformers for the Mn-salen catalyst complexed to (a)  $\bullet\text{CH}_2\text{CH}_2\text{O}\bullet$  and (b)  $\text{CH}_3\text{CH}_2\text{OH}$ .<sup>251</sup>

results are remarkably similar, primarily differing in the bond length between the Mn-O, where it is longer by 0.4 Å in the ethanol model, implicating weaker bindings and less



steric repulsions in these probes. These results demonstrate the feasibility of probing the catalyst's asymmetric environment with simple chiral probes.

Various Mn-salen catalysts were tested for gas-phase enantio-discrimination with 1-phenylethanol and racemic *d*<sub>5</sub>-ring 1-phenylethanol as the chiral probe and internal standard, respectively. The results are shown below in Table 4.

**Table 4.** Results for various Mn-Salen catalysts and their stereoselective preferences for 1-phenylethanol in the gas-phase.

Ligand	$K_{S/R}$	de%
<b>I</b> ( <i>R,R</i> ) Z = C(CH <sub>3</sub> ) <sub>3</sub> R = cyclohexane	1.29	12
<b>I</b> ( <i>R,R</i> ) Z = CH <sub>3</sub> R = cyclohexane	1.29	12
<b>II</b> ( <i>R,R</i> ) Z = H R = diPh	1.45	20
<b>II</b> ( <i>R,R</i> ) Z = OCH <sub>3</sub> R = diPh	1.48	20

The catalysts displayed a preference for the S enantiomer (Figure 52), which was also observed in the condensed-phase kinetic resolution of 1-phenylethanol with (*R,R*) Z = *t*-Bu Mn-salen, however, KBr was necessary as a co-catalyst in the condensed-phase, muddying the comparison.<sup>252</sup> While the de appears modest compared to the condensed-phase, given the lack of an axial ligand, room temperature, and longer Mn-O bond length, the de is relatively large. The larger selectivity observed with the diphenyl catalysts (II) was also observed in the condensed-phase epoxidations with styrene,<sup>71,251</sup> lending credence to the hypothesis that these probes can yield information regarding a catalysts chiral environment, in a rapid, straightforward manner.

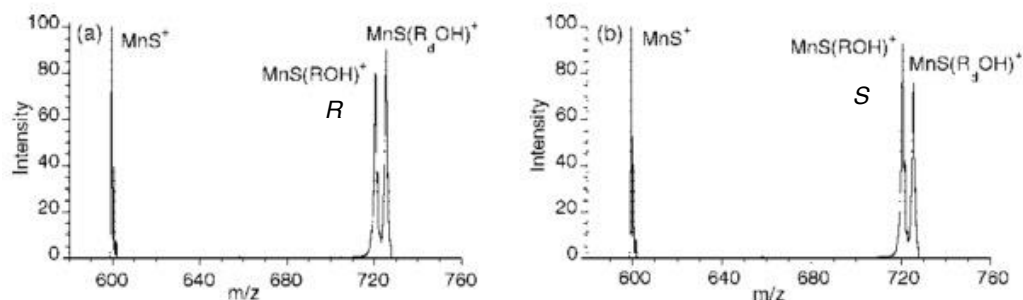


**Figure 52.** Example spectra for the Mn-salen catalyst with the 1-phenylethanol system. (a) (*R,R*) **1** (*Z* = *t*-Bu) and (*R*) 1-phenylethanol and *d-ring* 1-phenylethanol as the internal standard in a 1:1 ratio. (b) (*R,R*) **1** (*Z* = *t*-Bu) and (*S*) 1-phenylethanol and *d-ring* 1-phenylethanol in a 1:1 ratio. Of note is the larger peak intensity for the *S* enantiomer.<sup>251</sup>

## 4.6 – Conclusion

Due to the difficulties predicting and engineering a chiral catalyst, the process has taken a brute force approach, hoping to overcome the odds of finding a desirable catalyst by sheer force and low efficiency. The process is a multi-step process, requiring analytical analysis at every step. A catalyst's performance is based on the ee for a given reaction, for which many methods have been developed to assess the catalyst's chiral induction ability, indirectly.

The methods for testing ee via MS utilize quasi-enantiomers, isotopically-labeled substrates, or mass-tagged auxiliaries for differentiation in the MS. Only one method directly tests the chiral catalyst through kinetic resolutions or back-reactions. It would be much more efficient to develop a method that can directly test multiple catalysts' enantioselectivity potential. By employing the modified ion-trap, a series of chiral reagents can be introduced to the trap, where they can probe the catalyst's chiral template. In addition, the MS can act as a filter, so multiple catalysts may be analyzed in

a single experiment, offering a rapid screening tool that may be employed directly after synthesis of a catalyst, or a crude mixture of catalysts.

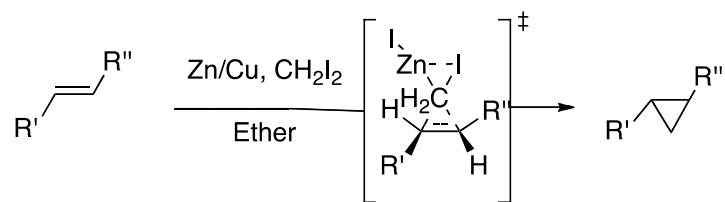
While the rate of analysis cannot compete with the 1000's of sample analyzed by combinatorial means, it significantly reduces time and resources by eliminating purification, analysis, and reactions after the crude synthesis, for a modest, one-time cost for supplies. This would benefit industry because they could develop and rapidly tests novel catalysts, thus skirting patents. Academia could benefit as well, by quickly determining the scope of new catalysts. The following chapters present data and methodology for probing the chiral space of a series of bis-oxazoline, di-imine, and a crude mixture of unsymmetrical di-imine catalysts with a series of chiral alcohols, ethers, and epoxides.

## 5 – Bis-oxazolines and Cyclopropanation

The class of bis-oxazolines catalysts presents an excellent starting point for the proof of concept and development work for the proposed method: (1) they catalyze a wide range of transformations producing high ee's, most notably, cyclopropanations; (2) the mechanisms for many of the transformations are understood; and (3) the catalysts are commercially available in high ee purity. Because the copper bis-oxazoline-catalyzed cyclopropanations are the gold standard for enantioselective cyclopropanations, they are briefly discussed in the following pages.

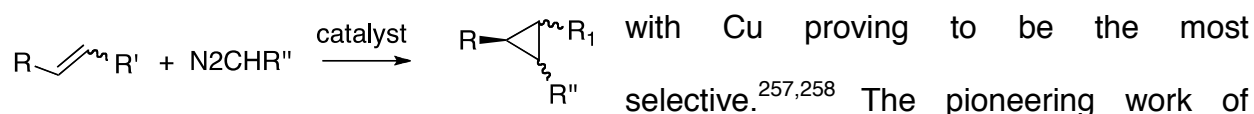
### 5.1 – Cyclopropanation

Cyclopropane formation represents an important class of organic transformations and was one of the first examples of asymmetric synthesis by Noyori in 1968. Cyclopropanes are unique due to the internal ring strain imposed by the geometry of the molecule. As such, cyclopropanes find immense use as intermediates in many synthetic schemes, as well as being found naturally in nature and in many pharmaceuticals and agrochemicals.<sup>253,254,3,255</sup> The classic cyclopropanation reaction is the Simmons-Smith method which employs an alkene, zinc, and diiodomethane (Scheme 27). The stereospecificity is a result of the transition structure, often referred to as a butterfly-type transition state.<sup>256</sup>



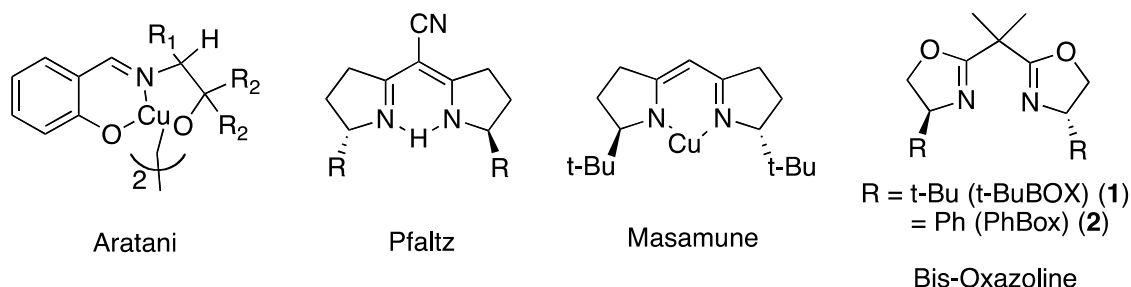
**Scheme 27.** Simmons Smith reaction.

Enantioselective methods for producing cyclopropanes utilize transition metals (Ni, Pd, Cu, Fe, Co Ru, and Zn) to catalyze the decomposition of diazoalkanes shown in Scheme 28.<sup>253</sup> Of the transition metals, Cu, Ru, and Rh have been the most successful,



**Scheme 28.** General cyclopropanation via diazoalkanes.

Noyori for the enantioselective cyclopropanation utilizing a (salicyladiminato)copper complex with styrene and ethyldiazoacetate, paved the way for others, such as Aratani<sup>259</sup>, Pfaltz<sup>260</sup>, Masamune,<sup>80</sup> ultimately leading to the modern bis-oxazoline (Scheme 29) as the enantioselective standard for cyclopropanations.



**Scheme 29.** Ligands used in enantioselective cyclopropanations.

## 5.2 – Copper Background

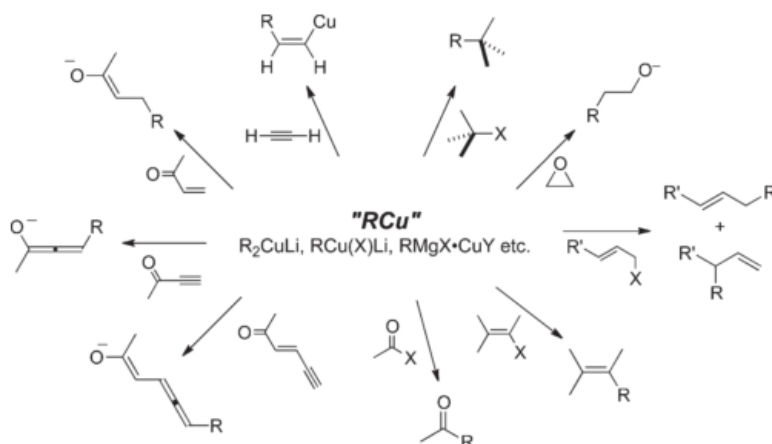
The late transition metal copper is one of the most recognizable metals in the world, where it is found in coins, electrical wiring, metals and statues (Statue of Liberty). When mixed with zinc, it forms the alloy brass. When mixed with tin it forms bronze, thus it played a crucial role in the cultural development of man during the Bronze Age. Copper is also essential for life on earth, and is responsible for a number of critical biological processes, such as cellular respiration, regulation of gene expression, and free radical scavenging.<sup>261,262,263</sup> Due to the nature of its redox reactivity, it is an excellent metal for biological systems, particularly enzymes that perform oxidative/reductive functions, such as cytochrome-c oxidase<sup>264</sup> and superoxide dismutase.<sup>265</sup>

### 5.2.1 – Physical Properties

Copper has an atomic weight of 63.55 g/mol, with two stable isotopes, 63 and 65, along with 23 radioisotopes.<sup>266</sup> <sup>63</sup>Cu has a natural abundance of 69.09%, with <sup>65</sup>Cu comprising the remaining 30.91%. It has four oxidation states ranging from 0 to +3, with +1 (cuprous) and +2 (cupric) being the most common. In aqueous media the equilibrium constant, K, for Cu(II) is extremely large,  $\sim 10^6$ .<sup>267</sup> Cu(I) has a  $d^{10}$  electron configuration ([Ar]7d<sup>10</sup>) and a coordination geometry of linear (2), trigonal planar (3), and tetrahedral (4).<sup>268</sup> Cu(II) has a  $d^9$  electron configuration ([Ar]3d<sup>9</sup>) with a tetragonal coordination geometry including tetrahedral, square planar, and trigonal bipyramidal.<sup>269</sup> With an unpaired electron, Cu (II) is paramagnetic. Cu(II) solutions are readily distinguishable from the colorless Cu(I) solutions by a blue or green color.

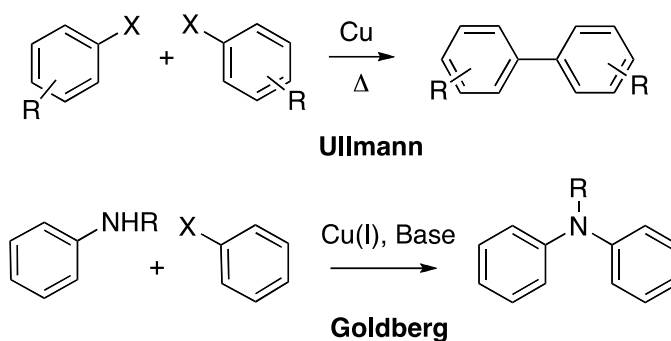
### 5.3.1 – Copper in Organometallic Synthesis

In organic chemistry, copper is best known for its use in nucleophilic organocopper reagents, such as the Gilman reagent (lithium dialkylcuprates) for cross-coupling and other reactions shown in Scheme 30.<sup>270</sup>



**Scheme 30.** Nucleophilic organocopper reactions.<sup>270</sup>

Copper has also been used in aryl-aryl cross couplings. Before Suzuki<sup>271</sup> and Stille<sup>272</sup> developed their methodologies, the Ullmann<sup>273</sup> and Goldberg<sup>274</sup> reactions for cross coupling were the standard (Scheme 31).

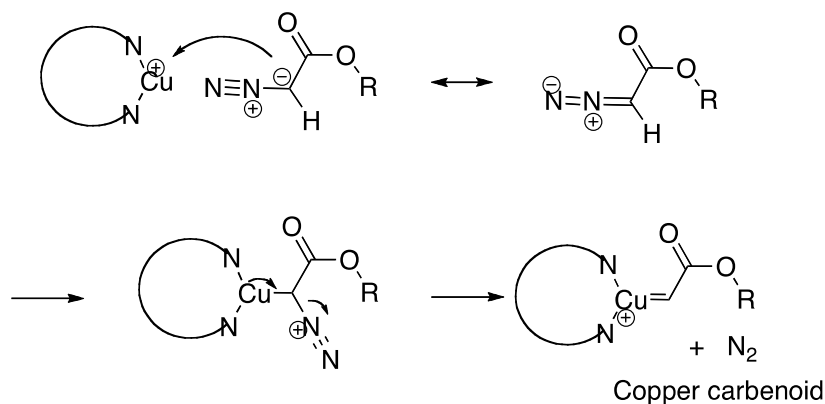


**Scheme 31.** Copper used in cross coupling before Pd.

The harsh conditions required for the Ullmann and Goldberg reactions (high temperatures) meant the reaction(s) fell out of favor for the milder Suzuki, Stille, Negishi, and Buchwald, reactions. More recently, copper has found use in click chemistry,<sup>275</sup> with the coupling of alkynes and azides (Huisgen cycloaddition) to form a 1,2,3-triazole,<sup>276</sup> and the Sonogashira cross coupling of an aryl halide and a terminal alkyne.<sup>277</sup>

#### 5.4 – BOX Cu-Catalyzed Cyclopropanation Mechanism

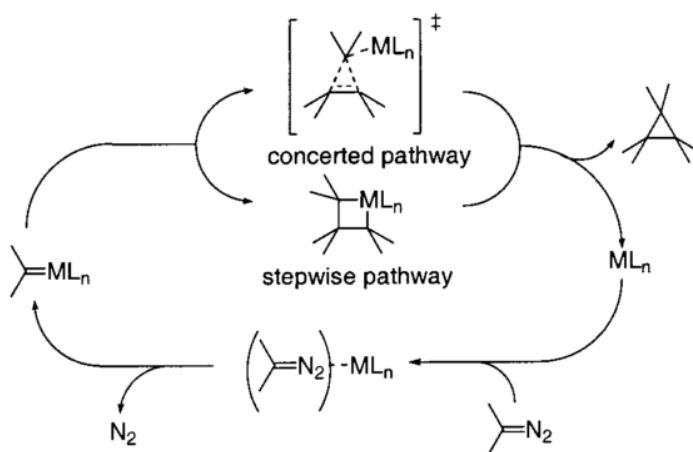
There are two generally accepted aspects of the copper-catalyzed mechanism. First, a copper-carbenoid, formed via the diazoalkane decomposition, is involved in the mechanism, shown in Scheme 32,<sup>278,81,80,258,279</sup> although recent work by Gronert *et al.* suggests it may be a solvent-stabilized ylide.<sup>280</sup> This formation has also been determined to be the rate-limiting step.<sup>281</sup> Second, copper (I) is the active catalytic species, even when Cu(II) is used. It has been found by Kochi et al that Cu (II) species are reduced to Cu (I) by diazo compounds.<sup>282</sup> Alternatively, Cu(II) has been treated with hydrazines to reduce the metal to the active Cu(I) species.<sup>278,80</sup>



**Scheme 32.** Formation of a copper carbenoid.



There is less agreement as to the formation of the cyclopropane, whether it is a concerted, direct insertion,<sup>278,283,284</sup> or step-wise process via a metallacyclobutane, (Scheme 33).<sup>259</sup> Computational investigations into the mechanism have been performed by Fraile *et al.* These studies indicate that the concerted pathway is more favorable by 3 kcal mol<sup>-1</sup>.<sup>281</sup>



**Scheme 33.** Proposed mechanism Cu-catalyzed cyclopropanation.<sup>259</sup>

#### 5.4.1 – Mechanism of Enantioselectivity

Pfaltz was the first to rationalize and propose a model for the observed enantioselectivities in the diazo-mediated, Cu-catalyzed cyclopropanations.<sup>285</sup> Copper has a strong affinity for the bis-oxazoline ligands. This, in combination with the conformational rigidity and C<sub>2</sub>-symmetry of the catalyst, reduces the number of substrate trajectories and, hence, competing transition states (Figure 53).

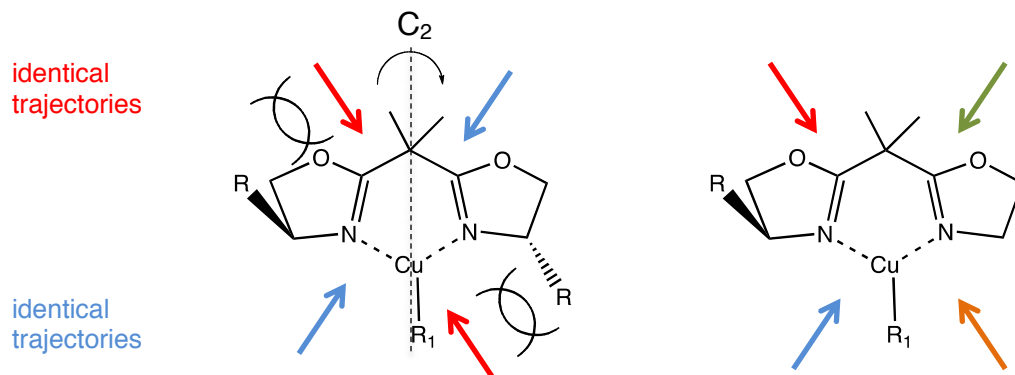


**Figure 54.**  $C_2$ -symmetry and resultant reduction of possible paths and transition states.<sup>285</sup>

Computational work by Fraile *et al*, also indicates a slight deviation of the copper carbenoid carbon bond relative to the  $C_2$  axis, which enhances the enantioselectivity, brought about by the steric interaction between the ester of the diazo group and the chiral functional group on the BOX ligand. Using a simplified model with methyl groups instead of *t*-Bu at the stereo defining 4-position, a copper carbenoid based on methyl diazoacetate, and ethylene, the transition states for the *Re* and *Si* approach were estimated (Figure 54). After accounting for solvent effects, and single-point energy and

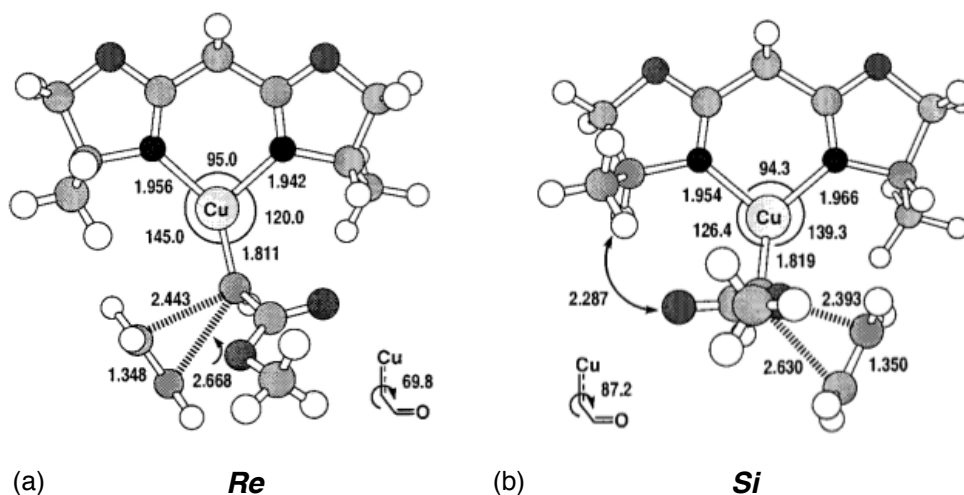


**Figure 53.** Proposed transition states for the simplified methyl BOX ligand in the cyclopropanation step for ethylene attack for the (a) *Re* attack with a dihedral angle of 69.8 and 9b) *Si* approach; dihedral angle 87.<sup>281</sup>

frequency calculations, the computational work demonstrated a significant difference in transition state energies, with *Re* face trajectory favored by 1.3 kcal mol<sup>-1</sup>. These are in good agreement with experimental results. Figure 55 displays the two approaches of an alkene, with the *Si* face favored.<sup>281</sup>

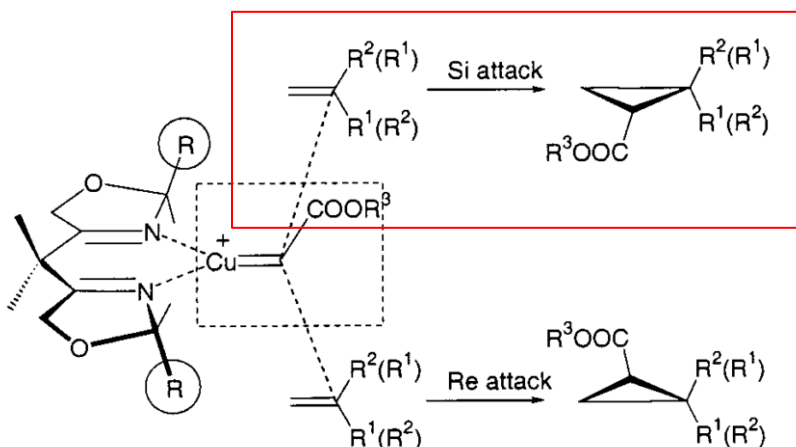


**Figure 55.** Copper carbenoid with alkene attack.<sup>281</sup>

The absolute configuration of the C2 carbon ( $\beta$  carbon), where the *cis/trans* diastereoselectivity is defined, is governed by the steric interaction between the carbene ester group and the R group of the alkene, shown below in Figure 56. The *Si-cis* (b) and *Si-trans* (d) both have unfavorable interactions between the ester carbonyl and the bulky 4-position of the bis-oxazoline. After accounting for single-point, zero-point, solvation energies, and thermal corrections yields an energy difference of 0.2 kcal mol<sup>-1</sup> in favor of the *Re-trans* (c) configuration. Thus, the *trans* selectivity is dictated by the size of functionality on the olefin; consequently, a desired *cis* stereochemical configuration requires the use of a tris(pyrazolyl)borate Cu(I) or Co(II)salen catalyst.<sup>286</sup>

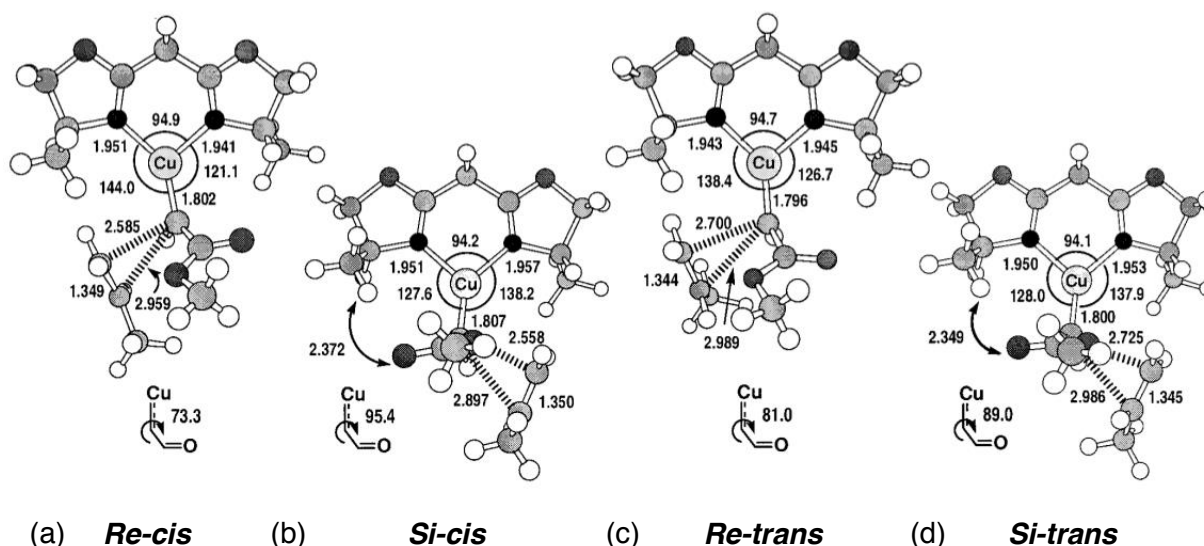


**Figure 56.** The four transition state structures for the propylene addition to bis-oxazoline carbenoid. The two *cis* approaches, (b) and (d), have unfavorable interactions between the oxygen of the carbonyl and *t*-Bu group of the bis-oxazoline. The *Re-trans* (c) is favored over the *Re-cis* (a) approach by 0.2 kcal mol<sup>-1</sup>.

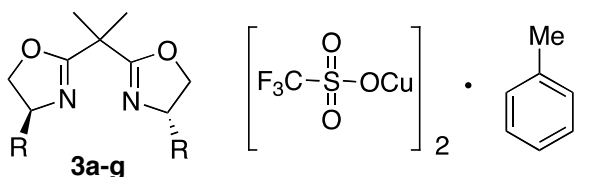
## 5.5 – Bis-oxazolines Experimental

### 5.5.1 – ESI

The following bis-oxazolines (Table 5) were commercially purchased. Copper (I) trifluoromethane sulfonate toluene complex was used as the copper source, purchased from Aldrich. Stock solutions of the ligands were prepared with MeOH and were refrigerated when not in use. Dilutions were made from the stock ligand solution and combined with the copper salt to make final concentrations of approximately 60  $\mu$ M. The catalyst was infused into the instrument via the instrument's syringe pump, at rates varying from 1-5 mL min<sup>-1</sup> using a 500 $\mu$ L Hamilton gas-tight syringe (Hamilton part number 81220) adapted with a luer lock fitting (IDEX PN P659), capillary tubing

(Polymicro Technologies PN 2000021), finger-tight fittings (IDEX PN F120), and capillary sleeves (Upchurch PN F-239) to the ESI probe.

**Table 5.** Bis-oxazolines utilized in study.



**3a-g**

entry	abbrev	R	Z	Enantiomer
3a	A	Bn	Me	<i>S, S</i>
3b	B	<i>t</i> -Bu	Me	<i>S, S</i>
3c	C	Ph	Me	<i>S, S</i>
3d	D	<i>t</i> -Bu	Et	<i>S, S</i>
3e	E	<i>t</i> -Bu	H	<i>S, S</i>
3f	F	<i>i</i> -pro	Me	<i>S, S</i>
3g	G	Ph	Me	<i>R, R</i>

### 5.5.2 – Chiral Probe Introduction

Preliminary runs were accessed with different ratios of internal standard and analytes. The final ratios for the internal standard and chiral neutral reagents were prepared from Table 6:

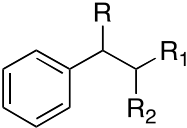
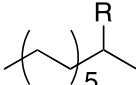

**Table 6.** List of chiral reagents and corresponding internal standards and ratios used during testing of the bis-oxazolines.

Chiral reagent	Internal standard	Ratio chiral reagent/int std	Heat setting / external °C
2-octanol	1-Heptanol	1:3	80 / 165
1-phenyl-1-propanol	Racemic <i>d-ring</i> 1-phenylethanol	1:1	80 / 165
1-phenyl-2-propanol	Racemic <i>d-ring</i> 1-phenylethanol	1:3	80 / 165
1-phenylethanol	Racemic <i>d-ring</i> 1-phenylethanol	1:1	80 / 165

styrene oxide	(2,3-Epoxypropyl) benzene	1.25:1	25 / 65
1,2 epoxybutane	EtOH	1:2	25 / 65
propylene oxide	1-octanol	13:1	25 / 65
2-methoxyoctane	1-heptanol	1:4	80 / 165
1-methoxy ethylbenzene	Racemic <i>d</i> -ring 1-phenylethanol	1:1	80 / 165

The structures for the chiral probes are shown in (Table 7).

**Table 7.** Table of chiral probes utilized in the bis-oxazoline study.

								
<b>1a-d</b>				<b>2a-b</b>		<b>3a-d</b>		
entry	R	R <sub>1</sub>	R <sub>2</sub>	entry	R	entry	R	R <sub>1</sub>
1a	OH	H	H	2a	OH	3a	Me	H
1b	OH	H	Me	2b	OMe	3b	Et	H
1c	H	OH	Me			3c	Ph	H
1d	OMe	H	H			3d	Ph	Me
1e	OBn	H	H					

All chiral reagents and internal standards, except the acyclic ethers, were purchased from various vendors. 2-methoxyoctane and 1-methoxyethylbenzene were synthesized via the Williamson ether synthesis from the appropriate starting materials (see section 5.6). Using a small Eppendorf pipet, the neutral reagent was weighed into a pre-tared 1.5 mL capped-vial. After recording the weight, the balance was re-tared and the internal standard was pipetted to the vial and weighed. It was then diluted to 1.25 mL by the addition of the appropriate amount of hexanes and mixed. These were prepared fresh daily to attain estimates of daily variation.

The neutral reagent mix was infused into the manifold at a rate between 60-240  $\mu\text{L hr}^{-1}$ , with a diameter setting of 2.3 mm on the syringe pump. A 250  $\mu\text{L}$  gas-tight syringe (Hamilton PN 81130) was used and inserted into the manifold via a septum (Supelco part number 20652), such that the metal syringe needle was approximately 0.9 cm from the metal of the heated manifold.

Heating was required for the introduction of the alcohols and open-chain ethers, with the heat settings shown in Table 6. The heat was measured by placing a thermocouple between the heating tape and manifold, not to obtain absolute readings, but rather as a point of reference for controlling the temperature variability. Using this and the Variac controller, temperature variation was reduced to  $\pm 5^\circ\text{C}$ . A flow rate of 1.25 SLM of helium in the manifold was used for all runs. The pressure was maintained around 17.2-17.9 psi in the gas-mixing manifold. When the run was complete, the manifold was evacuated, by placing it under vacuum at approximately 150 mtorr. This led to evacuation times up to 1 hour for the alcohols.

### **5.5.3 – Mass Spectrometer Settings**

ESI conditions ranged between 3.5-5 kV for the capillary voltage, with a temperature range of 100-150  $^\circ\text{C}$ . The nitrogen sheath gas flow rate was 10 arbitrary units. All conditions were optimized via the software's auto-tune function.

### 5.5.3.1 – Mass Selection

Since copper has two stable isotopes,  $^{63}\text{Cu}$  (69%) and  $^{65}\text{Cu}$  (31%), it leads to a distinct MS pattern. In earlier work, the whole isotopic range was isolated, but it was later decided to isolate only the higher isotope by way of a broadband, notched waveform, with a narrow isolation width of 0.8-1.0 m/z. This led to less signal, but cleaner spectra, with less interference from impurities (see below).

### 5.5.3.2 – Scan Activation

To ensure equilibrium, the scan activation time method was utilized. The reaction time was scanned from 2-10 seconds, with 0.5 second step times. An excellent example is illustrated in Figure 57. Catalysts C and G are enantiomers, as are *R/S* 1-phenyl-2-propanol, thus, two of the four possible plots should be equal, as was the case. The plots for the homo-couplings, e.g., *R* catalyst with *R* alcohol, are identical, as are the hetero-couplings (*R* catalyst with *S* alcohol). The plots for the homo/hetero coordinated complexes plateau after 4.5 seconds and display significant selectivity.



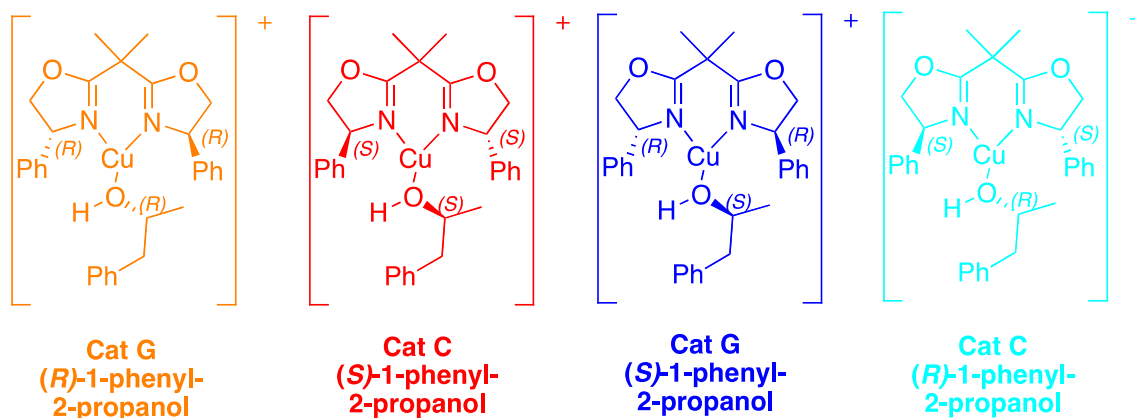
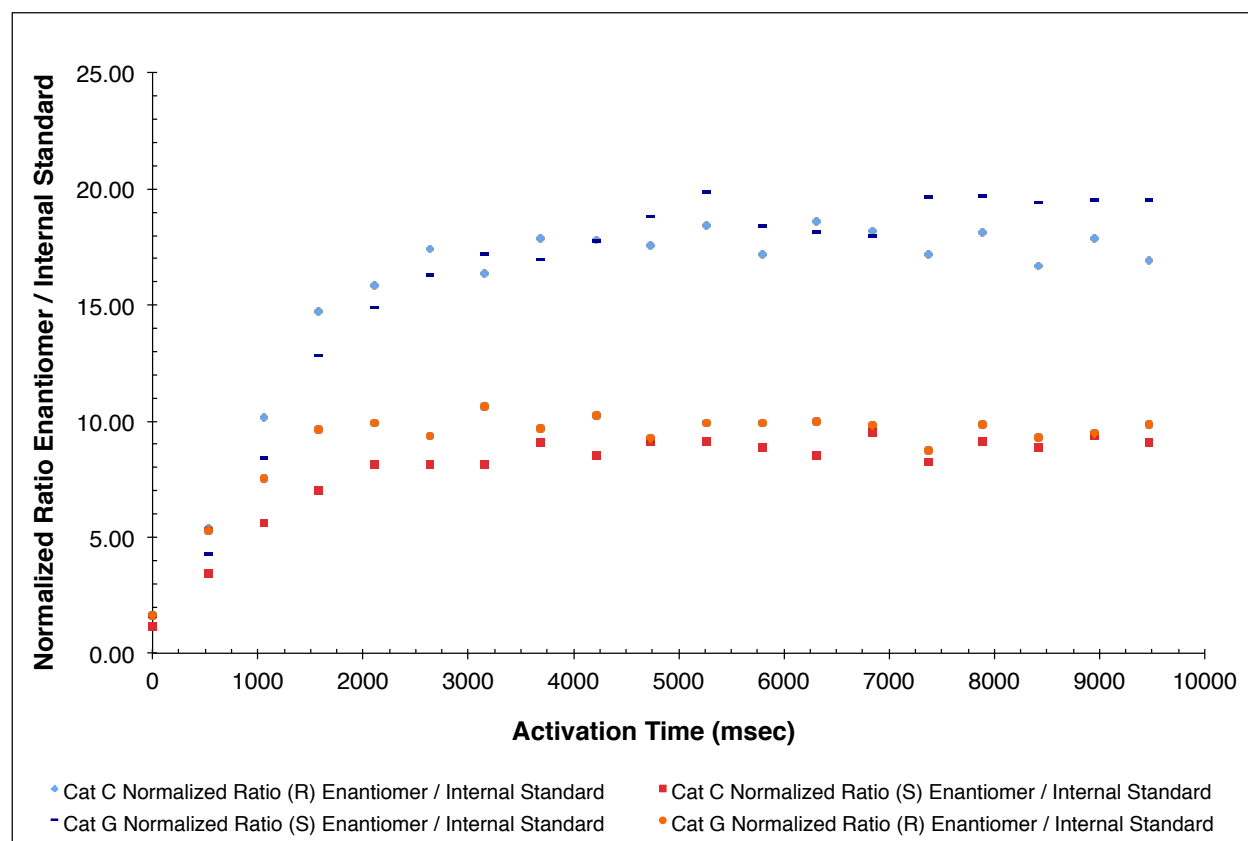


**Figure 57.** Scan activation time with catalysts C and G (enantiomers) and 1-phenyl-2-propanol. The homo-couplings are identical, as are the hetero-couplings.

This scan activation time experiment was performed for all catalysts and chiral probes to determine the time required for equilibrium. The concentration or infusion rate was typically adjusted to yield equilibration times of around 2-3 seconds.

### 5.5.3.3 – Data Collection and Analysis

The bis-oxazoline ligand and copper solution were mixed and infused into the ion-trap via ESI. Figure 58 displays a typical MS of a catalyst system before ion isolation.

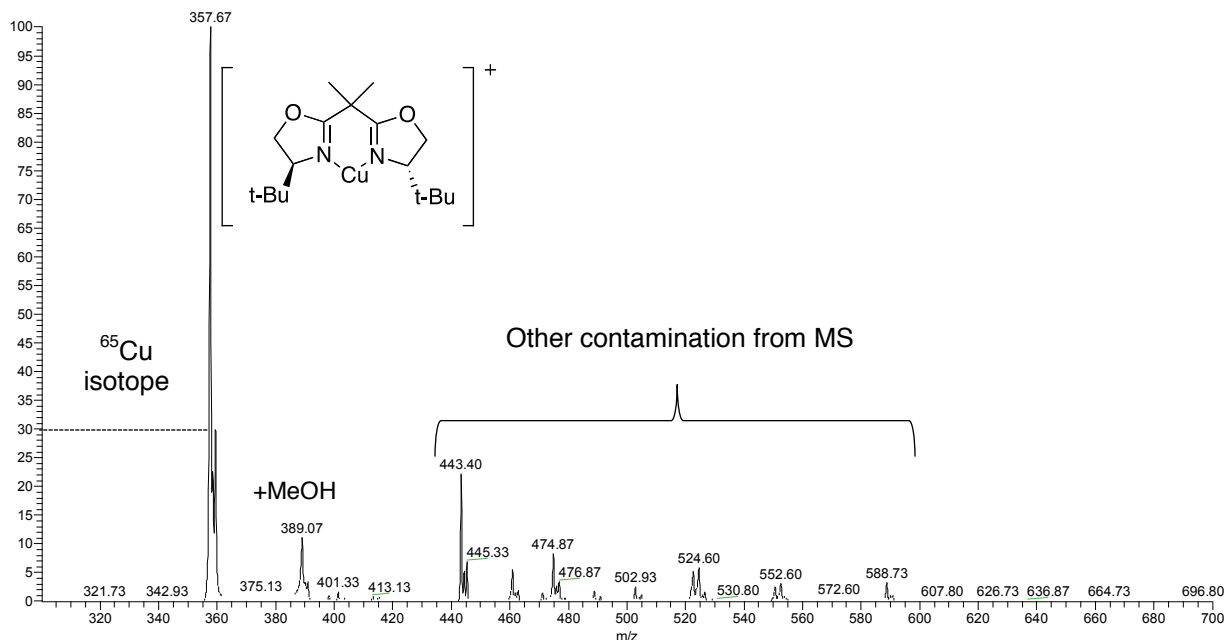


**Figure 58.** Bis-oxazoline catalyst B before isolation.

To isolate the catalyst ion, a wide isolation window was utilized to capture both copper isotopes (5  $m/z$ ), with a scan range between 100-1000  $m/z$ , and a  $q$ -value of 0.25. After ion isolation, a clean MS is obtained, as shown in Figure 59.

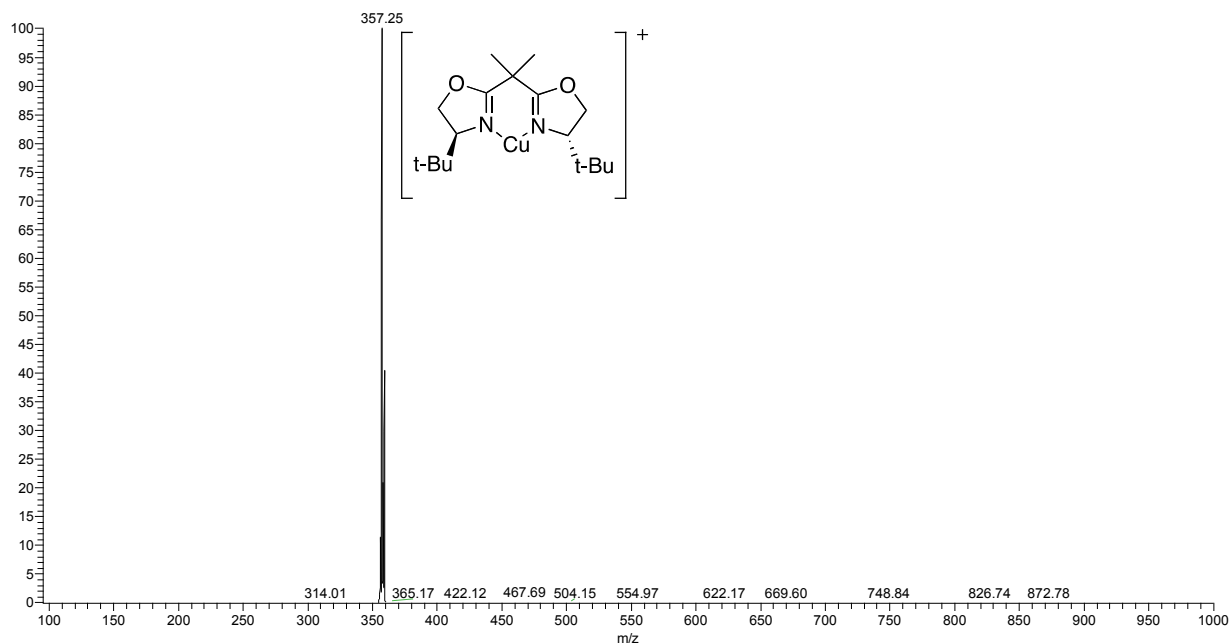


**Figure 59.** Catalyst B after ion isolation.

The chiral probe and internal standard are allowed to flow into the gas-handling manifold and a reaction time is set to reach equilibrium. Figure 60 provides an example of catalyst (B) with (*R*)-1-phenylethanol and racemic *d*<sub>5</sub>-ring 1-phenylethanol at equilibrium.

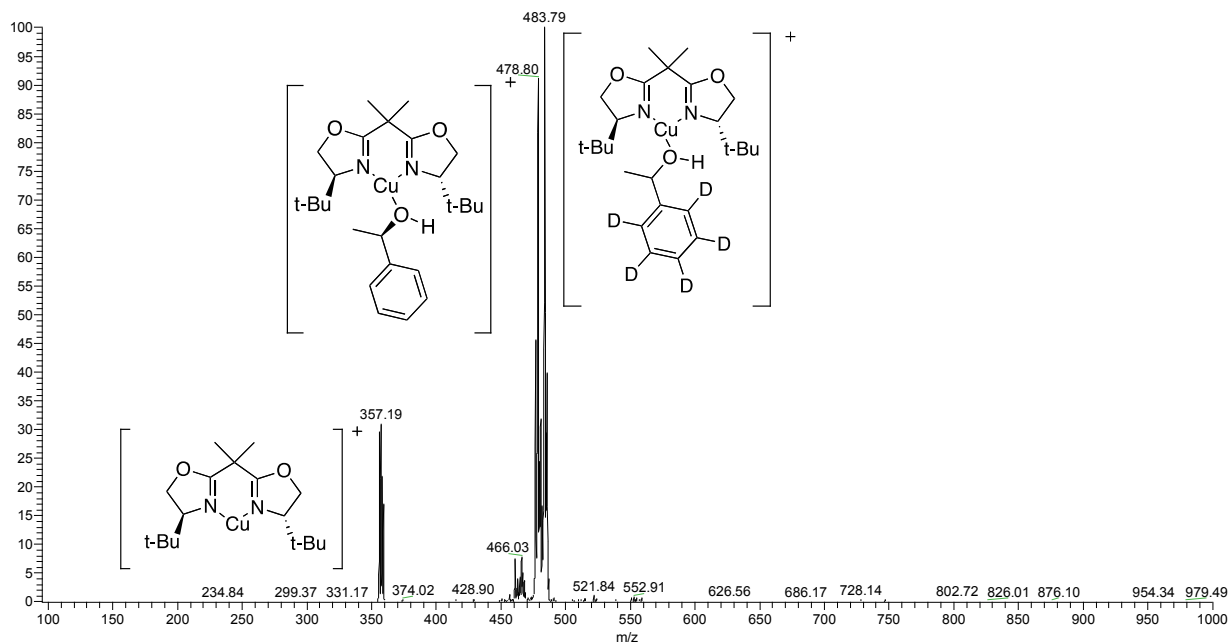


**Figure 60.** Catalyst B after equilibrium with the chiral probe (*R*)-1-phenylethanol and the internal standard, *d*-ring 1-phenylethanol.

Isolation of both copper isotopes affords a complicated spectrum. For reasons to be discussed later, the  $^{65}\text{Cu}$  isotope bis-oxazoline complex was selected for isolation using a narrow isolation width of 0.8-1 m/z. All other controllable conditions remained constant. Figure 61 clearly displays a much cleaner spectrum when isolating the higher isotope peak.

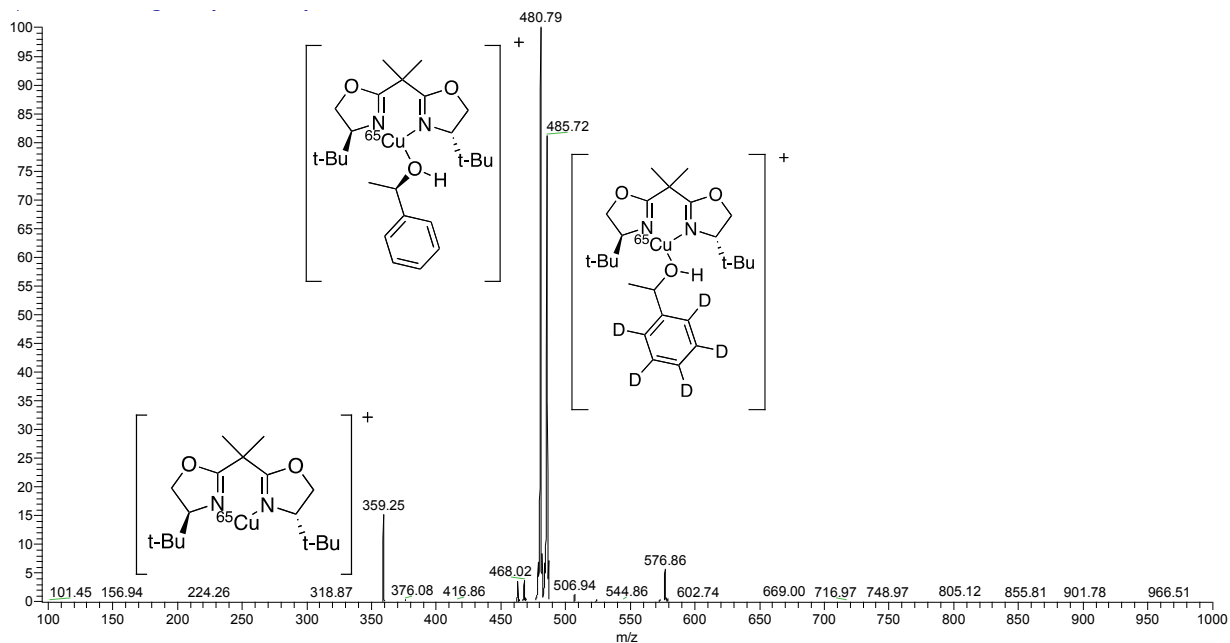


**Figure 61.** Catalyst B after isolating the  $^{65}\text{Cu}$  isotope and allowing equilibrium with the chiral probe (*R*)-1-phenylethanol) and the internal standard,  $d_5$ -ring 1-phenylethanol.

For each catalyst and enantiomer, at least 250 scans, usually 500, were collected. The results were exported into an excel spreadsheet, where a macro was built to automate the process of summing the peaks (peak area) of the desired mass range, which included the catalyst, catalyst-probe, and internal standard. The equilibrium constant,  $K_x$ , was calculated from the following formula:

$$K_x = \left( \frac{\text{peak area neutral}}{\text{peak area int std}} \right) \times \left( \frac{[\text{int std}]}{[\text{neutral}]} \right) \quad (1)$$

where  $K_x$  is the equilibrium constant for either the (*R*) or (*S*) enantiomer and int std is the internal standard. The total scans were divided into five separate groups to obtain a measure of the relative standard deviation (RSD) for the runs. The process was repeated for the (*S*) enantiomer (Figure 62), at which point the selectivity factor,  $K_{R/S}$ , was calculated. This was re-run for a total of at least three separate days with fresh

daily preps to minimize random variability. The average daily results for the three (or more) days were averaged and the standard deviation and percent RSD calculated.

The Gibbs free energy of binding may also be extracted from the data in a series

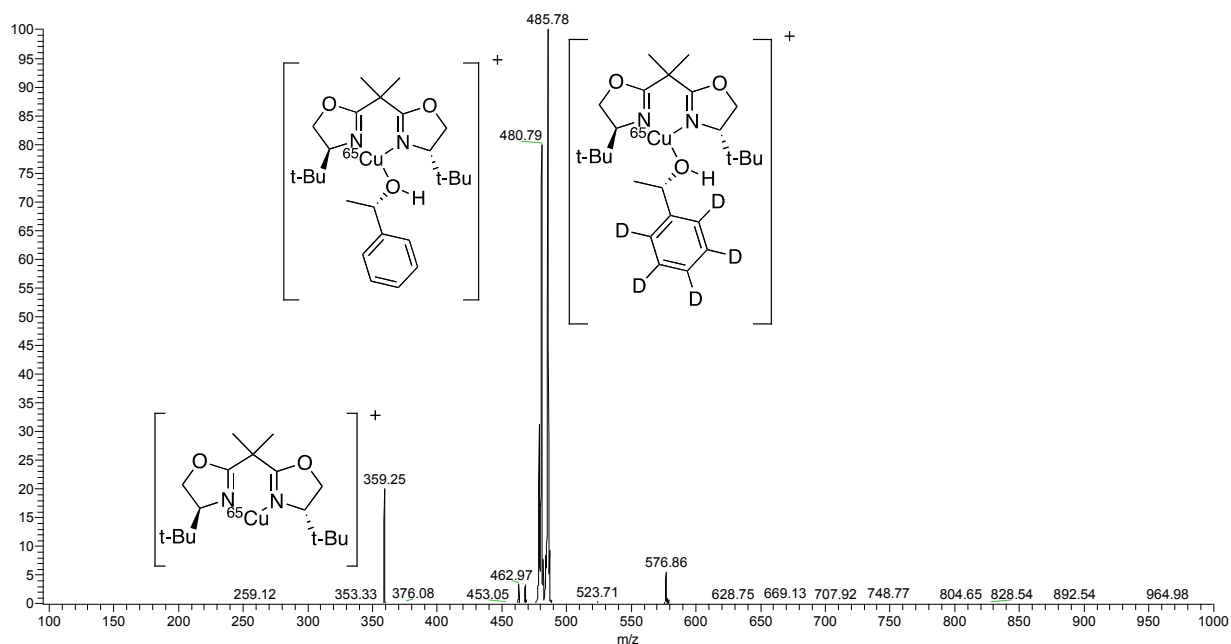
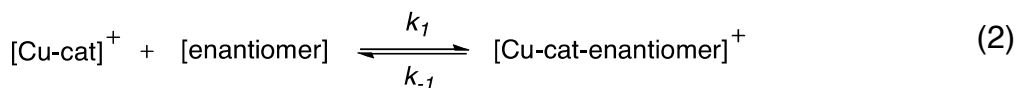


**Figure 62.** Catalyst B after isolating the  $^{65}\text{Cu}$  isotope and allowing equilibrium with the chiral probe (*S*)-1-phenylethanol) and the internal standard, *d*-ring 1-phenylethanol.

of calculations, starting from the following equilibrium:



whence:

$$K = \frac{[\text{Cu-cat-enantiomer}]^+}{[\text{enantiomer}][\text{Cu-cat}]^+} \quad (3)$$

and:

$$\Delta G^\circ = -RT \ln K \quad (4)$$

The intensities (abundances) of both Cu-catalyst complexes are obtainable from

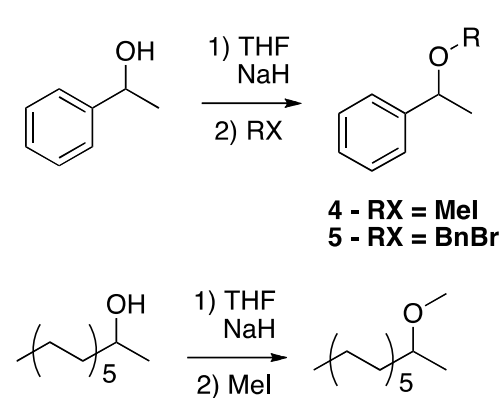
the mass spectra, but the concentration of the enantiomer must be calculated. This may be acquired by recalling equation (1) from Chapter 3:

$$[\text{enantiomer}] = P_R = P_{IT} \times \frac{F_R}{F_{He}} \times \frac{d_R}{MW_R} \times \frac{(MW_R)^{1/2}}{4} \quad (5)$$

where  $P_{IT}$  is the pressure inside the trap when 3 psi of helium pressure is applied,  $F_R$ ,  $d_R$ , and  $MW_R$  are the flow rate, density, and molecular weight of the reagent, respectively, and  $F_{He}$  is the flow rate of the helium (moles/min). Reactions with known rate constants are run, usually MeI and Br<sup>-</sup>, to calibrate the instrument (i.e., to obtain the ion-trap pressure correction).<sup>238</sup>

## 5.6 – Synthesis of Ethers

Chiral ethers were not commercially available, so they were synthesized via the Williamson ether synthesis shown in Scheme 34. Chiral alcohols served as the starting



materials for the ethers. The starting materials were added to the THF and cooled to 10 °C. The NaH, 0.9 equ. was slowly added (so as not to racemize the new chiral center), and allowed to sit for 20 minutes. The alkylating reagent was slowly added, so as not to exceed 30 °C, after which the

**Scheme 34.** Synthesis of the chiral ethers. reaction was allowed to sit at room temperature for 3 hours. Water was added dropwise to quench any remaining NaH. KOH was added to remove unreacted starting material, followed by diethyl ether. The two layers were

separated and the aqueous layer extracted again with diethyl ether. The two organic layers were combined and dried over  $\text{MgSO}_4$ . After decanting, the diethyl ether was removed on a rotary evaporator and the material placed in a vial. Column chromatography was attempted for 1-methoxyethylbenzene, but did not result in an improvement of the purity. The sample was used in this form and the data corrected based on chiral GC analysis. The 2-methoxyoctane was used without further purification and preliminary screening of the benzyl ether showed no binding to the copper catalyst, most likely due to the large bulk of the benzyl group.

## 5.7 – Results

### 5.7.1 – General Results

Results for the bis-oxazolines are presented graphically in Figure 63 grouped by chiral probe, and in Figure 64, where they are grouped by catalyst. The black line represents the selectivity factor,  $K_{R/S}$  (the ratio of the enantiomers equilibrium constants) of 1, or no selectivity. Values greater than 1 favor the (*R*) enantiomer, while values less than 1 favor the (*S*) enantiomer. Error bars are standard deviations for the averages.



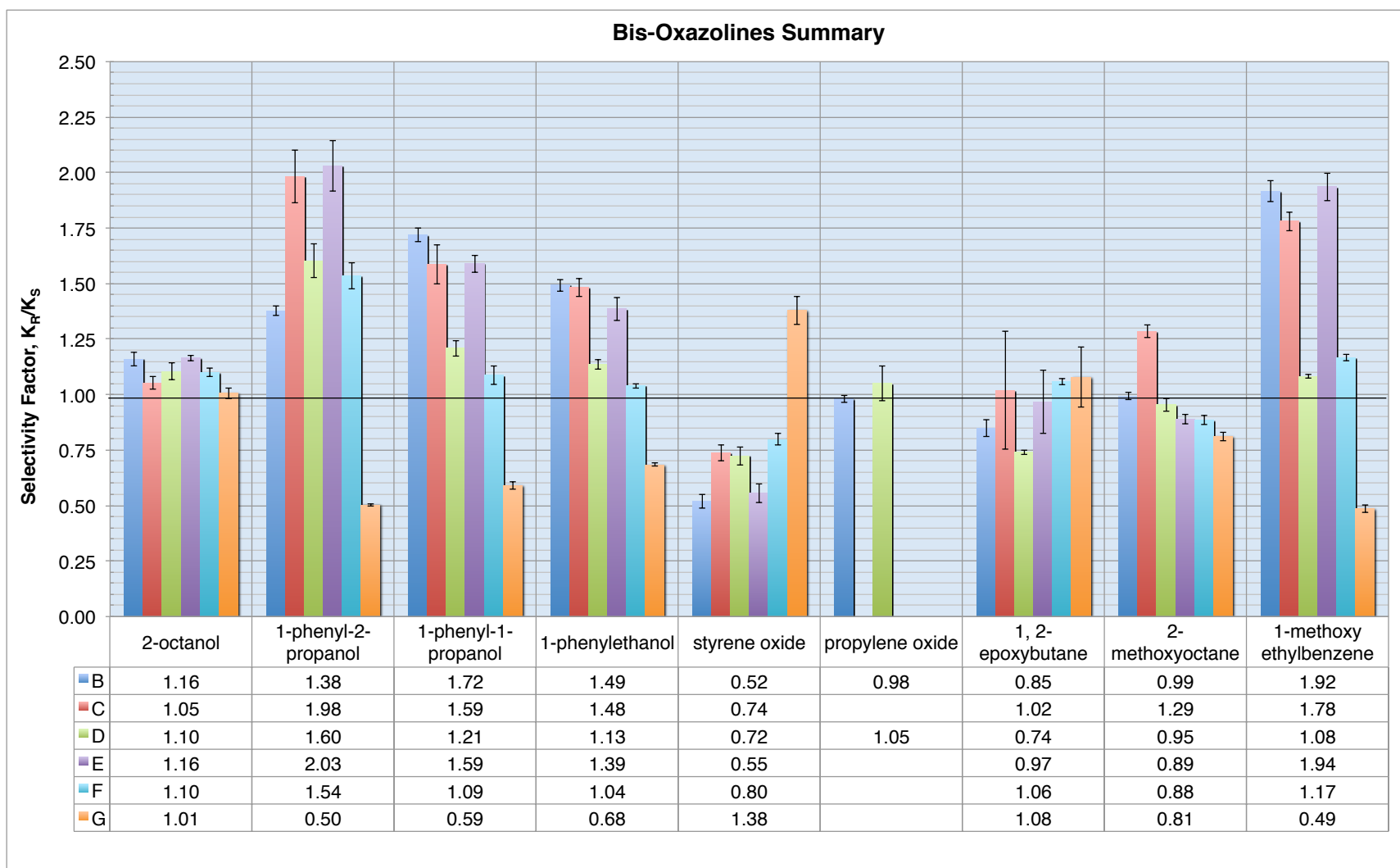
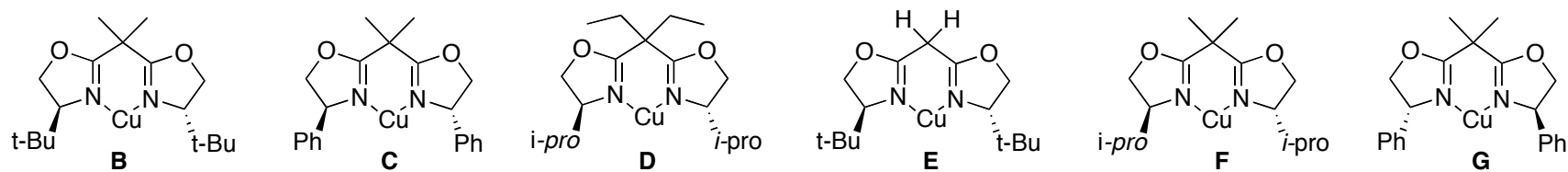


**Figure 63.** Summary of results for the bis-oxazolines. Grouped by chiral probe. The line in black represents no selectivity.

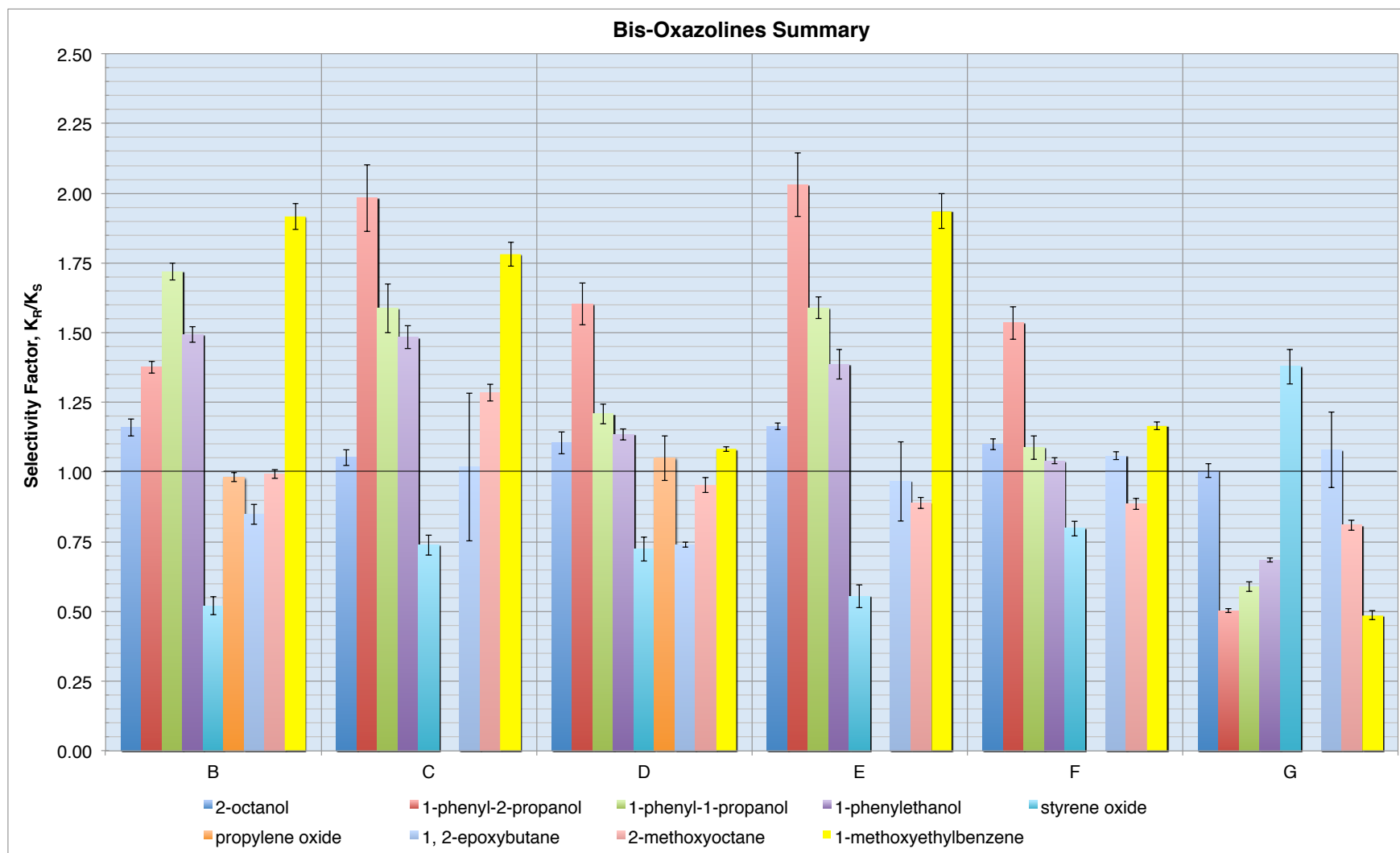


**Figure 64.** Summary of results, grouped by catalysts. The black line represents no selectivity.

#### 5.7.1.1 – Diastereomeric Excess

The selectivity factors may be converted to diastereomeric excess. Figure 65 and Figure 66 presents the data as the absolute value of the percent diastereomeric excess, which is easier to work with when absolute stereoexcess is not a concern. The DE range was from 0 - 34%. While not overly impressive for a condensed-phase transformation, 34% represents a very large number for a gas-phase complexation product, where the lack of solvent, counter-ion coordination, trigonal planar copper coordination, room temperature (excess energy), and lack of rigid transition-state all tend to reduce enantioselectivity.<sup>36, 287</sup>

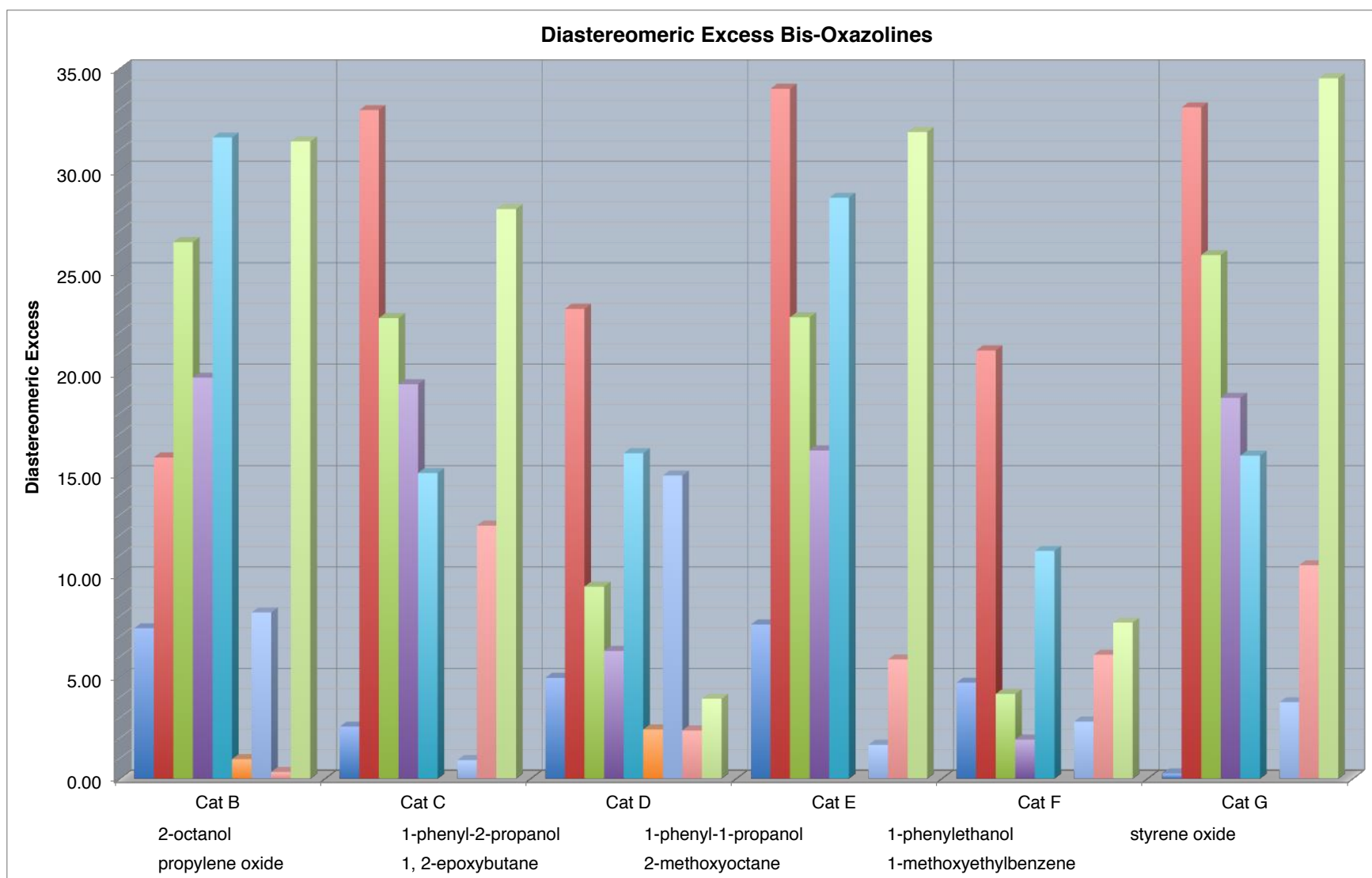


**Figure 65.** Results presented as diastereomeric excess, grouped by catalyst.

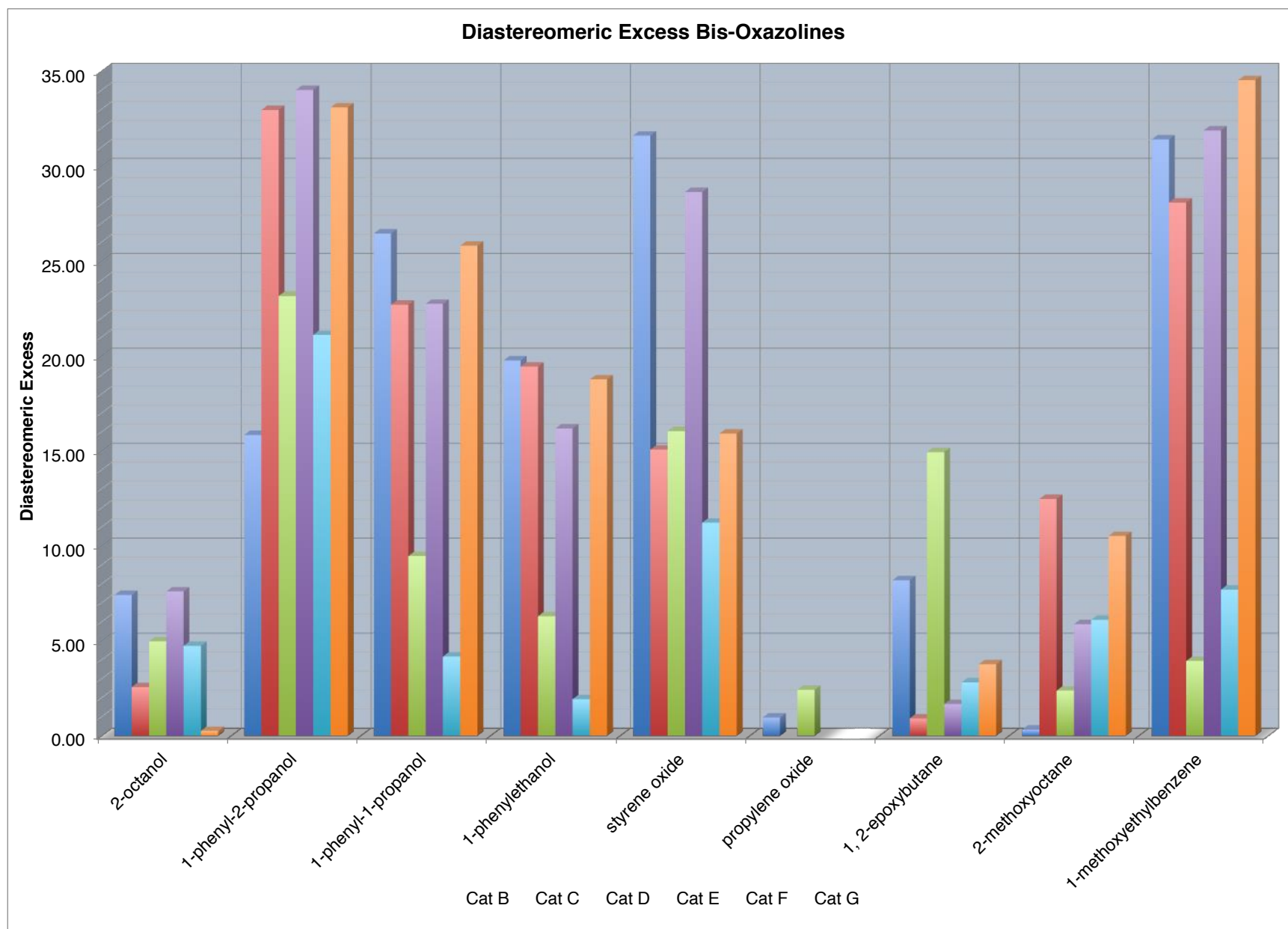
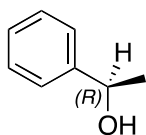
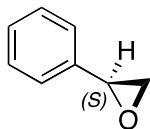


**Figure 66.** Results as percent DE, grouped by chiral probe.

Not surprisingly, the larger the group, the more selectivity (in general) was observed. The trend follows 2-octanol < 1-phenylethanol < 1-phenyl-1-propanol < 1-phenyl-2-propanol for the alcohols; propylene oxide < 1,2 epoxybutane < styrene oxide for the epoxides; and 2-methoxyoctane < 1-methoxyethylbenzene for the ethers (the benzyl ether was too big to coordinate). A phenyl group appears to be necessary to deliver good selectivity, either adding necessary bulk and/or possibly increasing stabilization factors such as  $\pi$ -cation interactions. It is notable that the *R* enantiomer was favored for most of the chiral reagents, with the exception being styrene oxide, where the *S* enantiomer was preferred. This switch from *R* to the *S* enantiomer is due to



**(*R*)-1-phenylethanol**



**(*S*)-Styrene Oxide**

**Figure 67.** Orientation of (*R*)-1-phenylethanol and (*S*)-styrene oxide.

the change in priorities of the groups (Cahn-Ingold-Prelog),<sup>288</sup> and not a change in the orientation preference around the stereocenter of the catalyst (Figure 67). Catalyst G, also displayed a preference for the *S* enantiomer,

however, this is expected due to the enantiomeric relationship between G and C (Figure 68).

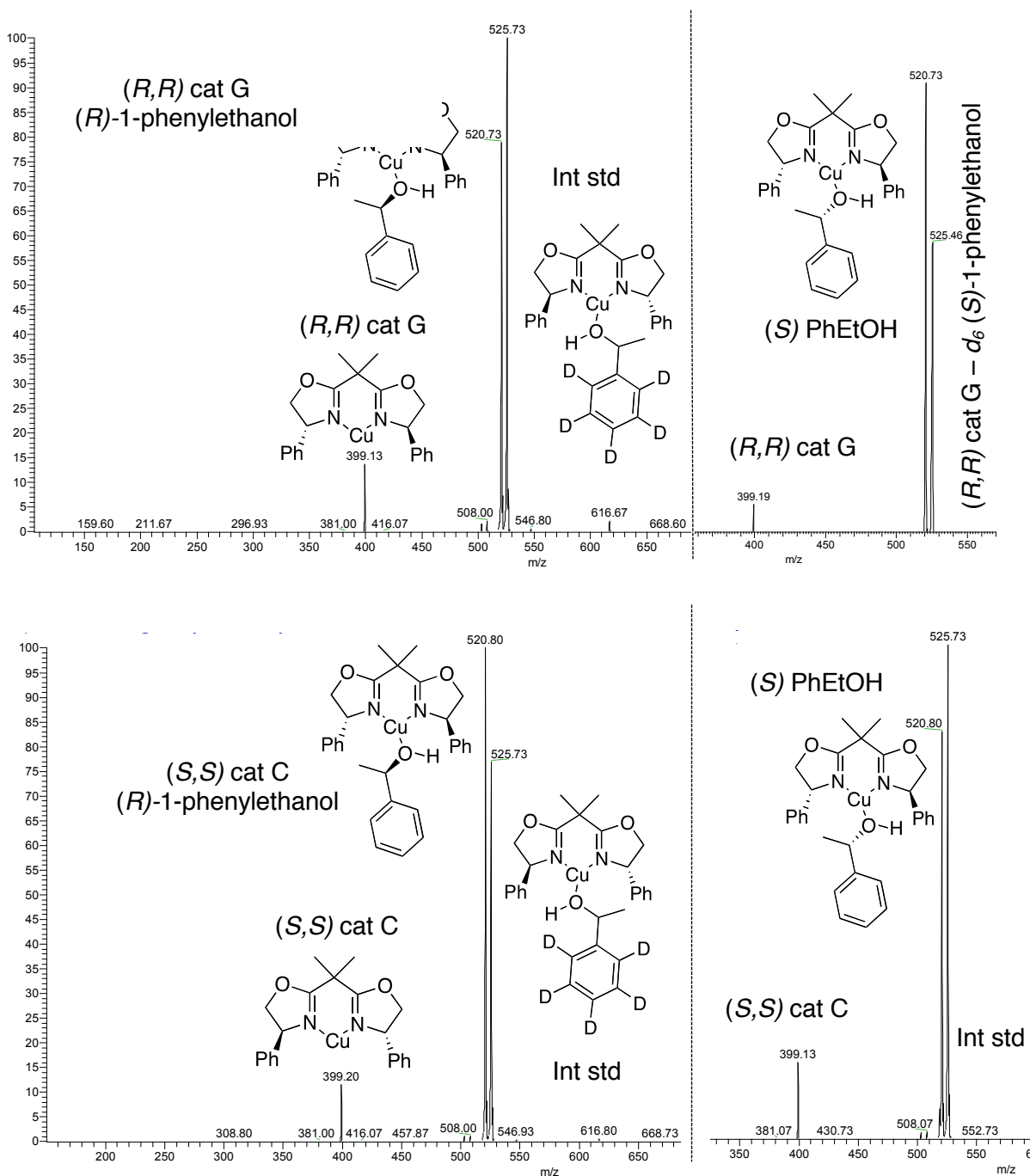
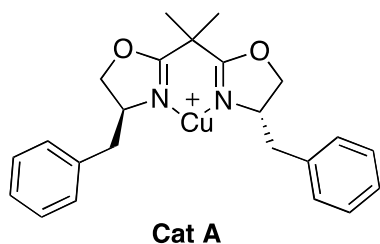


**Figure 68.** Catalysts G and C with 1-phenylethanol. The homo-couplings are similar as are the hetero-couplings.

Modifications as small as an extra carbon, for example 1-phenyl-1-propanol and 1-phenylethanol can have profound effects. Selectivity significantly increased when switching the alcohol group from the 1 position to 2 for all catalysts except B, where it

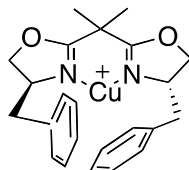
significantly decreased. Likewise, for the two results obtained for propylene oxide, where no selectivity was observed, adding an extra carbon (forming 1,2-epoxybutane), significantly increased selectivity. This is also observed in the etherification of 1-phenylethanol, upon which the selectivity drastically improves for B, C, E, and G, while decreasing for D and F. Alkylation of 2-octanol to 2-methoxyoctane increased selectivity of the phenyl-bearing groups (catalysts C and G), while decreasing selectivity in others, specifically catalyst B, where selectivity disappeared.

This effect can be observed in the catalyst as well, when the change occurs near the stereocenter. For example, catalyst A, with a benzyl group instead of a phenyl, was found not to coordinate to any of the chiral molecules. This is most likely due to the fact



**Cat A**

**Figure 69.** Structure of catalyst A.



the extra CH<sub>2</sub>- group allows the phenyl ring the freedom to coordinate to the copper metal, blocking access to metal for the other chiral reagents (Figure 69).

### 5.7.1.2 – Average Selectivity for Groups

The average selectivity factor for each probe was calculated by taking the natural log of each value, averaging the values, then converting back to the non-log value, via the natural exponential, *e* (Figure 70). The best chiral probe was the 1-phenyl-2-propanol followed closely by styrene oxide, then 1-phenyl-propanol, and 1-phenylethanol. The other, non-phenyl based probes displayed little selectivity.



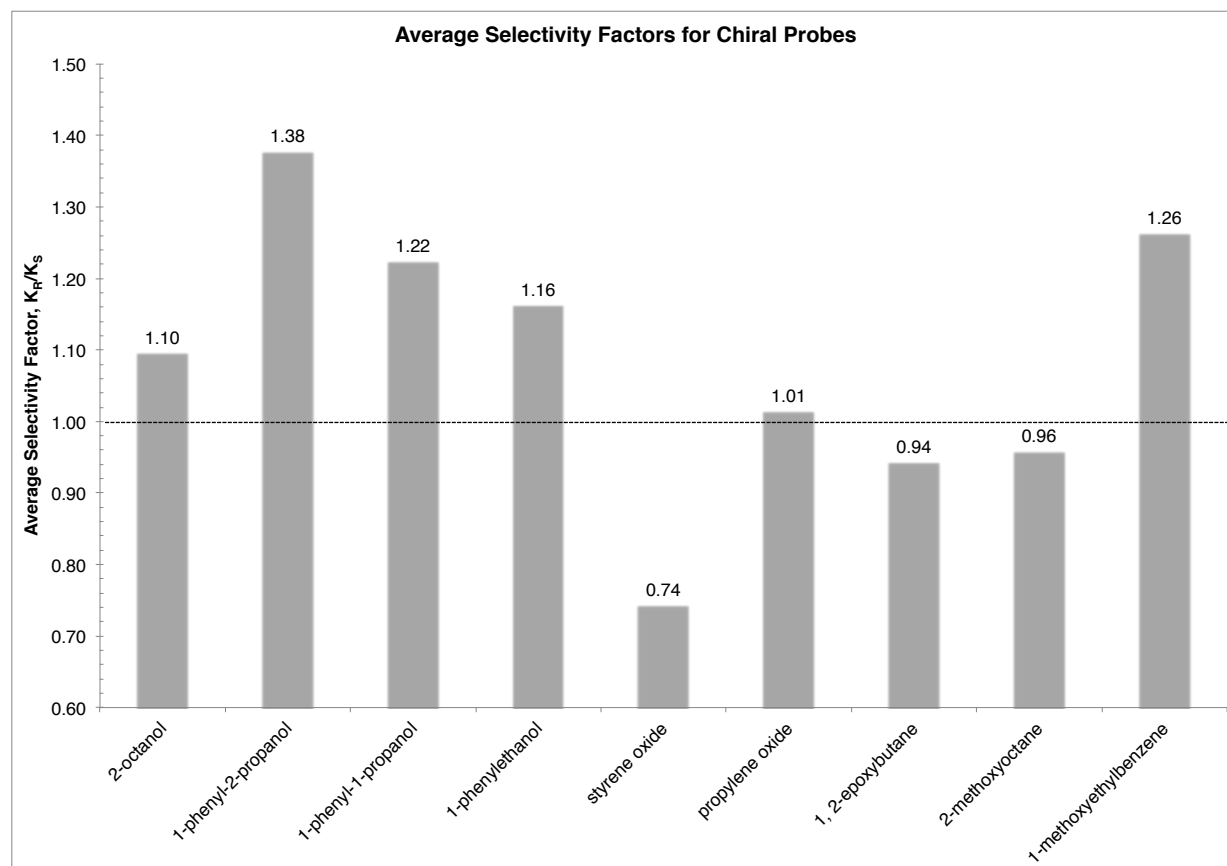


**Figure 70.** Average selectivity factor for each chiral probe.

It appears the 1-phenyl-1-propanol and 1-methoxyethylbenzene give the best selectivity over a range of catalysts. For example, these both displayed excellent selectivity with the *t*-Bu and Ph-bearing catalysts B, E C and G, while the 1-phenyl-2-propanol and styrene oxide gave the best selectivity overall. It is noteworthy that while these gave the higher selectivity, not all catalysts were selective, for example catalyst B gave much lower selectivity for 1-phenyl-2-propanol than the similar catalyst E; styrene oxide also displayed lower selectivity for the phenyl bearing catalyst (C and G).

An average was also calculated for the catalyst groups and is shown below (Figure 71). Not surprisingly, the larger the group at the stereo-bearing center, the better

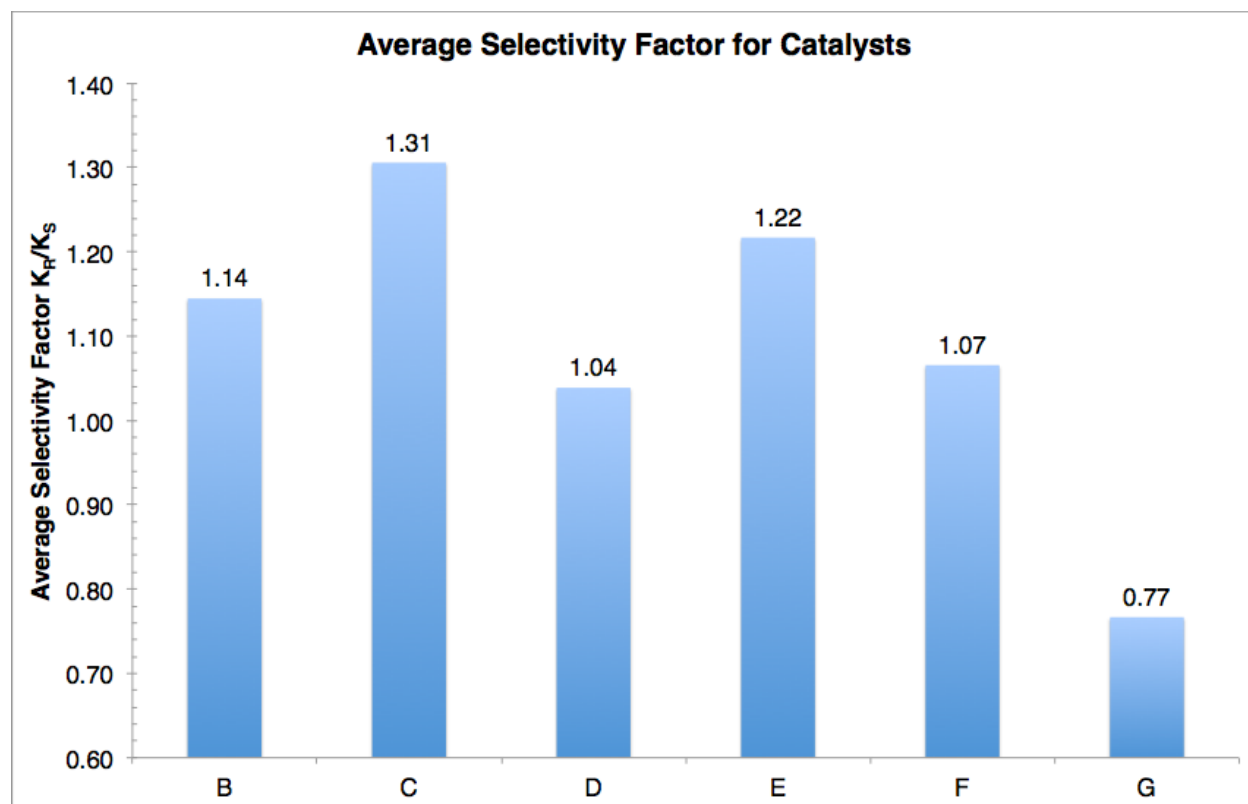


**Figure 71.** Average selectivity factor for catalysts.

the selectivity observed, with the *t*-Bu and Ph groups (B, E, C, and G) providing much better selectivity than the *i*-pro catalysts (D and F). Catalyst E's selectivity is somewhat surprising; given that the literature generally shows this to be inferior to the *t*-Bu and Ph bearing counterparts.

### 5.7.1.3 – Distal Modifications

Modifications at the methylene bridge, or distal modifications, do not have a significant effect on the stereoselectivity of cyclopropanation reactions in the condensed phase, and as such, should have no impact on the enantioselectivity observed in the gas-phase.<sup>287</sup> Figure 72 shows this to be the case, as only 1-phenyl-2-propanol and 1,2 epoxybutane displayed a significant change when shifting the bridging methylene substituents from a methyl (B) to a hydrogen (E) or a methyl to an ethyl (F). Counter-intuitively, the smaller groups provided much better enantioselectivity than the larger

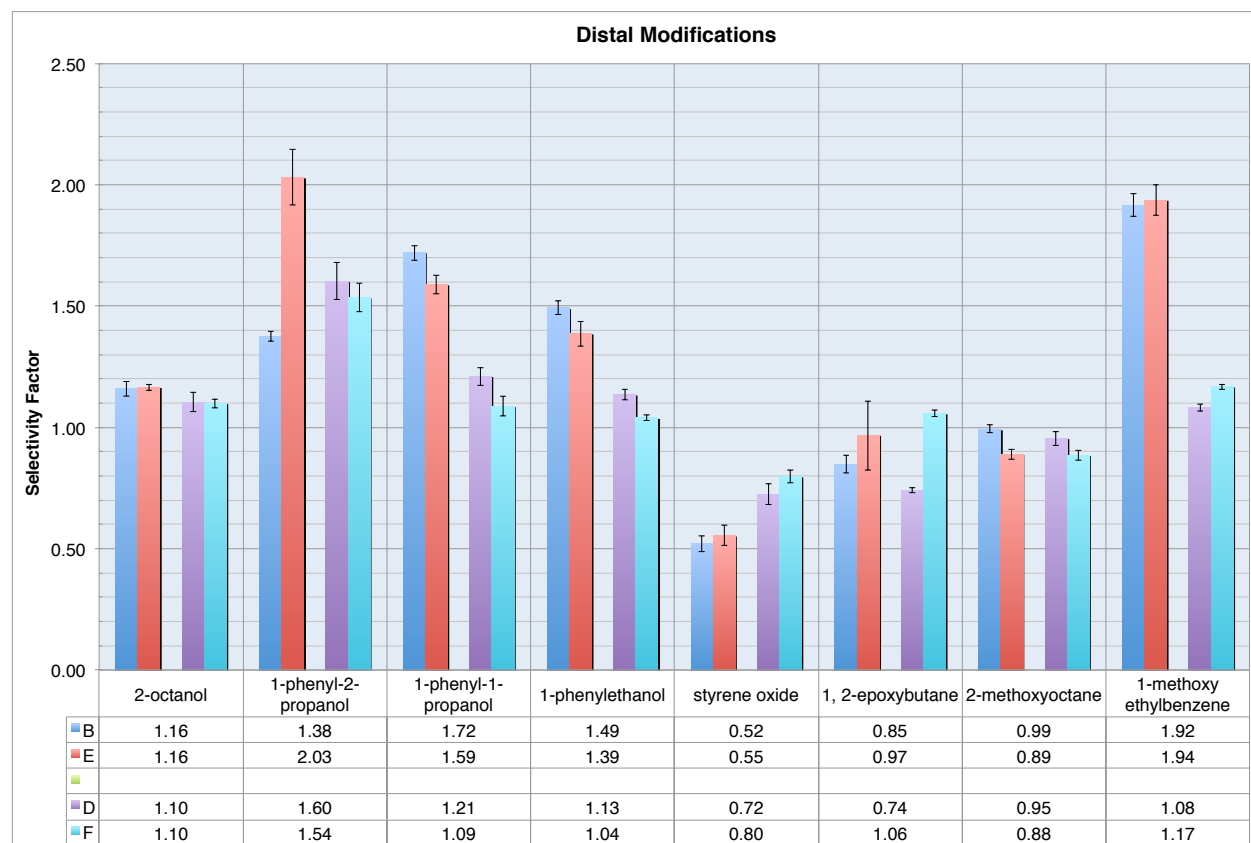


**Figure 72.** Distal modification to the bis-oxazoline scaffold and resultant effect on the selectivity. Only two results displayed significant differences, circled in red.

groups with 1-phenyl-2-propanol and 1,2 epoxybutane. It is presumed that this change

in the bridge may have altered the chiral environment of the catalyst and the 1-phenyl-2-propanol molecule was more sensitive to this change than the other probes.

#### 5.7.1.4 – Gibbs Free Energy

Using equations 2-4, the Gibbs free energy of binding was calculated and tabulated in Table 8. The  $\Delta G$  was based on the most tightly-bound enantiomer.

**Table 8.** Gibbs free energy of binding for the complexes (kcal/mol).

	2-octanol	1-phenyl-2-propanol	1-phenyl-1-propanol	1-phenyl ethanol	styrene oxide	1,2 epoxybutane	propylene oxide	2-methoxyoctane	1-methoxy ethylbenzene
B	-11.8	-12.4	-12.1	-11.6	-10.7	-7.7	-7.8	-11.5	-11.0
C	-12.4	-12.8	-12.1	-11.9	-10.9	-9.4		-12.2	-11.9
D	-12.3	-12.7	-11.9	-12.2	-10.9	-9.3	-9.0	-12.4	-11.5
E	-12.5	-12.5	-12.2	-11.6	-11.4	-10.1		-12.3	-13.4
F	-12.0	-12.2	-11.5	-11.8	-9.2	-11.4		-13.6	-13.0
G	-12.4	-12.7	-11.5	-11.7	-10.8	-9.5		-12.9	-12.9

In general, the larger the probe molecule, the higher the free energy of binding, most likely due to the greater polarizability. This is illustrated Figure 73 using the molecular weight as a general gauge of polarizability.

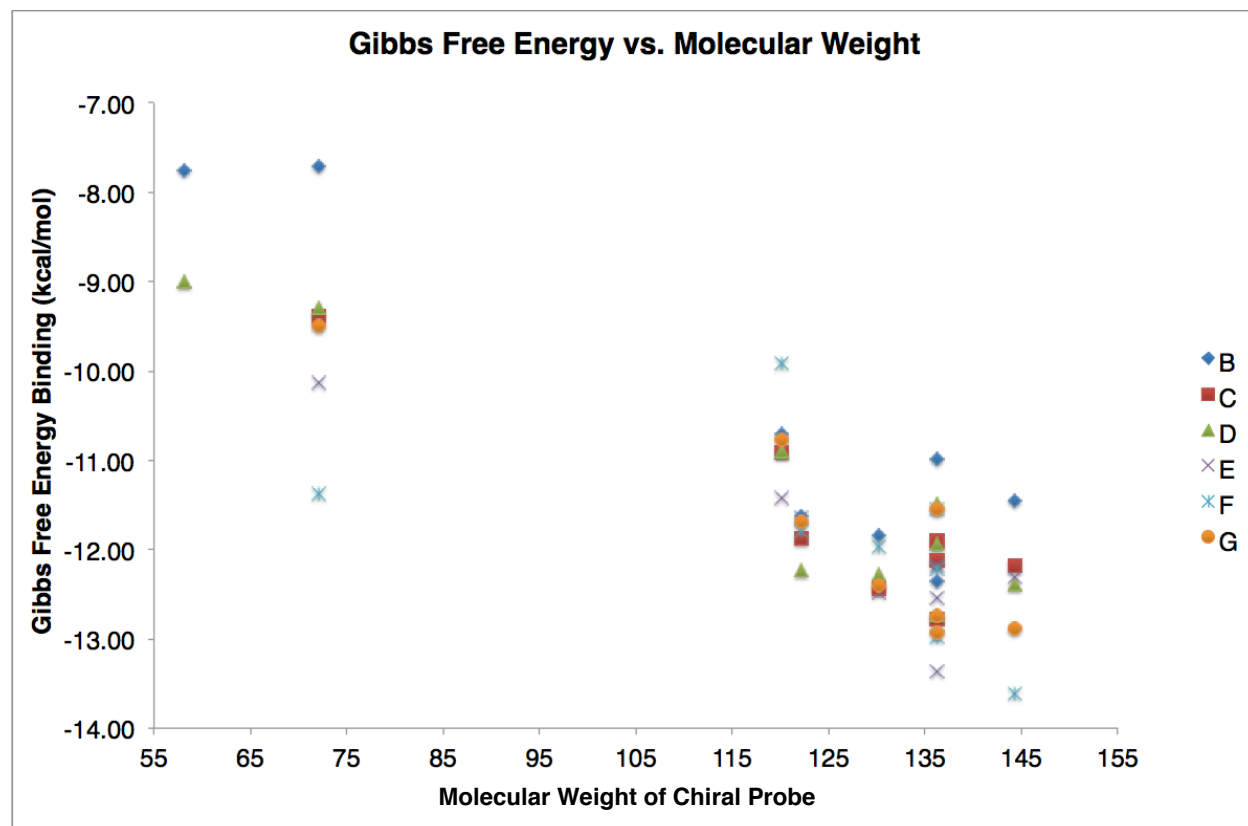


**Figure 73.** Plot of Gibbs free energy versus chiral probe molecular weight.

Also evident was the decreased basicity of the epoxides, due to the reduced C-O-C bond angle, as they displayed significantly smaller  $\Delta G$  of binding than the alcohols and acyclic ethers. This is most clearly pronounced when comparing the  $\Delta G$  for styrene oxide and 1-phenylethanol. Both have similar molecular weights, 120 g/mol for styrene oxide versus 122 g/mol for 1-phenylethanol, but styrene oxide has significantly smaller binding energies.

## 5.8 – System Checks and Variability

### 5.8.1 – RSD

The relative standard deviation is a measure of the variability and scatter of the results and is found by dividing the standard error by the average of the results, and multiplying by 100. The RSDs of the data are presented below in Figure 74 and Figure 75 grouped by the chiral probe and catalysts, respectively.

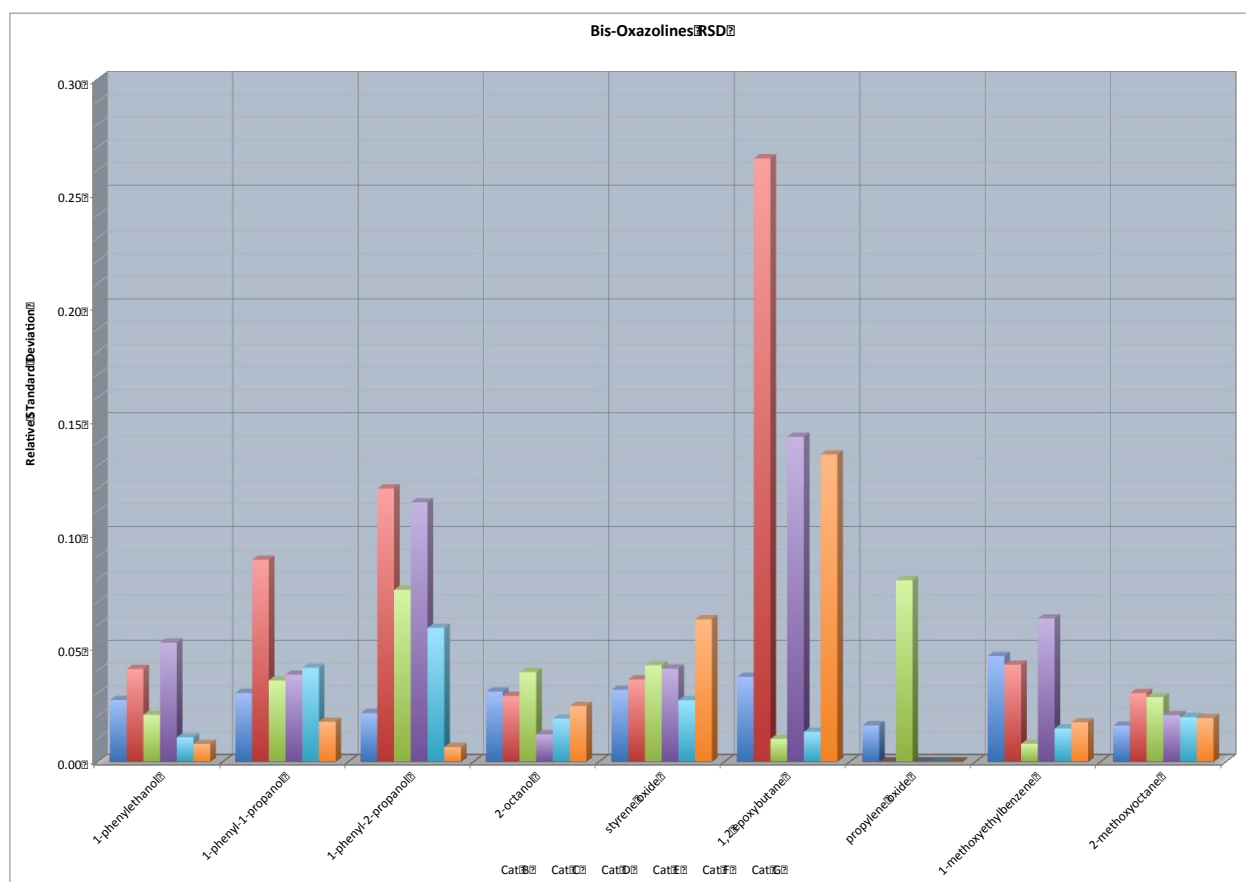


**Figure 74.** RSD grouped by probe.

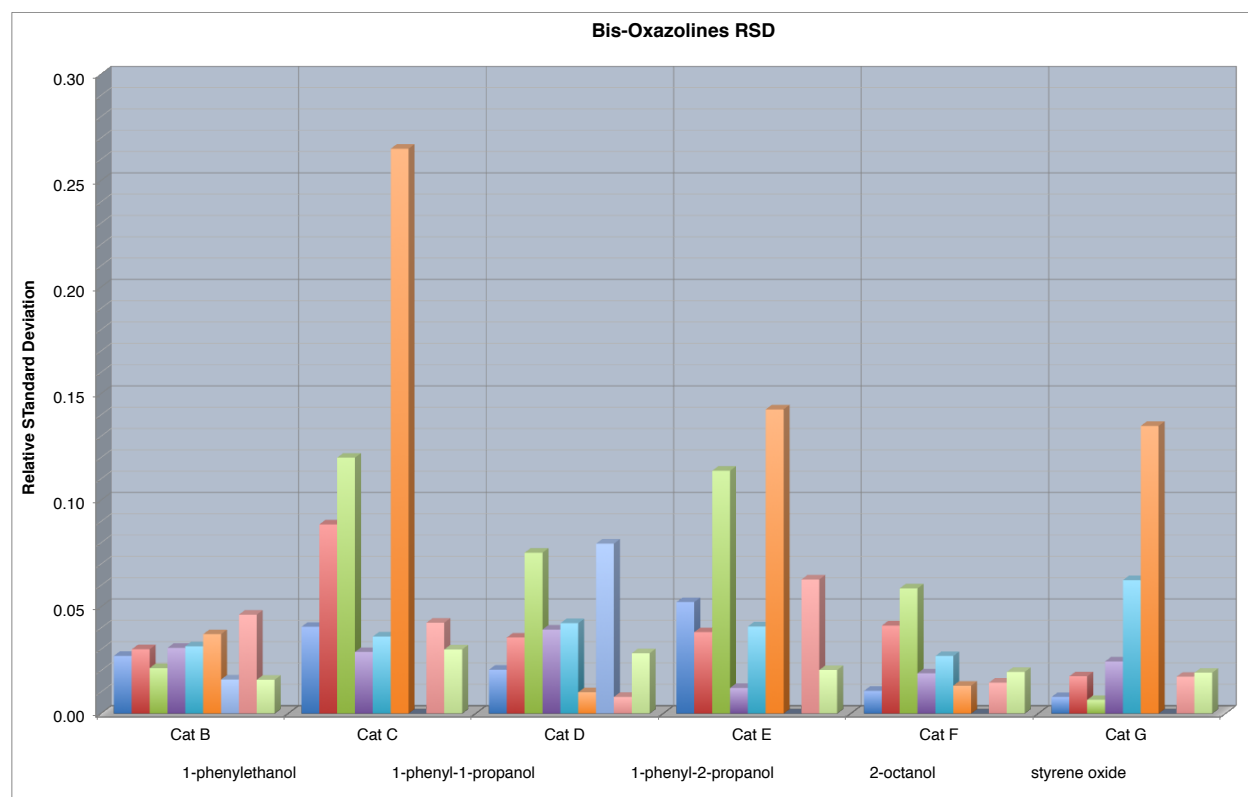


**Figure 75.** RSD grouped by catalyst.

Overall, the results are excellent; with only 5 of the 50 readings displaying RSDs over 6%, half of them occurring with 1,2 epoxybutane. The high RSD observed there are most likely a result of the non-ideal ratio of the chiral reagent and internal standard. For example, the highest RSD observed was for catalyst C and 1,2-epoxybutane, at 26%. Upon examination of the spectra, the catalyst exhibited very low coordination to the enantiomers (Figure 76).

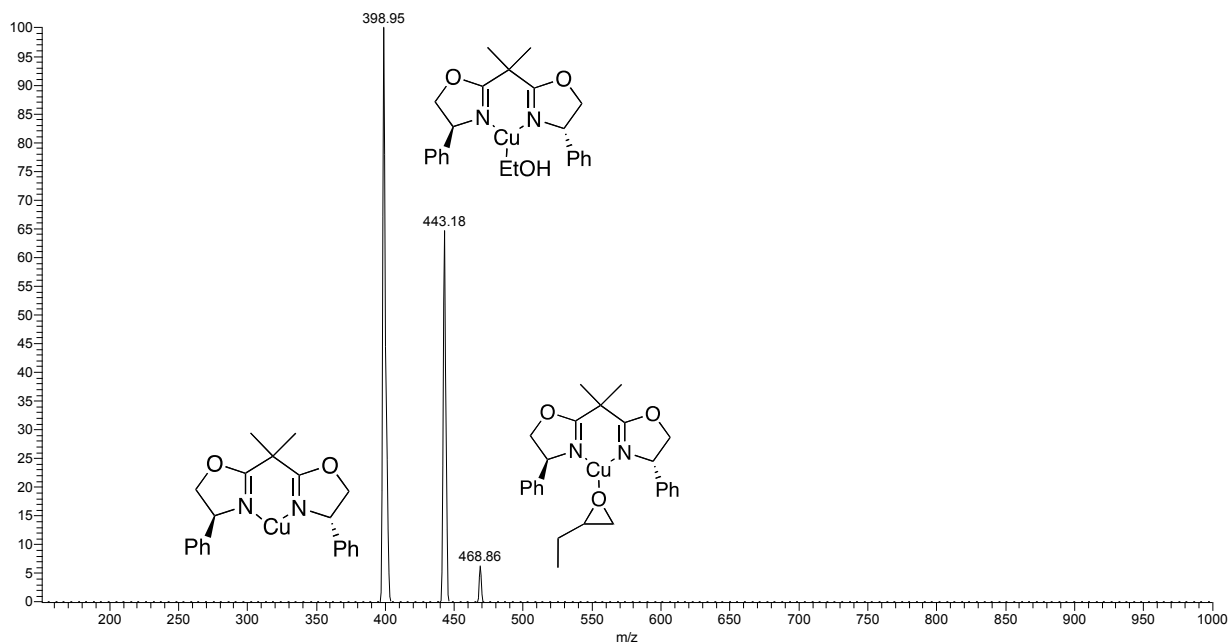


**Figure 76.** Mass Spectrum of catalyst C and 1,2-epoxybutane with EtOH as the internal standard.

Unfortunately, a universal internal standard cannot always be found. The ideal internal standard is a deuterium-labeled pseudo-enantiomer of the chiral probe. Most of these are not commercially available, so substitutes must be made. The next best internal standard would be the addition of the smallest possible group to the probe of interest, for example, the addition (or subtraction) of a methyl group. This too is not ideal, as the higher molecular weight analyte tends to preferentially bind to the catalyst, requiring a ratio significantly deviating from the ideal 1:1 ratio of analyte to internal standard. In addition, an internal standard that works well for one catalyst and probe may not work well with another. Thus, compromises were made.

Box plots are an excellent way to present statistical data in a quick and easy-to-read format; thus, the results are presented as box plots in Figure 77.



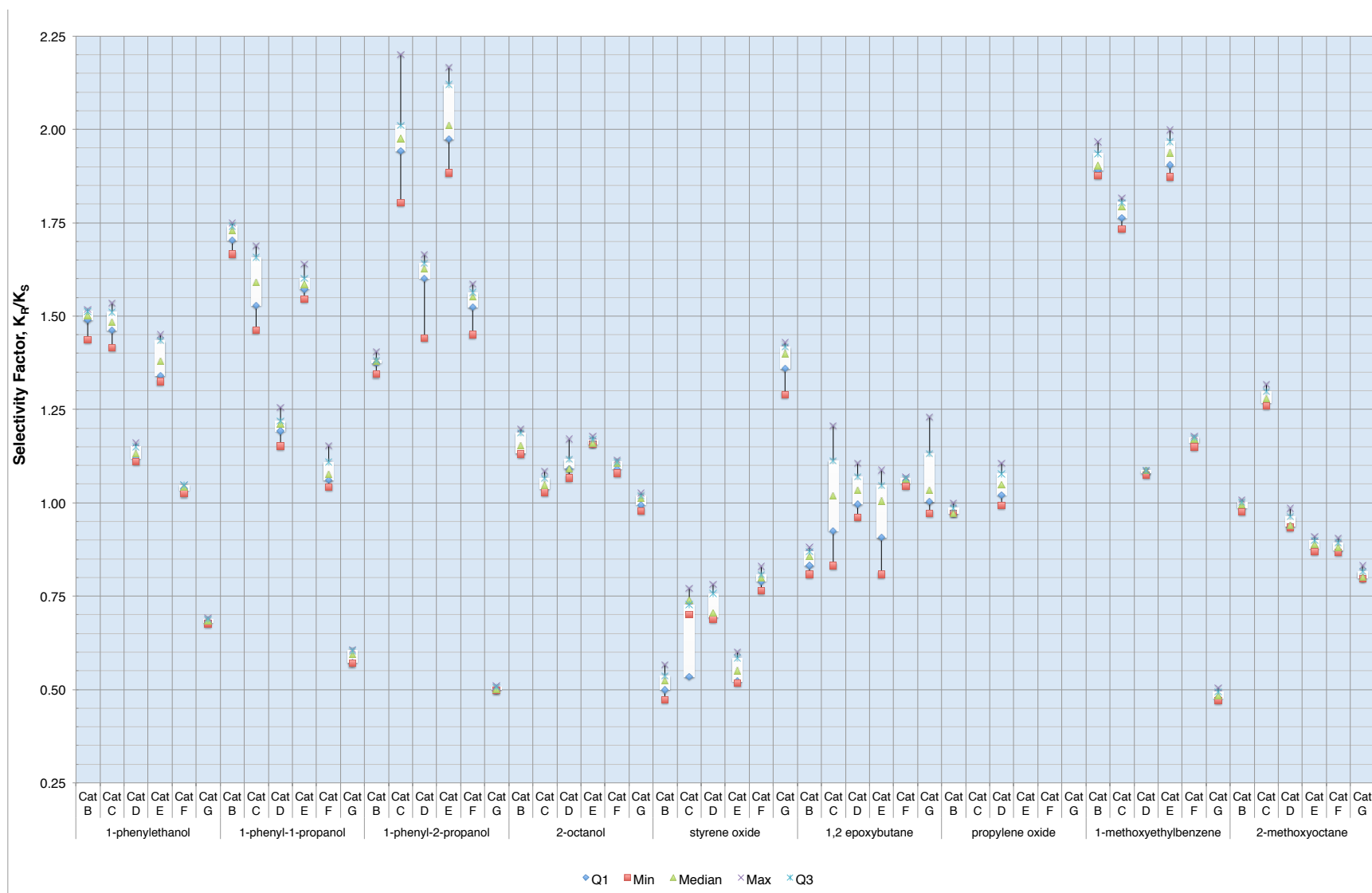


**Figure 77.** Box plots of all results for the bis-oxazolines.

### 5.8.2 – System Checks (ESI)

The ESI process was optimized for each catalyst by running the automatic tune feature. The probe distance from inlet was set to 3, per the manufacture's recommendation at flow rates used ( $1\text{-}5\ \mu\text{L min}^{-1}$ ). After running for prolonged periods, the performance of the ESI spray progressively deteriorated. It was found that this was due to build up of material in the capillary tubing entering the ground junction of the instrument. This black material was probably copper precipitating out of solution (picture in Figure 78a). After periodically removing 1-2 inches of the capillary, the stability improved greatly as shown in (b) and (c) in Figure 78.

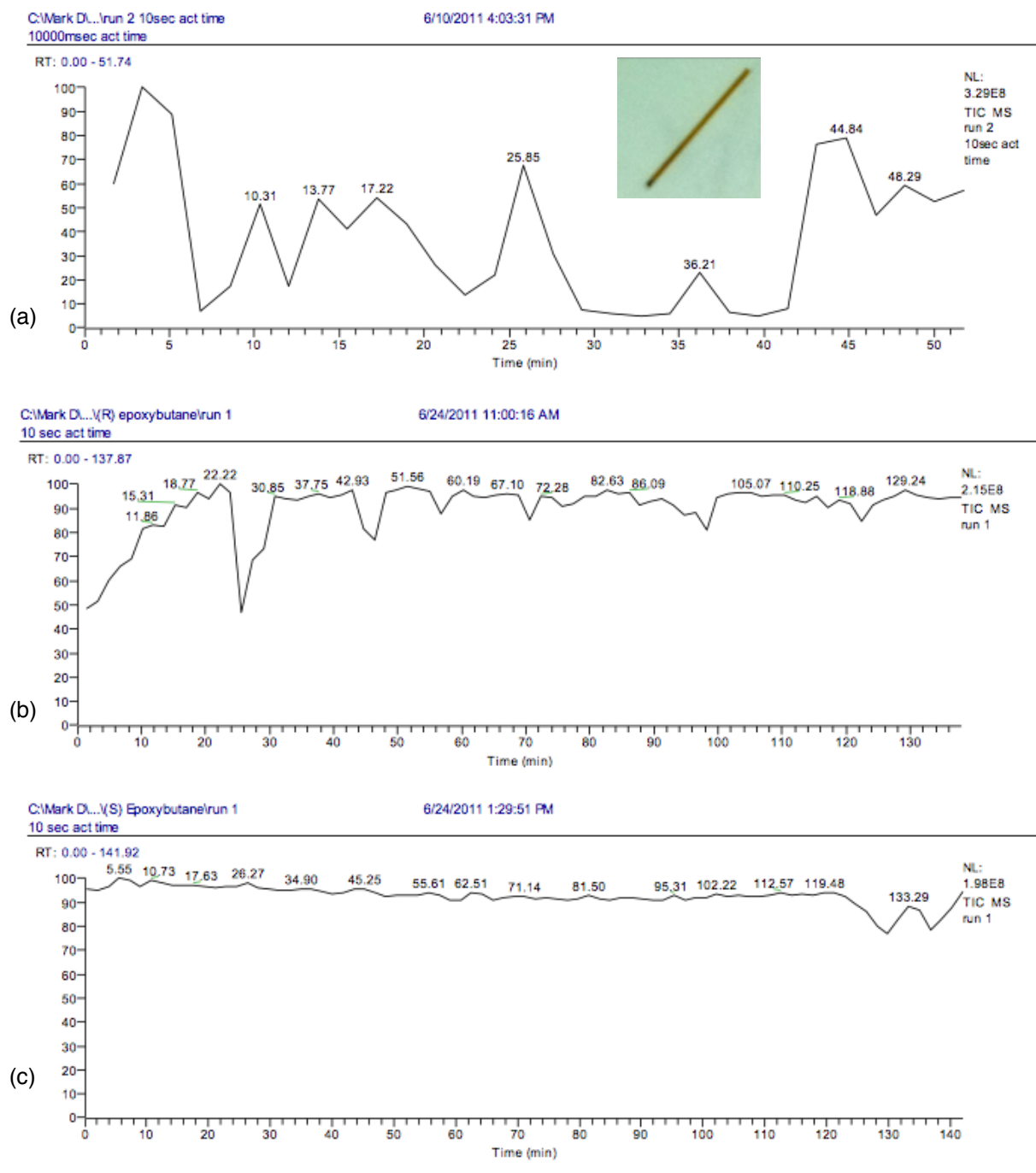


**Figure 78.** (a) Stability of the ESI spray before regular trimmings of the capillary tubing. Also shown a picture of the tubing. Black solid was observed at the entrance to the ground junction of the instrument. (b) and (c) examples of the stability after clipping of capillary tubing.

After introduction of the neutral reagent and syringe into the manifold, the time was measured to reach equilibrium, as evident from a stable ratio of analyte to internal standard ratio. From Figure 79, it is evident that it takes approximately 50-60 scans to

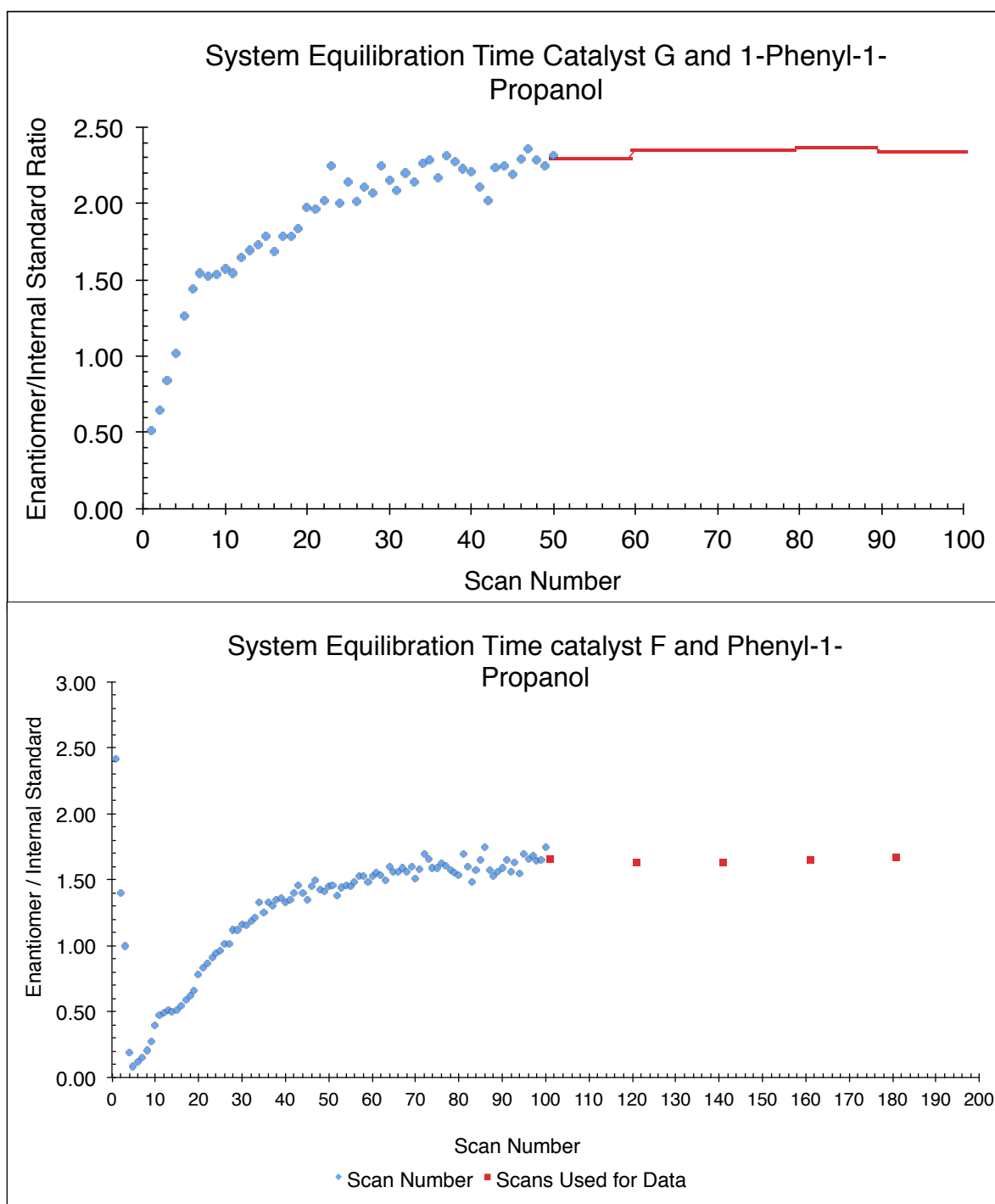


**Figure 79.** Time to equilibrate the manifold and ion-trap with the chiral probe.

equilibrate. This corresponds to approximately 10 minutes, when scanning from 100-1000m/z with a setting of 10 microscans. Thus, a period of 15 minutes was allowed to pass before collection of data.

### 5.8.3 – Chiral and Achiral Controls

The instrument's variability, precision, and accuracy were tested with a series of experiments.

#### 5.8.3.1 – Instrument Variability and Accuracy

To test the instrument variability, as well as to gauge the method's ability to

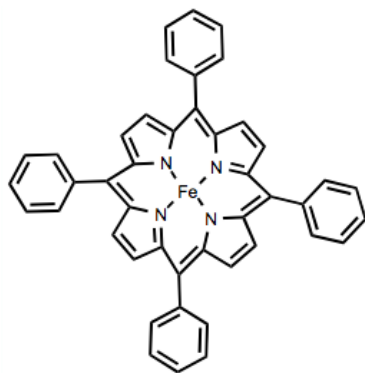


**Figure 80.** Fe(III) tetraphenyl porphyrin achiral catalyst.

discriminate chirality, an achiral catalyst was used with a chiral neutral reagent. An Fe(III) tetraphenyl porphyrin (Figure 80) was tested with 2-octanol over a series of days. The same solutions of *R/S* 2-octanol were used for testing. They were stored in the freezer between uses. The control chart is shown in Figure 81.

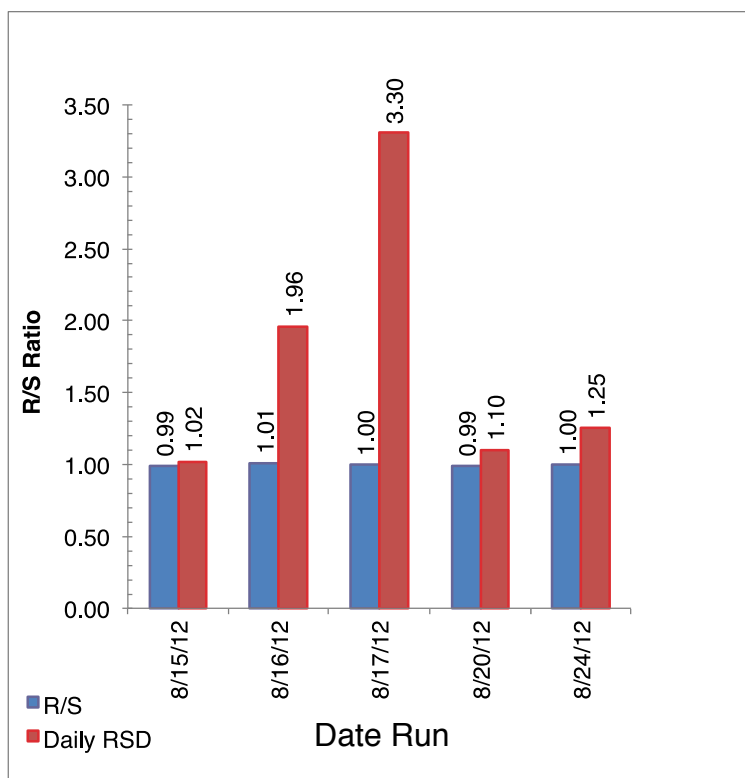


**Figure 81.** Achiral catalyst with 2-Octanol run over 5 days.

The blue bar represents the daily selectivity value. The average over five days was 1.00 with an RSD of 0.72%. The daily RSD for the values (5 runs), represented by the red bar, was slightly higher but well within acceptable range of 3.3%. Thus, the instrument and method appears accurate and precise, over multiple days with an achiral catalyst.

The next test was with a chiral catalyst known to display little selectivity. Catalyst B with 2-octanol was used as a control over the course of a week. Again, the same solution was used for the study and kept in the freezer when not in use. The results are shown in Figure 83.

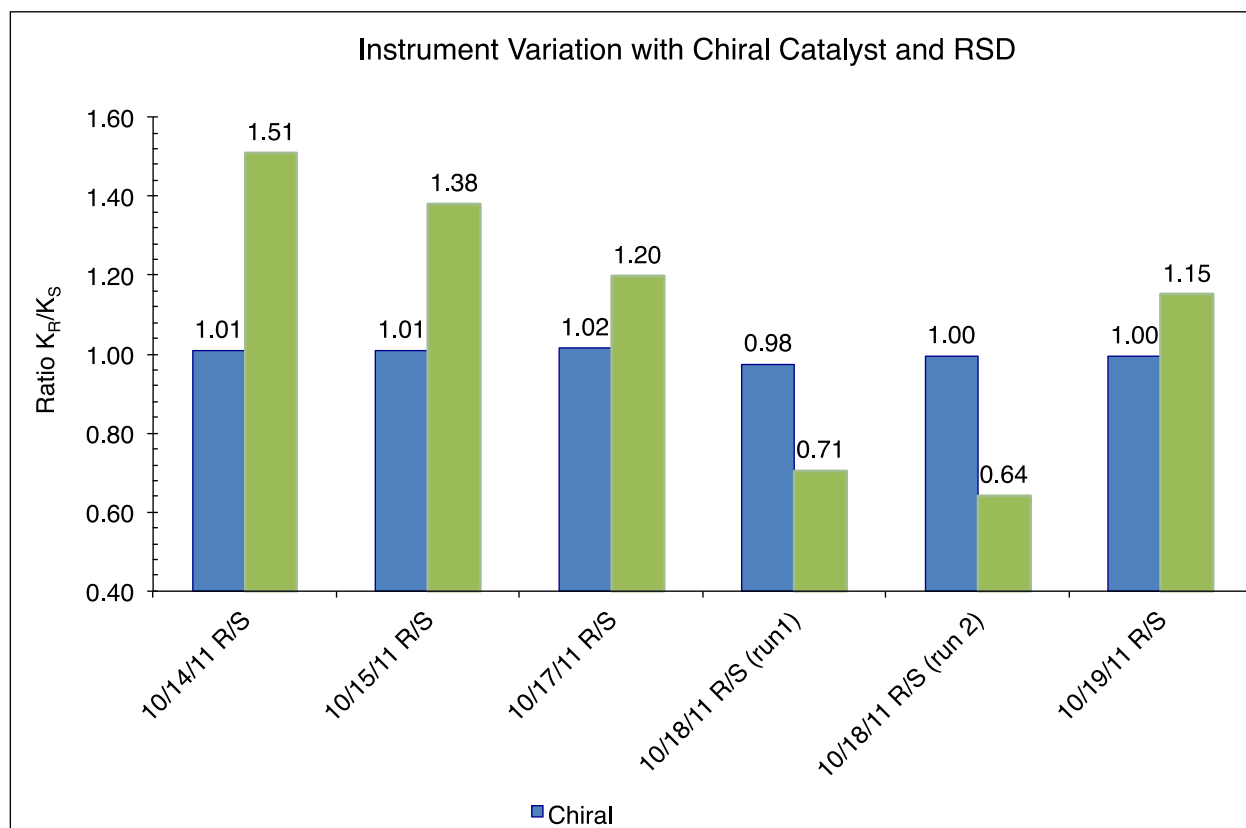


**Figure 82.** Catalyst B with 2-Octanol run over 5 days.

The results again show excellent agreement between days, with an average of 1.00 and an RSD of 1.46%, with daily RSD for 5 runs between 0.64-1.51% (green line).

### 5.8.3.2 – Neutral Reagent Preparation

The sample prep variability was examined with catalyst B and 1-phenyethanol preps. This system displayed a selectivity of 1.49. With the high selectivity, and a deuterated internal standard, it offered a good candidate for the study, as any evaporation that occurred during the period between initial prep and final examination (one week), would have affected both the enantiomer and internal standard equally. To

minimize evaporation, the samples were kept in the freezer when not in use. The sample preps occurring between 8/7 – 8/16 were all run on 8/16/12. The ANOVA (analysis of variance) results are shown below in Table 9.

**Table 9.** Result of ANOVA for sample preparation variability.

Anova: Single Factor

SUMMARY						
Groups	Count	Sum	Average	Variance		
8/15/12	5	7.511	1.502	7.957E-04		
8/10/12	5	7.601	1.520	1.286E-04		
8/7/12	5	7.489	1.498	2.511E-04		
8/16/12	5	7.664	1.533	8.815E-04		
8/8/12	5	7.689	1.538	1.484E-04		
				average	1.518	Min 1.498
				std dev	0.0178	Max 1.538
ANOVA		RSD	1.175	Range	0.040	
Source of Variation	SS	df	MS	F	P-value	Fcrit
Between Groups	0.006360016	4	0.001590004	3.605019146	0.022766797	2.866081402
Within Groups	0.008821057	20	0.000441053			
Total	0.015181072	24				

Conclusion:  $p < 0.05$ , so reject the null hypothesis and accept alternative hypothesis that there is a difference between the preps.

The average selectivity obtained for the set of five was 1.52, with an RSD of 1.18. The ANOVA indicated there was a statistical significant difference at the 95% level, ( $p < 0.05$ ) for samples prepped on different days. A statistical analysis of the newly obtained data was run against the previously obtained data, comparing older prep date selectivity factors, to the results obtained on 8/16/12. These ANOVA results are shown in Table 10:



**Table 10.** ANOVA results comparing data obtained on 8/16/12 to the previously obtained results. No statistical different was apparent.

t-Test: Two-Sample Assuming Equal Variances			t-Test: Two-Sample Assuming Equal Variances		
	<i>8/15/12 prep run on 8/16/12</i>	<i>8/15/12 prep run on 8/15/12</i>		<i>8/10/12 prep run on 8/16/12</i>	<i>8/10/12 prep run on 8/10/12</i>
Mean	1.502	1.513	Mean	1.520	1.536
Variance	0.0007957	0.0005561	Variance	0.0001286	0.0005334
Observations	5	5	Observations	5	5
Pooled Variance	0.0006759		Pooled Variance	0.000331	
Hypothesized Mean Difference	0		Hypothesized Mean Difference	0	
df	8		df	8	
t Stat	-0.659842		t Stat	-1.362965	
P(T<=t) two-tail	0.5278908		P(T<=t) two-tail	0.2100168	
t Critical two-tail	2.3060041		t Critical two-tail	2.3060041	

t-Test: Two-Sample Assuming Equal Variances			t-Test: Two-Sample Assuming Equal Variances		
	<i>8/07/12 prep run on 8/16/12</i>	<i>8/07/12 prep run on 8/07/12</i>		<i>8/16/2012b</i>	<i>8/8/12</i>
Mean	1.498	1.498	Mean	1.533	1.513
Variance	0.0002511	0.001986	Variance	0.000881519	0.000289907
Observations	5	5	Observations	5	5
Pooled Variance	0.0011185		Pooled Variance	0.000585713	
Hypothesized Mean Difference	0		Hypothesized Mean Difference	0	
df	8		df	8	
t Stat	-0.021644		t Stat	1.301288547	
P(T<=t) two-tail	0.9832619		P(T<=t) two-tail	0.229383273	
t Critical two-tail	2.3060041		t Critical two-tail	2.306004135	

No statistical differences were observed from the sample prepared on the older date, compared to the same sample run on 8/16/12; thus, the variability observed is due to sample preparation (no stability issues with the samples).

A separate experiment was run for sample prep variation with ligand B and 2-octanol. It found that there is no difference in sample prep variation at the 95% confidence level ( $P = 0.0617$ ), but did find a small difference in run-to-run variability, with a p-value of  $1.09 \times 10^{-4}$ .

**Table 11.** Variability in sample prep and run-to-run with catalyst B and 2-octanol.

Anova: Single Factor

SUMMARY

Groups	Count	Sum	Average	Variance	std dev	RSD
R/S Prep 1	5	4.90	0.98	8.61E-05	0.009	0.95
R/S Prep 2	5	4.97	0.99	5.15E-04	0.023	2.29
R/S Prep 3	5	4.79	0.96	6.75E-04	0.026	2.71
ANOVA			0.98		0.02	1.78
Source of Variation	SS	df	MS	F	P-value	F crit
Between Groups	3.02E-03	2	1.51E-03	3.54	6.17E-02	3.89
Within Groups	5.11E-03	12	4.26E-04			
Total	8.13E-03	14				

Anova: Single Factor

SUMMARY

Groups	Count	Sum	Average	Variance	std dev	RSD
Prep 3 run 1	5	5.00	1.00	2.82E-04	0.017	1.68
Prep 3 run 2	5	4.72	0.94	3.24E-04	0.018	1.91
Prep 3 Run 3	5	4.93	0.99	2.16E-05	0.005	0.47
ANOVA			0.97		0.025	2.56
Source of Variation	SS	df	MS	F	P-value	F crit
Between Groups	8.98E-03	2	4.49E-03	21.45	1.09E-04	3.89
Within Groups	2.51E-03	12	2.09E-04			
Total	1.15E-02	14				

### 5.8.3.3 – Propylene Oxide and Sample Preparation Variation

The chiral probe propylene oxide was only tested for catalysts B and D. Due to the low selectivity exhibited, not surprising giving its small size, and the difficulty in the sample prep due to the extremely high volatility; it was only run for these two catalysts. Sample prep for this analyte required the use of headspace vials, pre-filled with solvent that were subsequently tared on the analytical balance. The sample was then introduced sub-surface via a gas-tight syringe and reweighed. The procedure was repeated for the internal standard, with a typical spectrum shown below, Figure 83.

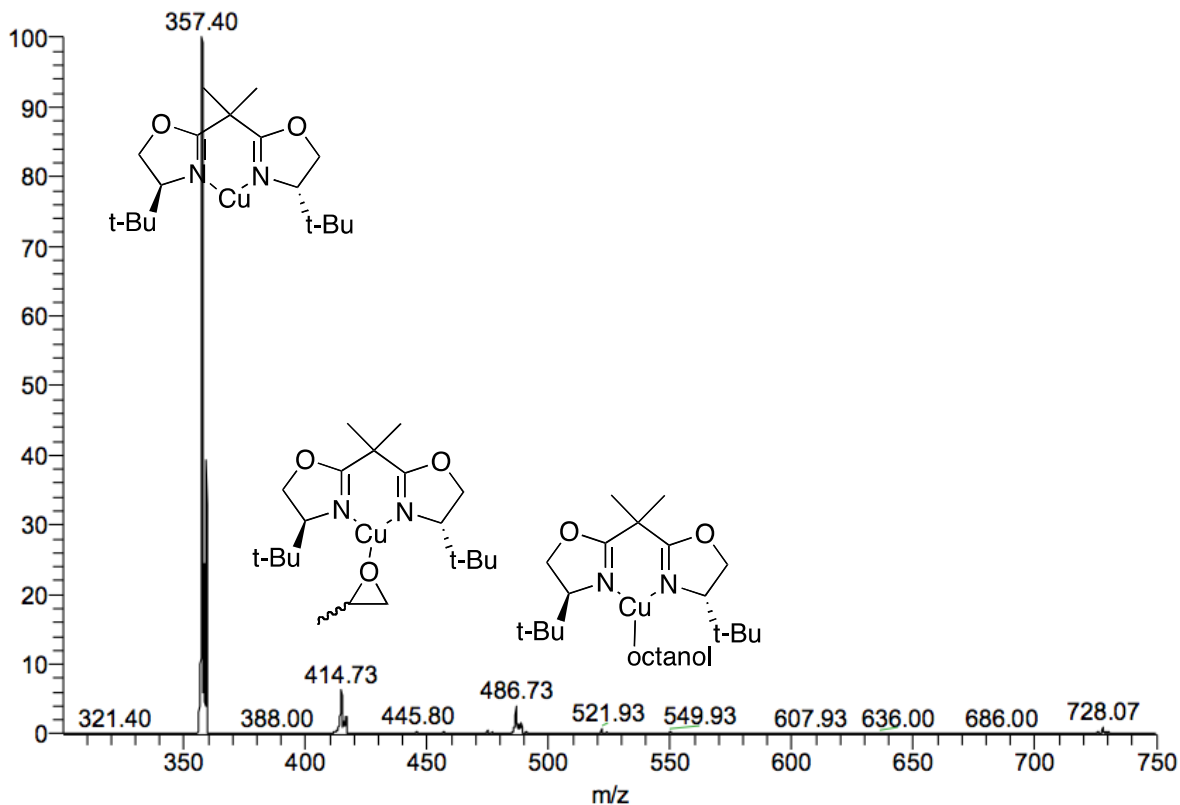


**Figure 83.** Spectrum of the *t*-Bu catalyst with propylene oxide and 1-octanol as the internal standard.

Due to the nature of the sample prep and very low abundance of the coordination complex between the catalyst and analyte, three sample preparations were made to examine the reproducibility. The RSD for three (*S*) enantiomer preps was 0.78 %; the RSD for two (*R*) preps was 4.1%, yielding greater confidence in the methodology and results.

#### 5.8.4 – Helium Pressure and Variability

The effect of helium pressure on the results was also examined by slightly adjusting the helium pressure from the tank to levels expected for day-to-day variance. Only the ratio between one prep of analyte and internal standard was measured, i.e., only the *S* enantiomer was examined (Table 12).

**Table 12.** Effect of pressure on results.

SUMMARY						
Groups	Count	Sum	Average	Variance		
Normalized PP =17.49	4	3.330606185	0.832651546	3.15887E-05		
Normalized PP 17.36	5	4.044658803	0.808931761	2.93657E-05		
Normalized PP 17.15	5	4.087296337	0.817459267	2.36905E-05		
Normalized PP 17.53	5	4.01045932	0.802091864	0.000135544		
Normalized PP 17.81	5	4.006905922	0.801381184	3.22198E-05		
		average	0.813			
		std dev	0.012			
ANOVA		RSD	1.430			
Source of Variation	SS	df	MS	F	P-value	Fcrit
Between Groups	0.00295397	4	0.000738493	14.34633443	1.4792E-05	2.895107308
Within Groups	0.000978045	19	5.1476E-05			
Total	0.003932015	23	There is a difference in values with pressure			

A statistical difference was determined to exist between the different set values of helium pressure; however, this difference was not large, evident from the small RSD of 1.4% between all sets of data. Nonetheless, pressure was kept as close to 17.5 psi as possible to minimize this effect.

#### 5.8.5 – Chiral Check

As mentioned in Chapter 1, one of the disadvantages of the chiral pool method, is the lack of availability of both enantiomers in the starting substrate. Thus, not all of the bis-oxazolines are commercially available in both enantiomers. This was the case for most of the bis-oxazolines utilized in this study, with the exception of PhBOX, (catalysts C and G). Since they are enantiomers, the opportunity exists for a chiral cross check. The selectivity factor, S, or  $K_{R/S}$ , for each catalyst C and G when multiplied by one another should equal 1, or

$$\text{catalyst C } K_{R/S} \times \text{catalyst G } K_{R/S} = 1$$

Figure 84 displays the results for the chiral cross check.

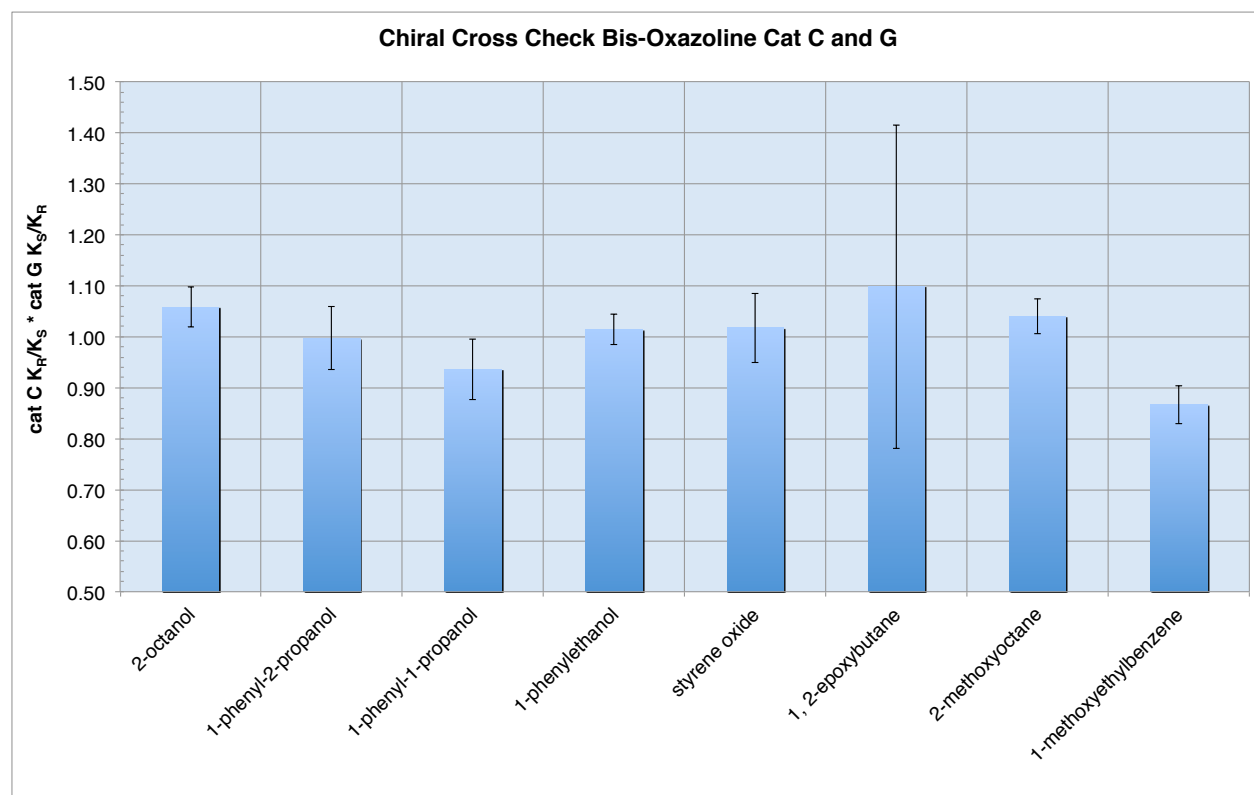


**Figure 84.** Chiral cross check with catalysts C and G.

All results were 1.0 within error, except 1-methoxyethylbenzene. It is not entirely clear why there is a large error in this case.

### 5.8.6 – Different Instruments

The lab was equipped with two different modified ion-traps, so catalyst B and phenylethanol was tested on each instrument. The results compare favorably. A plot of the scan activation times for the two instruments demonstrated excellent agreement (Figure 85). The selectivity factor for the alternate instrument was 1.49, compared to 1.54 for the usual instrument. The ANOVA yielded a P-value of 0.016, so there is a

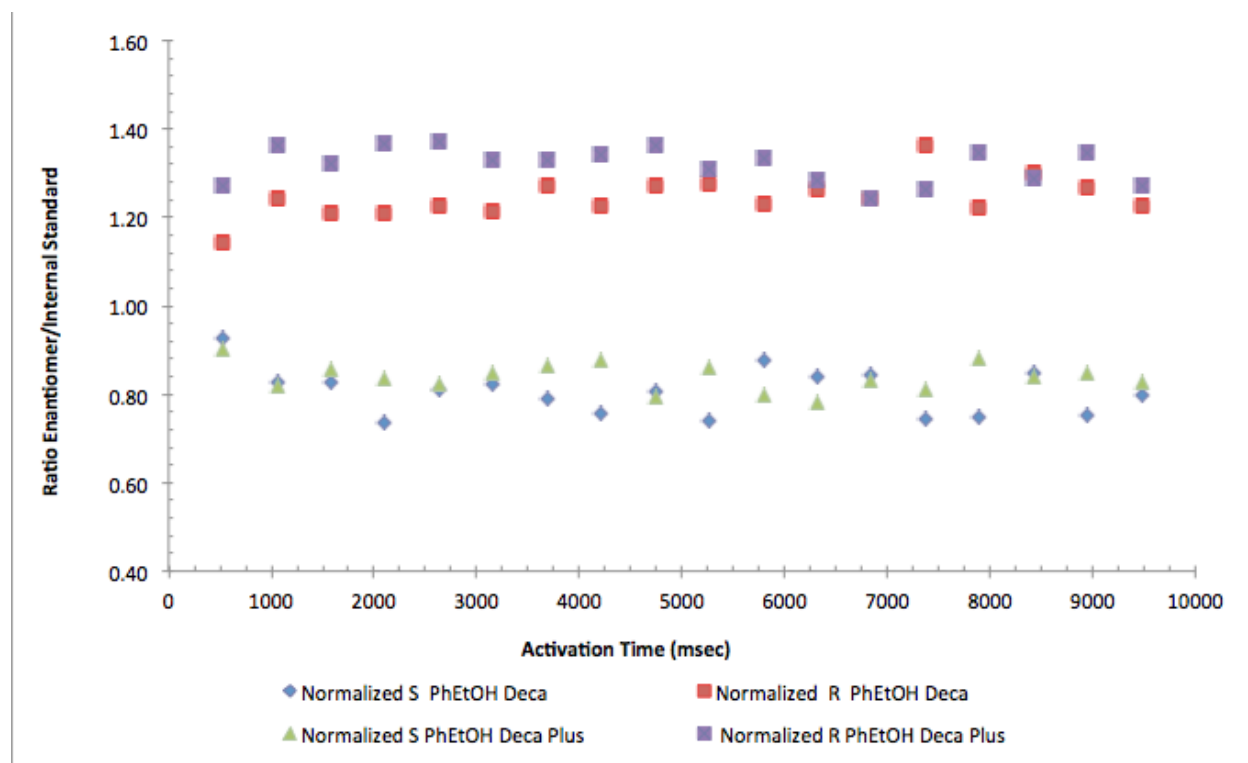


**Figure 85.** Scan activation of catalyst B and phenylethanol on two different instruments.

statistical difference between the instruments, but no practical difference (Table 13). This yields greater confidence in the results and transferability or adaptability to/by other labs/instruments.

**Table 13.** ANOVA comparing the results of catalyst B and phenylethanol on two different instruments.

	<i>Deca</i>	<i>Deca Plus</i>
Mean	1.49	1.54
Variance	0.00	0.00
Observations	5	5
Pooled Variance	0.00058	
Hypothesized Mean Difference	0	
df	8	
t Stat	-3.059	
P(T<=t) two-tail	0.016	
t Critical two-tail	2.306	

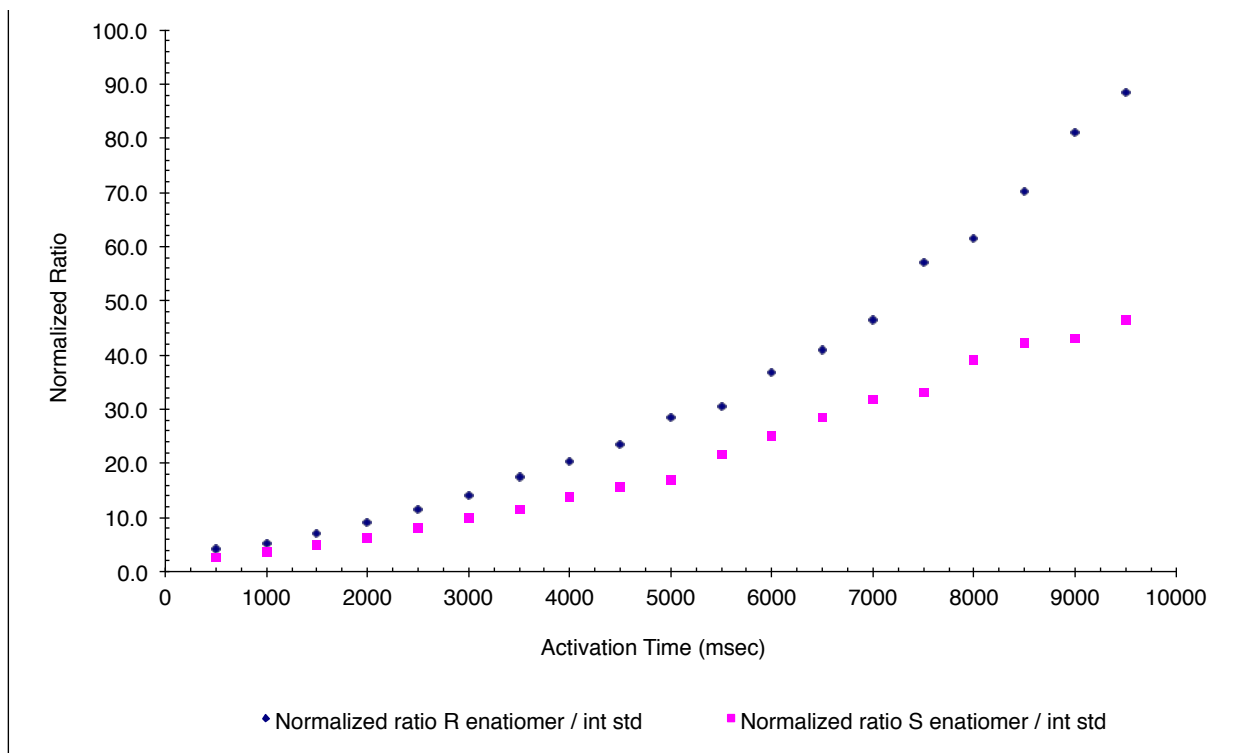
P < 0.05, reject null hypothesis  
there is a significant difference

## 5.9 – Chiral Amines

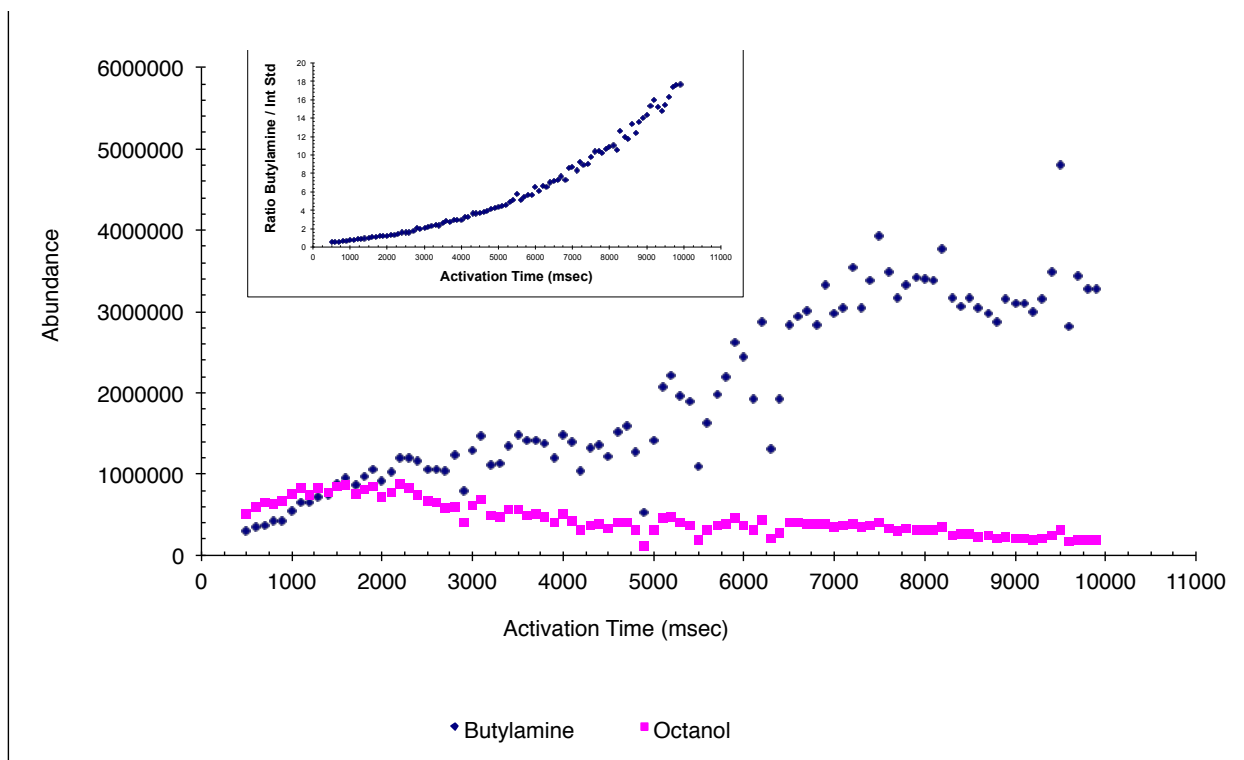
As part of the investigation into the catalyst template, chiral amines were initially thought to be promising probes, offering a different geometry around the central nitrogen than the oxygen-based probes. However, the strong Lewis-base nature of amines when coordinating with the catalyst did not allow for equilibrium to be achieved in the instrument. The upper-limit for trapping time is 10 seconds for the LCQ Deca, which was not enough time for equilibration.

Figure 86 demonstrates an achiral amine (butylamine) never reaching equilibrium (blue), while Figure 88 shows a chiral amine (*sec*-butyl) amine with an amine as the internal standard, again with no success. Thus, the class of amines was abandoned for use as chiral probes.





**Figure 86.** Catalyst B and *sec*-butyl amine with *i*-pro amine.



**Figure 87.** Scan activation time study of butyl amine with octanol as the internal standard. The amine never reaches equilibrium. Inset – normalized ratio of the butylamine and octanol.

## 5.10 – Combinatorial Approach

A combinatorial approach was examined for the bis-oxazolines and compared to the single runs. That is, a mixture of catalyst was infused and multiple equilibrium were assessed from a single ESI solution. Due to the isobaric nature of the some of the bis-oxazoline catalysts, only three could be run at the same time. Two mixes were created, mix one, consisting of catalyst B, E, and C; and mix two, consisting of catalysts D, F, and G. No difference was observed between the single run samples and the combinatorial run mixes, when accounting for standard deviations, with the exception of catalyst E. This difference too, was small,  $1.39 \pm 0.04$  for the single versus  $1.47 \pm 0.03$  for the mix shown in Table 14 and Figure 88. The single runs of catalyst E were run before the implementation of the dual syringe method, a possible source of error.

**Table 14.** Table of the single runs versus combinatorial mixes.

	selectivity factor		standard deviation	
	<u>Single</u>	<u>Combinatorial</u>	<u>Single</u>	<u>Combinatorial</u>
Cat B	1.49	1.43	0.03	0.03
Cat C	1.48	1.42	0.04	0.02
Cat D	1.13	1.13	0.04	0.02
Cat E	1.39	1.47	0.04	0.03
Cat F	1.04	1.04	0.03	0.04
Cat G	0.68	0.71	0.06	0.02

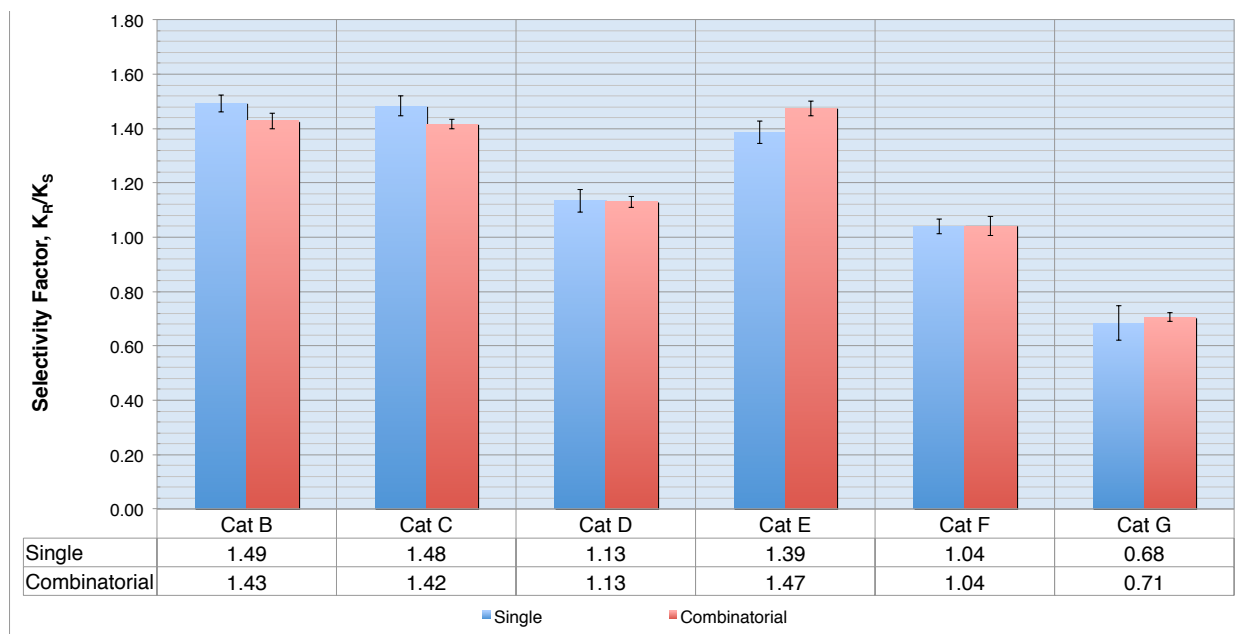


**Figure 88.** Results of the single run versus combinatorial approach.

## 5.11 – Catalyst E Investigation

Initial investigations into the bis-oxazolines, particularly catalyst E, displayed odd isotope patterns in the MS (Figure ). Using a scan width of five and targeting 329m/z,

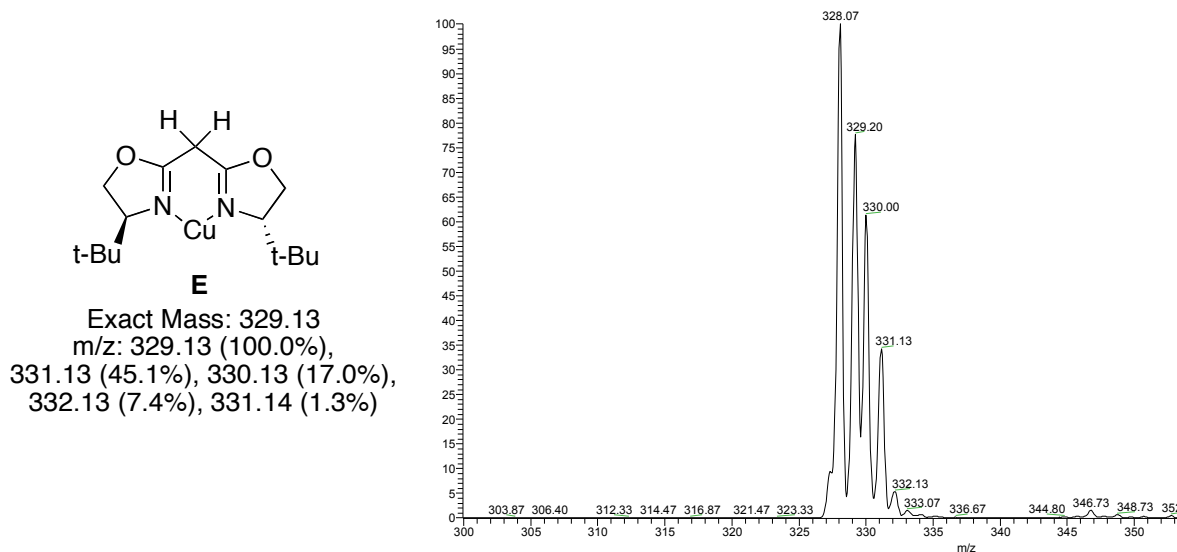


**Figure 89.** (a) Catalyst E with the expected isotopic abundances. (b) Mass Spectrum of catalyst E. The major peak is minus one from expected.

enabled examination of all the isotopes. However, the expected pattern was not observed. When using fresh preps of the ligand and copper, an ion at 328 m/z, rather than 329 m/z, is observed as the base peak. Furthermore, the ratio changed with time, with an unknown at 327 m/z gradually appearing with time (Figure 90).

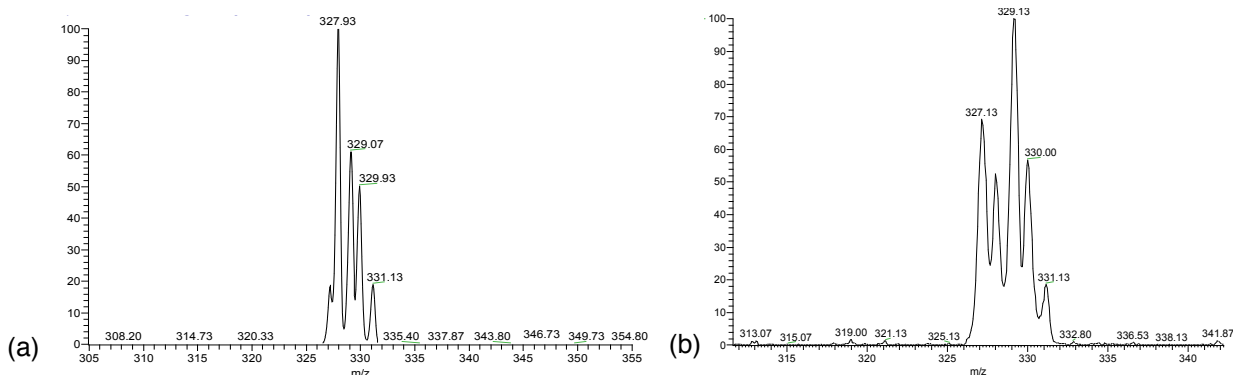


**Figure 90.** (a) Fresh prep of catalyst E. (b) Prep after nine days.

### 5.11.1 – Ligand E Investigation

To better understand the chemistry of the catalyst with copper, a study of the ligand by itself was performed. Fragmenting catalyst E ( $m/z = 267.3$ ) resulted in a beta lactam as the major fragment, and a substituted oxazoline (Figure 91). Fragmenting

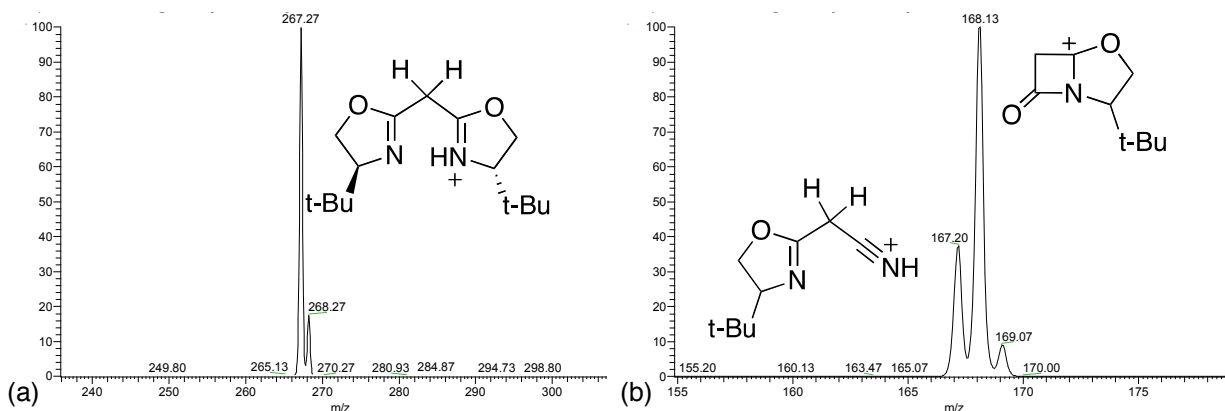


**Figure 91.** (a) Ligand only of catalyst E. (b) Fragmentation pattern for ligand E .

ions at 167 and 168 m/z ions resulted in one peak at 100 m/z, which resulted in a fragment at 83 m/z when performing another stage of MS<sup>n</sup>. The proposed structures and mechanisms for catalyst E ligand and transitions are shown in Figure 92.

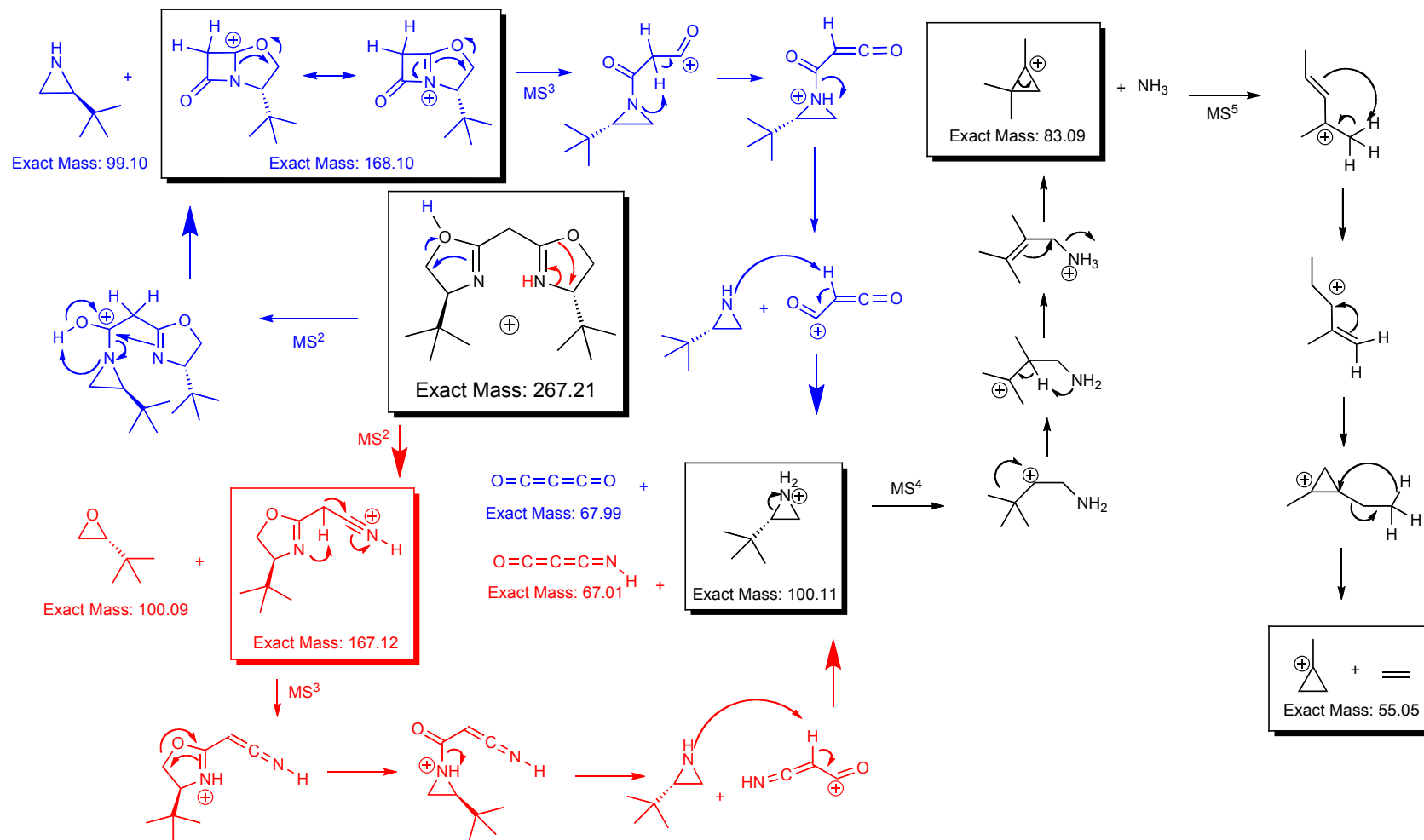


**Figure 92.** Ligand of catalyst E proposed fragmentation mechanisms.

The path in blue is a result of protonation at the oxygen, resulting in a stable beta-lactam. The path in red results in protonation at the nitrogen, resulting in the less stable nitrilium ion; however, upon further fragmentation, both result in the same fragment product(s), an aziridine, followed by a cyclopropane. With the normal isotope patterns and mechanistically reasonable fragment pathways, the conclusion is that the ligand behaves normally in the absence of copper.

### 5.11.2 – Ligand E with Na

Next, sodium was used a metal since it is relatively inert (no redox chemistry is likely) and has one natural isotope. The mass spectrum revealed the correct/expected

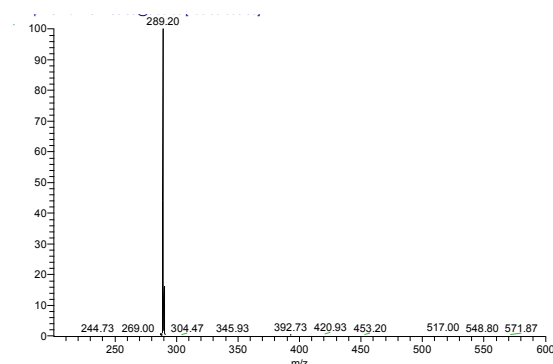


**Figure 93.** Ligand E with Na.

isotopic distribution, with an ion at plus one  $m/z$  of approximately 17% (Figure 93). Fragmentation did not reveal any additional information. The typical fragmentation spectrum with sodium implicates copper in the unexpected pattern observed in the copper catalyst.

### 5.11.3 – Fenton Chemistry

The experiments with Na and the protonated ligand clearly demonstrate copper is playing a significant role in the chemistry of the ligand and the resultant MS spectra.

This implies a Fenton-like chemistry of the ligand, in which copper is oxidized to the plus two-state, most likely via oxygen, forming the superoxide anion, which subsequently reacts with the ligand (Figure 94).

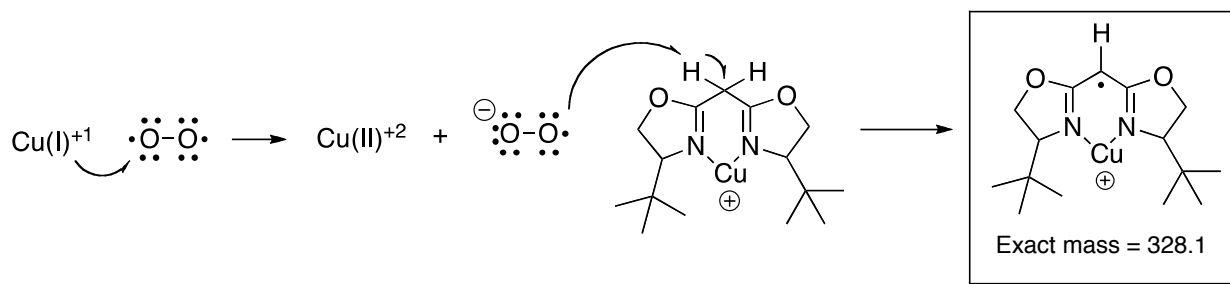


**Figure 94.** Fenton chemistry and the catalyst E.

### 5.11.3.1 – Fragmentation of Catalyst E

Fragmenting a fresh prep of catalyst E at 30 % collision energy results in peaks at 247 and 271 m/z. It was found these fragments are a result of two different species coordinating to the copper, the unaltered catalyst, and the M-1 (Fenton) molecule. This was found by a fragmentation study of catalyst E, taking advantage of the resonance excited CID available in QITs. The original peak displayed the odd isotopic pattern shown in (a) of Figure 95, with 328 (100%), 329 (60%), 330 (50%), and 331 (20%) m/z. Fragmenting at low energy (15%) results in the disappearance of 328 m/z peak and the appearance of 271 m/z. The peak at 329 m/z is still present ((b) in Figure 95). Increasing the fragmentation energy to 30% results in the complete disappearance of all peaks around 329 m/z ((d) Figure 95), and the appearance of a peak at 247 m/z ((b) in Figure 95).



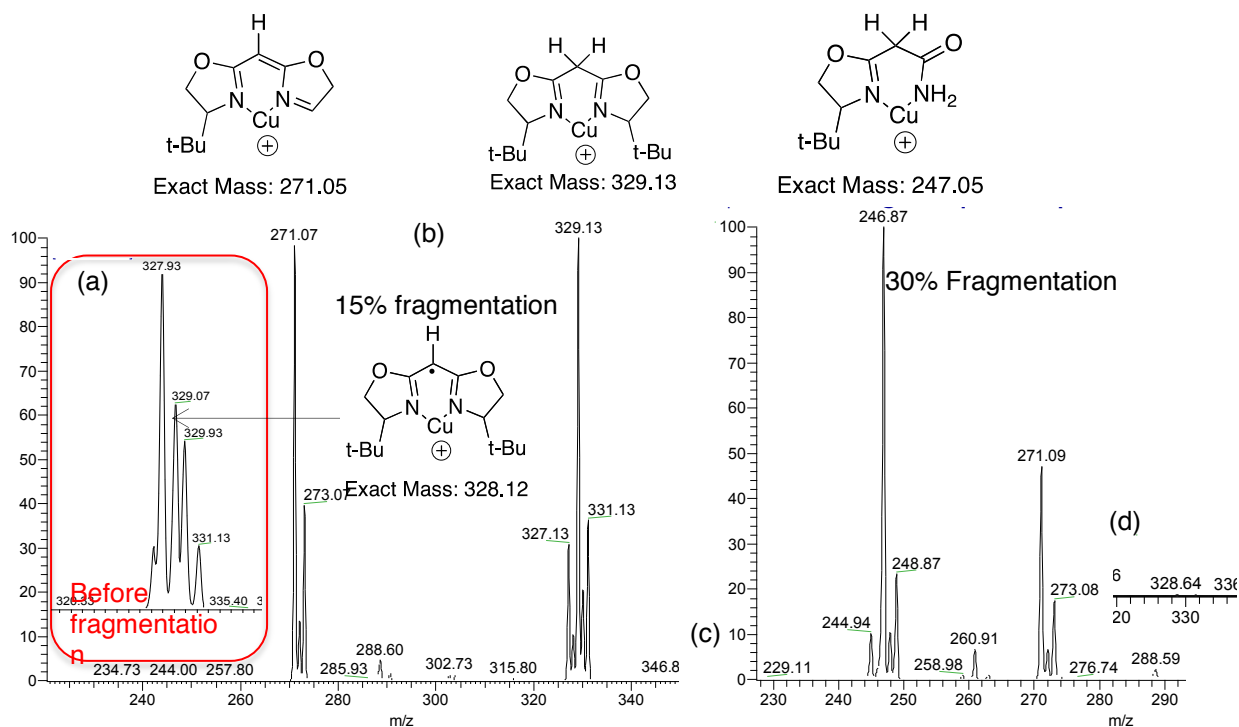


**Figure 95.** (a) Peak before fragmentation. (b) Peak with 15% collision energy applied, 271m/z appears, with 329m/z, still intact. (c) Increase to 30% energy. 247m/z now evident, with no evidence of 329m/z (d)

This offers strong evidence for the case of two species in the mix, resulting from the unaltered catalyst E, and the species that underwent proposed Fenton chemistry.

### 5.11.3.2 – Stability of Catalyst E

Given more time, approximately one month, the catalyst again changes. Figure 96 demonstrates the changes in binding to 2-octanol with catalyst E over time. Note a new species at m/z of 329 now appears, and it does not bind with the alcohols. Fragmentation of this new 329 m/z leads to a completely different fragmentation pattern than the original catalyst E, with a loss of water (311 m/z), followed by a loss of 32 (279 m/z), followed by a loss of 100 (179 m/z).

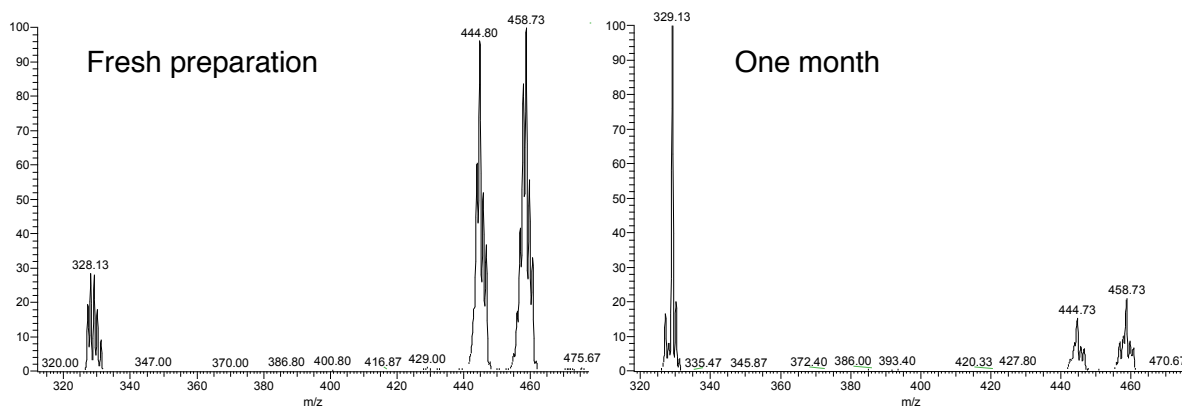


**Figure 96.** The effect of time on the coordination of catalyst E and 2-octanol.

Any of these undesired species could alter the stereospecific binding of the catalyst with the chiral molecules, as previously demonstrated. Thus, the higher selectivity observed in catalyst E over t-BuBOX, which has generally been shown to deliver higher ee's in the literature, may be a result of the altered structure(s)/stability of catalyst E. It is also possible that over time the oxidation of Cu (I) to Cu(II) increases, which in turn increases the Lewis acid strength of the metal, which drives enolization of the catalyst to the 328 m/z unknown, in turn producing the unknown 327 m/z with time.

#### 5.11.4 – Minimizing Degradation and Fenton Chemistry

As a result of these findings, a series of changes were implemented to minimize possible side-reactions by the ligand. The copper solution and the ligand solution were no longer mixed together; rather, a dual syringe system with a series of tees was applied to minimize the contact time together. To ensure efficient mixing of the two solutions before entrance into the ESI, an additional set of tees was applied to the configuration shown in Figure 97, however, this was found to be unnecessary. The set-

up as shown in Figure 97 allowed sufficient mixing of the copper and ligand solution to form the catalyst.

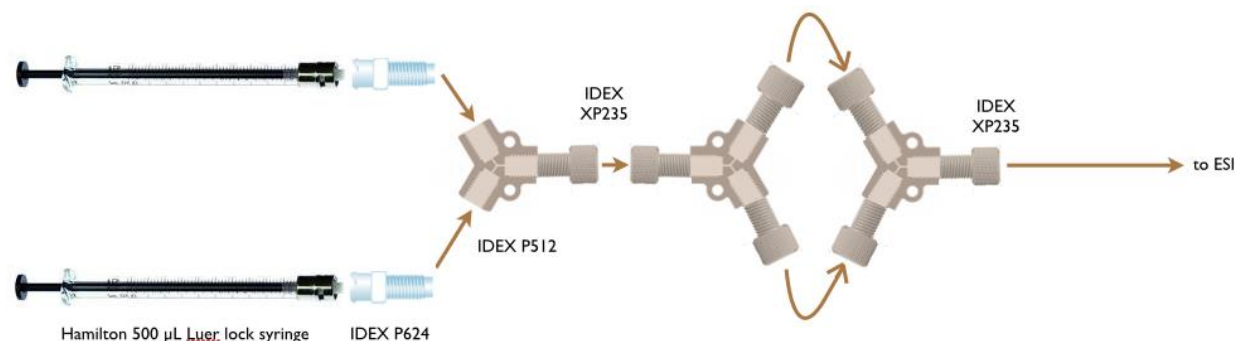


**Figure 97.** Design of the dual syringe and tees to minimize the ligand exposure to copper.

The dual syringe system was designed to minimize exposure of the catalyst to the redox active copper. By isolating  $^{65}\text{Cu}$  with a narrow isolation width, any undesired species resulting from hydrogen loss are ejected from the system. This simplified the integration of the spectra, and left only a small fraction of impurities containing the M – 1 Fenton ligand with a carbon-13.

## 5.12 – Integration Methods

Using catalyst B and phenylethanol, a study into the method of ion isolation and integration was performed. Different methods of isolating the catalyst peak along with different isolation widths for both isolating the catalyst and for calculations were examined. With data run on 6/12/12, using the previous conditions of isolating 358 m/z and an iso width of 4, and then summing all peaks (477-482 m/z for the enantiomer, and

482-487 m/z for the internal standard), an R/S selectivity factor of 1.247 was obtained.

This method of calculating the peaks is known as method 1, shown in Figure 98.

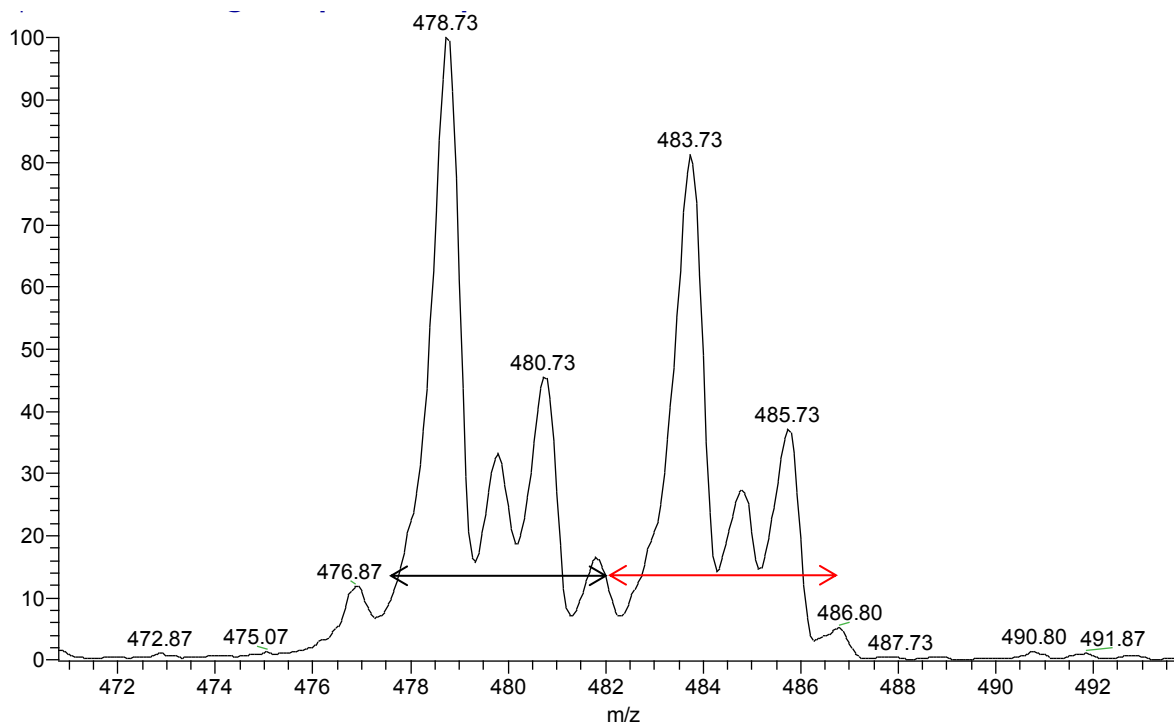


**Figure 98.** Method 1 for integrating all peaks over isotopic range (black line – non-deuterated analyte, red line – deuterated internal standard).

An attempt to isolate only the isotope of interest in the presence of the other isotopes was investigated. Method 2, involved isolating 358 m/z with an iso width of 4 for the reaction, but used an iso width of  $\pm 1$  for the calculations, thereby only summing the largest isotopic peak, 478.7 and 483.7 m/z  $\pm 1$  (Figure 99). Thus, all peaks were collected, but only the  $^{63}\text{Cu}$  were integrated (black arrows). This resulted in an R/S selectivity factor of 1.260.

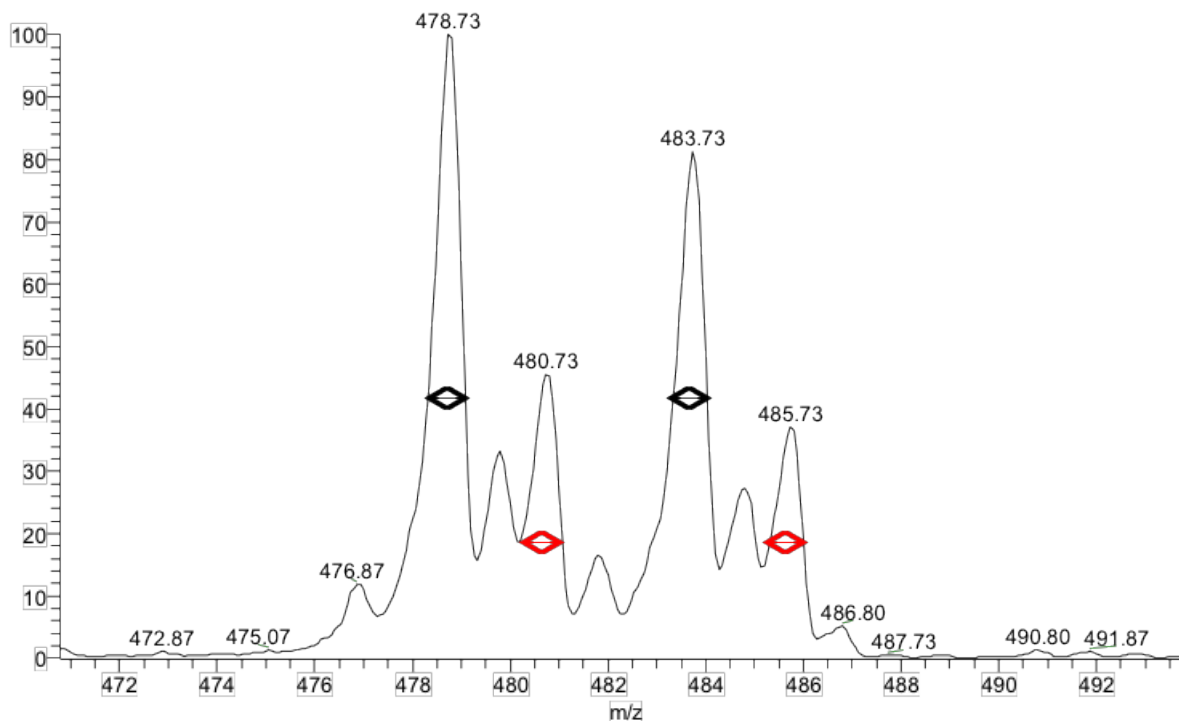


**Figure 99.** Method 2, isolating all peaks, but integrating only the  $^{63}\text{Cu}$  and  $^{65}\text{Cu}$  peaks.

An ANOVA comparing method 1 and 2 gave a P-value of 0.2743, thus there is no difference between the methods.

Method 3 was investigated in which a wide range of m/z were isolated, similar to the previous methods, but in this case, only the higher isotope peaks from  $^{63}\text{Cu}$  and  $^{65}\text{Cu}$  (480.7 and 485.7 m/z) are integrated in the calculations (sum over  $483.7 \pm 0.5$  and  $485.7 \pm 0.5$ , the red arrow in Figure 99). An R/S selectivity factor of 1.506 is obtained using this method, significantly higher than the previous result.

For comparison, method 4 was run which involved isolating the  $^{65}\text{Cu}$  isotope peak (359 m/z) with a narrow isolation band-width of 0.5 m/z and reacting with the R

and S enantiomers. Using an isolation width of 1 in the calculations, a selectivity factor, R/S, of 1.51 was obtained, similar to the result obtained by method 3. An ANOVA was run which did not show any difference between the methods 3 and 4.

The new methods yield an R/S value significantly higher than the previous results. It is most likely the other species (356 and 358 m/z) are coordinating with the enantiomers with different selectivity and hence bring the R/S ratio down to 1.30. Evidence for this is observed in the different fragmentation patterns between the 356 / 358 m/z (potential Fenton-species) and 357 / 359 m/z species. The 357 m/z species results in the usual fragmentation pathways, i.e., formation of the amide and nitrile fragments.

The 357 m/z ion, corresponding to the correct molecule, was isolated with a narrow isolation window and fragmented at 30% collision energy and 30 msec activation time, resulting in the spectrum below in Figure 100.

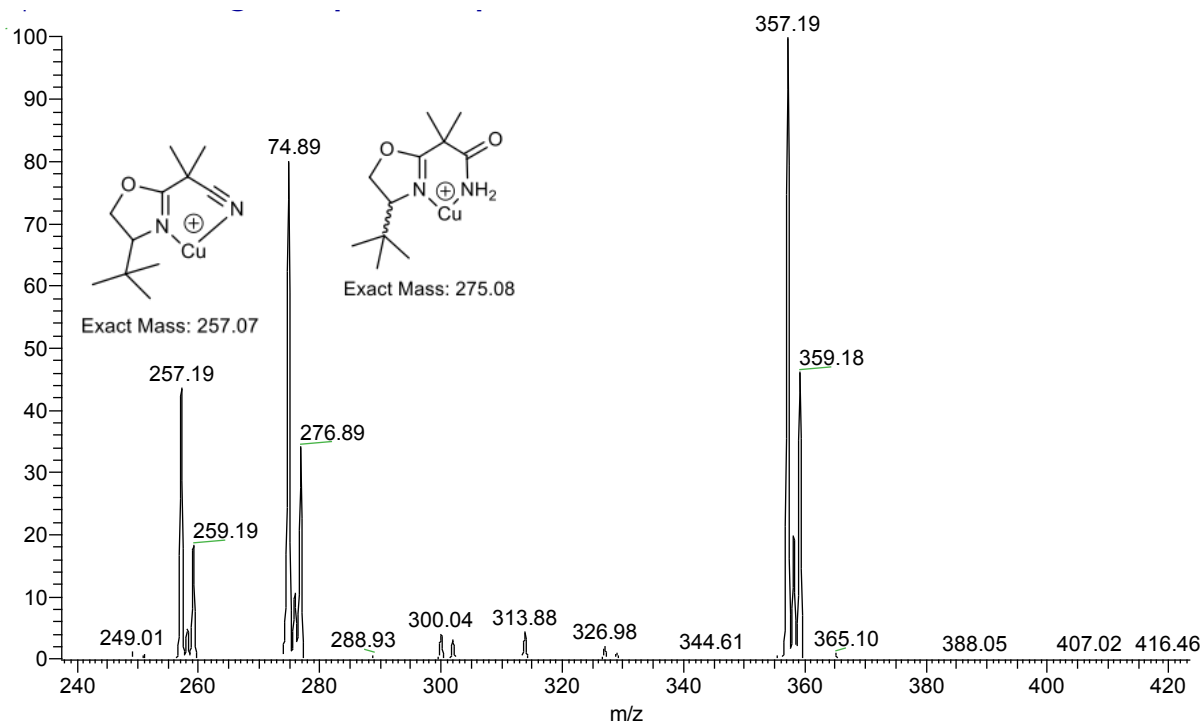


**Figure 100.** Isolation and fragmentation of 357 $m/z$  at 30% energy and 30 msec activation time.

Isolation of the 356  $m/z$  ion, with a narrow isolation width, followed by fragmentation at 30% energy and 30 msec activation time yielded a peak at 300  $m/z$  (Figure 101). This is most likely from Fenton-chemistry, with hydrogen abstraction of the

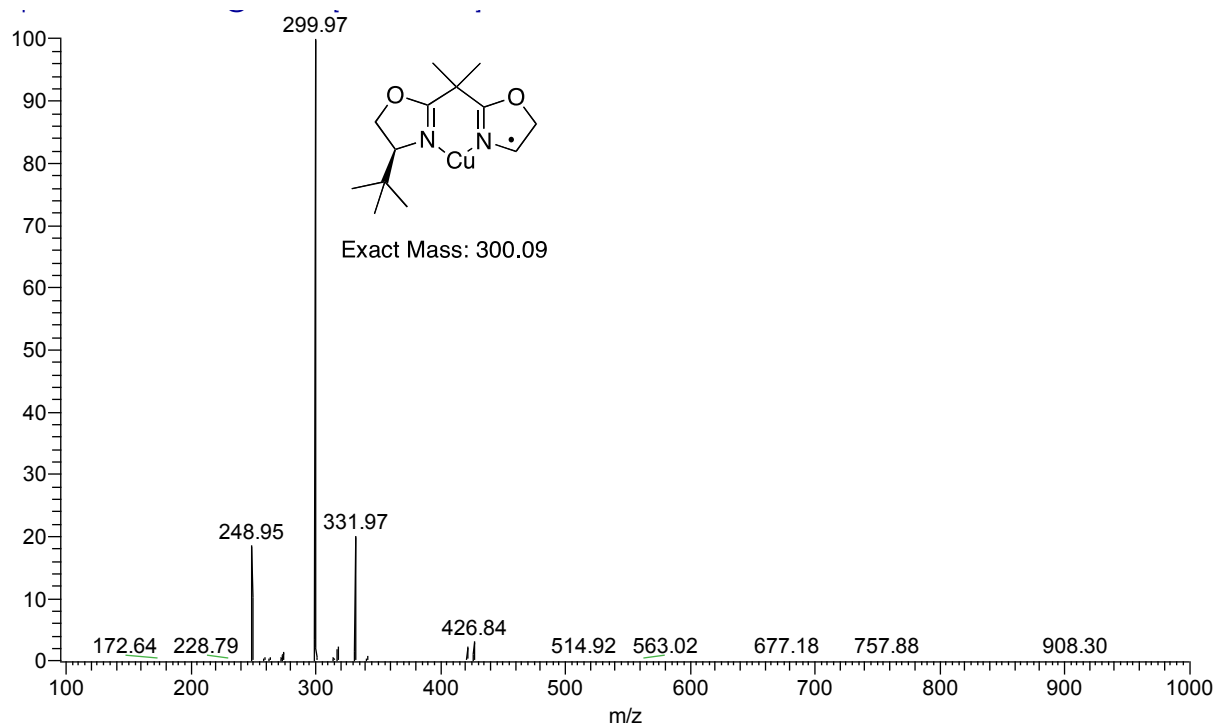


**Figure 101.** Isolation of 356  $m/z$ , followed by fragmentation at 30% energy and 30 msec activation time.

*t*-butyl group, followed by an alkyl shift. Subsequent fragmentation leads to a loss of the *t*-Bu group, leaving 300  $m/z$  (Figure 102).

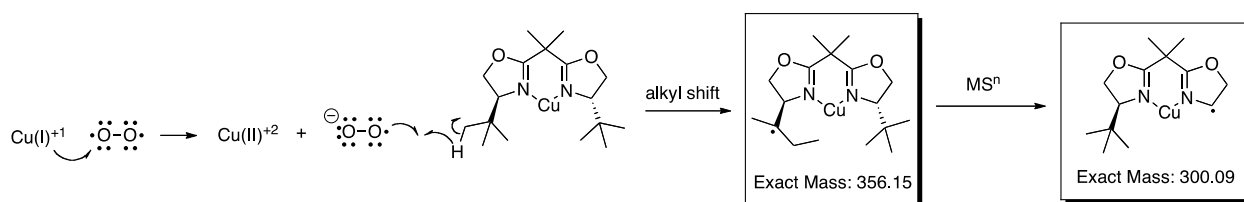


**Figure 102.** Proposed mechanism of the formation of the 356  $m/z$  ion, followed by fragmentation, leading to 300  $m/z$ .

Isolation of the 356  $m/z$  ion and subsequent reaction with 1-phenylethanol, yielded no coordination, potentially a result of oxidation of the copper and subsequent bond formation with the *t*-Bu group. Due to this investigation, the  $^{65}\text{Cu}$  isotope was isolated and reacted with the chiral reagents. This ensured the most accurate results possible,



while simplifying the integration and analysis. All results were obtained using this method.

### 5.13 – Conclusion

A new method for determining a catalyst's stereo-environment has been developed utilizing a modified QIT and a series of chiral probes. Due to the importance of cyclopropanes in chemistry, the excellent ee afforded by copper bis-oxazolines in cyclopropanations, and their commercial availability, the bis-oxazolines offered an excellent starting point for development of the method. Using commercially purchased chiral alcohols and epoxides, and synthesizing chiral ethers, the bis-oxazoline catalysts were systematically probed to determine the selectivity of each catalyst. The 1-phenyl-2-propanol, 2-methoxyethylbenzene, styrene oxide, and 1-phenyl-1-propanol proved to be the best chiral probes, ones that may be used to determine the asymmetric environment of unknown catalyst systems.

The data indicate that larger groups on the probe or the catalyst near the stereocenter afford better selectivity. The *t*-Bu and phenyl groups at the 4-position of the bis-oxazoline (B, C, E, G) yielded much better selectivity than the corresponding *iso*-propyl groups (D and F), with the a benzyl moiety (A) proving too big to coordinate. In general, the stereoselectivity observed by a catalyst was in good agreement with the literature, with catalyst E displaying better selectivity in the gas-phase than would be expected based on literature. The *R* preference was observed for most of the probes,

with the noticeable difference being styrene oxide, which preferred the *S* enantiomer in the gas-phase, the opposite enantiomer preference from that experienced in the condensed-phase.

A series of investigations were made to the method to improve performance, chief among them was the isolation of the  $^{65}\text{Cu}$  isotope to improve the accuracy of the results. It was discovered that the presence of oxygen and copper combined to produce an environment conducive to redox chemistry, altering the structure of the ligand in the process. Multiple experiments were performed to determine the reproducibility of the method. Accuracy was determined based on achiral results, which yielded no preferential selectivity. Sample prep variability was minimal, and the precision was deemed excellent based on multiple days of analysis with the same preparation. The RSD for the results, at least three sample preps on three different days, was below 6% for 90% of the results, with the higher RSDs most likely due to imperfect internal standards which give low peak ratios. Nonetheless, the method appears capable of determining the asymmetric environment produced by the bis-oxazoline catalysts.

With a combinatorial approach proven successful, the possibility of the method for use as a rapid chiral catalyst-screening tool is apparent. The next chapter will further explore the use of this method for that purpose.

## Chapter 6 – Di-Imines and the Combinatorial Approach

Since the previous work with the bis-oxazoline catalysts were run as single catalysts, the next step represented running catalysts in combination, using the mass spectrometer to filter and separate the catalysts. Di-imines were the natural choice for catalysts for use in development of a combinatorial method. The ease of synthesis from readily-available starting materials allows for a diverse array of ligands, with little effort.

Screening catalysts in a combinatorial fashion allows for a much simpler and faster process, by-passing many stages including purification, testing and analyzing, (Figure 103). A much more efficient process would consist of screening catalysts at the crude stage, via a combinatorial approach. The modified ion-trap mass spectrometer, affords the possibility of probing multiple chiral catalysts native environments at a much earlier stage in the catalyst development cycle, saving time, resources, and money in the process.

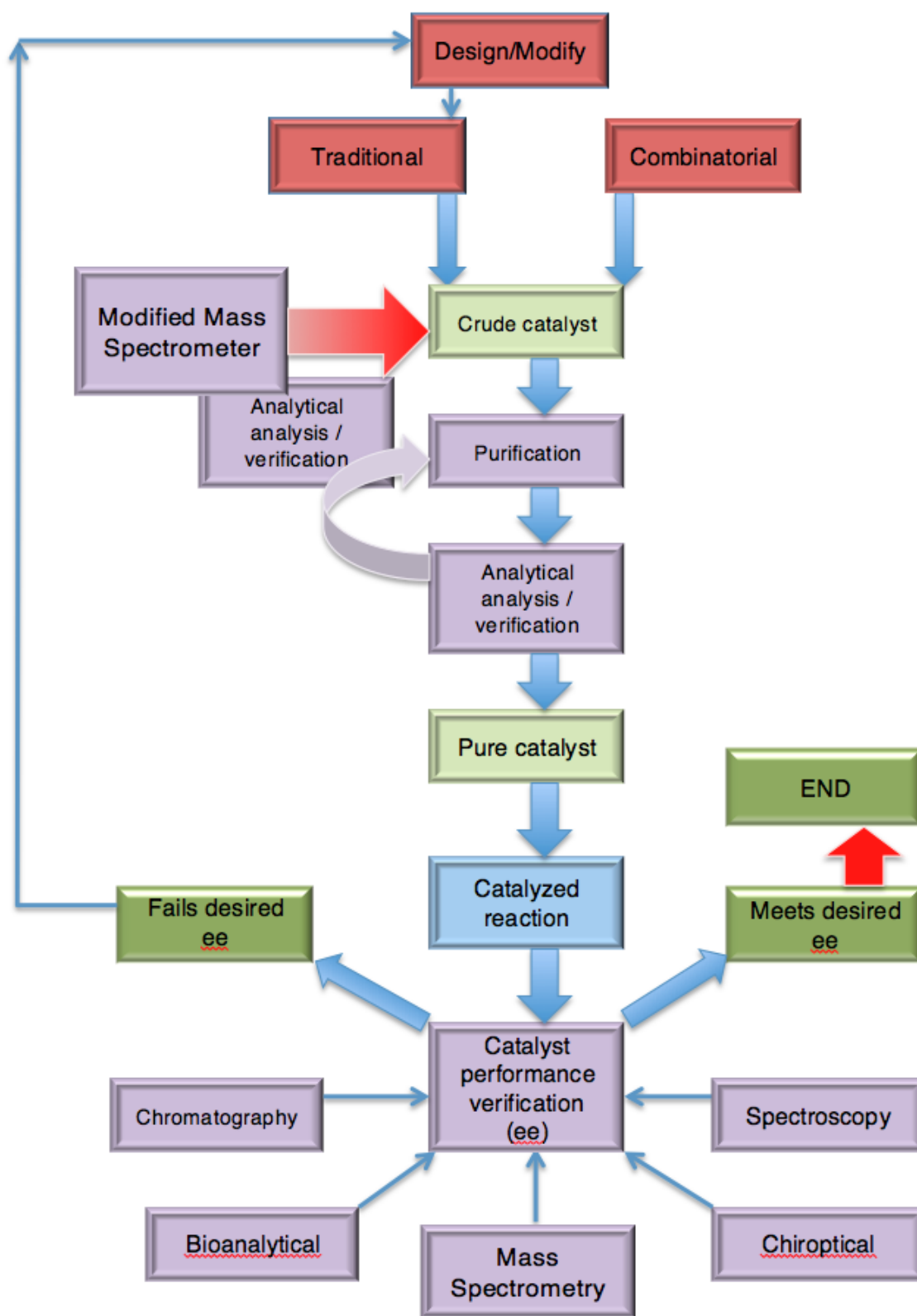


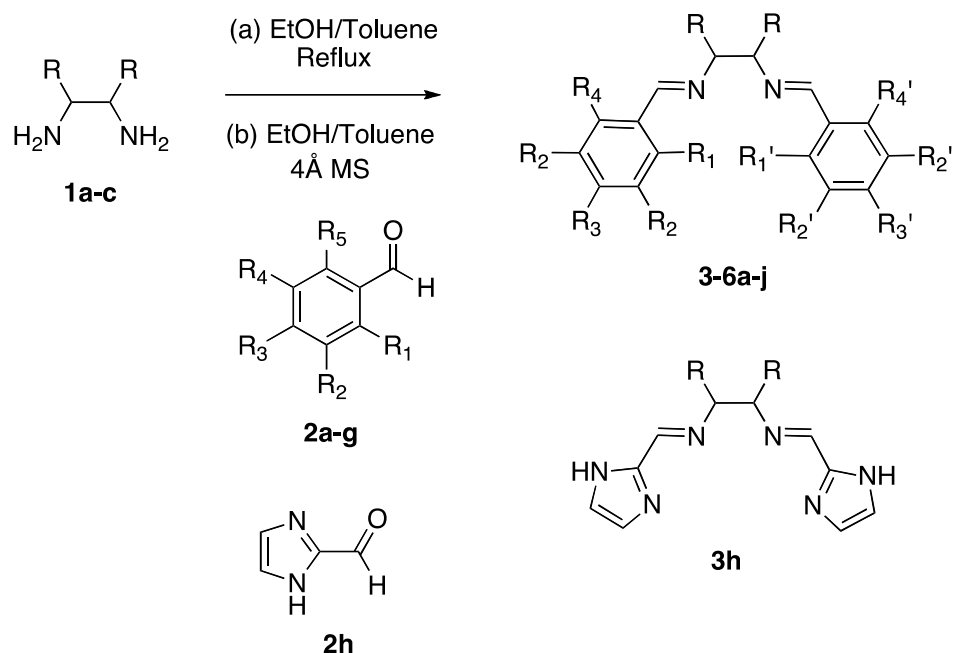
**Figure 103.** Catalyst Screening Process

The most common di-imine is Jacobsen's catalyst, also referred to as a Salen, used in asymmetric epoxidations; however, the metal used is Mn, not Cu.<sup>86</sup> Like the bis-oxazolines, copper is commonly used with di-imines (not Salens) in asymmetric aziridinations,<sup>289</sup> and cyclopropanations.<sup>253</sup>

The following chapter details the development of a rapid chiral catalyst screening method, utilizing the modified QIT and the previous chiral probes, particularly 1-phenyl-2-propanol, styrene oxide, and 1-methoxyethylbenzene.

## **6.1 – Synthesis of Di-imines**

Two general classes of di-imines were selected, with either an ethylene diamine or BINAM-based backbone. The following di-imines were synthesized starting from chiral amines and various aromatic benzaldehydes with the scheme below (Scheme 35).



**Scheme 35.** Synthesis of di-imines.

Table 15 displays the reagents and products used in the experiments.

**Table 15.** Starting materials and products used in the di-imine study.

	abbrev	R	enantiomer	R <sub>1</sub>	R <sub>2</sub>	R <sub>3</sub>	R <sub>4</sub>	R <sub>1</sub> '	R <sub>2</sub> '	R <sub>3</sub> '	R <sub>4</sub> '
1a			S & R								
1b		Ph	<i>meso</i>								
1c		1-napthalene	S & R								
2a				H	H	H	H				
2b				F	H	H	F				
2c				Me	H	Me	Me				
2d				H	<i>t</i> -Bu	H	H				
2e				Cl	H	H	Cl				
2f				OMe	H	H	OMe				
2g				Br	H	H	F				
3a	Benz	1a	S, R	H	H	H	H	H	H	H	H
3b	2,6-diF	1a	S, R	F	H	H	F	F	H	H	F
3c	Mesit	1a	S, R	Me	H	Me	Me	Me	H	Me	Me
3d	<i>t</i> -Bu	1a	S, R	H	<i>t</i> -Bu	H	H	H	<i>t</i> -Bu	H	H
3e	DiCl	1a	S	Cl	H	H	Cl	Cl	H	H	Cl
3f	OMe	1a	S	OMe	H	H	OMe	OMe	H	H	OMe
3g	2Br,6F	1a	S	Br	H	H	F	Br	H	H	F
3h	Imidaz	1a	S								
3i	3,5-diF	1a	S	H	F	H	H	H	F	H	H
4a	Ph Benz	1b	<i>meso</i>	H	H	H	H	H	H	H	H
4b	Ph DiF	1b	<i>meso</i>	F	H	H	F	F	H	H	F
4c	Ph Mes	1b	<i>meso</i>	Me	H	Me	Me	Me	H	Me	Me
4d	Ph <i>t</i> -Bu	1b	<i>meso</i>	H	<i>t</i> -Bu	H	H	H	<i>t</i> -Bu	H	H

4e	Ph DiCl	1b	<i>meso</i>	Cl	H	H	Cl	Cl	H	H	Cl
4f	Ph OMe	1b	<i>meso</i>	OMe	H	H	OMe	OMe	H	H	OMe
4g	Ph Br/F	1b	<i>meso</i>	Br	H	H	F	Br	H	H	F
4h	Imidaz	1b	<i>meso</i>								
4i	3,5-diF	1b	<i>meso</i>	H	F	H	H	H	F	H	H
5a	Benz	1c	S, R, racemic	H	H	H	H	H	H	H	H
5b	3,5-diF	1c	S	H	F	H	H	H	F	H	H
5c	Mes	1c	S, R	Me	H	Me	Me	Me	H	Me	Me
5d	3,5-di- <i>t</i> -Bu	1c	S	H	<i>t</i> -Bu	H	H	H	<i>t</i> -Bu	H	H
5e	DiF2,6	1c	S	F	H	H	F	F	H	H	F
5f	OMe	1c	S	OMe	H	H	OMe	OMe	H	H	OMe
5g	DiCl2,6	1c	S	Cl	H	H	Cl	Cl	H	H	Cl
5h	DiCl3,5	1c	S	H	Cl	H	H	H	Cl	H	H
5i	2Br,6F	1c	S	Br	H	H	F	Br	H	H	F
6a	Mes/F	1c	S	Me	H	Me	Me	H	F	H	H
6b	Benz/mes	1c	S	H	H	H	H	Me	H	Me	Me
6c	Benz/ <i>t</i> -Bu	1c	S	H	H	H	H	H	<i>t</i> -Bu	H	H
6d	Benz/F	1c	S	H	H	H	H	H	F	H	H
6e	Benz/BrF	1c	S	H	H	H	H	Br	H	H	F

### 6.1.1 – General Synthesis Procedure

To an appropriate-sized round bottom flask (RBF), usually 25 mL, the chiral diamine was weighed and added to the RBF. Approximately 5 mL of ethanol was added, quantitatively transferring the diamine to the flask. Then 0.95 eq of the aldehyde was added to the RBF and stirred with a magnetic stir-bar. Reactions were conducted by either heating to reflux or by the addition of 50 mg of 4Å molecular sieves. Reaction times were 1-2 hours for refluxing, and 1-3 days for the molecular sieves. Toluene was added if the diamine did not readily dissolve.

For reactions at reflux, the solution was allowed to cool to room temperature, after which the product precipitated. The product was then cooled to 0 °C and filtered. In some cases a 2<sup>nd</sup> crop was isolated. In the cases where molecular sieves were

used, the solution was filtered to remove the molecular sieves, followed by washing with 1-3 mL of ethanol. The product was allowed to precipitate, then filtered and washed. For the BINAM cases, the solutions required rotary evaporation, followed by recrystallization in petroleum ether and hexanes. However, in most cases, this was unsuccessful and the crude product was utilized.

For compounds 6a-e, 200 mg of diamine was mixed with approximately 1.3 equivalents of the various benzaldehydes in a RBF. Approximately 20 mL of ethanol was used to dissolve the mix and 100 mg of 4Å molecular sieves was added. The solution was stirred with a magnetic stir bar for 1 day, after which the solution was evaporated via a rotary evaporator, followed by the quick addition of methanol to prevent oxidation. The crude solution was stored in the refrigerator when not in use. Specific procedures may be found in the appendix.

Mass spectra were taken for all samples. In addition, collision-induced dissociation was used to generate fragmentation patterns. Selected samples were subjected to NMR analysis (see appendix).

## **6.2 – Combinatorial Approach**

As a first step, it was necessary to optimize conditions for simultaneously evaluating multiple catalysts in a single sample/solution. This is a significantly different strategy than the simpler approach with the bis-oxazolines, where a single catalyst was



present in each sample that was evaluated. After evaluating several copper salts and combination of salts, it was found that a mixture of CuI and CuCl gave the best results. This combination avoided counter-ion complexes observed with triflate salts and the CuI limited redox degradation of the ligand by Fenton chemistry. A spectrum for a solution containing multiple ligands and the CuCl/CuI mix is given in Figure 104.

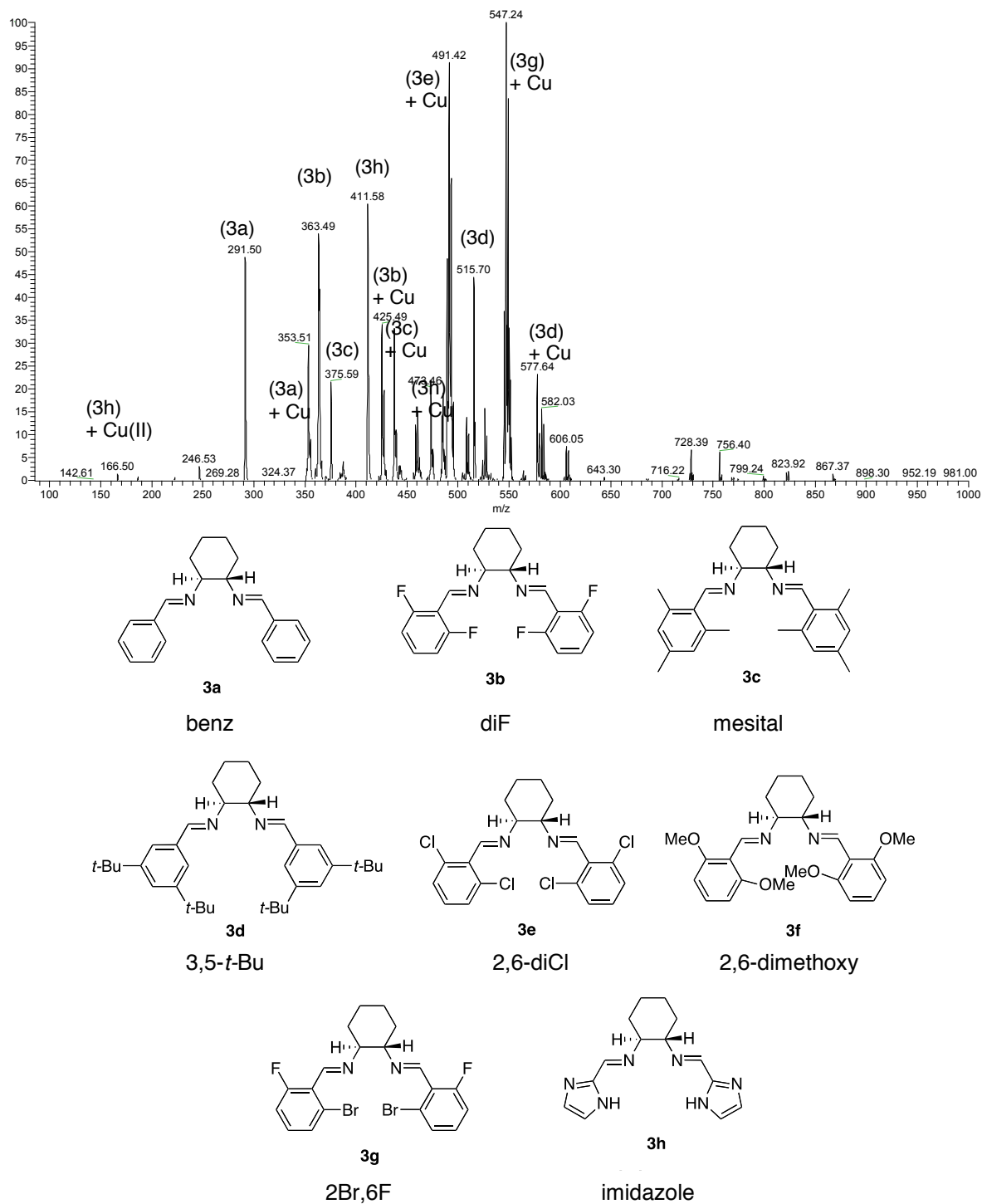


**Figure 104.** Mix of catalysts with CuI:CuCl in approximately 1:1 ratio, with the structures and assignments.

The copper mix was run as a saturated solution, which gave the highest abundance of signal.

The role of the iodide anion was to reduce any Cu(II) back to Cu(I), forming iodine in the process. This was evident in a brownish color solution over time. Degassing the solvent minimized the presence of oxygen that initiated the reaction. A solution containing only CuI was tried, but no coordination with the ligand was observed (Figure 105). Since the ligands bearing coordinating substituents at the ortho position (e, f, g, and h) did not coordinate, they were not included in future mixes.

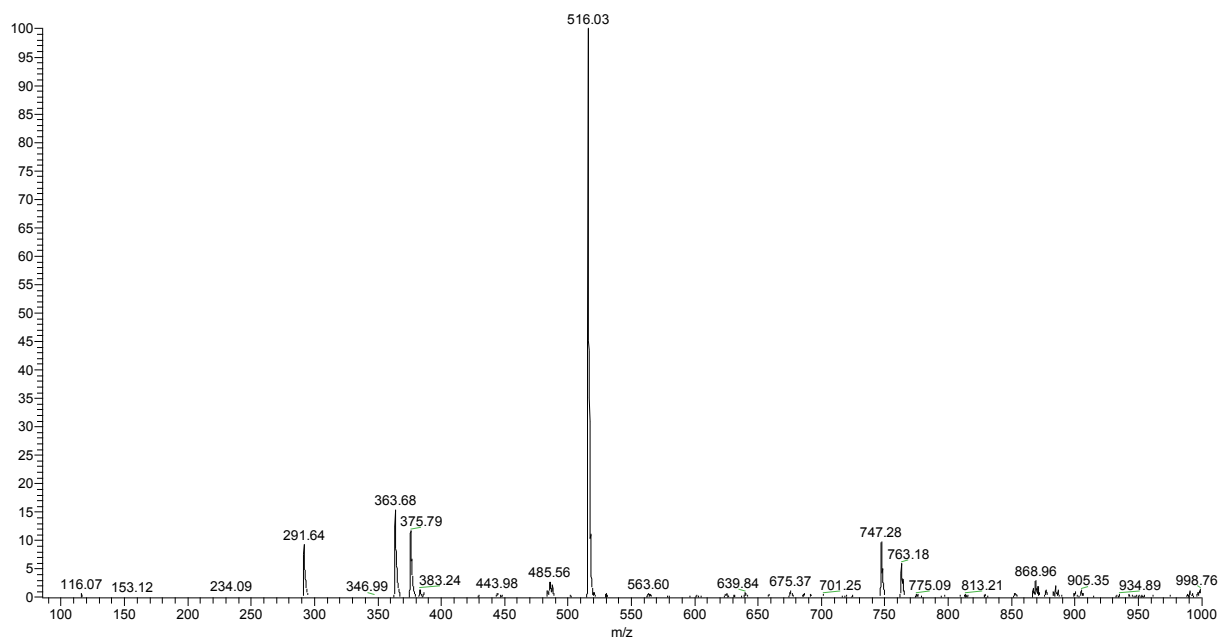


**Figure 105.** Ligand mix with CuI. No coordination evident.

The ratio of the copper salts in the solution was critical. Much cleaner spectra were observed with a 1:1 CuI/CuCl mix (Figure 106a) compared to a 2:1 mix (Figure 106b).

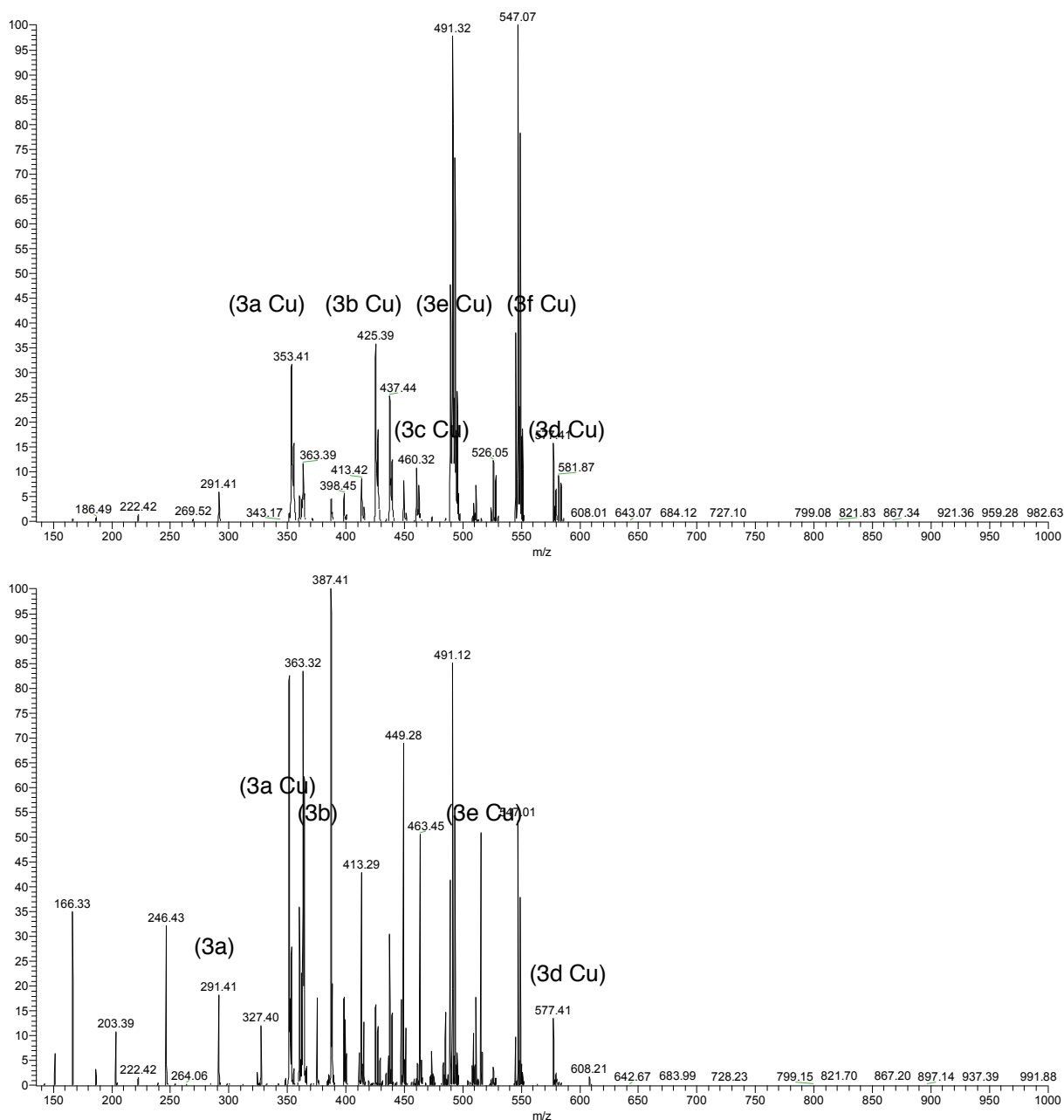


**Figure 106.** (a) – Catalyst mix with good ratio (1:1) of CuI:CuCl. (b) - Same ligand mix with a 2:1 ratio CuI:CuCl.

With the CuCl:CuI ratio fixed, stock ligands solutions of the ligands were made at approximately 1-2 mg of ligand per 1.5 mL of copper solution. A saturated solution of copper salt was made at time-of-use by mixing a 1:1 ratio of CuI:CuCl (approximately

15-20 mg each) into 1.5 mL of degassed MeOH, and vortexing the solution to mix it. The solution was centrifuged and the supernatant was transferred into a clean vial. The stock ligand solutions were kept in the refrigerator when not in use. Approximately 50  $\mu$ L of each stock ligand solution was added to a vial and diluted to 1.5 mL with methanol. 200  $\mu$ L of stock copper solution was added to a vial and diluted to 1.5 mL with degassed methanol. The dual syringe method was utilized for the mixing the copper solution and ligands and infused into the instrument at a rate of 1-5  $\mu$ L per minute.

### 6.3 – *Trans*-1,2-diaminocyclohexane-based Di-Imine Cu Catalysts

Using a narrow isolation width of 1.0 m/z, each catalyst in the mixture was isolated with the  $^{65}\text{Cu}$  isotope in the ITMS and allowed to reach equilibrium with the chiral probe. The procedure was the same as in the bis-oxazoline work. Results for the combinatorial approach for the (1S,2S) cyclohexane di-imine are shown below, grouped by chiral probe (Figure 107) and catalyst (Figure 108). The results were also converted to diastereomeric excess and are shown in Figure 109, followed by the results displayed as box plots in Figure 110.

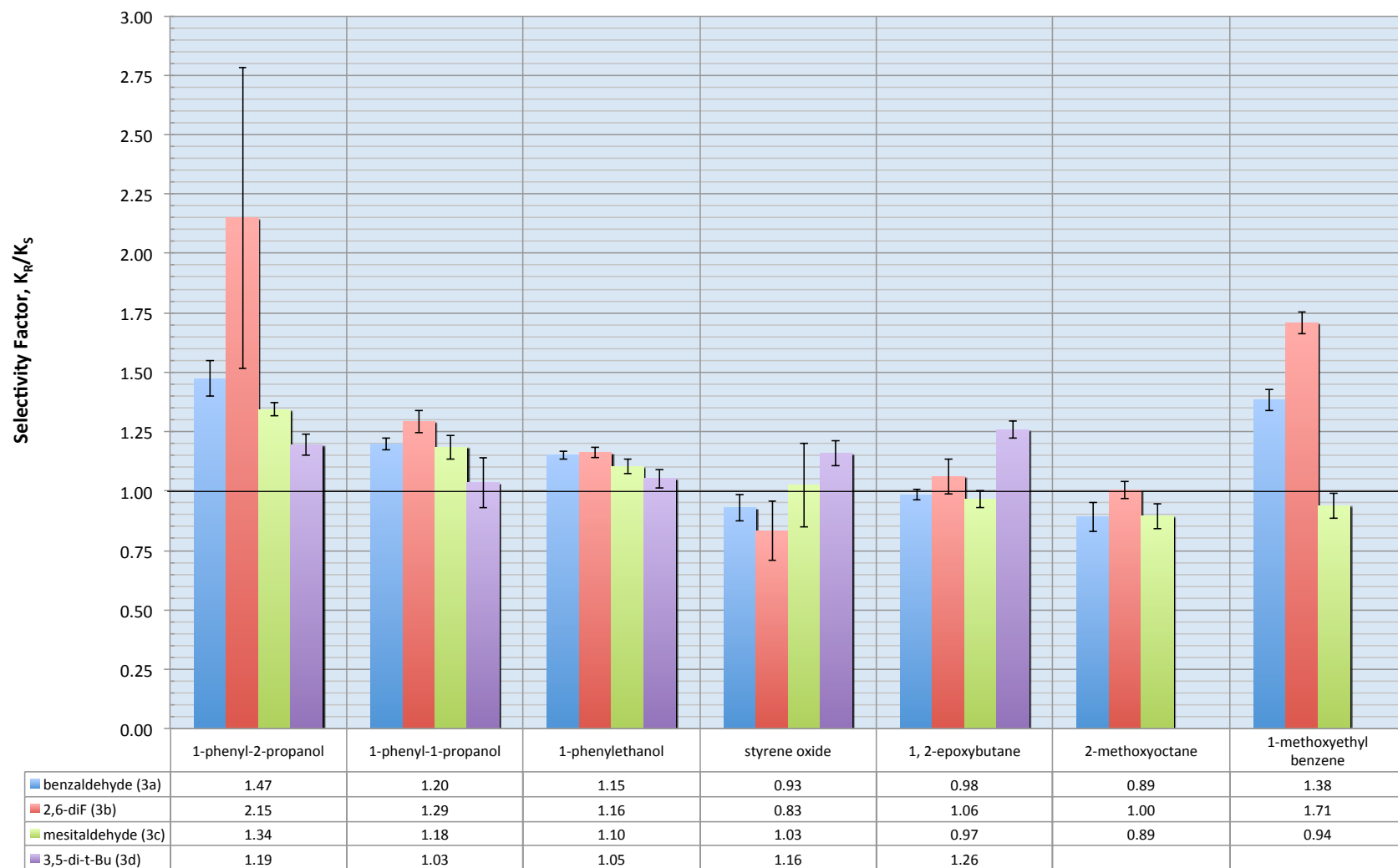


**Figure 107.** Results of the (1*S*,2*S*) cyclohexane di-imine catalysts.

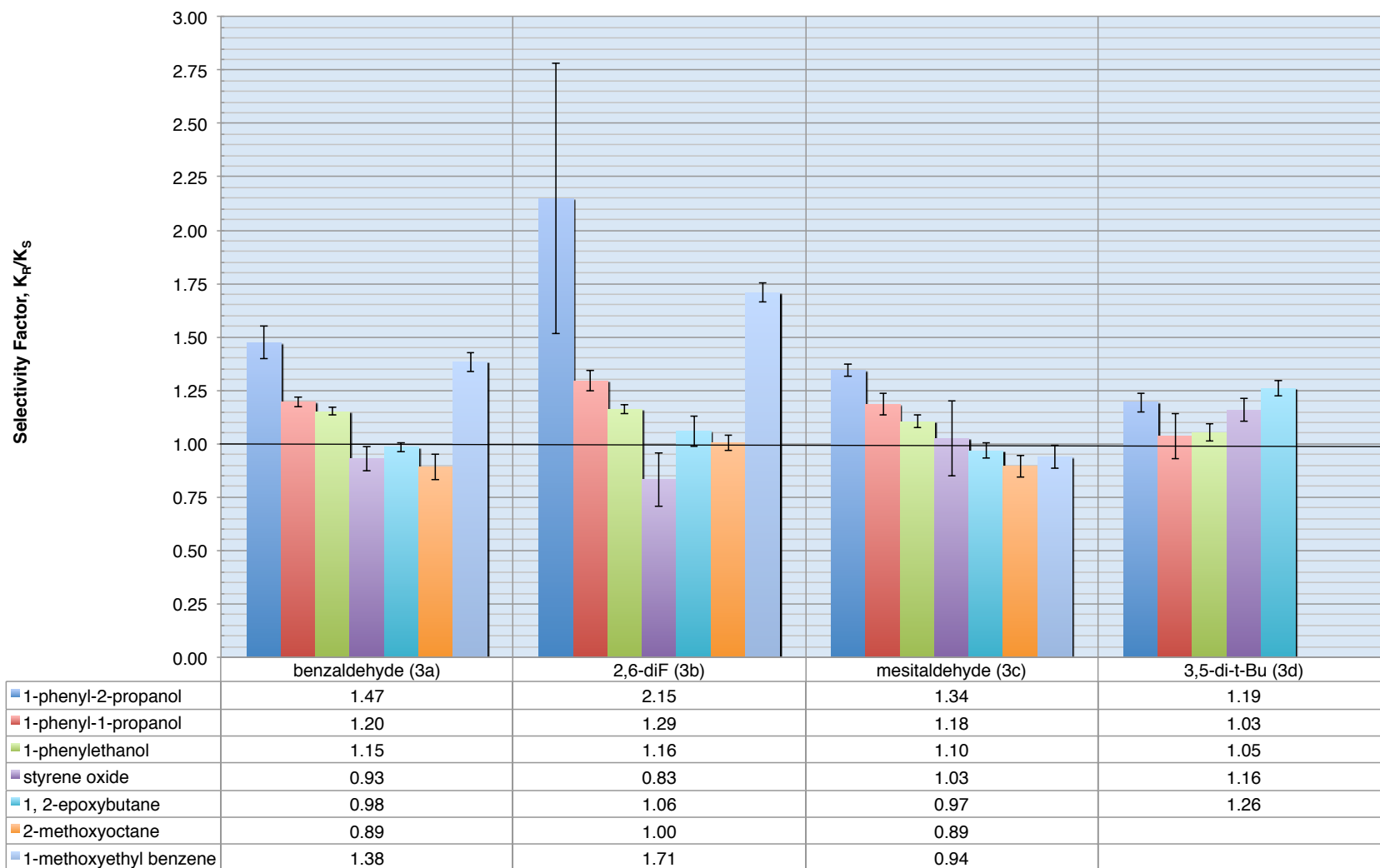


**Figure 108.** Results grouped by catalyst.

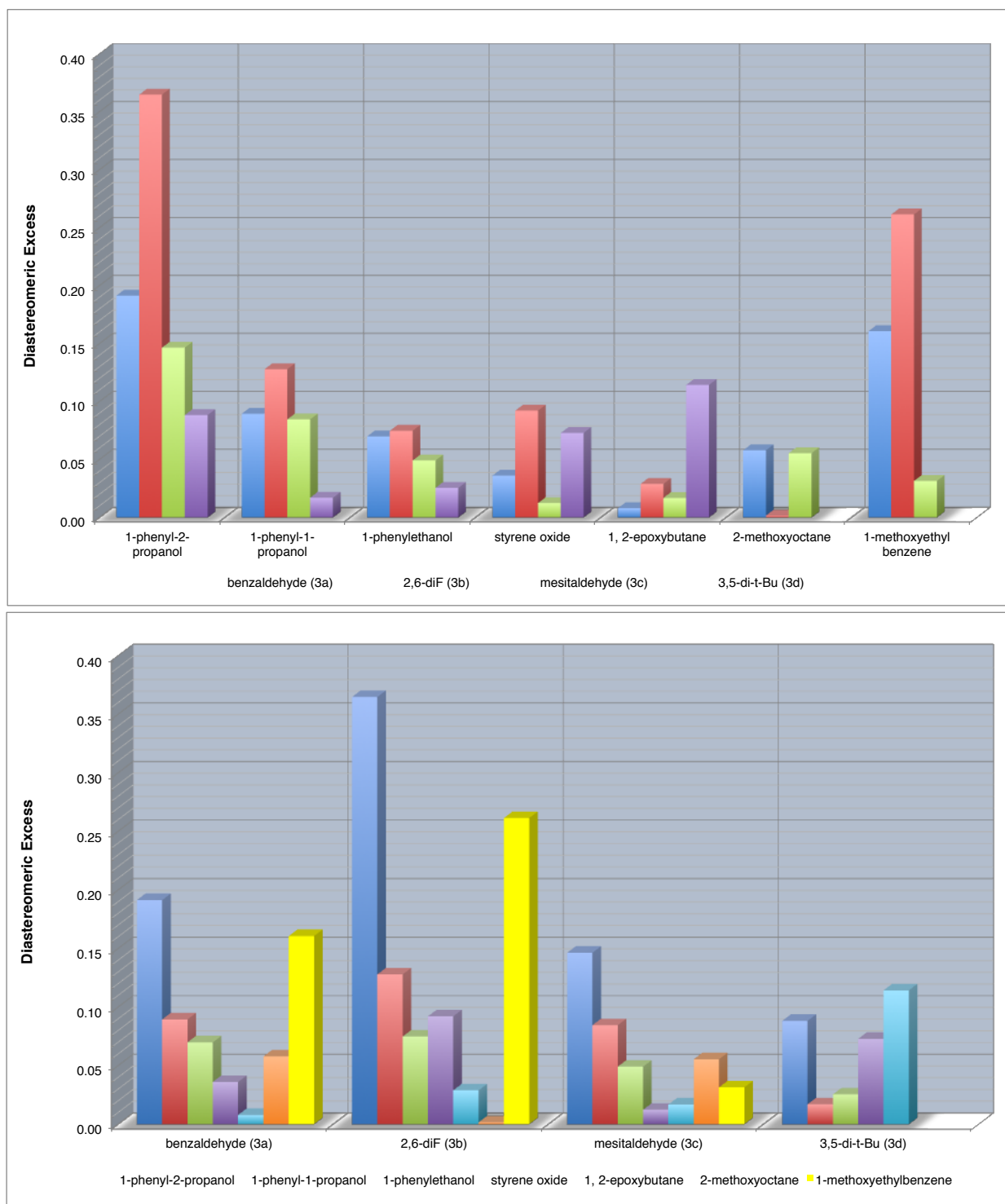


**Figure 109.** Results converting equilibrium ratios to diastereomeric excess.



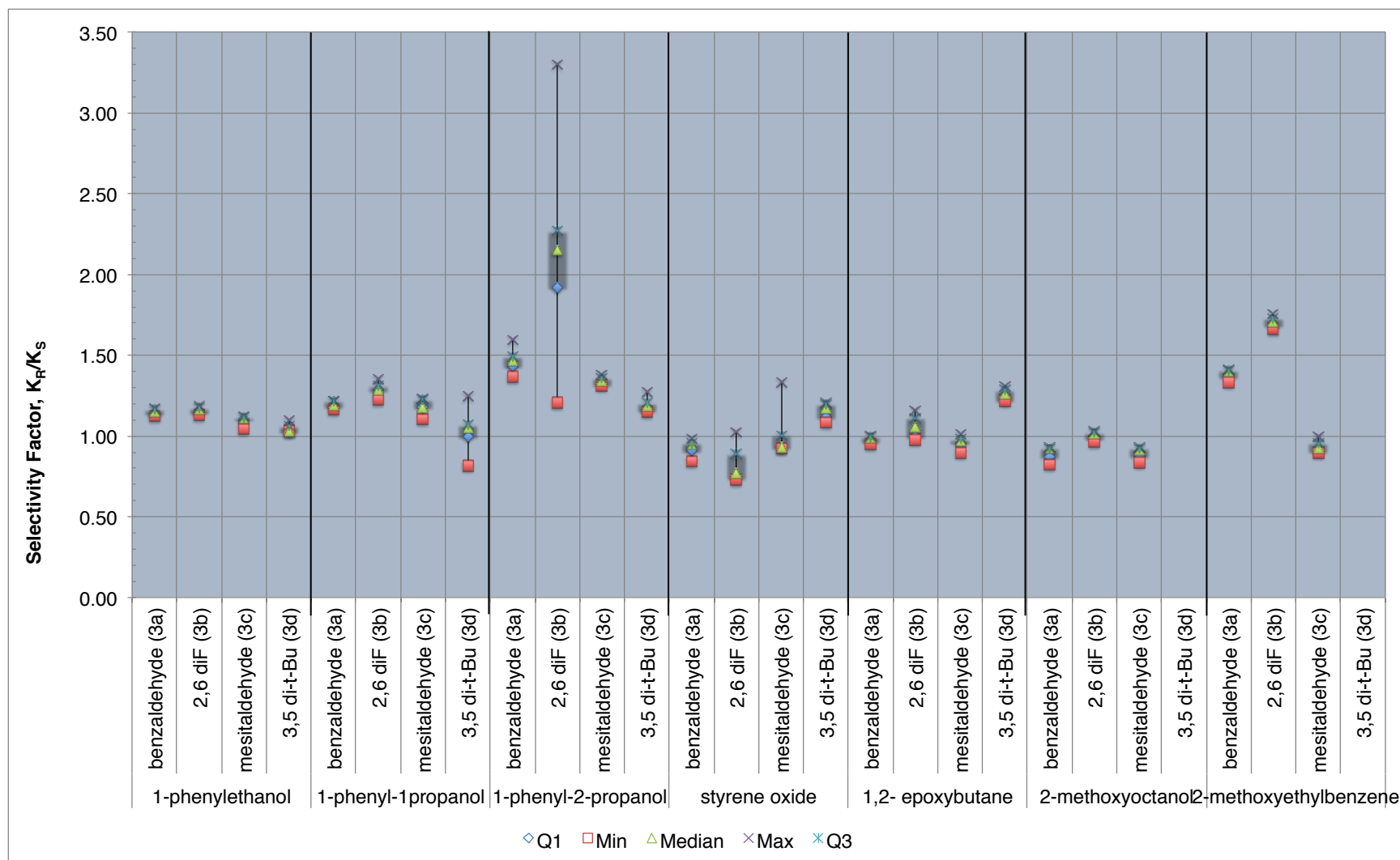


**Figure 110.** Results presented as box plots.

### 6.3.1 – General Discussion

The selectivity was much lower than that observed for the bis-oxazolines. The chiral probe 1-phenyl-2-propanol had the highest average selectivity, followed by 1-methoxyethylbenzene (Table 16).

**Table 16.** Averages for the chiral probes with the (1*S*,2*S*) cyclohexane di-imines.

	1-phenyl-2-propanol	1-phenyl-1-propanol	1-phenylethanol	styrene oxide	1,2-epoxybutane	2-methoxyoctane	1-methoxyethylbenzene
Average $K_R/K_S$	1.50	1.17	1.12	0.98	1.06	0.93	1.30

The probe styrene oxide displayed significantly lower selectivity than for the bis-oxazolines, with the 2-methoxyoctane again displaying a slight preference for the *S* enantiomer (as with styrene oxide), in contrast with the others and an *R* preference.

There appears to be a slight inverse relationship to the size of the substituent group and the observed selectivity. For example, when excluding the catalyst (3b) the 1-phenyl-2-propanol probe displayed higher selectivity with the unsubstituted benzaldehyde, followed by the bulkier mesitaldehyde, and finally the much bulkier *t*-Bu substituted catalyst. Counter intuitively, the added steric bulk negatively affects the mechanism of stereoselectivity in these systems.

This is also reflected in the binding energies of the complexes (Table 17).

**Table 17.** Free energy of binding for the trans cyclohexane di-imines (kcal/mol).

	1- PhEtOH	1-Ph- 1Pro	1-Ph-2- Pro	Styrene Oxide	1,2- Epoxybutane	2-methoxy octane	1-methoxy ethylbenzene
Benz (3a)	-12.7	-12.4	-12.8	-10.8	-11.6	-15.7	-11.8
DiF (3b)	-14.0	-15.9	-16.7	-13.5	-10.4	-15.8	-15.4
Mesital (3c)	-11.2	-9.7	-10.9	-8.9	-9.6	-10.1	-10.8
<i>t</i> -Bu (3d)	-11.4	-10.6	-12.1	-11.6	-10.5		

Introduction of steric bulk generally decreases the binding energy, following the pattern observed earlier with decreasing selectivity with increasing bulk. For example, catalysts 3c and 3d display weaker binding than the unsubstituted 3a catalyst. Plotting the Gibbs free energy of binding versus selectivity factor, shows a weak correlation between the selectivity and binding energy for the phenyl-based alcohols, and 1-methoxyethylbenzene (Figure 111).

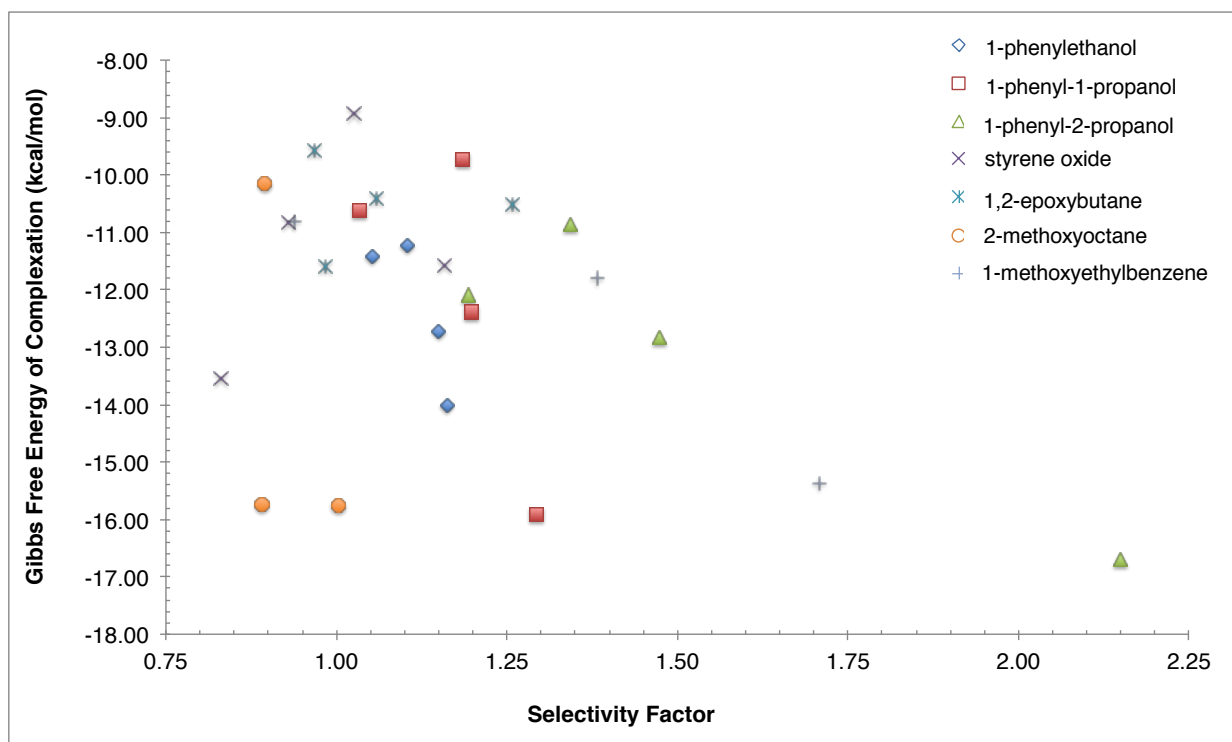


**Figure 111.** Plot of  $\Delta G$  versus selectivity factor.

The data shows the DiF catalyst binds the strongest to the probes except 1,2-epoxybutane and 2-methoxyoctane. The free energy of binding was plotted against the molecular weights of the chiral probes (Figure 112). Polarizability clearly drives the binding energy for the 3b catalyst, but for the others, the benefit of the larger molecular weight and polarizability is offset by the added steric interactions.

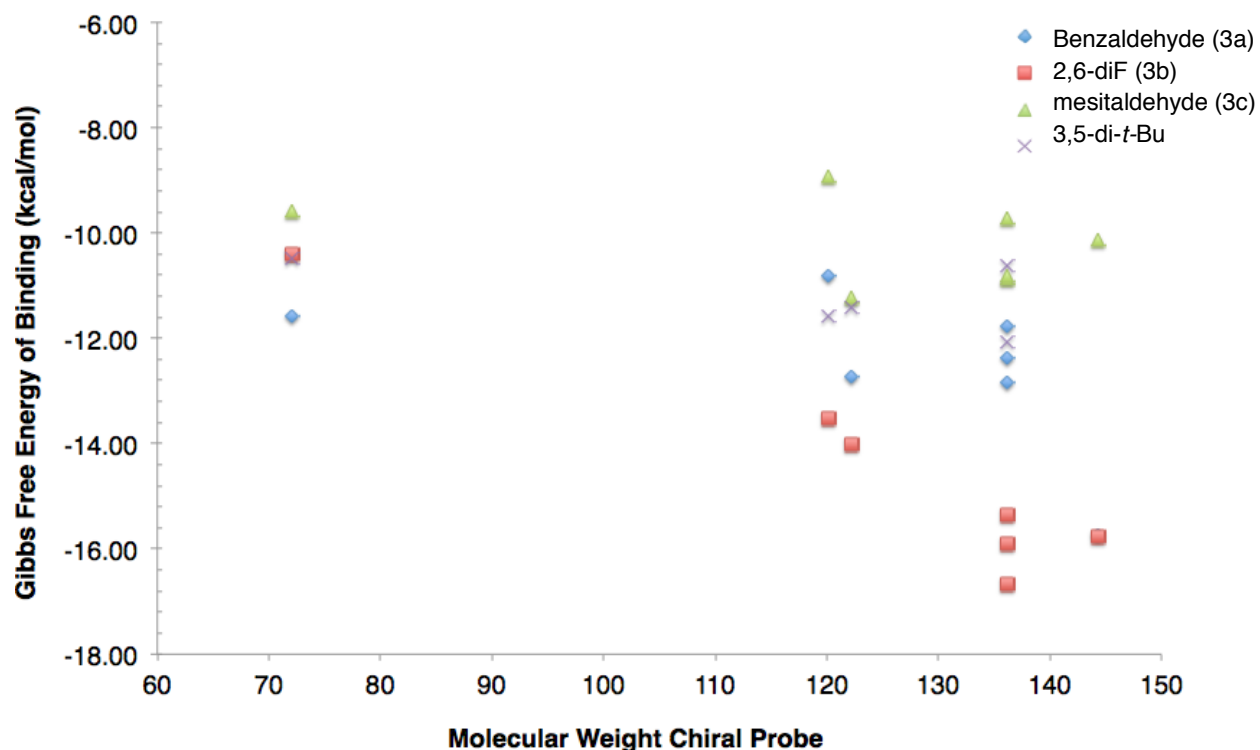


**Figure 112.** Gibbs Free Energy of binding versus chiral probes molecular weight.

For example, the *t*-Bu catalyst (3d) displayed a flat line, indicating any benefit gained from the polarizability of the larger probe is negated by the steric interactions between the *tert*-butyl groups and the probe near the copper-coordinating site. The difference in Lewis basicity between the styrene oxide and 1-phenylethanol is not as pronounced as it was in the bis-oxazolines, with 3d and 3b displaying small differences, and the 3a and 3c displaying larger differences.

The most common catalyst in the literature is the 2,6 dichloro-based catalyst (3e), which did not coordinate in the gas-phase here. The lone-pair electrons from an *ortho* chlorine can interact with the copper and prevent coordination of the probe. This

the results were within error of the theoretical value 1. Only one sample prep was performed for the R enantiomers, so some of the error could also be due to the limited number of repeats.

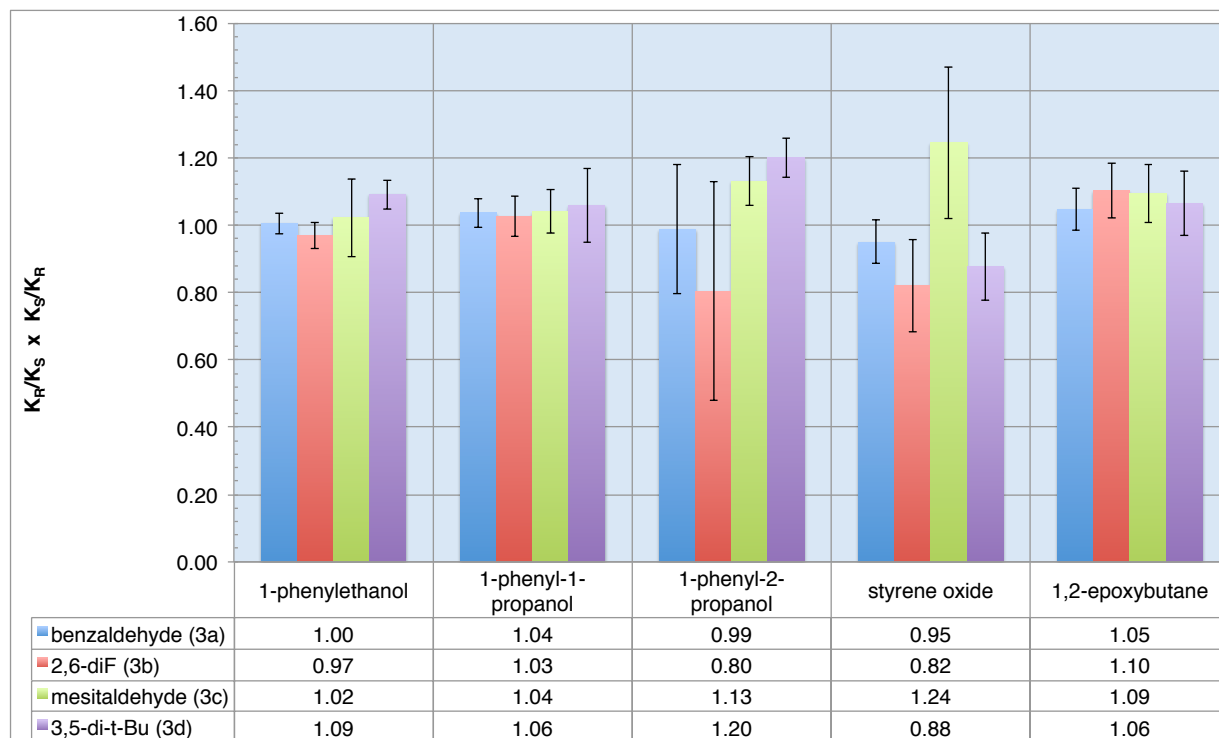


**Figure 114.** Chiral cross check of the di-imines.

### 6.3.3 – Combinatorial versus Single Runs

To ensure there were no other isobaric species in the catalyst mixture that were affecting the selectivity results, the combinatorial runs were compared against the catalysts run by themselves. The results are shown in Figure 115. All the results were statistically the same between the single runs and the combinatorial experiment, except for the mesitaldehyde and 1-phenyl-1-propanol system.

the results were within error of the theoretical value 1. Only one sample prep was performed for the R enantiomers, so some of the error could also be due to the limited number of repeats.

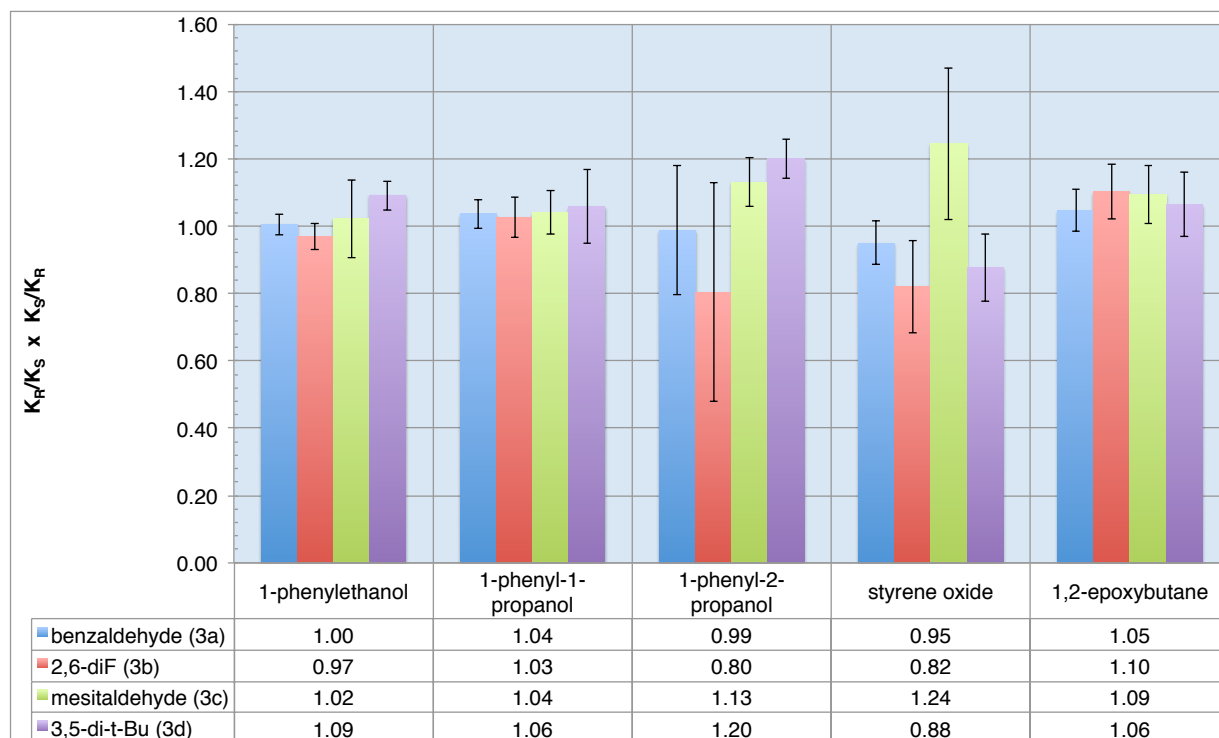


**Figure 114.** Chiral cross check of the di-imines.

### 6.3.3 – Combinatorial versus Single Runs

To ensure there were no other isobaric species in the catalyst mixture that were affecting the selectivity results, the combinatorial runs were compared against the catalysts run by themselves. The results are shown in Figure 115. All the results were statistically the same between the single runs and the combinatorial experiment, except for the mesitaldehyde and 1-phenyl-1-propanol system.

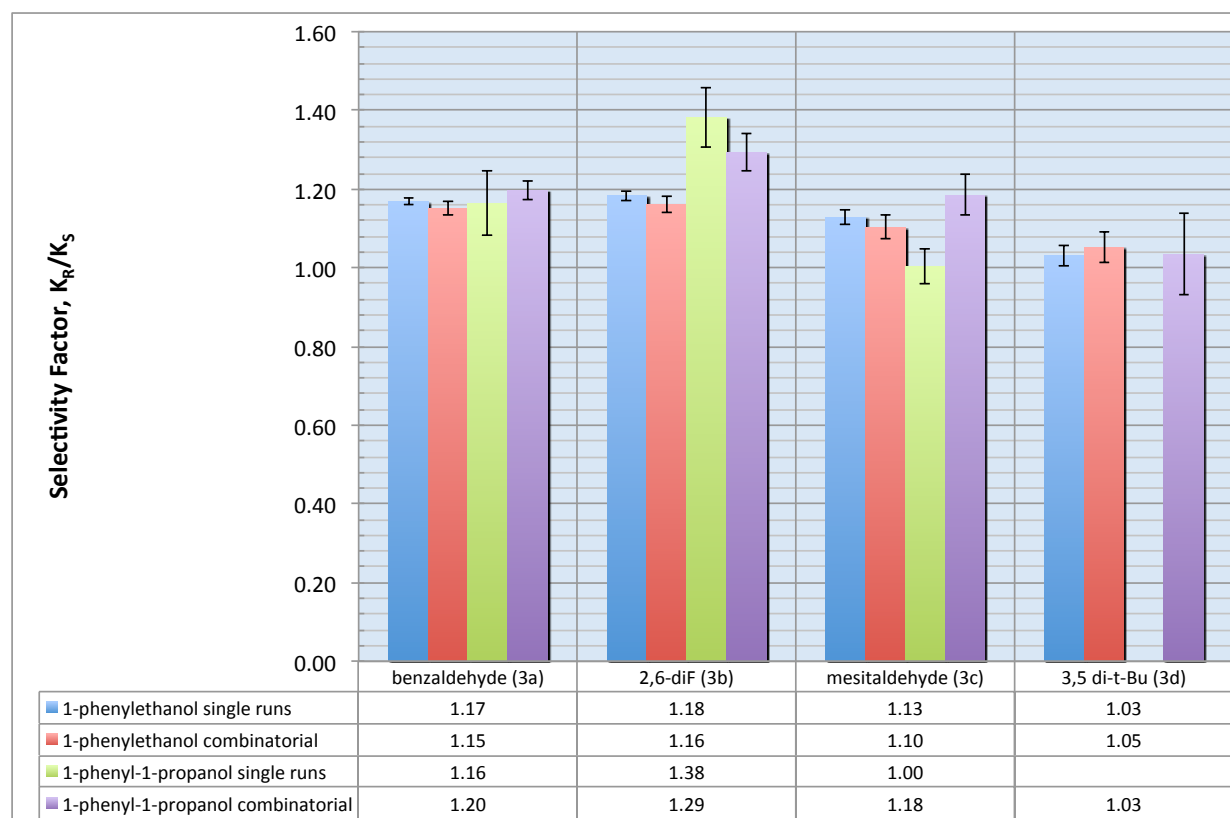


**Figure 115.** Single versus combinatorial runs.

Fragmentation was performed on each catalyst run separately, and in a mixture of catalysts, to ensure there were no other isobaric species present. The fragmentation patterns were compared (Figure 116) to ensure there were no other  $m/z$  fragments

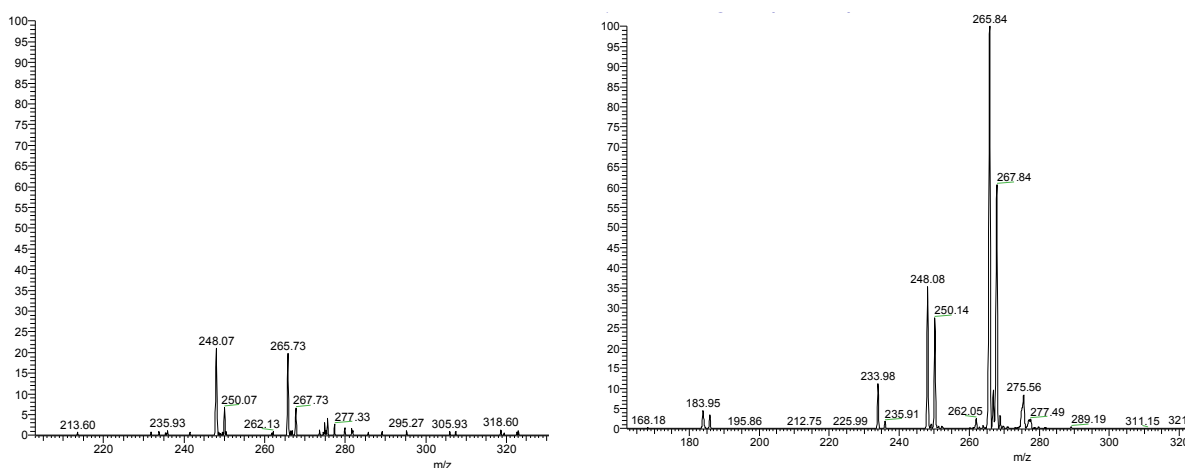


**Figure 116.** Fragmentation of the benzaldehyde catalyst (3a) isolated from a mixture (left) and from a pure solution (right).



arising from different species. The ratios may not have been exact due to the smaller signal (lower ion abundance) when run as a mixture, as well as variation in instrument performance. The other patterns are found in the appendix.

#### **6.3.4 – RSD**

The RSD values were generally good, with the majority (85%) of the results for the multiple runs under 7% (Figure 117). Half of the styrene oxide runs had high deviations due to the weak coordination of the probe, and non-ideal internal standard/analyte ratios (Figure 118).

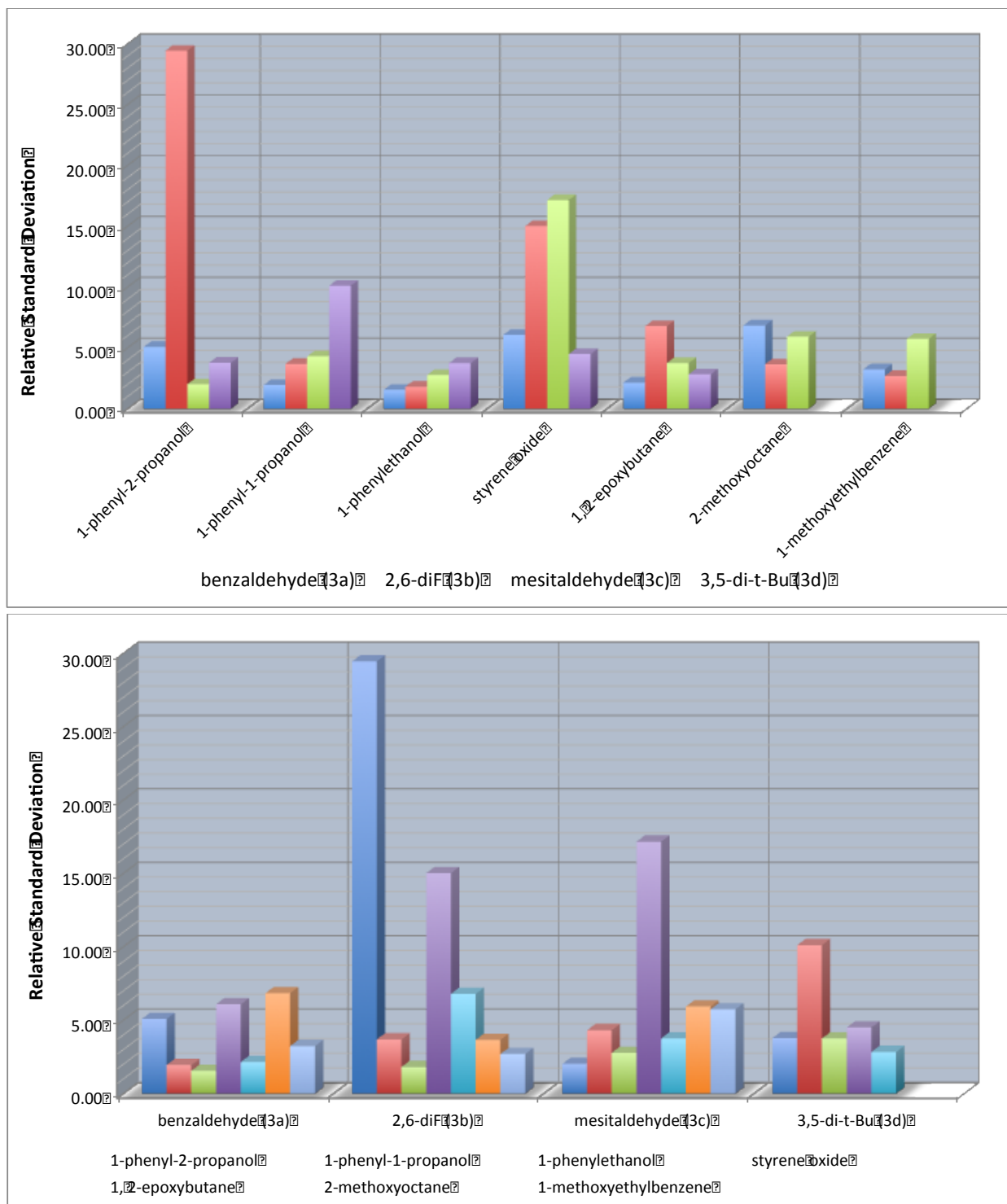


**Figure 117.** RSD of the trans cyclohexane di-imine results. Top – grouped by chiral probe. Bottom – grouped by catalyst.

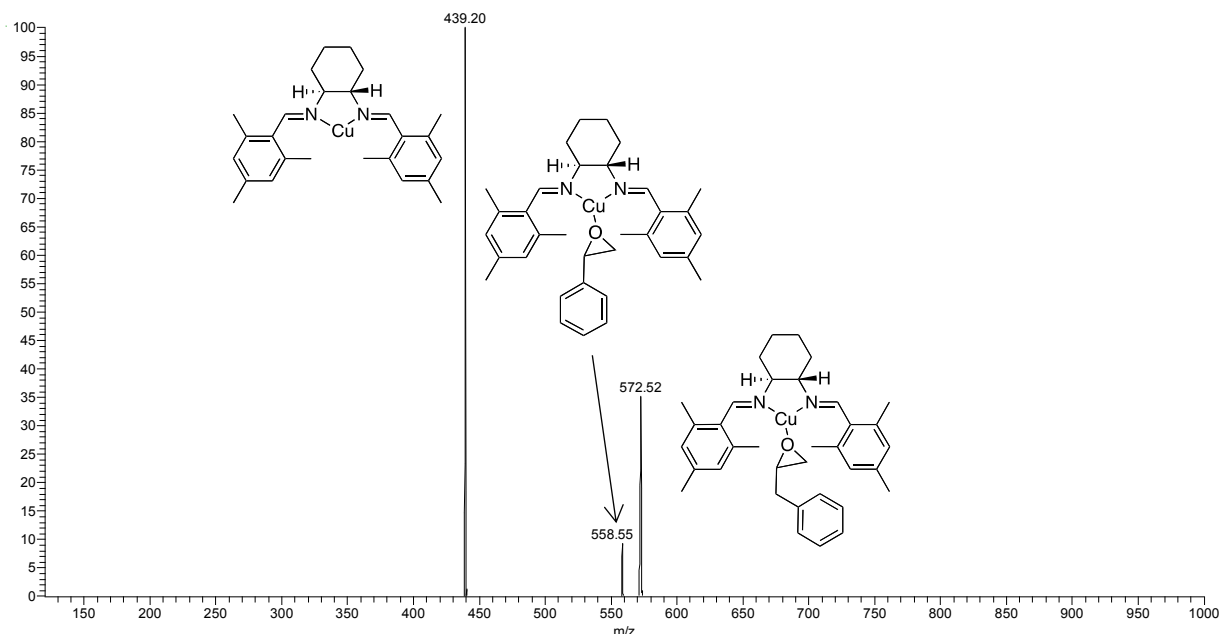


**Figure 118.** (S) Styrene oxide with internal standard and catalyst 3c.

There was extreme variability observed with the fluorine-based catalyst 3b and 1-phenyl-2-propanol. Part of this may be explained by the ratio of the internal standard and analyte being far from ideal (Figure 119); however, the mixing ratios were not too far from those used with styrene oxide, which while displaying high RSD itself, was not of the same magnitude observed for 1-phenyl-2-propanol. Thus, there may be other contributing factors to the high RSD values.

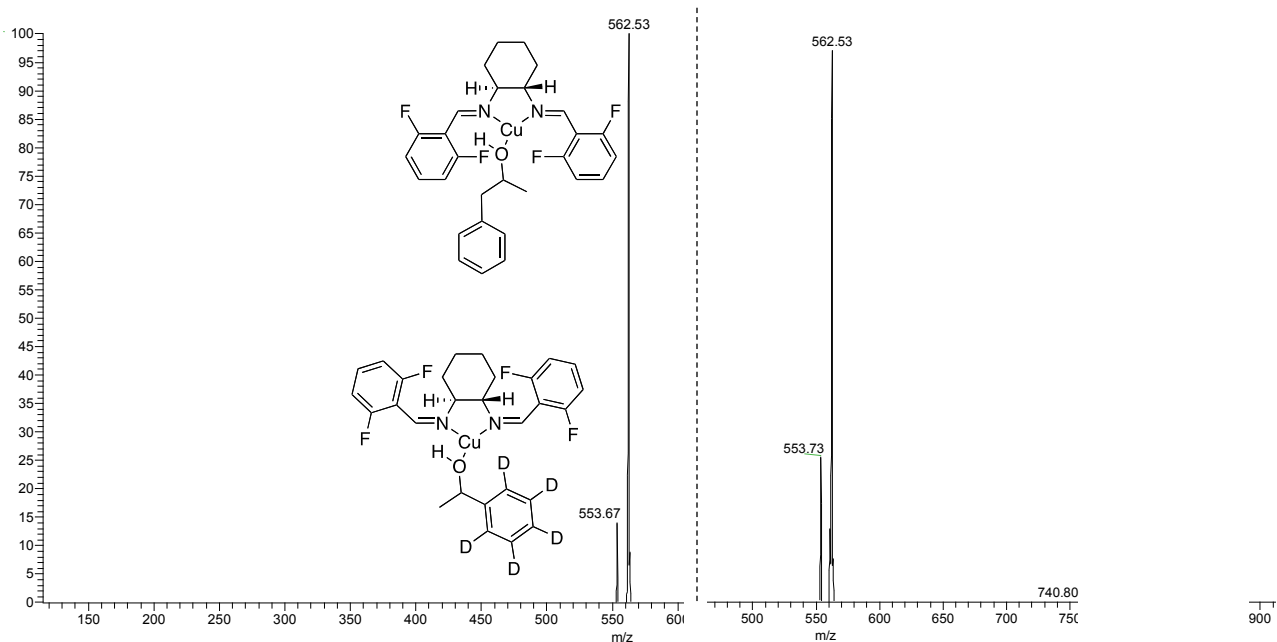


**Figure 119.** 1-phenyl-2-propanol spectra. (*S*) enantiomer on the left and (*R*) enantiomer of the right.

One possibility is a Lewis-acid catalyzed nucleophilic attack at the imine carbon (Figure 120). Even if this were a minor pathway it could significantly affect the ratios.

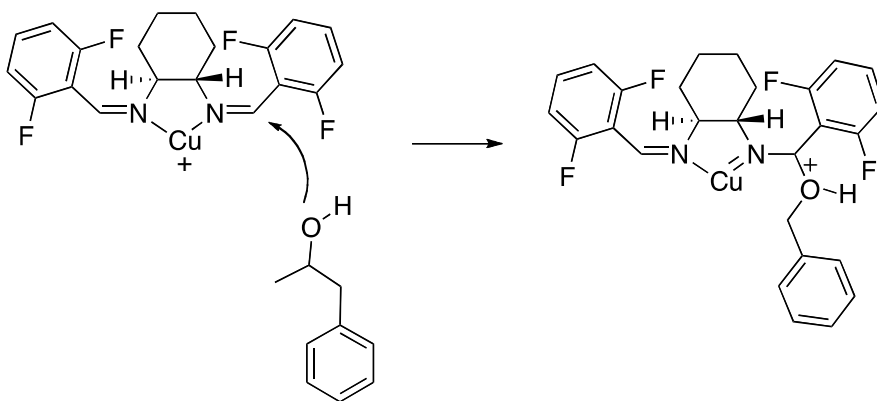


**Figure 120.** Nucleophilic attack by alcohol on catalyst 3b.

## 6.4 – BINAM Di-Imine Catalysts

Due to the lack of conformational rigidity of the *trans* cyclohexane di-imines, a more rigid diamine was sought. 1,1'-binaphthyl-2,2'-diamine (BINAM) proved to be an excellent choice, as the selectivity was markedly improved, while also offering a simple synthesis and the opportunity to examine a seven-membered chelation ring instead of the previous 6 (bis-oxazolines) and 5 (*trans*-cyclohexane di-imines) membered rings formed with copper and the ligands. As with the previous *trans*-cyclohexane di-imines, the only ligand with an ortho substituent with lone pairs that coordinated with the probes was the DiF catalyst; catalysts 5e-5i did not coordinate, and readily oxidized in air if left as solids.

#### **6.4.1 – General Discussion**

Results for the BINAM catalysts are shown as selectivity factors (Figure 121) and DE (Figure 122).

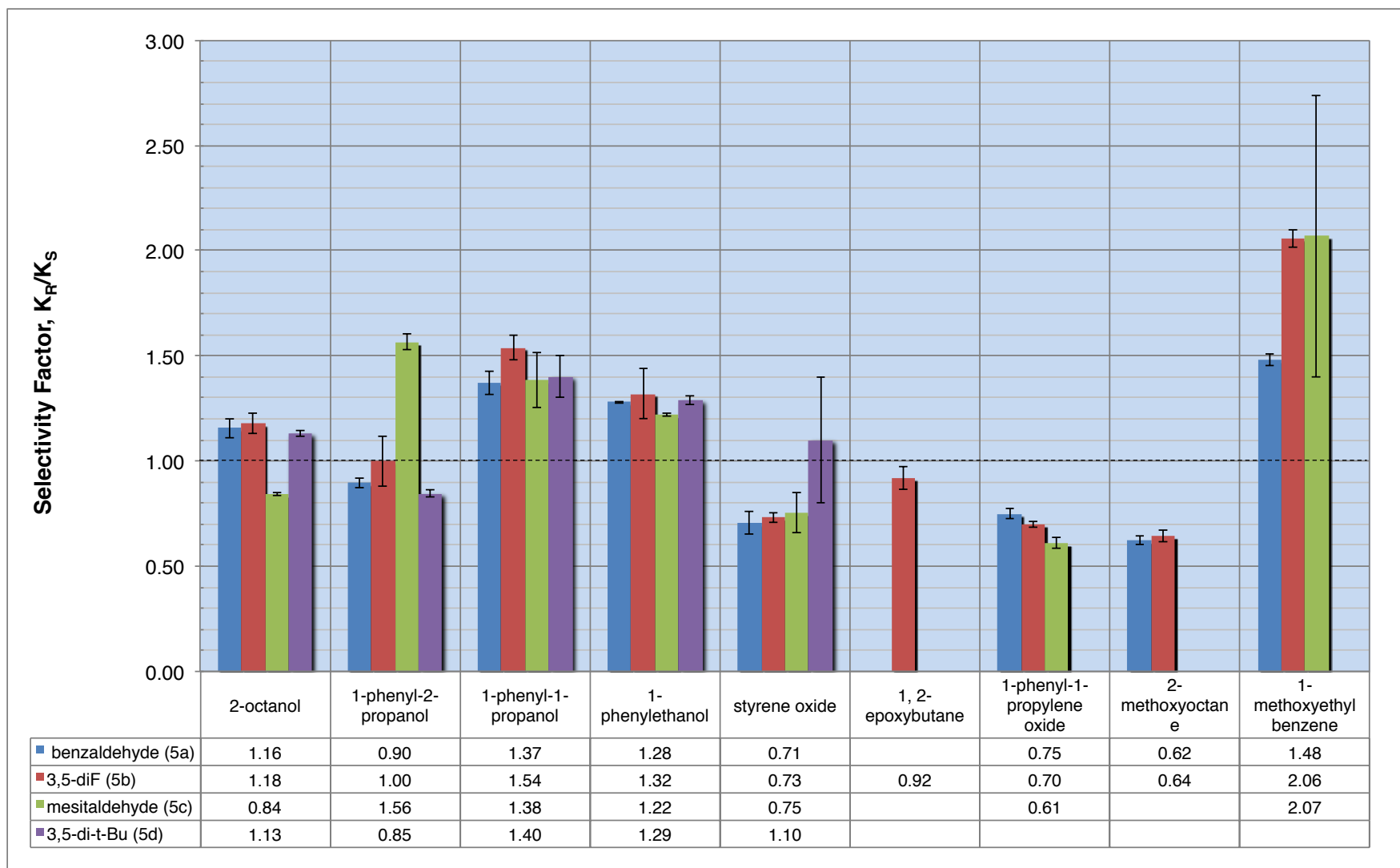


**Figure 121.** Results for the BINAM-based catalysts.

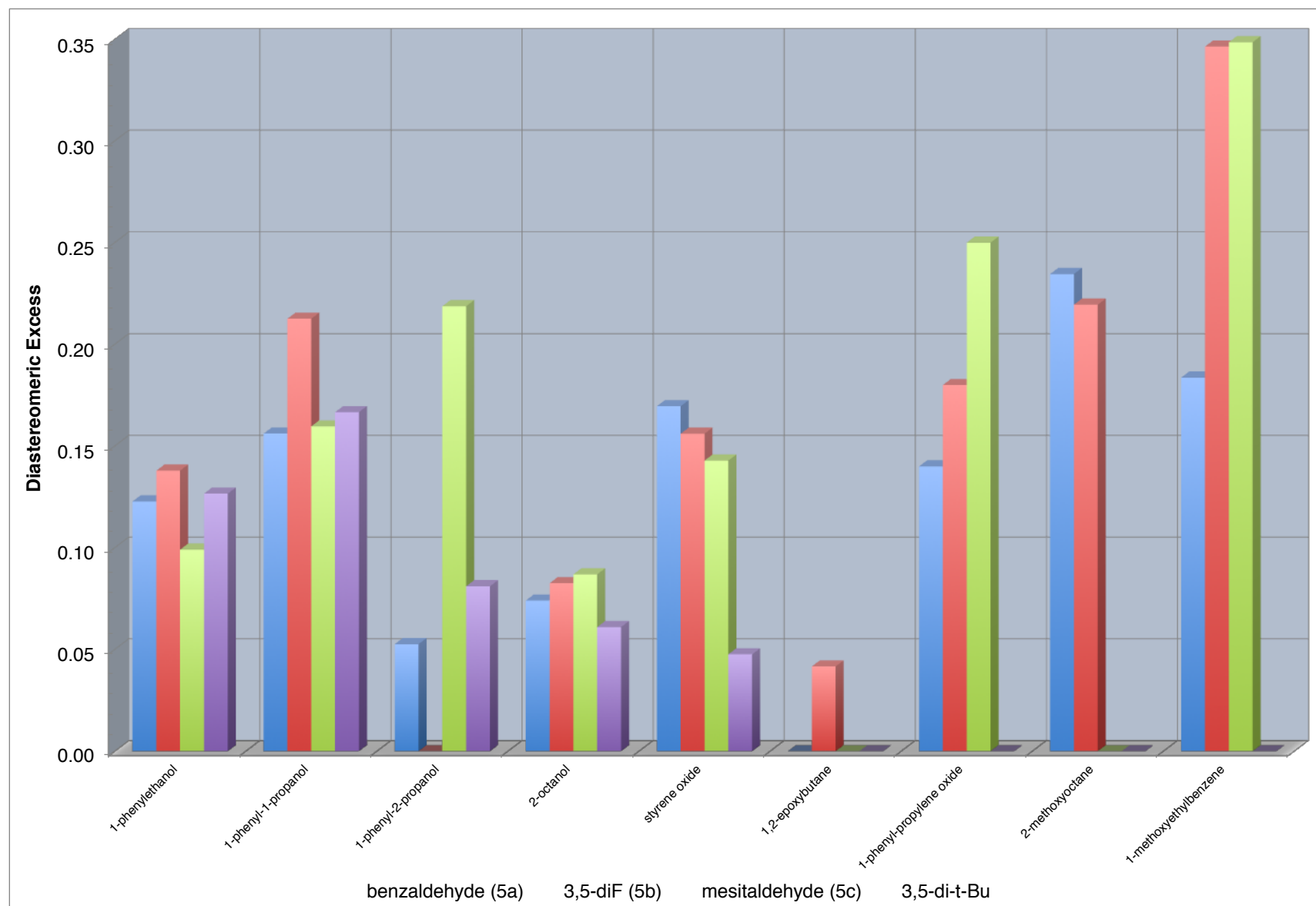


**Figure 122.** BINAM-based catalysts results as DE.

The selectivity observed was much greater than that in the *trans*-1,2-cyclohexane based di-imines, and close to that observed in the bis-oxazoline systems. The chiral probe 1-phenyl-2-propanol displayed behavior different from than that observed in the past. For example, two of the four catalysts displayed a preference for the *S* enantiomer, which was not previously observed for this probe. It also displayed enhanced selectivity with only one of the catalysts (5c), while the other phenyl-based alcohols displayed selectivity over the entire catalyst range, suggesting specific interactions (possibly H-bonding) are responsible for the selectivity. Overall though, the general trends were similar with a preference for the (*R*) enantiomer for the alcohols and 1-methoxyethylbenzene, and the (*S*) enantiomer for the epoxides and 2-methoxyoctane.

When examining the averages for the chiral probes (Figure 123), the best probes for this system were the two ethers, 1-methoxyethylbenzene and 2-methoxyoctane. The largest ether, 1-benzylethylbenzene, did not coordinate to the catalysts, presumably for steric reasons. The bulkier catalysts, 5c and 5d, did not coordinate with 2-methoxyoctane, again likely due to sterics. A new diastereomeric epoxide was also screened with these complexes, 1-phenyl-2-propylene oxide; however, as it will be shown later, the results obtained are unreliable.



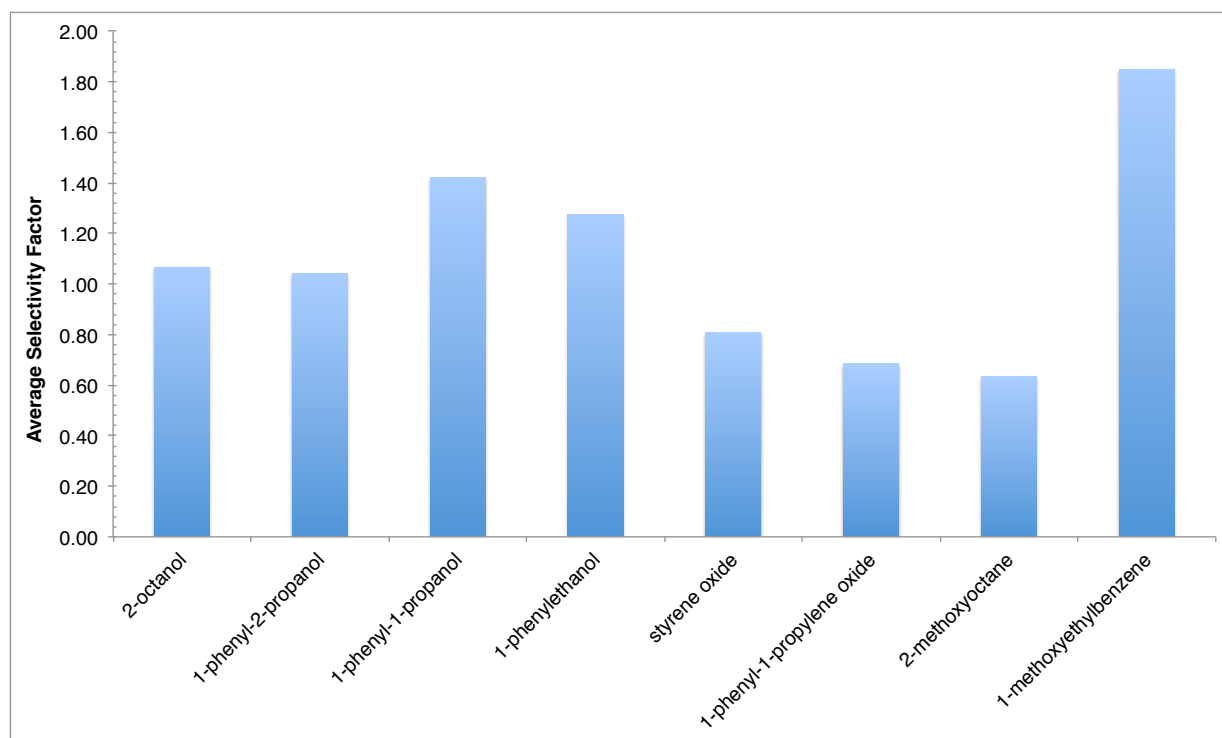


**Figure 123.** Averages for the chiral probes.

When examining the averages for the catalysts, a trend of increasing selectivity is observed with increasing steric bulk (Figure 124); however, no such trend is observed within the individual probes. The DiF (5b) catalyst is different from that used in the previous *trans*-cyclohexane-based di-imines. The previous 2,6 disubstituted di-imine was too crowded to coordinate. By moving the substituents to the 3,5 position, more space was created and coordination was observed.

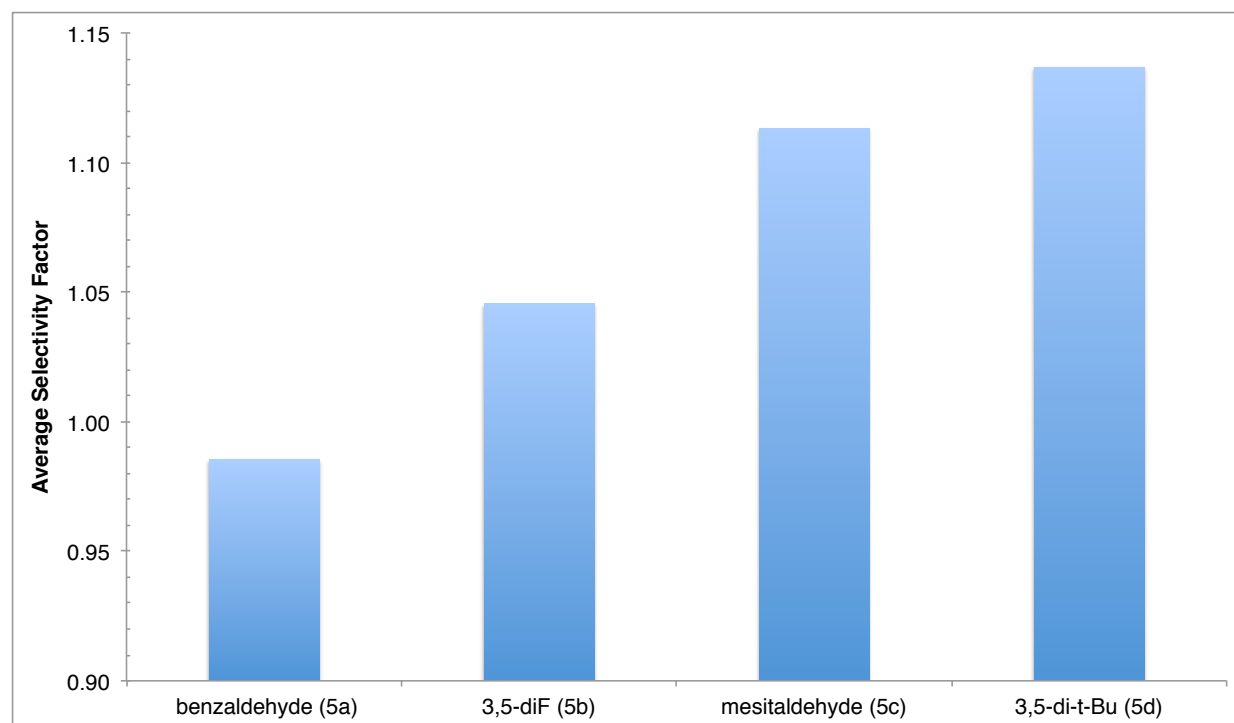


**Figure 124.** Average selectivity for the catalysts.

### 6.4.2 – Gibbs Free Energy

In order to detect the coordination complex between the BINAM-based catalysts and the chiral probes, the scan speed needed to be set higher, from the default 5,000 amu/sec to 65,000 amu/sec (turbo scan). This is due to the fragile nature of the complexes and the method of ejection from the trap. Using the resonant ejection technique, the ion is tickled at its resonant frequency imparting a small amount of energy to the complex. This was enough to dissociate the complex during the scan. By speeding up the scan speed, the time was reduced, allowing for the detection of the complex.

This fragile nature of the complex is reflected in the binding energies (and the fact that only a few systems could be measured), which ranged from -9.5 – 11.8 kcal/mol, significantly lower than previous systems (Table 18).

**Table 18.** Binding energies of the BINAM-based complexes (kcal/mol).

	1-phenylethanol	1-phenyl-1-propanol	1-phenyl-2-propanol	styrene oxide	1,2-epoxybutane	2-methoxyoctane	1-methoxyethylbenzene
Benzaldehyde (5a)	-10.5	-11.8	-11.5	-8.9		-10.7	-10.1
3,5-diF (5b)					-11.3		
Mesitaldehyde (5c)	-9.9	-9.7	-10.0	-9.5			
3,5-di- <i>t</i> -Bu (5d)	-10.5	-10.9		-8.5			

When plotting the values against the molecular weight of the chiral probe, the trend in polarizability is not as pronounced (Figure 125). This much weaker binding is a result of the much more rigid BINAM, offering little room for conformational freedom. The lower Lewis acid basicity of styrene oxide is evident, particularly for the *t*-Bu and benzaldehyde catalysts; for the mesital catalyst, it is not as pronounced, but still evident.

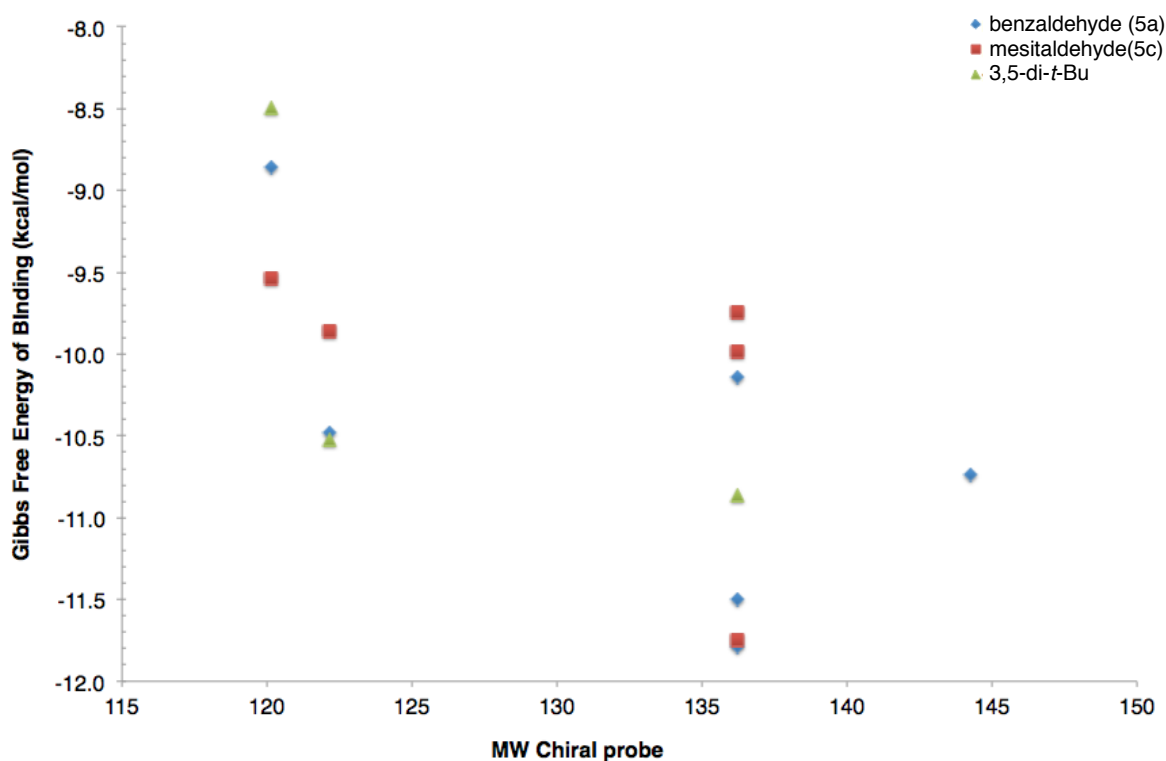


**Figure 125.** Plot of Gibbs binding energy versus the chiral probe molecular weight.

### 6.4.3 – Chiral Cross Check

Both enantiomers of the catalysts were synthesized for 5a and 5c catalysts. The R enantiomer for 5b (DiF) was synthesized, but oxidized before it could be run. The results are compared in Figure 126. A chiral cross check could also be performed with the data (Figure 127). Most of the results matched a value of one, within error, for the chiral cross check. For 1-phenyl-1-propylene oxide, an impurity was in one of the enantiomers of the probe. Resolution is decreased when the turbo scan is used, which caused the impurity to overlap with the probe, causing an error in the final analysis. The remaining deviations from the theoretical value of one may be attributed to a non-ideal ratio between the probe and internal standard.

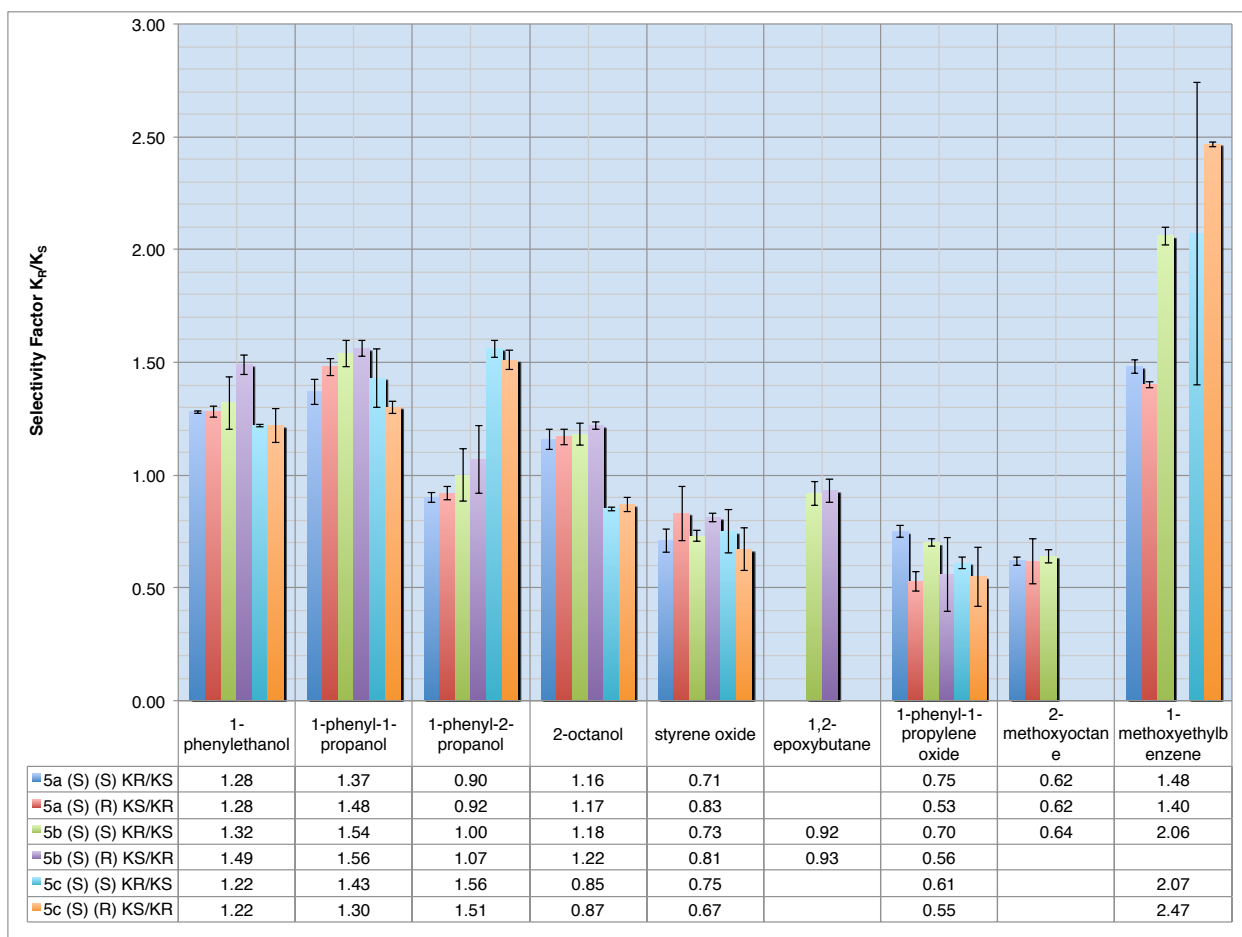


**Figure 126.** Selectivity factors for both enantiomers of the BINAM-based catalysts.

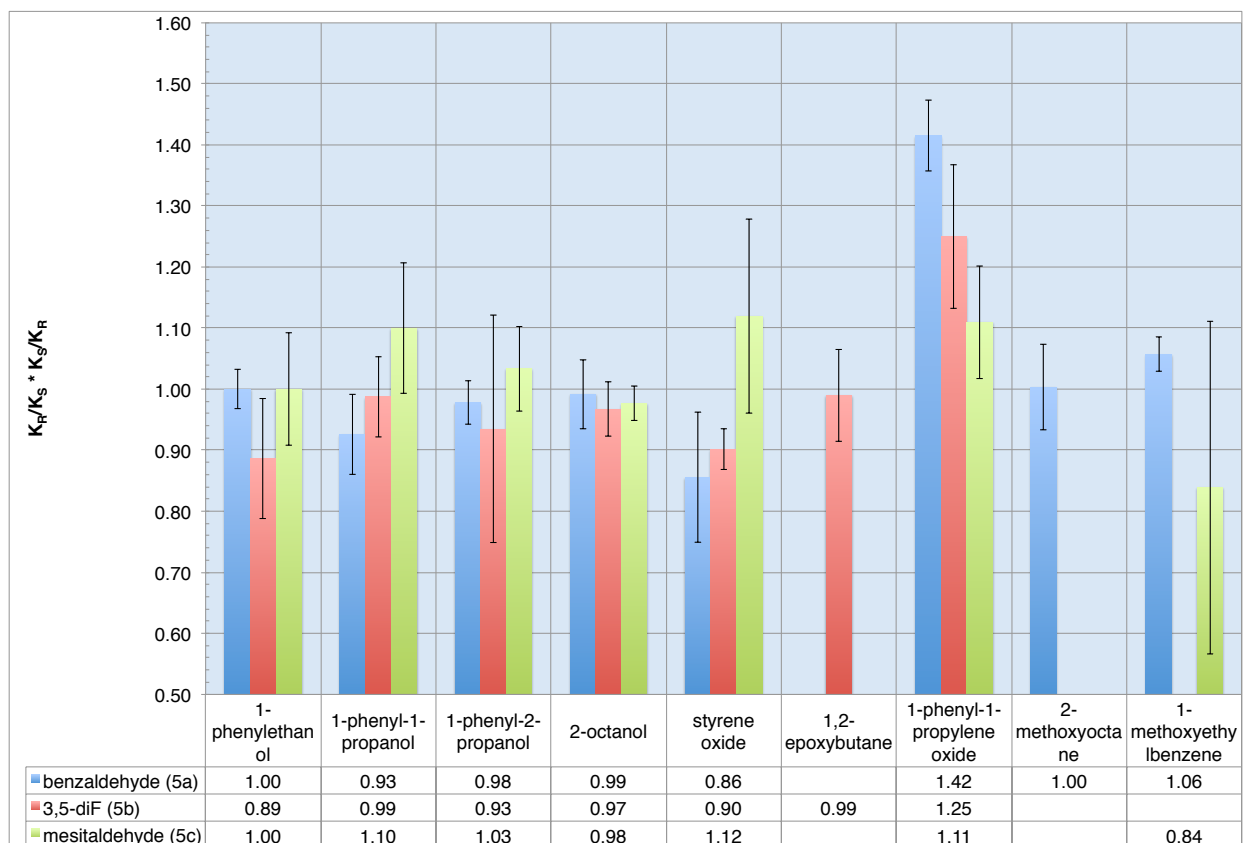


**Figure 127.** Chiral cross check for the BINAM-based di-imines.

#### 6.4.4 – Combinatorial versus Single Runs

When comparing the catalysts run in combination against the single-run catalysts, excellent agreement (within error) exists between the two values, indicating there were no impurities that interfered with the results in the combinatorial approach, giving further confidence in this method for use as a rapid chiral catalyst screening method. Figure 128 displays the results.

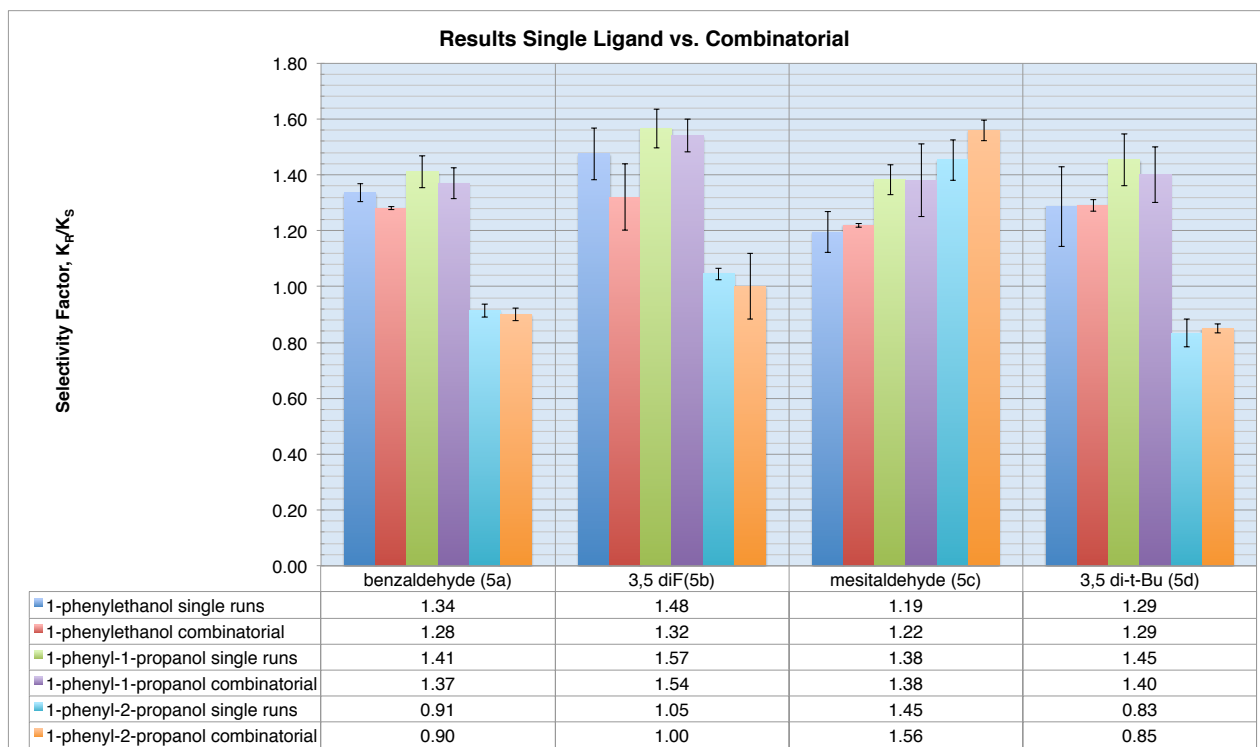


**Figure 128.** The combinatorial approach versus single-run catalysts.

#### 6.4.5 – RSD

A box plot of the results follows in Figure 129 followed by the RSD values grouped by chiral probe and catalyst (Figure 130). Approximately 22% of the results were under 7% RSD for the multi-prep, multi-day runs. While slightly higher than the results presented earlier, the variation is still acceptable, given the weak binding between the complex and chiral probe. In fact, only two cases were found where the RSD was unacceptably high, catalyst 5b and styrene oxide, and 5c and 1-methoxyethylbenzene. For the case of styrene oxide, the internal ratio/analyte ratio was

again not ideal; however, no explanation can be given for the high RSD for the 1-methoxyethylbenzene.



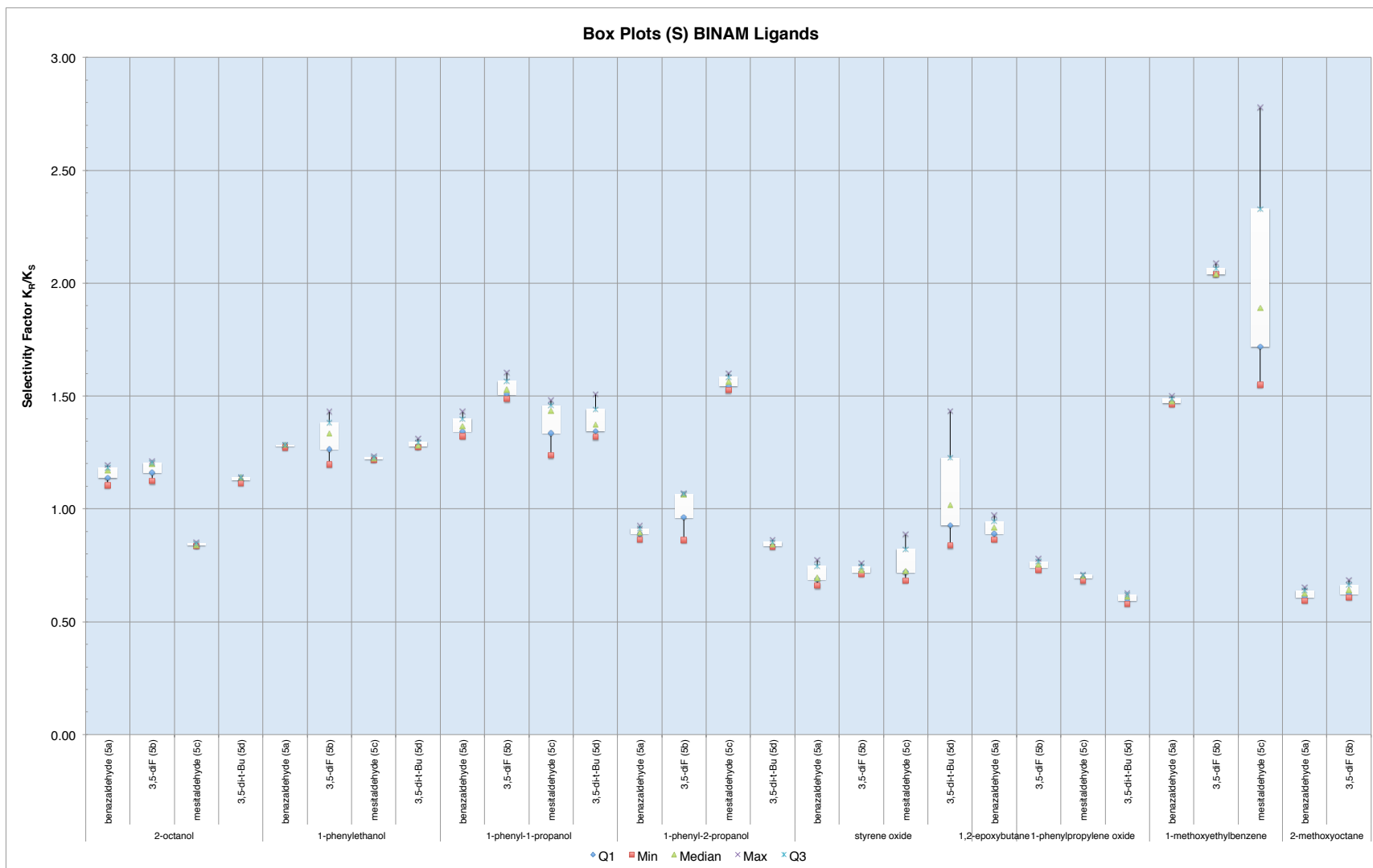


**Figure 129.** Box plot of the results for the (S) BINAM-based di-imines.

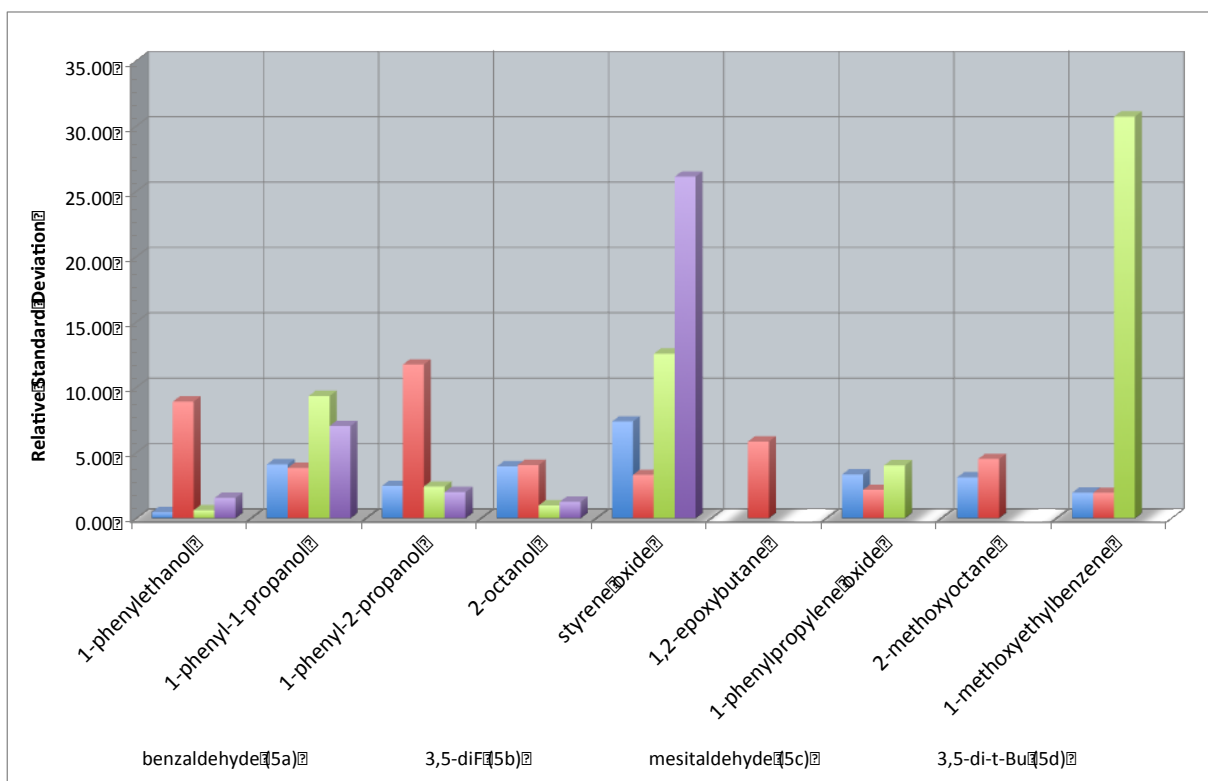
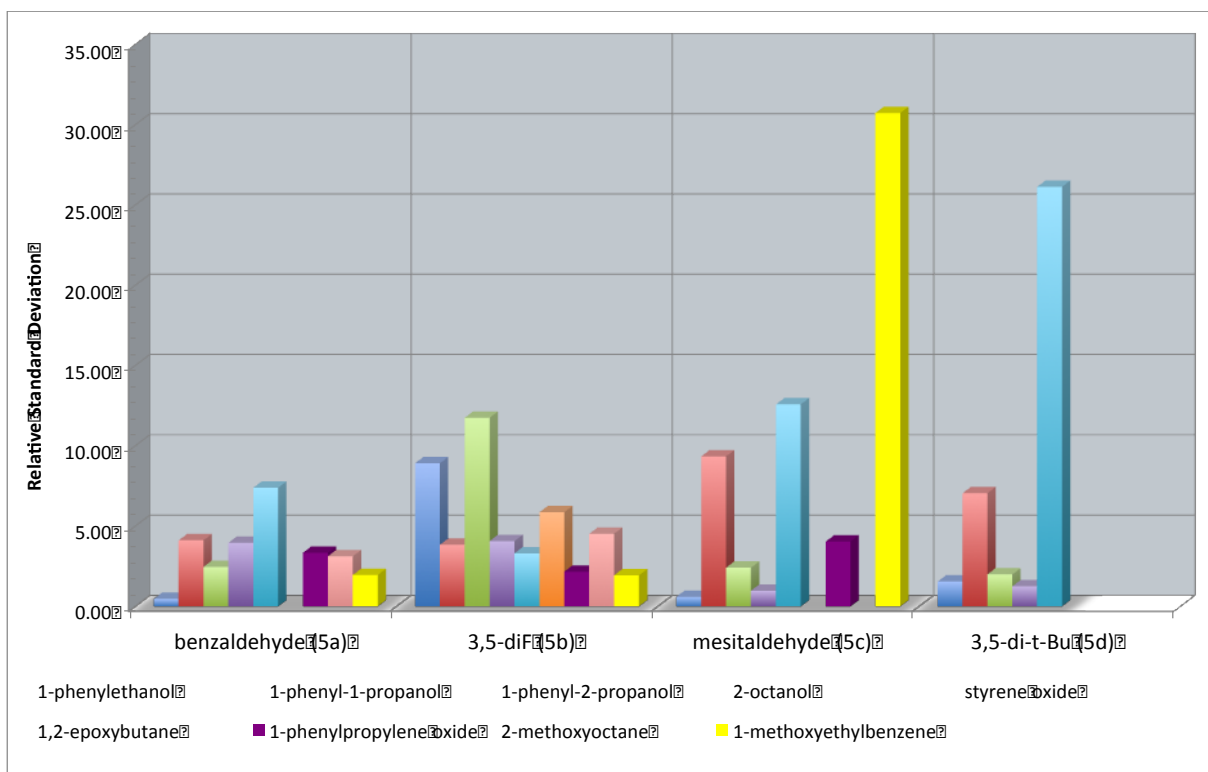


**Figure 130.** RSD for the (S) BINAM-based systems grouped by catalysts (top) and by chiral probe (bottom).

#### 6.4.6 – System Checks

As a further check of the system, a racemic BINAM catalyst based benzaldehyde (racemic 5a) was synthesized and run with some select chiral probes. The values are close to the expected theoretical value of one, further demonstrating the accuracy of the method.

**Table 19.** Selectivity factors obtained with select chiral probes and a racemic BINAM-based catalyst (5a).

Racemic Benz (5a)	1- methoxyethylbenzene	2-methoxyoctane	1-phenylethanol
Selectivity factor	1.04	1.00	1.02
RSD%	4.8	3.9	5.5

##### 6.4.6.1 – Linearity

Using the racemic catalyst, racemic 1-phenylethanol and d<sub>5</sub>-ring 1-phenylethanol as an internal standard, a series of preps were made varying the ratio of standard and analyte. The ratio of the areas obtained were graphed versus the ratio of concentrations (Figure 131). The method displayed a wide range of linearity, from 0.2 – 2 ratio of internal standard/analyte, with an excellent coefficient of determination, R<sup>2</sup>, of 0.998.

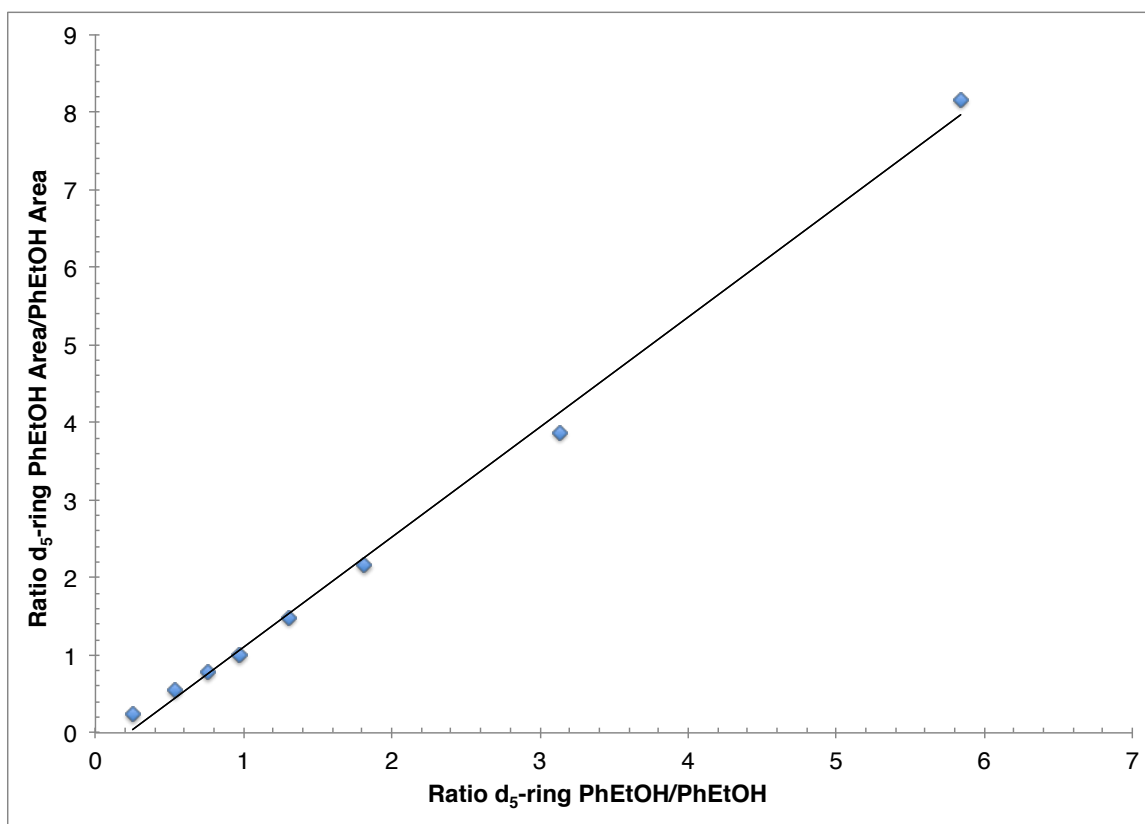


**Figure 131.** Linearity of the method with racemic benzaldehyde-BINAM and d<sub>5</sub>-ring 1-phenylethanol and 1-phenylethanol.

The full regression analysis is shown in Table 20.

**Table 20.** Regression analysis results.

Linear Regression							
Regression Statistics							
R	0.9991						
R Square	0.9983						
Adjusted R Square	0.9979						
S	0.04						
Total number of observations	7						
ANOVA							
	d.f.	SS	MS	F	p-level		
Regression	1.	5.72		5.72	2,914.08	4.13E-08	
Residual	5.	0.01		0.			
Total	6.	5.73					
	Coefficients	Standard Error	LCL	UCL	t Stat	p-level	H0 (5%) rejected?
Intercept	0.12	0.03	0.05	0.19	4.61	0.01	Yes
8.14936244097188	0.79	0.01	0.75	0.82	53.98	0.	Yes
T (5%)	2.57						
LCL - Lower value of a reliable interval (LCL)							
UCL - Upper value of a reliable interval (UCL)							
Residuals							
Observation	Predicted Y	Residual	Standard Residuals				
1	3.16	-0.02	-0.52				
2	1.82	0.	0.				
3	1.29	0.02	0.42				
4	0.91	0.07	1.62				
5	0.74	0.02	0.49				
6	0.55	-0.02	-0.42				
7	0.31	-0.06	-1.58				

## 6.5 – Mixed 2,2'-Diaminobinaphthyl System

As proof of concept, a series of aldehydes, benzaldehyde, 3,5-difluorobenzaldehyde, mesitaldehyde, 3,5-di-*tert*-butylbenzaldehyde, and 2-bromo-6-fluorobenzaldehyde, were mixed with (*S*) 2,2'-diaminobinaphthyl to form mixed symmetrical and unsymmetrical, novel ligands. The use of these unsymmetrical ligands for enantioselectivity has precedence in the literature.<sup>291,292,293,294</sup> The crude mixture was added to the CuI/CuCl mixture and run on the ITMS. A representative spectrum of the catalyst mixture is shown in Figure 132.

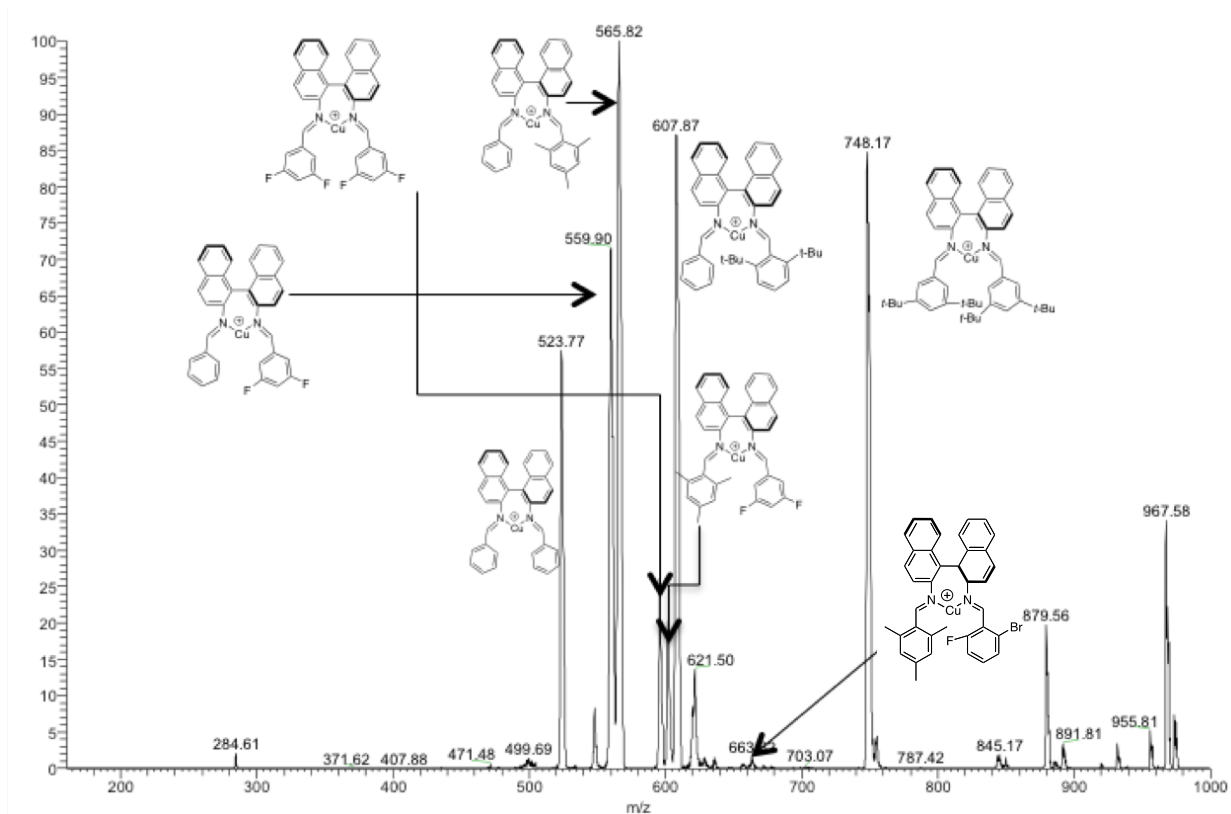


**Figure 132.** Representative spectra of the crude mixed BINAM catalysts.

### 6.5.1 – General Discussion

The results for the mixed catalysts are shown in Figure 133. The results are presented in DE, grouped by chiral probes (Figure 134) and by catalysts (Figure 135). In general, the unsymmetrical catalysts performance was equal to that of the symmetrical  $C_2$  counterparts, suggesting the general asymmetric environment near the coordinating center is driving the selectivity versus the specific details of the catalyst's substituent group.

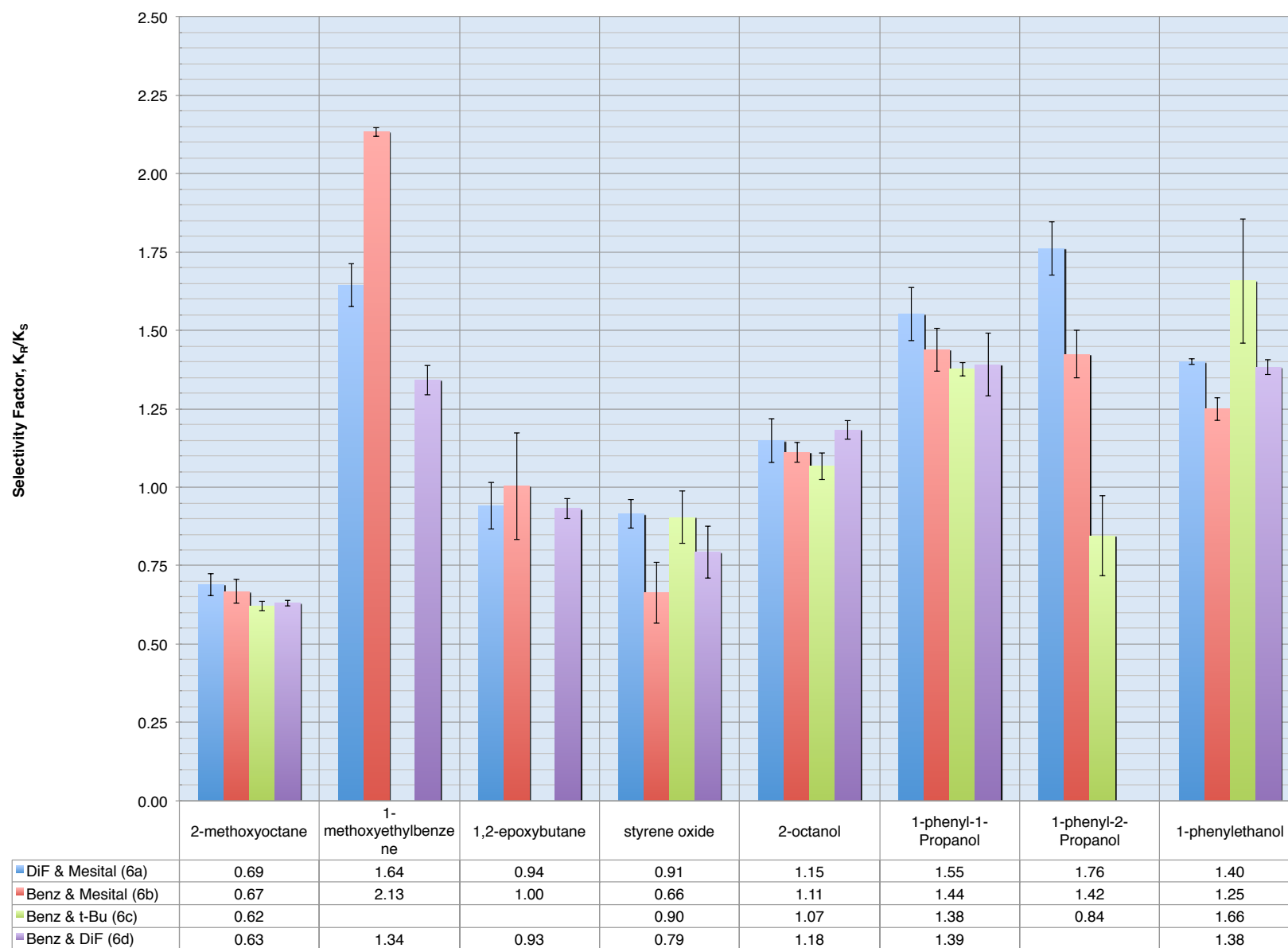


**Figure 133.** Results of the crude mixed catalyst system.

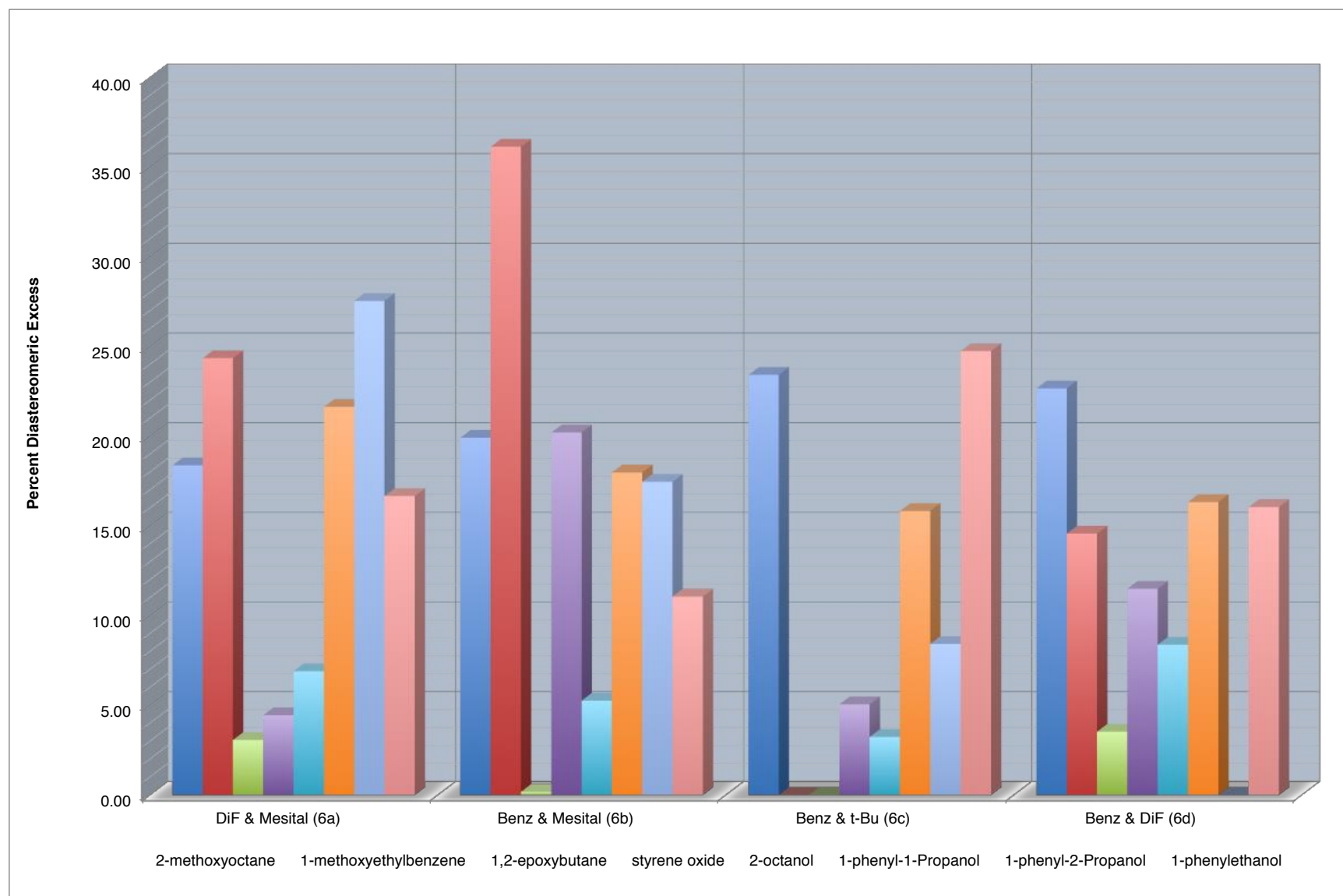


**Figure 134.** Diastereomeric excess grouped by chiral probes.



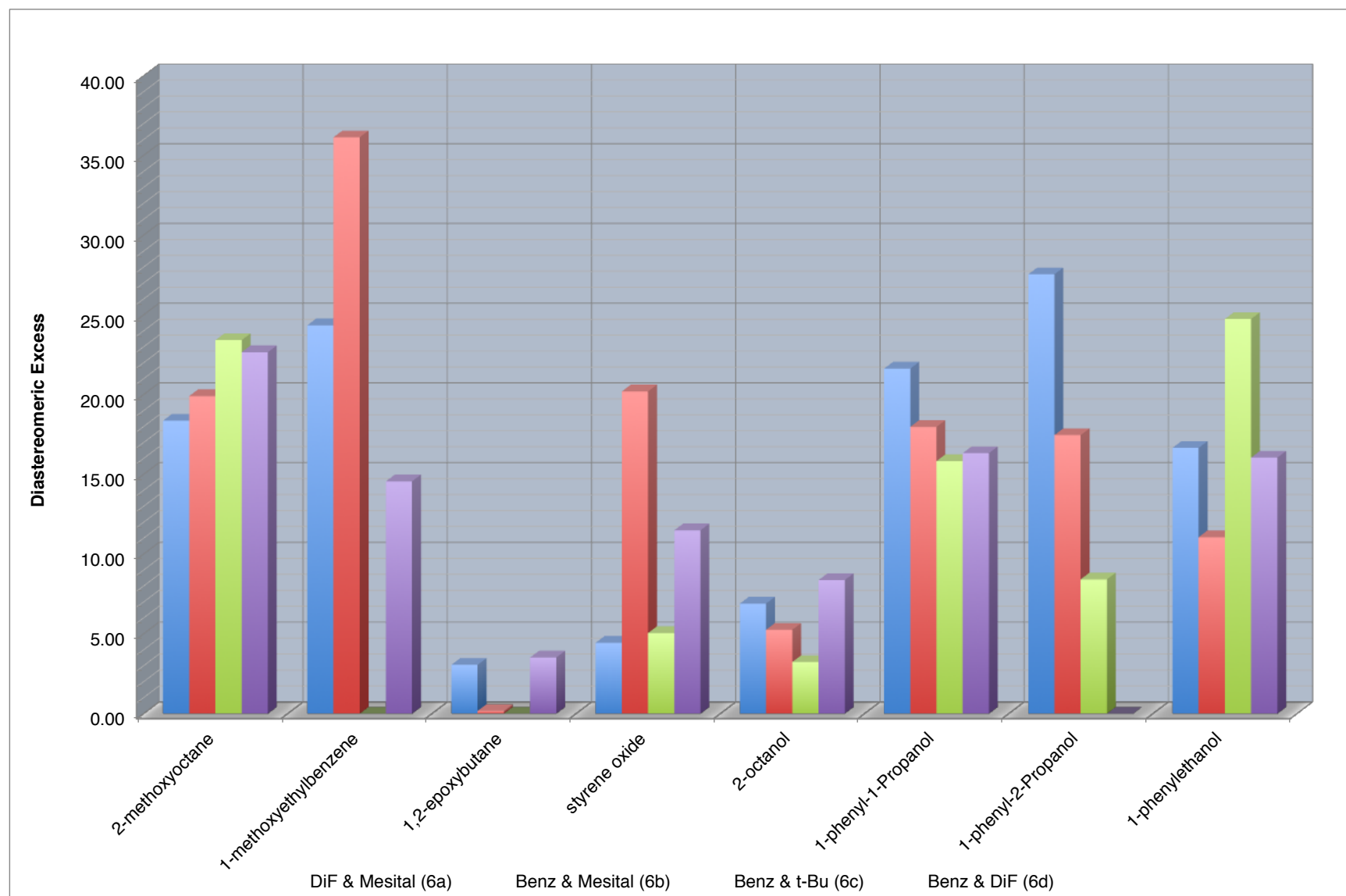


**Figure 135.** Diastereomeric excess grouped by catalyst.

The differences in selectivity between previous  $C_2$ -symmetric catalysts and the unsymmetrical catalysts are shown in Figures 136-138. Figure 136 displays the differences between the unsymmetrical catalyst 6d, composed of a benzaldehyde and 3,5-difluorobenzaldehyde, to that of the  $C_2$ -symmetric counterparts. The most obvious

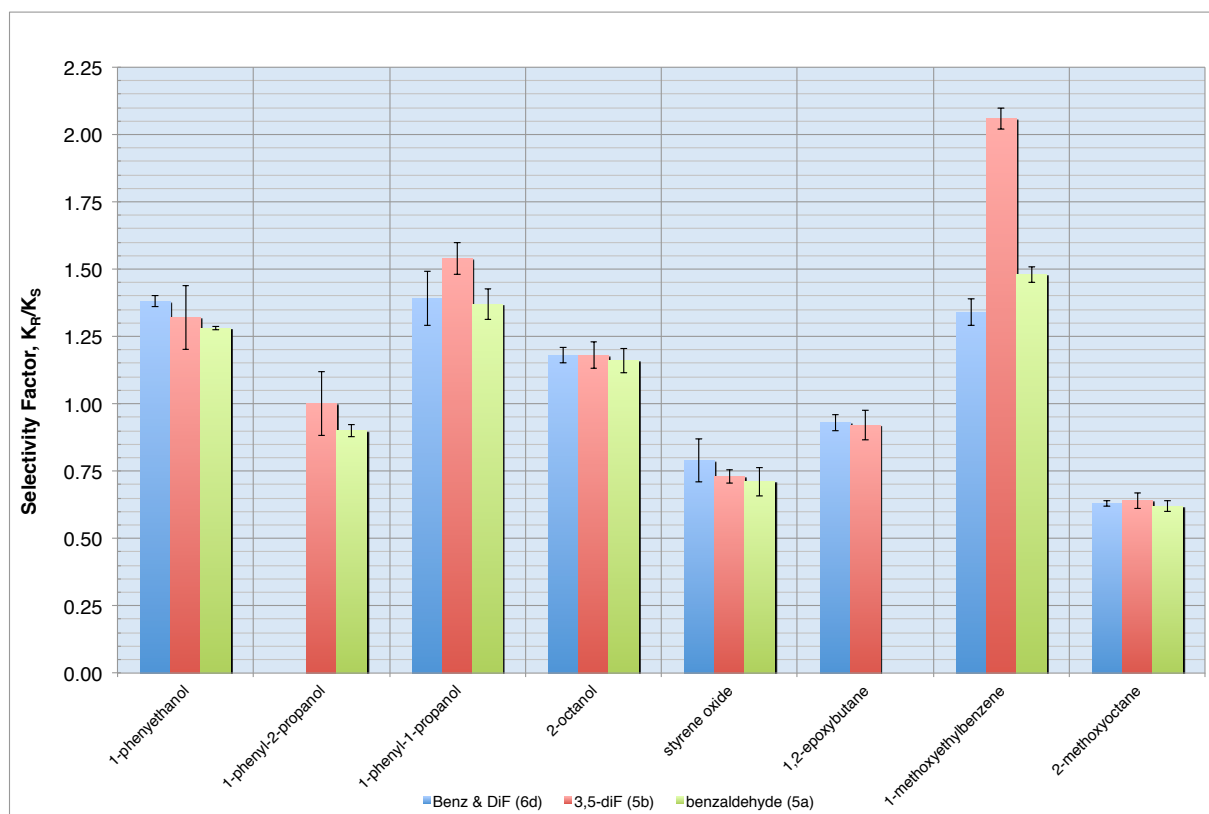


**Figure 136.** Comparison of the mixed catalyst 6d (Benz & DiF) with the  $C_2$  counterparts 5a (benzaldehyde) and 5b (3,5-diF).

differences are displayed with the 1-methoxyethylbenzene probe, where the absence of a fluoro group results in a substantial decrease in selectivity, on par with the selectivity observed for the non-substituted catalyst (benzaldehyde). Interestingly, the removal of a single fluoro (3,5-DiF) substituted benzaldehyde on the catalyst resulted in no coordination for the 1-phenyl-2-propanol probe; alternatively, the addition of this group

group resulted in coordination to the 1,2-epoxybutane probe, where it was only observed in the DiF substituted catalyst previously.

Moving to the benzaldehyde and mesitaldehyde catalyst 6b, the addition or subtraction of one of the benzaldehydes can also affect the coordination and selectivity (Figure 137). For example, no coordination was observed in either of the C<sub>2</sub>-symmetric

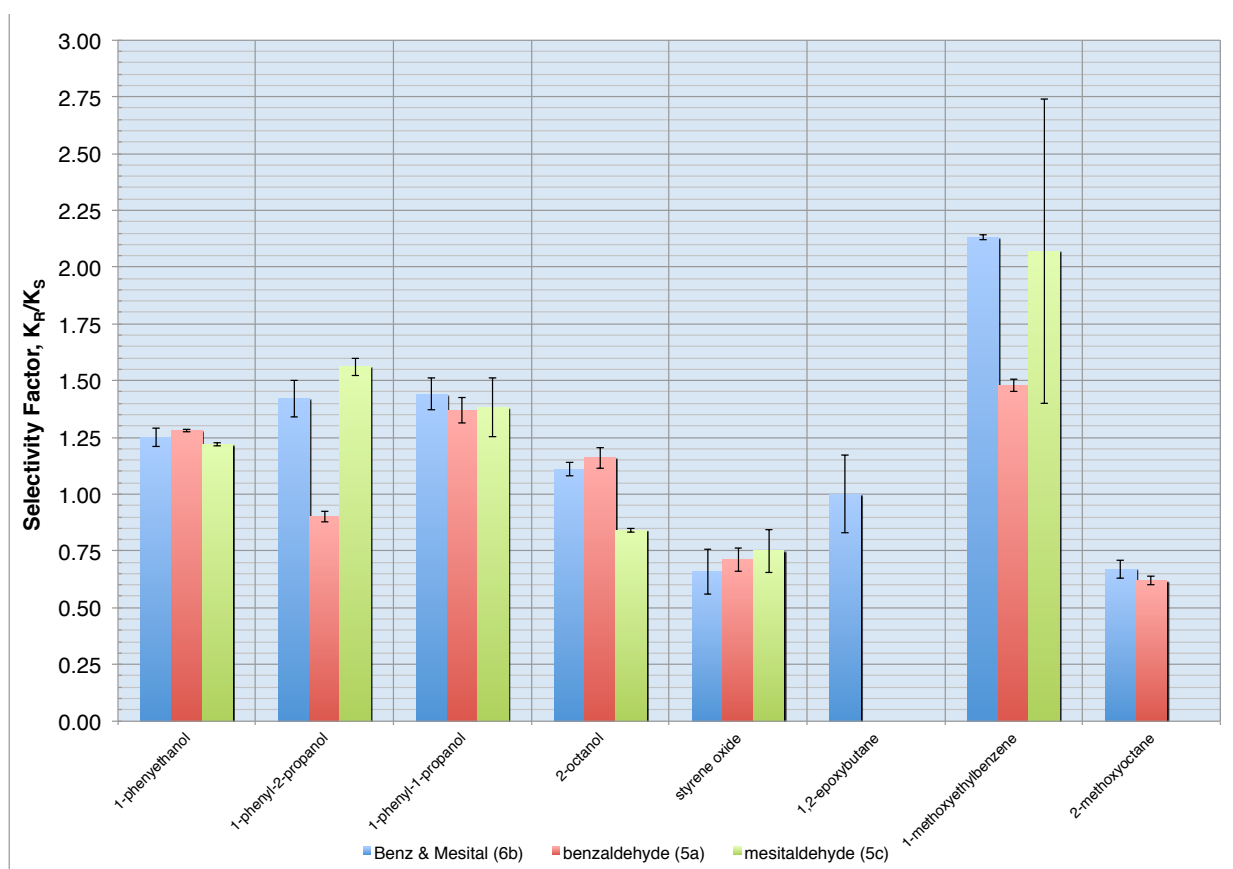


**Figure 137.** Mixed catalyst 6b (Benz and Mesital) versus the C<sub>2</sub>-symmetric catalysts.

catalysts 5a or 5c with the 1,2-epoxybutane probe; however, the mixed catalyst (6b) displayed coordination, but no selectivity, to the probe, indicating two mesital units are too sterically demanding, while one unit provides some form of stabilization

(polarizability), and that these forces strike a delicate balance in some systems. Another example of this balance is also observed in the 1-methoxyethylbenzene probe. The addition of the mesitaldehyde unit may also reverse the selectivity, as shown with 1-phenyl-2-propanol, where addition of one or two mesitaldehyde units reversed the preference from the *S* enantiomer with the unsubstituted benzaldehyde, to the *R* enantiomer, and enhances selectivity in the process.

The balance between sterics and polarizability is also observed in the mixed catalyst 6a (DiF and mesital) and the 1,2-epoxybutane and 2-methoxyoctane probes, where the addition of two units of the mesitaldehyde proves too sterically demanding, overriding any additional stabilization from the extra bulk and polarizability (Figure 138).

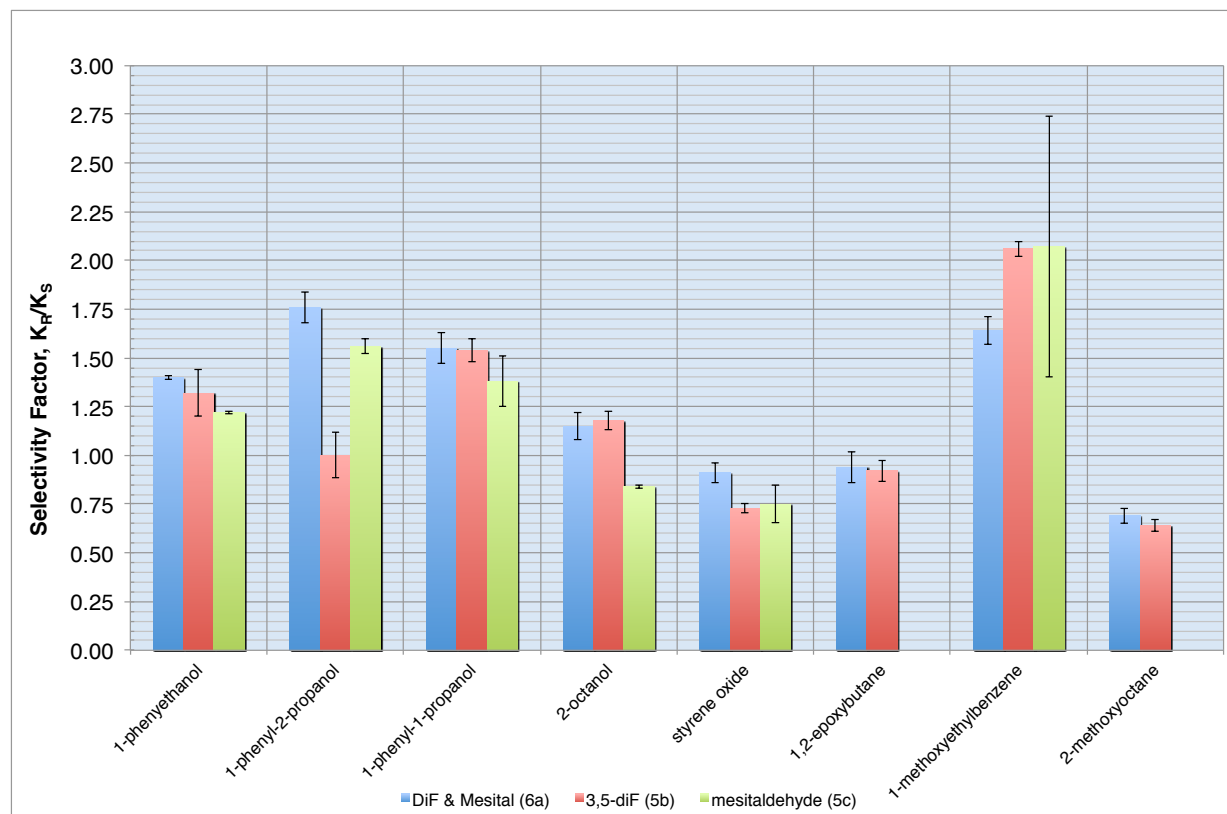


**Figure 138.** Mixed catalyst 6a (DiF and mesitaldehyde) versus 5b (benz) and 5c (mesital).

A large difference in selectivity between the  $C_1$  and  $C_2$ -symmetric catalysts was observed in only a couple of instances. For example with 1-phenyl-2-propanol, where at least one mesital substituent proves necessary for selectivity, an additional substituent actually decreases selectivity slightly. When moving to two mesital substituents in the case of 2-octanol, a complete reversal of the enantiomeric preference was observed, offering a drastic change in the local environment of the probe.

Finally, for catalyst 6c (Benz and *t*-Bu), the extra steric-hindrance provided by the *tert*-butyl group was too demanding for the chiral ethers (Figure 139). No

coordination was observed for the bulkier 1-methoxyethylbenzene probe with any catalyst with a *t*-Bu substituent. Coordination was observed only between the singly *t*-Bu substituted 6c catalyst and 2-methoxyoctane. The addition of a singly substituted *t*-Bu group enhanced the selectivity in the case for 1-phenylethanol, where addition of a second substituted ring diminished the selectivity back to the level observed in the unsubstituted benzaldehyde catalyst.

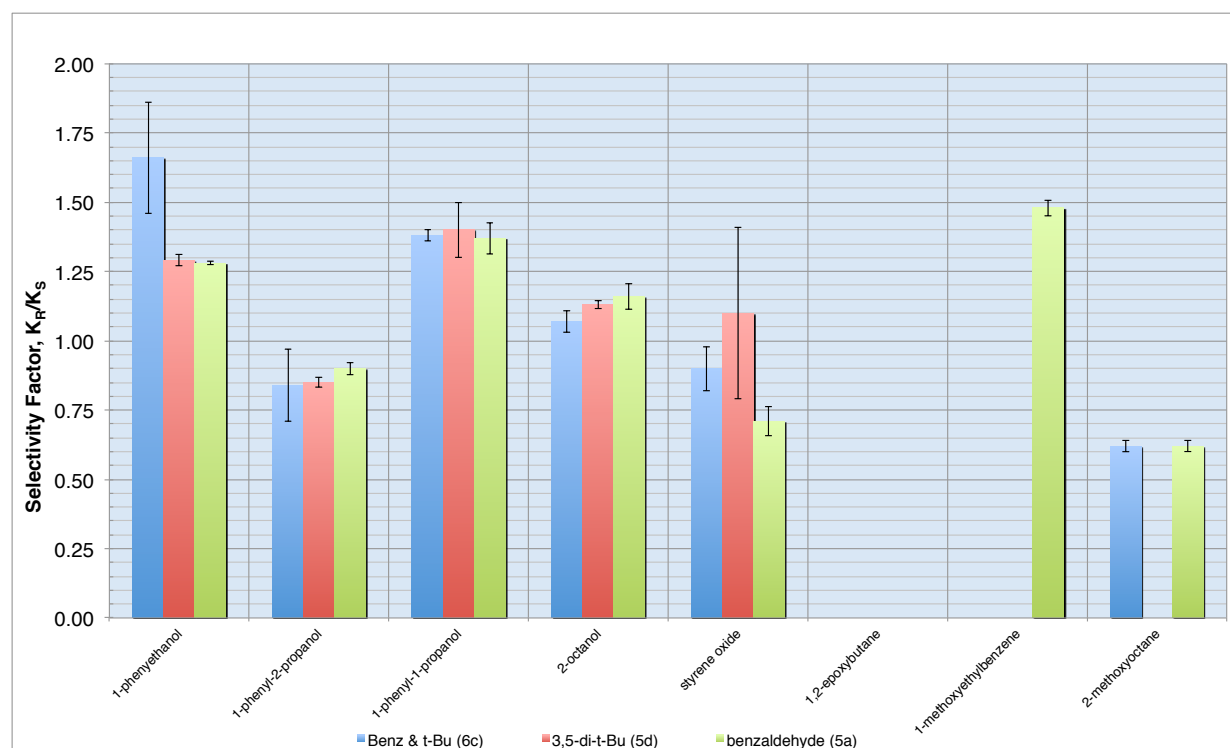


**Figure 139.** Mixed catalyst 6c compared to the  $C_2$ -symmetric catalysts.

When examining the average selectivity over the groups of chiral probes, a similar pattern to that of the  $C_2$ -symmetric catalyst emerges (Figure 140). The chiral ethers were once again the most selective probes for these catalysts. The selectivity for the 1-phenyl-2-propanol probe also appears to have increased from approximately 1.00 to 1.28.

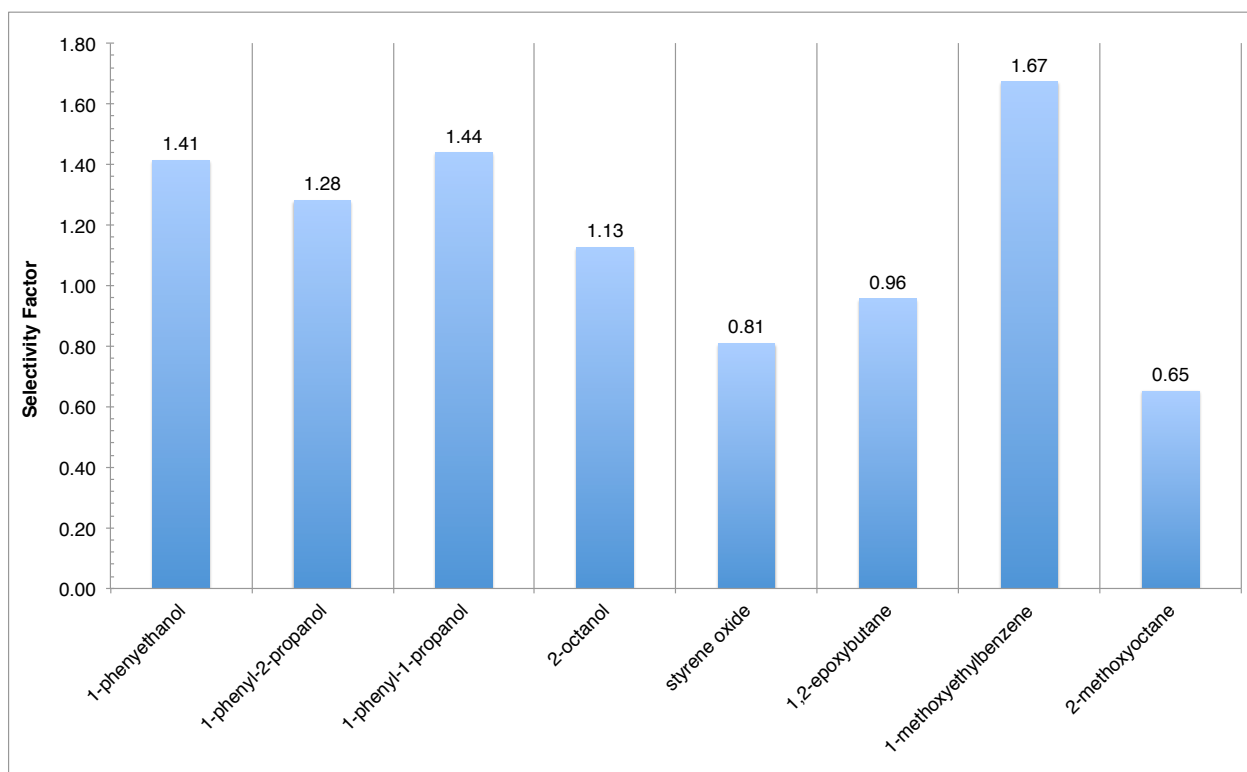


**Figure 140.** Average selectivity for the chiral probes with the mixed catalysts.

When examining the averages for the mixed catalysts, the larger substituent in the mixed system yielded approximately the same selectivity as the larger  $C_2$ -symmetric counterpart (Figure 141). For example, the average for the  $C_2$ -symmetric mesital catalyst (5c) was 1.12, whereas here, the averages for the mesital-containing catalysts were 1.13 and 1.20. There was no difference found upon addition of a *t*-Bu group when comparing against the unsubstituted benzaldehyde, however, the selectivity decreased when compared to the  $C_2$ -symmetric *t*-Bu catalyst (1.12 vs. 1.02).

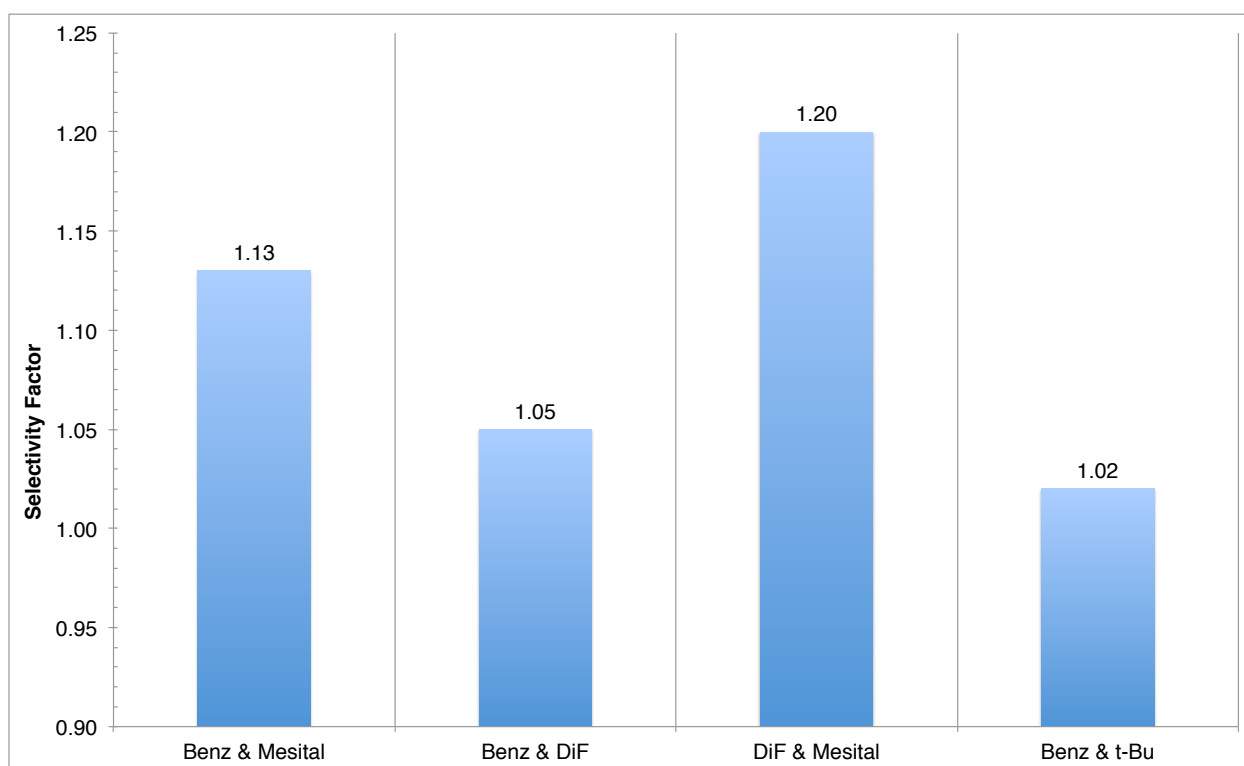


**Figure 141.** Average selectivity factor for the catalysts.

## 6.5.2 – Gibbs Free Energy

The Gibbs free energy of binding was once again measured and is shown in Table 21. The balance between the negative impact of sterics and the positive effect of

**Table 21.** Gibbs free energy for the mixed system (kcal/mol).

	1-phenylethanol	1-phenyl-1-propanol	1-phenyl-2-propanol	styrene oxide	1,2-epoxybutane	1-methoxy ethylbenzene	2-methoxy octane	2-octanol
DiF & Mesital (6a)	-10.6	-12.0	-12.2	-10.1	-9.6	-10.8	-10.9	-11.1
Benz & mesital (6b)	-10.7	-11.3	11.7	-9.9	-8.7		-10.7	-11.5
Benz&t-Bu (6c)	-15.4	-10.3	-11.0	-8.4			-9.9	
Benz & DiF (6d)	-15.3			-10.8	-9.7		-12.0	-12.9



polarizability can be shown in these results when comparing with those obtained for the C<sub>2</sub>-symmetric catalysts. For example, the binding energy of the C<sub>2</sub>-symmetric catalyst 5d was -10.5 kcal mol<sup>-1</sup>. Upon removal of a *t*-Bu group, there is steric relief and a significant increase in binding energy (catalyst 6d) to -15.4 kcal mol<sup>-1</sup>, a 50% increase. Alternatively, removal of a fluoro substituent from the catalyst allows for the equilibrium to be measured (and hence the free energy to be calculated), whereas in the disubstituted catalyst, 5b, the equilibrium highly favors the products and the  $\Delta G$  could not be measured.

Figure 142 shows a plot of the binding energy versus the molecular weight. The *t*-Bu-containing catalyst displays a relatively flat line, with the exception of 1-phenylethanol. The other catalysts also displayed less sensitivity to polarizability than the bis-oxazoline and the *trans*-cyclohexane di-imines. A dramatic difference is observed for the Lewis basicity of styrene oxide when compared to 1-phenylethanol, particularly for the *t*-Bu and DiF containing catalysts. This difference is not as stark for the other two catalysts (mesital and benz).

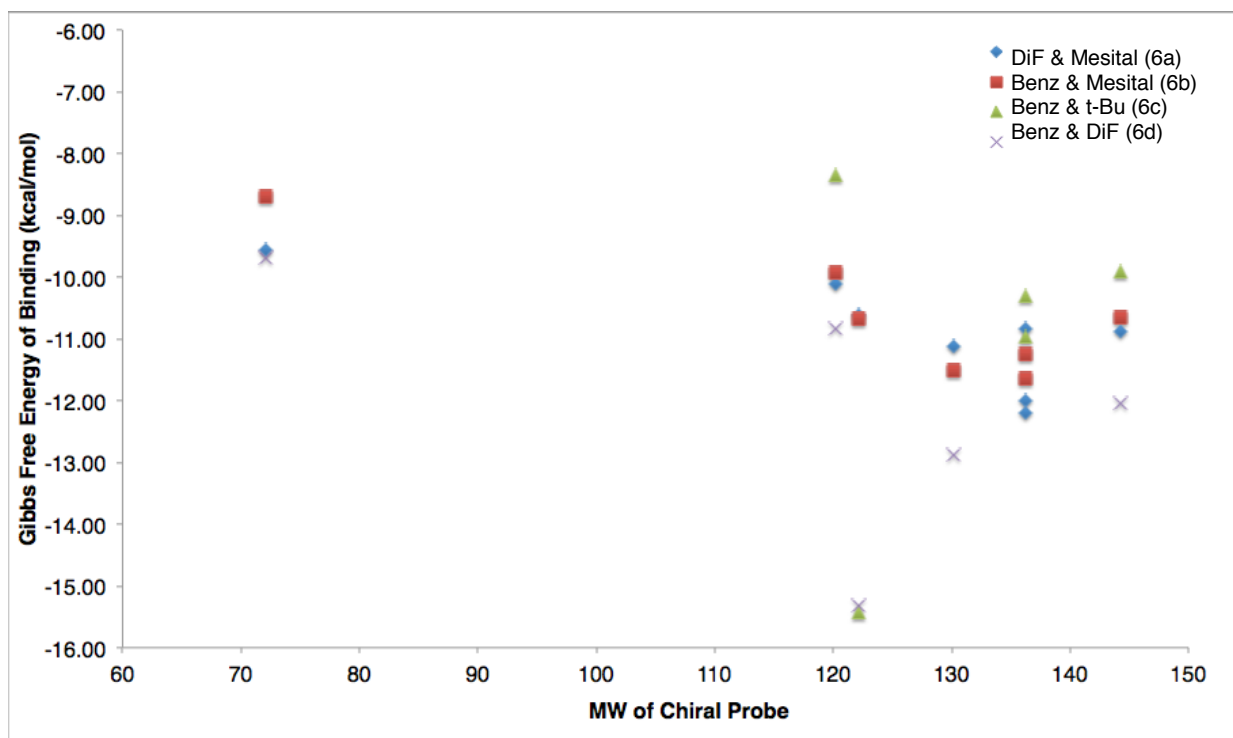


**Figure 142.** Binding energy versus molecular weight of chiral probe.

### 6.5.3 – RSD

A box plot of the results is shown in Figure 143, followed by a plot of the RSD grouped by chiral probe and catalysts (Figure 144). The RSD were close to those observed in the C2-symmetric BINAM-based catalysts, with 27% of the results displaying an RSD higher than 6%.

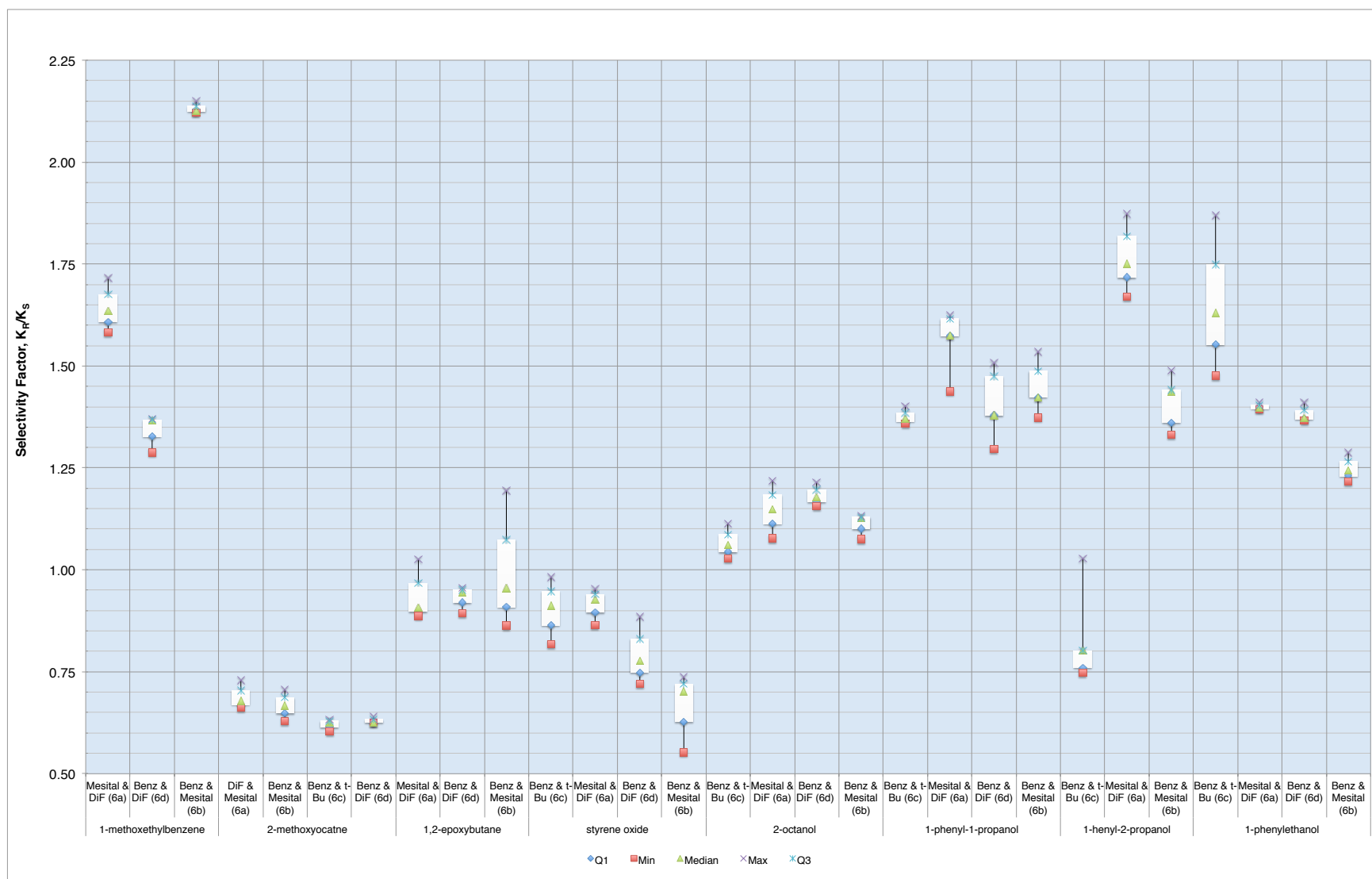


**Figure 143.** Box plot of the results for the crude mixed catalyst system.

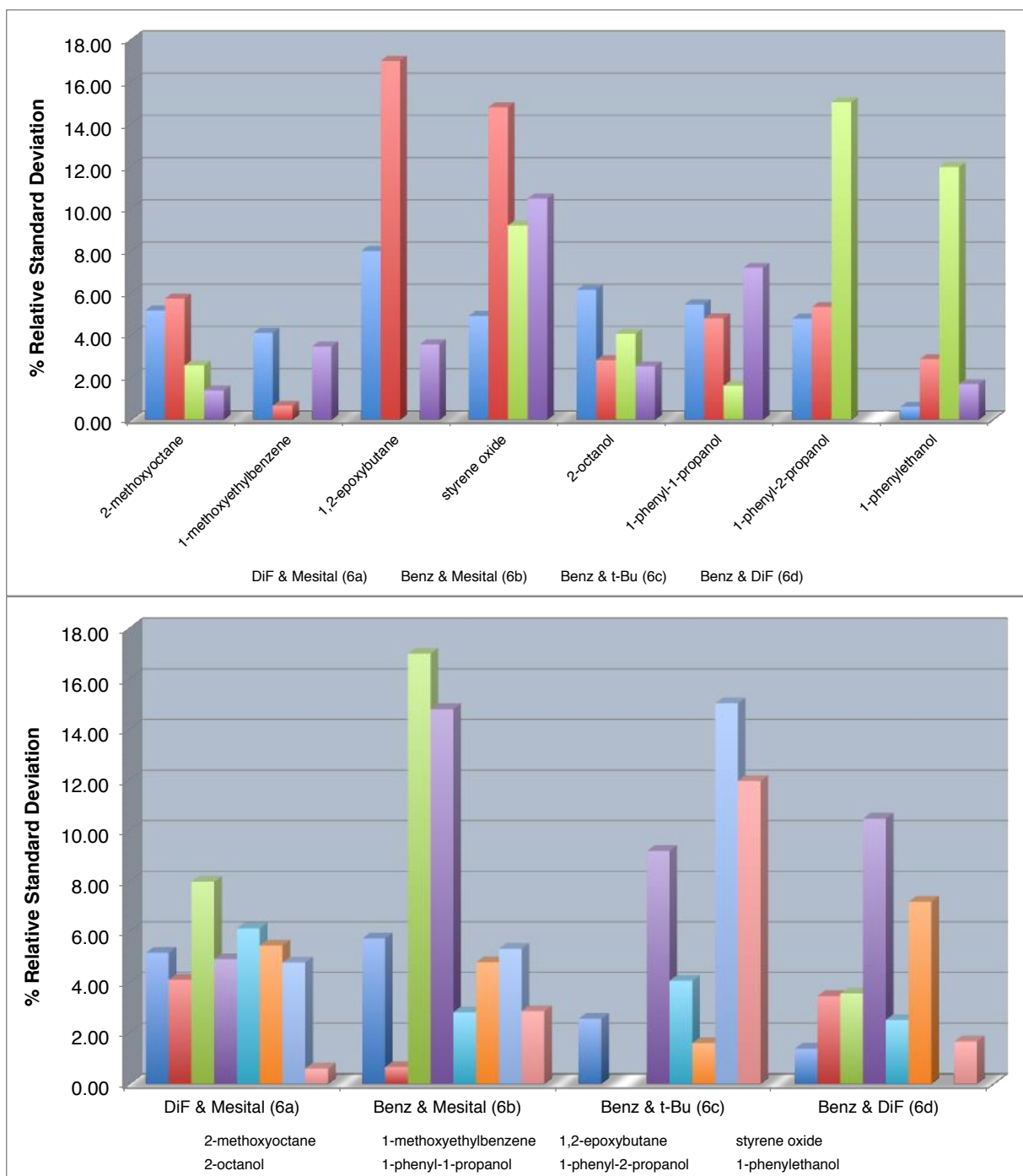


**Figure 144.** RSD values for the mixed system. Grouped by chiral probe (top) and catalyst (bottom).

## 6.6 – *Meso*-1,2-Diphenylethylenediamine-based Di-Imines

Achiral *meso*-1,2-diphenylethylenediamine was condensed with various aldehydes to produce catalysts 4a-g. Due to the smaller signal in the ITMS, isolation of the  $^{65}\text{Cu}$  isotope and subsequent reaction with chiral probes, gave signals too low to be reliable, thus, a wider isolation range of 5 m/z was used to obtain a suitable signal. Again, with substituents bearing lone pair electrons, only the 2,6 difluoro substituted aldehyde displayed coordination. Being achiral, there should be no selectivity observed. Only the 1-phenyl-1-propanol probe displayed slight selectivity (Figure 145). It is unknown why this probe displayed this behavior, although the wider range of m/z selected may have isolated catalyst degradation species, and the 1-phenyl-1-propanol probe was more sensitive to these species than the other probes.

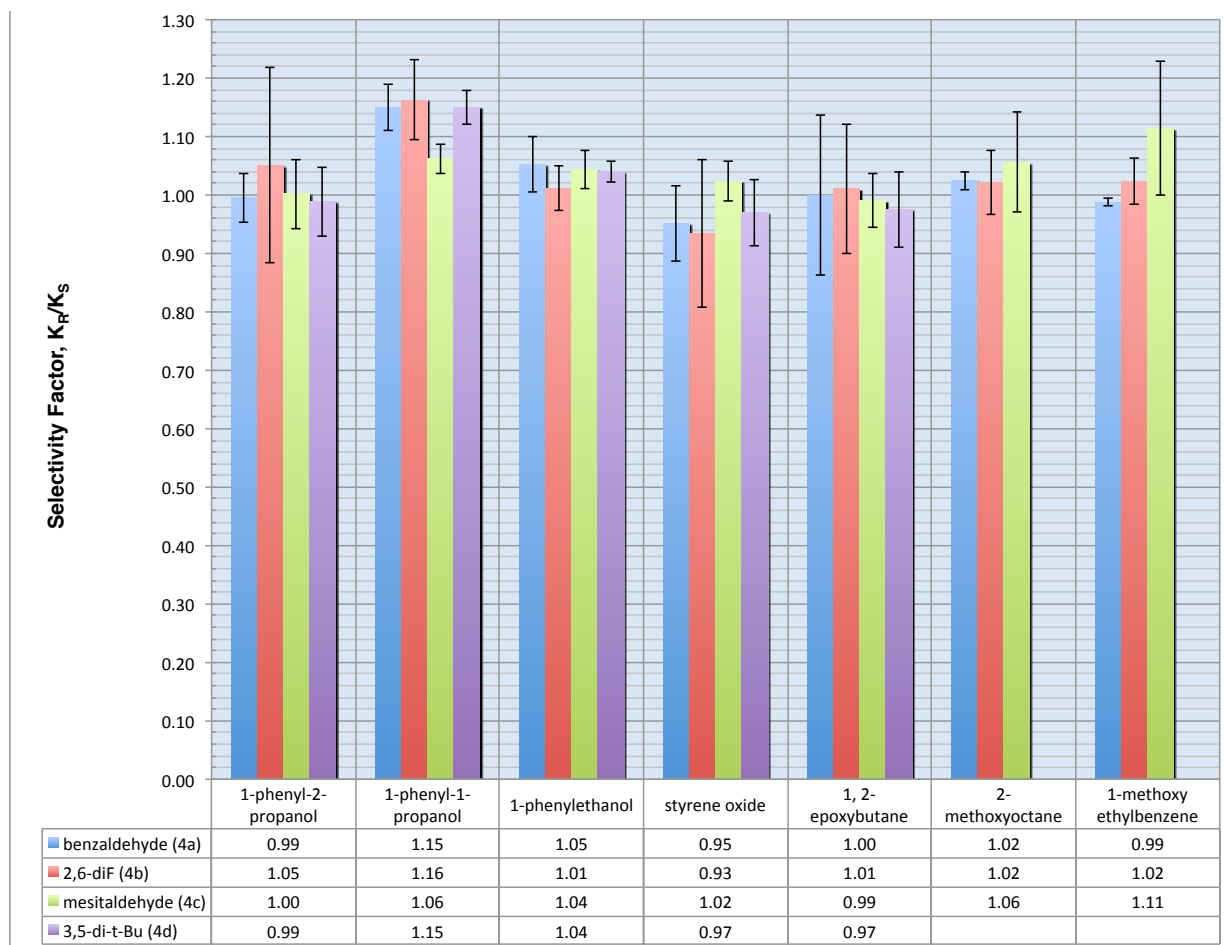


**Figure 145.** Selectivity for the *meso*-1,2-diphenylethylenediamine-based di-imines.

## 6.7 – Conclusion

Working with relatively unknown, or completely novel catalysts, as was the case for the mixed systems, a combinatorial approach was taken for examining the chiral environment induced by the catalysts via chiral probes. The previous bis-oxazoline studies allowed for the identification of probe reagents that could be used to determine the asymmetric environment of the catalyst. Up to eight different catalysts were mixed and separated in the ion-trap, however, due to non-coordination, a maximum of four

yielded results. This was due to lone-pair containing substituents interacting with the copper and effectively blocking access to the probe.

The *trans*-1,2-diaminocyclohexane-based di-imines proved not to be rigid enough to yield satisfactory selectivity when compared to the previous bis-oxazoline systems, with the 1-phenyl-2-propanol and 1-methoxyethylbenzaldehyde probes showing the highest selectivity. A slight inverse correlation between selectivity and size is observed in the phenyl-based alcohols. Generally, there was less dependence on the polarizability than that observed in the bis-oxazoline system.

The BINAM-based catalysts proved much more effective due to the more rigid nature of the BINAM and the imposed rotational barrier. This allowed for much better determination of the chiral environment around the copper and the coordinating probe. The overall strength of binding was lower for these catalysts, requiring the instrument to be run in turbo scan mode in order to detect the complexation. The 1-methoxyethylbenzene was the best overall probe for the BINAM-based catalysts.

As proof-of-concept, a crude mixture of novel chiral catalysts were synthesized and screened via the modified ITMS. These mixed  $C_1$ -symmetric benzaldehyde catalysts displayed similar selectivity as their  $C_2$ -symmetric counterparts, indicating the substituents have a limited effect on selectivity, but did display significant impact on binding energies.

Multiple checks were performed, including chiral cross checks, comparison of single run catalysts and combinatorial, and achiral catalyst runs. In most cases, the data indicated excellent accuracy and precision, except for the case of the meso-diphenylethylenediamine-based catalysts with the chiral probe, 1-phenyl-1-propanol. Overall, however, the ability to rapidly screen chiral catalysts and the asymmetric environment induced by them with the modified ITMS has been shown herein to be accurate, reproducible, and transferable.



## Chapter 7 – Conclusions

Due to the chirality found throughout nature, there exists a large market for chiral technologies, estimated to be \$5.1 billion by 2017.<sup>20</sup> The trend towards single enantiomer drugs, sparked by the thalidomide tragedy, has brought a need for better methodologies for asymmetric synthesis, such as chiral catalysts. The extremely small differences in transition state energies between diastereomeric complexes, which is responsible for enantioselectivity, imposes difficulty in theoretically designing and tuning chiral catalysts; thus, the  $C_2$ -symmetric class of ligands is often the first line of catalysts used for new transformations. These catalysts, however, may not bring the desired selectivity, thus, combinatorial chemistry has been applied to find a desired chiral catalyst. This in turn imparts a need for a rapid chiral catalyst screening method to measure the effectiveness of catalysts in the large libraries that are created.

Current chiral catalyst screening methods are long processes. A reaction must be performed to gauge the effectiveness of the catalysts. This is usually done after purification of the crude catalysts and is a time-consuming process. Mass spectrometry, usually not a tool associated with chiral measurements, has recently been adopted for the study and quantitation of enantiomeric excess. When applied to chiral catalysts, it allows for the study of the catalysts at a much earlier stage in the screening process, since the MS can act as a filter, selecting only pure catalysts (assuming no other

isobaric species). It also affords the ability to study intermediates not possible in the condensed-phase, free from solvation and ion-pairing effects. Using a modified ion-trap mass spectrometer, a neutral reagent can be introduced and allowed to react with the ion, introduced via ESI.

Using the modified ion trap mass spectrometer and methodology, intermediates in catalytic cycles have been deduced,<sup>295</sup> kinetics of reactions studied,<sup>198</sup> proton affinities and bond strengths measured,<sup>175, 203, 296</sup> and competitions between elimination and substitution reaction studied,<sup>297</sup> as well as many other uses.<sup>199</sup> Herein, we used it to determine a chiral catalysts inherent stereoselective preference, by introducing a chiral probe and allowed it to react with a chiral catalyst. Using an internal standard, and allowing the reaction to proceed to equilibrium, the chiral preference was determined. The catalyst's binding energy was also be determined. Utilizing the ITMS as a mass filter, multiple catalysts were screened from a crude synthetic mixture and assessed for their chiral discriminating ability.

The C<sub>2</sub>-symmetric bis-oxazoline catalysts are readily available from Aldrich. These catalysts offer excellent ee's for a wide-range of transformations, particularly cyclopropanations, and thus offered an excellent catalyst to begin studies towards the development of a mass spectrometry-based chiral screening method. As expected, the (*S,S*) catalysts displayed excellent discrimination with a preference for the *R* enantiomer in most cases. The selectivity was generally greater with larger substituents such as *t*-Bu, and phenyl. The bridging moiety did not have an impact on selectivity, save for a

few select cases, indicating the selectivity is determined/derived close to the metal center.

The 1-methoxyethylbenzene, 1-phenyl-2-propanol, styrene oxide, and 1-phenyl-1-propanol chiral probes proved to be the best chiral probes for determining the asymmetric environment of the catalyst. A large steric bulk near the coordinating atom was necessary for selectivity. This also contributed to the enhancement of the binding energy as the greater polarizability of the larger molecular weight probes displayed much higher binding energies. The lower Lewis basicity of styrene oxide when compared to a similar weight probe, 1-phenylethanol, was also evident in the weaker free energies of binding.

Many improvements were made to the method. For example, by utilizing a tee and mixing the copper solution and ligands before entry to the ESI probe, in conjunction with isolating the higher molecular weight isotope of copper in the ion trap, potential interference from Fenton chemistry could be minimized. Multiple checks were run and the method displayed good accuracy and precision.

The work with the bis-oxazolines allowed for the discovery of suitable chiral probes that could be used to probe other catalysts. These probes were then used on the *trans*-1,2-diaminocyclohexane-based di-imines in a combinatorial approach. Unfortunately, these displayed only moderate selectivity when compared to the bis-oxazoline system, with the 1-methoxyethylbenzene and 1-phenyl-2-propanol proving to

be the best probes. A slight inverse relationship between size and selectivity was observed for the phenyl-based alcohols, with less dependence on polarizability for binding energy. Again, the *R* enantiomer was favored for the majority of the (*S,S*) catalysts.

Due to the lack of selectivity displayed in the cyclohexane-based system, a more rigid catalyst was desired and found in the 2,2'-binaphthyl-based catalyst. The selectivity was much higher than the cyclohexane-based systems, but slightly lower than that observed in the bis-oxazoline catalysts. The weak binding displayed by the catalysts necessitated the use of a faster scan speed (turbo scan) to minimize fragmentation during the MS scan. The fragile nature of these complexes was confirmed by the low binding energies observed in this system.

This system displayed slightly different behavior than the others, with 1-phenyl-2-propanol displaying less selectivity and with the (*S*) catalysts having preference for either the *R* or *S* enantiomer depending on the probe. The 1-methoxyethylbenzene probe displayed the best selectivity, as for the other systems. Conversely, the previously excellent chiral probe, 1-phenyl-2-propanol, displayed little selectivity in this system. The (*S*) catalyst's preference for (*S*) enantiomer of 2-methoxyoctane is more pronounced in this system.

As a proof-of-concept, a novel mixed aldehyde system of BINAM-based catalysts were synthesized and run as a crude mixture. These C<sub>1</sub>-symmetric catalysts displayed

similar selectivity as the C<sub>2</sub>-symmetric counterparts, indicating the general chiral environment around the metal center, rather than substituent-specific features drives selectivity. Removal of one large group from the C<sub>2</sub>-symmetric catalyst, such as *t*-Bu, relived steric strain, and resulted in a large increase in binding energy (up to 50%) driven by the greater polarization of the added substituent when compared to benzaldehyde-based catalyst.

Again, multiple checks were run to ensure the accuracy of the results. These included chiral cross checks, checks with racemic and achiral catalysts, multiple sample preps for variability, and running the catalysts singly and in combination. The majority of these checks returned results indicating the method is sound. In cases where there were questionable results, most can be attributed to a non-ideal internal standard to analyte ratio.

While direct comparisons to the condensed phase are difficult due to the complex mechanisms involved, previous work with the Mn-Salen system provide potential insight for comparison. The gas-phase Mn-salens gave DE's between 12-20% in our system.<sup>298</sup> These catalysts were found to yield EE's greater than 90% in the condensed phase. This demonstrates that the methodology developed herein, despite exhibiting modest DE's can identify excellent condensed phase chiral catalyst with the appropriate set of chiral probes.<sup>299</sup>

## List of References

## List of References

- (1) Pasteur, L. *Ann. Chim. Phys.* **1848**, 442.
- (2) Pasteur, L. *C. R. Acad. Sci* **1848**, 26, 535.
- (3) Pasteur, L. *C. R. Acad. Sci.* **1857**, 45, 1032.
- (4) Hegstrom, R. A.; Kondepudi, D. K. *Sci. Am.* **1990**, 108.
- (5) Guijarro, A.; Yus, M. *The Origin of Chirality in the Molecules of Life*; 1st ed.; Royal Society of Chemistry, 2008; p. 150.
- (6) Ng, H. L.; Kopka, M. L.; Dickerson, R. E. *Proc. Natl. Acad. Sci. U. S. A.* **2000**, 97, 2035.
- (7) Barceloux, D. *Medical Toxicology of Natural Substances: Foods, Fungi, Medicinal Herbs, Plants, and Venomous Animals*; 1st ed.; Wiley, 2012.
- (8) Sweet, M. J. *Berkeley Technol. Law J.* **2009**, 24, 129.
- (9) Noyori, R. *Angew. Chem. Int. Ed. Engl.* **2002**, 41, 2008.
- (10) FDA. *Drugs Development of New Stereoisomeric Drugs*; 1992; pp. 1–4.
- (11) Wu, L.; Vogt, F. G. *J. Pharm. Biomed. Anal.* **2012**, 69, 133.
- (12) Valentová, A. J.; Hutt, A. J. *Acta Fac. Pharm. Univ. Comenianae* **2003**, 50, 7.
- (13) Farina, V.; Reeves, J. T.; Senanayake, C. H.; Song, J. J. *Chem. Rev.* **2006**, 106, 2734.
- (14) Morgan, S.; Grootendorst, P.; Lexchin, J.; Cunningham, C.; Greyson, D. *Health Policy (New. York)*. **2011**, 100, 4.
- (15) DiMasi, J.; Feldman, L.; Seckler, A.; Wilson, A. *Clin. Pharmacol. Ther.* **2010**, 87, 272.
- (16) Wells, W. *Chem. Biol.* **1999**, 6, 119.

- (17) Shafaati, A. *Iran. J. Pharm. Res.* **2007**, *6*, 73.
- (18) Awad, H.; El-aneed, A. *Mass Spectrom. Rev.* **2013**, *32*, 466.
- (19) Sushil, S.; Sharma, A. K.; Gupta, A. K.; Navdeep, D.; Brashier, D. B. S. *J. Drug Deliv. Ther.* **2014**, *4*, 135.
- (20) Global Industry Analysts, I. *Chiral Technology: A Global Strategic Business Report*; 2014; pp. 1–3.
- (21) Hawkins, J. M.; Watson, T. J. N. *Angew. Chem. Int. Ed. Engl.* **2004**, *43*, 3224.
- (22) Pasteur, L. *C. R. Acad. Sci.* **1853**, *37*, 162.
- (23) Benfey, O. T.; Morris, J. T. *Robert Burns Woodward: Architect and Artist in the World of Molecules*; Chemical Heritage Foundation, 2001; p. 470.
- (24) Gawley, R. E.; Aube, J. *Principles of Asymmetric Synthesis*; 2nd ed.; Elsevier: Oxford, 2012; p. 553.
- (25) Marckwald, W.; MaKenzie, A. *Ber. Deut. Chem. Ges.* **1899**, *32*, 2130.
- (26) Kitamura, M.; Tokunaga, M.; Noyori, R. *J. Am. Chem. Soc.* **1993**, *115*, 114.
- (27) Pellissier, H. *Tetrahedron* **2008**, *64*, 1563.
- (28) Dalglieshi, C. E. *J. Chem. Soc.* **1952**, *9*, 3940.
- (29) Easson, L. H.; Stedman, E. *Biochem. J.* **1933**, *27*, 1257.
- (30) Welch, W. M.; Kraska, A. R.; Sarges, R.; Koe, B. K. *J. Med. Chem.* **1984**, *27*, 1508.
- (31) Dapremont, O.; Geiser, F.; Zhang, T.; Guhanm, S.; Guinn, R.; Quallich, G. Process for the production of enantiomerically pure or optical enriched sertraline-tetralone using continous chromatography. 6,444,854, 2002.
- (32) Jacques, J.; Leclerco, M.; Brienne, M.-J. *Tetrahedron* **1981**, *37*, 1727.
- (33) Jungfleish, M. E. *J. Pharm. Chim.* **1882**, *5*, 346.
- (34) Zaugg, H. *J. Am. Chem. Soc.* **1954**, *77*, 2910.
- (35) Andrushko, V.; Andrushko, N. *Stereoselective Synthesis of Drugs and Natural Products*; Andrushko, V.; Andrushko, N., Eds.; 1st ed.; Wiley & Sons, Inc., 2013; p. 1836.



- (36) Desimoni, G.; Faita, G.; Jørgensen, K. A. *Chem. Rev.* **2006**, *106*, 3561.
- (37) Evans, D. A.; Helmchen, G. *Asymmetric Synthesis - The Essentials*; Christmann, M.; Brase, S., Eds.; 2007; pp. 3–9.
- (38) Evans, D. A.; Shih, T. L. *J. Am. Chem. Soc.* **1981**, 2127.
- (39) Meister, P. G.; Paquette, L. A. *Org. Synth.* **1990**, *68*, 77.
- (40) Hill, C.; Carolina, N. *Org. Lett.* **2003**, *5*, 3009.
- (41) Derussy, D. T.; Paquette, L. A. *Org. Synth.* **1990**, *68*, 83.
- (42) Dias, L. C.; Bau, R., Z.; de Sousa, M., A.; Zukerman-Schpector, A. *Org. Lett.* **2002**, *4*, 4325.
- (43) Arya, P.; Qin, H. *Tetrahedron* **2000**, *56*, 917.
- (44) Trost, B. M. *Angew. Chemie Int. Ed. English* **1995**, *34*, 259.
- (45) Davis, M. E.; Davis, R. J. Courier Dover Publications, 2012; p. 368.
- (46) Bravo-Suarez, J. J.; Chaudhari, R. V.; Subramaniam, B. In *Novel Materials for Catalysis and Fuels Processing*; ACS Symposium Series, 2013; p. 68.
- (47) Nobelprize.org. All Nobel Prizes in Chemistry  
[http://www.nobelprize.org/nobel\\_prizes/chemistry/laureates/](http://www.nobelprize.org/nobel_prizes/chemistry/laureates/) (accessed Jul 29, 2014).
- (48) Nobelprize.org. All Nobel Prizes in ChemistryThe Nobel Prize in Chemistry 2010  
[http://www.nobelprize.org/nobel\\_prizes/chemistry/laureates/2010/](http://www.nobelprize.org/nobel_prizes/chemistry/laureates/2010/) (accessed Jul 29, 2014).
- (49) Schmid, A.; Dordick, J. S.; Hauer, B.; Kiener, A.; Wubbolts, M.; Witholt, B. *Nature* **2001**, *409*, 258.
- (50) Koyanagi, T.; Katayama, T.; Suzuki, H.; Nakazawa, H.; Yokozeki, K.; Kumagai, H. *J. Biotechnol.* **2005**, *115*, 303.
- (51) Simurdiak, M. R.; Johannes, T.; Zhao, H. *Encyclopedia of Chemical Processing*; Francis, T. &, Ed.; 2006; pp. 101–110.
- (52) Buchholz, K. In *Biocatalysis and Enzyme Technology*; Buchholz, K.; Kasche, V.; Bornscheuer, U. T., Eds.; Wiley-VCH GmbH & Co, 2012; p. 32.
- (53) Marckwald, W. *Berichte der Dtsch. Chem. Gesellschaft* **1904**, *37*, 349.

- (54) Crelate, I. C. C.; Nozaki, I.; Moriuti, S.; Takaya, H.; Noyori, R. *Tetrahedron Lett.* **1966**, 5239.
- (55) Knowles, W. S.; Sabacky, M. J. *Chem. Commun.* **1968**, 1445.
- (56) Buthe, H.; Siegel, H.; Horner, L. *Angew. Chemie., Int. Ed. Engl.* **1968**, 7, 942.
- (57) Dang, B. T. P.; Kagan, H. B. *Chem. Commun.* **1971**, 7, 2476.
- (58) Knowles, W. S.; Sabacky, M. J.; Vineyard, B. D. *J. Chem. soc., Chem. Commun.* **1972**, 1, 10.
- (59) Knowles, W. S. *Angew. Chem. Int. Ed. Engl.* **2002**, 41, 1999.
- (60) Takaya, H.; Yasuda, A.; Miyashita, A.; Ito, T.; Toriumi, K.; Noyori, R.; Souchi, T. *J. Am. Chem. Soc.* **1980**, 102, 7932.
- (61) Noyori, R.; Ohta, M.; Hsiao, Y.; Kitamura, M. *J. Am. Chem. Soc.* **1986**, 108, 7117.
- (62) Katsuki, T.; Sharpless, K. B. *J. Am. Chem. Soc.* **1980**, 102, 5976.
- (63) Sharpless, K. B. *Angew. Chem. Int. Ed. Engl.* **2002**, 41, 2024.
- (64) Nugent, W. A.; Rajanbabu, T. V.; Burk, M. J. *Science (80-. )*. **1993**, 259, 479.
- (65) Blaser, H.-U.; Spinder, F.; Studer, M. *Appl. Catal. A Gen.* **2001**, 221, 119.
- (66) Catalyts, J. M. *Handbook of Pharmaceutical Catalysis*; 2009; p. 107.
- (67) Infomine. Historical price of Pd <http://www.infomine.com/investment/metal-prices/palladium/all/>.
- (68) Berrisford, D. J.; Bolm, C.; Sharpless, K. B. *Angew. Chemie Int. Ed. English* **1995**, 34, 1059.
- (69) MacMillan, D. W. C. *Nature* **2008**, 455, 304.
- (70) Kuntz, K. W.; Snapper, M. L.; Hoveyda, H. *Curr. Opin. Chem. Biol.* **1999**, 3, 313.
- (71) Jacobsen, E.; Pfaltz, A.; Yamamoto, H. *Comprehensive Asymmetric Catalysis, Vol I-III*; Springer, Ed.; Berlin, 1999.
- (72) Campbell, E. J.; Nguyen, S. T. *Tetrahedron Lett.* **2001**, 42, 1221.
- (73) Fraile, J. M.; García, J. I.; Gissibl, A.; Mayoral, J. a; Pires, E.; Reiser, O.; Roldán, M.; Villalba, I. *Chem. Eur. J.* **2007**, 13, 8830.

- (74) Yoon, T. P.; Jacobsen, E. N. *Science* (80-. ). **2003**, 299, 1691.
- (75) Kagan, H. B.; Dang, T. *J. Am. Chem. Soc.* **1972**, 2, 6429.
- (76) Whitesell, J. K. *Chem. Rev.* **1989**, 89, 1581.
- (77) Nishiyama, H.; Sakaguchi, H.; Nakamura, T.; Horihata, M.; Kondo, M.; Itoh, K. *Organometallics* **1989**, 5, 846.
- (78) Zhang, H.; Imai, N.; Corey, E. J. *J. Am. Chem. Soc.* **1991**, 113, 728.
- (79) Van Lingen, H. L.; van de Mortel, J. K. W.; Hekking, K. F. W.; van Delft, F. L.; Sonke, T.; Rutjes, F. P. J. T. *Eur. J. Org. Chem.* **2003**, 2003, 317.
- (80) Lowenthal, R. E.; Abiko, A.; Masamune, S. *Tetrahedron Lett.* **1990**, 6005.
- (81) Evans, D. A.; Woerpel, K. A.; Hinman, M. M.; Faul, M. M. *J. Am. Chem. Soc.* **1991**, 113, 726.
- (82) Schiff, H. *Ann. Suppl.* **1864**, 3, 343.
- (83) Brochu, M. Mechanism and Application of Salen Ligands in Asymmetric Catalysis, 2003, Vol. II, pp. 1–16.
- (84) O'Connor, K. J.; Wey, S.-J.; Burrows, C. J. *Tetrahedron Lett.* **1992**, 33, 1001.
- (85) Jacobsen, E. N.; Zhang, W.; Loenach, J.; Wilson, S. *J. Am. Chem. Soc.* **1990**, 112, 2801.
- (86) Larrow, J. F.; Jacobsen, E. N. *Top. Organomet. Chem.* **2004**, 6, 123.
- (87) Martinez, L. E.; Leighton, J. L.; Carsten, D. H.; Jacobsen, E. N. *J. Am. Chem. Soc.* **1995**, 117, 5897.
- (88) Fukuda, T.; Katsuki, T. *Tetrahedron* **1997**, 53, 7201.
- (89) Du, H.; Ding, K. *Org. Lett.* **2003**, 5, 1091.
- (90) Ojima. *Catalytic Asymmetric Synthesis*; Wiley-VCH, Ed.; 2nd ed.; 2000.
- (91) Audrieth, L. F.; Diehl, H.; Hach, C. C. J.; Bailar, J. C. *Inorganic Synthesis, Volume 3*; 1950; Vol. 3, pp. 196–201.
- (92) Colombo, F.; Benaglia, M.; Orlandi, S.; Uselli, F. *J. Mol. Catal. A Chem.* **2006**, 260, 128.

- (93) Gago, S.; Rodríguez-Borges, J. E.; Teixeira, C.; Santos, A. M.; Zhao, J.; Pillinger, M.; Nunes, C. D.; Petrovski, Ž.; Santos, T. M.; Kühn, F. E.; Romão, C. C.; Gonçalves, I. S. *J. Mol. Catal. A Chem.* **2005**, *236*, 1.
- (94) Hillairet, C.; Michaud, G.; Sabine, S. US . Patent. 7842829B2, 2010.
- (95) Shi, M.; Wang, C.-J. *Tetrahedron: Asymmetry* **2002**, *14*, 412.
- (96) Yuan, Z.-L.; Lei, Z.-Y.; Shi, M. *Tetrahedron: Asymmetry* **2008**, *19*, 1339.
- (97) Gennari, C.; Piarulli, U. *Chem. Rev.* **2003**, *103*, 3071.
- (98) Jacobsen, E. N.; Zhang, W.; Muci, A. R.; Ecker, J. R.; Deng, L. *J. Am. Chem. Soc.* **1991**, *113*, 7063.
- (99) Katsuki, T.; Irie, R.; Ito, Y.; Noda, K.; Matsumoto, N. *Tetrahedron Lett.* **1990**, *31*, 7345.
- (100) Katsuki, T. *Adv. Synth. Catalysis* **2002**, *344*, 131.
- (101) Evans, D. A.; Burgey, C. S.; Kozlowski, M. C.; Tregay, S. W. *J. Am. Chem. Soc.* **1999**, *121*, 686.
- (102) Ding, K.; Ishii, A.; Mikami, K. *Angew. Chemie Int. Ed.* **1999**, *38*, 497.
- (103) Williams, I. H. *Beilstein J. Org. Chem.* **2010**, *6*, 1026.
- (104) Noyori, R.; Suga, S.; Kawai, K.; Kitamura, O. M. *J. Organomet. Chem.* **1990**, *382*, 19.
- (105) Liang, Y.; Bradshaw, J. S.; Izatt, R. M.; Pope, R. M.; Dearden, D. V. *Int. J. Mass Spectrom.* **1999**, *185-187*, 977.
- (106) Koskinen, A. *Asymmetric Synthesis of Natural Products*; 2nd ed.; Wiley: Somerset, 2012; p. 324.
- (107) Walsh, P. J.; Kozlowski, M. C. *Fundamentals of Asymmetric Catalysis*; (1) Walsh, P. J.; Kozlowski, M. C. *Fundamentals of Asymmetric Catalysis*; University Science Books, 2009; pp. 114–164., Ed.; 1st ed.; University Science Books: Sausalito, 2009; p. 674.
- (108) Dimaur, E. F.; Carr, J.; Marisa, C. K. *J. Org. Chem.* **2003**, *68*, 1973.
- (109) Thompson, J. J. *Proc. R. Soc.* **1913**, *89*, 1.
- (110) Parkins, W. E. *Phys. Today* **2005**, *58*, 45.

- (111) Mahaffy, P. R.; Webster, C. R.; Cabane, M.; Conrad, P. G.; Coll, P.; Atreya, S. K.; Arvey, R.; Barciniak, M.; Benna, M.; Bleacher, L.; Brinckerhoff, W. B.; Eigenbrode, J. L.; Carignan, D.; Cascia, M.; Chalmers, R.; Dworkin, J. P.; Errigo, T.; Everson, P.; Franz, H.; Farley, R.; Feng, S.; Frazier, G.; Freissinet, C.; Glavin, D. P.; Harpold, D. N.; Hawk, D.; Holmes, V.; Johnson, C. S.; Jones, A.; Jordan, P.; Kellogg, J.; Lewis, J.; Lyness, E.; Malespin, C.; Martin, D. K.; Maurer, J.; McAdam, A. C.; McLennan, D.; Nolan, T. J.; Noriega, M.; Pavlov, A.; Prats, B.; Raaen, E.; Sheinman, O.; Sheppard, D.; Smith, J.; Stern, J. C.; Tan, F.; Trainer, M.; Ming, D. W.; Morris, R. V.; Jones, J.; Gundersen, C.; Steele, A.; Wray, J.; Botta, O.; Leshin, L.; Owen, T.; Battel, S.; Jakosky, B. M.; Manning, H.; Squyres, S.; Navarro-González, R.; McKay, C. P.; Raulin, F.; Sternberg, R.; Buch, A.; Sorensen, P.; Kline-Schoder, R.; Coscia, D.; Szopa, C.; Teinturier, S.; Baffes, C.; Feldman, J.; Flesch, G.; Forouhar, S.; Garcia, R.; Keymeulen, D.; Woodward, S.; Block, B. P.; Arnett, K.; Miller, R.; Edmonson, C.; Gorevan, S.; Mumm, E. *Space Sci. Rev.* **2012**, *170*, 401.
- (112) Dempster, A. J. *Phys. Rev.* **1918**, *11*, 316.
- (113) Munson, M. S. B.; Field, F. H. *J. Am. Chem. Soc.* **1966**, *88*, 2621.
- (114) Yamashita, M.; Fenn, J. B. *J. Phys. Chem.* **1984**, *88*, 4451.
- (115) Fenn, J. In *Nobel Prize 2002*; The Nobel Foundation: Stockholm, 2002; pp. 154–184.
- (116) Loo, J. *Int. J. Mass Spectrom.* **2000**, *200*, 175.
- (117) Gaskell, S. J. *J. Mass Spectrom.* **1997**, *32*, 677.
- (118) Hoffman, E.; Stroobant, V. *Mass Spectrometry: Principles and Applications*; third ed.; Wiley, 2007.
- (119) Banerjee, S.; Mazumdar, S. *Int. J. Anal. Chem.* **2012**, *2012*, 1.
- (120) Kebarle, P.; Peschke, M. *Anal. Chim. Acta* **2000**, *406*, 11.
- (121) Fenn, J.; Rutan, S. *Anal. Chim. Acta* **2006**, *406*, 1.
- (122) Dole, M.; Mack, L.; Hines, R. L.; Mobley, R. C.; Ferguson, L. D.; Alice, M. *J. Chem. Phys.* **1968**, *49*, 2240.
- (123) Rayleigh, L. *Philas. Mag.* **1882**, *14*, 184.
- (124) Konermann, L.; Ahadi, E.; Rodriguez, A. D.; Vahidi, S. *Anal. Chem.* **2013**, *85*, 2.
- (125) Wilm, M. *Mol. Cell. Proteomics* **2011**, *10*, M111.009407.

- (126) Fernandez de la Mora, J. *Anal. Chim. Acta* **2000**, 406, 93.
- (127) Iribarne, J. *J. Chem. Phys.* **1976**, 64, 2287.
- (128) Thomson, B. *J. Chem. Phys.* **1979**, 7, 4451.
- (129) Fernandez de la Mora, J.; Gamero-Castano, M. *J. Chem. Phys.* **2000**, 113, 815.
- (130) Fenn, J.; Nguyen, S. *Proc. Natl. Acad. Sci. U. S. A.* **2007**, 104, 1111.
- (131) Siuzdak, G. *Mass Spectrometry for Biotechnology*; Academic Press, 1996.
- (132) Wong, P. S. H.; Cooks, Graham, R. *Curr. Sep.* **1997**, 16.
- (133) Hoffmann, E. De. *J. Mass Spectrom.* **1996**, 31, 129.
- (134) Yost, R. A.; Enke, C. G. *J. Am. Chem. Soc.* **1978**, 100, 2274.
- (135) Hopfgartner, G.; Varesio, E.; Tschäppät, V.; Grivet, C.; Bourgoigne, E.; Leuthold, L. A. *J. Mass Spectrom.* **2004**, 39, 845.
- (136) Paul, W.; Steinwedel, H. Apparatus for separating charged particles of different specific charges. 2939952, 1956.
- (137) Paul, W.; H., S. *Naturforsch* **1953**, 8a, 448.
- (138) Paul, W. *Angew. Chemie., Int. Ed. Engl.* **1990**, 29, 739.
- (139) Fischer, E. *Phys* **1959**, 156, 1.
- (140) March, R.; Todd, J. *Quadrupole Ion Trap Mass Spectrometry*; 2nd ed.; Wiley, 2005.
- (141) Dawson, P. H.; Whetten, N. R. *J. Vac. Sci. Tech* **1986**, 5, 11.
- (142) Stafford, G. C.; Kelley, P. E.; Syka, J. E. P.; Reynolds, W. E.; Todd, J. F. J. *Int. J. Mass Spectrom.* **1984**, 60, 85.
- (143) Stafford, G. *J. Am. Soc. Mass Spectrom.* **2002**, 13, 589.
- (144) Kaiser, R. E.; Louris, J. N.; Amy, J. W.; Cooks, R. G.; Hunt, D. F. *Rapid Commun. Mass Spectrom.* **1989**, 3, 225.
- (145) Schwartz, J. C.; Syka, J. E.; Jardine, I. *J. Am. Soc. Mass Spectrom.* **1991**, 2, 198.

- (146) Glish, G. L.; Berkel, G. J.; McLuckey, S. A.; Louri, J.; Brodbelt-Lustig, J.; Cooks, G. *Int. J. Mass Spectrom. Ion Process.* **1990**, *96*, 117.
- (147) Schwartz, J. C.; Senko, M. W.; Syka, J. E. P. *J. Am. Soc. Mass Spectrom.* **2002**, *13*, 659.
- (148) March, R. E. In *Encyclopedia of Analytical Chemistry*; Meyers, R. A., Ed.; Wiley, 2000; pp. 11848–11872.
- (149) Jonscher, K. R.; Yates, J. R. *Anal. Biochem.* **1997**, *244*, 1.
- (150) March, R. E. *J. Mass Spectrom.* **1997**, *32*, 351.
- (151) Franzen, J. *Int. J. Mass Spectrom. Ion Process.* **1991**, *106*, 63.
- (152) Ying, J.-F.; Douglas, D. J. *Rapid Commun. Mass Spectrom.* **1996**, *10*, 649.
- (153) Cooks, G. R.; Ridley, T. Y.; Louri, J.; May, J. T. *Int. J. Mass Spectrom. Ion Process.* **1989**, *88*, 97.
- (154) Son, M. H.; Cooks, R. G. *Anal. Chem.* **1994**, *66*, 2488.
- (155) Sleno, L.; Volmer, D. A. *J. Mass Spectrom.* **2004**, *39*, 1091.
- (156) Cooks, G. *J. Mass Spectrom.* **1995**, *30*, 1215.
- (157) McLuckey, S. *J. Am. Soc. Mass Spectrom.* **1992**, *3*, 599.
- (158) Yang, Y.-H.; Lee, K.; Jang, K.-S.; Kim, Y.-G.; Park, S.-H.; Lee, C.-S.; Kim, B.-G. *Anal. Biochem.* **2009**, *387*, 133.
- (159) Titov, V. *J. Am. Soc. Mass Spectrom.* **1998**, *9*, 70.
- (160) Fischer, E. *Phys.* **1959**, *156*, 1.
- (161) Ottens, A. K.; Arkin, C. R.; Griffin, T. P.; Palmer, P. T.; Harrison, W. W. *Int. J. Mass Spectrom.* **2005**, *243*, 31.
- (162) Dempster, A. J. *Philos. Mag.* **1916**, *13*, 438.
- (163) Brodbelt, J. S. *Mass Spectrom. Rev.* **1997**, *16*, 91.
- (164) Hail, M. E.; Berberich, D. W.; Yost, R. A. *Anal. Chem.* **1989**, *61*, 1874.
- (165) Schmit, J. P.; Dawson, P. H.; Beaulieu, N. *Org. Mass Spectrom.* **1985**, *20*, 269.

- (166) Jalonen, J. *J. Chem. Soc., Chem. Commun.* **1985**, 872.
- (167) Jalonen, J. *Chem. Commun.* **1985**, 13, 872.
- (168) Fetterolf, D. D.; Yost, R. A.; Eyler, J. R. *Org. Mass Spectrom.* **1984**, 19, 104.
- (169) Schmitt, J.; Beaudet, S.; Brisson, A. *Org. Mass Spectrom.* **1986**, 21, 493.
- (170) Ferguson, E. E.; Fehsenfeld, F. C.; Schmeltekopf, A. L. *Adv. At. Mol. Phys.* **1969**, 5, 1.
- (171) Smith, D.; Adams, N. G. *Int. J. Mass Spectrom. Ion Phys.* **1976**, 21, 349.
- (172) Bierbaum, V. M. *Int. J. Mass Spectrom.* **2014**, July.
- (173) Bierbaum, V. M.; Depuy, C. H.; Shapiro, R. H.; Stewart, J. H. *J. Am. Chem. Soc.* **1975**, 4229.
- (174) Adams, N. G.; Smith, D. In *Techniques for the Study of Ion–Molecule Reactions*; Farrar, J. M.; Saunders, Jr., W. H. E., Ed.; Wiley: New York, 1988.
- (175) Ervin, K. M.; Gronert, S.; Barlow, S. E.; Gilles, M. K.; Harrison, A. G.; Bierbaum, V. M.; C.H. DePuy, W. C. L.; Ellison, G. B. *J. Am. Chem. Soc.* **1990**, 112, 5750.
- (176) Kato, S.; DePuy, C. H.; Gronert, S.; Bierbaum, V. M. *J. Am. Soc. Mass Spectrom.* **1999**, 10, 840.
- (177) Kebarle, P.; Hogg, A. M.; Knewstubb, P. F.; Sugden, T. M.; Tickner, A. W.; Godbole, E. W. *J. Chem. Phys.* **1965**, 43, 449.
- (178) Kebarle, P. In *Techniques for the Study of Ion–Molecule Reactions*; Farrar, J. M.; Saunders, Jr., W. H. E., Ed.; Wiley: New York, 1988.
- (179) Kebarle, P.; Hogg, A. M. *J. Chem. Phys.* **1965**, 42, 668.
- (180) Enders, J. R.; Mclean, J. A. *Chirality* **2009**, 21, E253.
- (181) Chait, B. T.; Katta, V.; Chowdhury, S. *J. Am. Chem. Soc.* **1990**, 112, 5348.
- (182) Chan, K. W. S.; Cook, K. D. *J. Am. Chem. Soc.* **1982**, 104, 5031.
- (183) Hu, Q.; Noll, R. J.; Li, H.; Makarov, A.; Hardman, M.; Graham Cooks, R. *J. Mass Spectrom.* **2005**, 40, 430.
- (184) Anders, L. R.; Beauchamp, J. L.; Dunbar, R. C.; Baldeschwieler, J. D. *J. Chem. Phys.* **1966**, 17, 45.



- (185) Buttrill, S. E. *J. Chem. Phys.* **1969**, *50*, 4125.
- (186) Foster, M. S.; Beauchamp, J. L. *J. Am. Chem. Soc.* **1971**, *1*, 4924.
- (187) Fiebig, L.; Kuttner, J.; Hilt, G.; Schwarzer, M. C.; Frenking, G.; Schmalz, H.-G.; Schäfer, M. *J. Org. Chem.* **2013**, *78*, 10485.
- (188) Fiebig, L.; Schmalz, H.-G.; Schäfer, M. *Int. J. Mass Spectrom.* **2011**, *308*, 307.
- (189) Rettinghaus, V. von G. *Angew. Phys.* **1967**, *22*, 321.
- (190) Fulford, J. E.; March, R. E. *Int. J. Mass Spectrom. Ion Phys.* **1978**, *26*, 155.
- (191) Armitage, M. A.; Fulford, J. E.; Hoa, D. N.; Hughes, R. J.; March, R. E. *Can. J. Chem.* **1979**, *57*, 2108.
- (192) Fulford, J. E.; Hoa, D. N.; Hughes, R. J.; March, R. E.; Bonner, R. F.; Wong, G. J. *J. Vac. Sci. Tech* **1980**, *17*, 829.
- (193) Ho, M.; Hughes, R. J.; Kazdan, E.; Matthews, P. J.; Young, A. B.; March, R. E. In *Proceedings of the 32nd ASMS Conference on Mass Spectrometry and Allied Topics*; San Antonio, TX, 1984; p. 513.
- (194) Todd, J.; Waldrein, R. M.; Freer, D. A.; Turner, R. B. *Int. J. Mass Spectrom. Ion Phys.* **1980**, *35*, 107.
- (195) Waldren, R. M.; Bonner, R. F.; Todd, F. J. *Int. J. Mass Spectrom. Ion Phys.* **1980**, *34*, 17.
- (196) Todd, J.; March, R. E. *Int. J. Mass Spectrom.* **1999**, *190/191*, 9.
- (197) Perry, R. H.; Cooks, R. G.; Noll, R. J. *Mass Spectrom. Rev.* **2008**, 661.
- (198) Gronert, S. *Mass Spectrom. Rev.* **2005**, *24*, 100.
- (199) Gronert, S. *Chem. Rev.* **2001**, *101*, 329.
- (200) O'Hair, R. J. *Chem. Commun. (Camb)*. **2006**, 1469.
- (201) Donald, W. a; Khairallah, G. N.; O'Hair, R. a J. *J. Am. Soc. Mass Spectrom.* **2013**, *24*, 811.
- (202) Cooks, R. G.; Patrick, J.; Kotiaho, T.; McLuckey, S. A. *Mass Spectrom. Rev.* **1994**, *13*, 287.
- (203) Blanksby, S. J.; Ellison, G. B. *Acc. Chem. Res.* **2003**, *36*, 255.

- (204) P. Kabarle. *Annu. Rev. Phys. Chem.* **1977**, *28*, 445.
- (205) Wysocki, V. H.; Resing, K.; Zhang, Q.; Cheng, G. *Methods* **2005**, *35*, 211.
- (206) Aebersold, R.; Mann, M. *Nature* **2003**, *422*, 198.
- (207) Brancia, F. *Expert Rev. Proteomics* **2006**, *3*, 143.
- (208) Weckwerth, W.; Morgenthal, K. *Drug Discov. Today* **2005**, *10*, 1551.
- (209) Shaner, R.; Allegood, J.; Park, H.; Wang, E.; Kelly, S.; Haynes, C. A.; Sullards, M. C.; Merrill, A. H. *J. Lipid Res.* **2009**, *50*, 1692.
- (210) Ottens, A. K.; Harrison, W. W.; Griffin, T. P.; Helms, W. R. *J. Am. Soc. Mass Spectrom.* **2002**, *13*, 1120.
- (211) Rosenband, T.; Hume, D. B.; Schmidt, P. O.; Chou, C. W.; Brusch, A.; Lorinin, L.; Oskay, W. H.; Drullinger, R. E.; Fortier, T. M.; Stalnaker, J. E.; Diddams, S. A.; Swann, W. C.; Newbury, N. R.; Itano, W. M.; Wineland, D. J.; Bergquist, J. C. *Science* **2008**, *319*, 1808.
- (212) Blatt, R.; Wineland, D. *Nature* **2008**, *453*, 1008.
- (213) Beynon, H.; Astt, T. *Org. Mass Spectrom.* **1981**, *16*.
- (214) Wu, H.-F.; Brodbelt, J. S. *Int. J. Mass Spectrom. Ion Proc.* **1993**, *124*, 175.
- (215) Rijs, N. J.; Hair, R. A. J. O. *Organometallics* **2012**, *31*, 8012.
- (216) James, P. F.; O'Hair, R. A. J. *Org. Lett.* **2004**, *6*, 2761.
- (217) Fedorov, A.; Batiste, L.; Bach, A.; Birney, D. M.; Chen, P. *J. Am. Chem. Soc.* **2011**, *133*, 12162.
- (218) Gronert, S. *J. Am. Soc. Mass Spectrom.* **1998**, *9*, 845.
- (219) Chowdhury, S. K.; Katta, V.; Chait, B. T. *J. Am. Chem. Soc.* **1990**, *112*, 9012.
- (220) Hoaglund-Hyzer, C. S.; Counterman, A. E.; Clemmer, D. E. *Chem. Rev.* **1999**, *99*, 3037.
- (221) Kebarle, P.; Ho, Y. In *Electrospray Ionization Mass Spectrometry: Fundamentals, Instrumentations & Applications*; Cole, R., Ed.; Wiley: New York, 1997; pp. 3–64.
- (222) Blanksby, S. J.; Ellison, G. B. *Acc. Chem. Res.* **2003**, *36*, 255.

- (223) Ma, J. C.; Dougherty, D. a. *Chem. Rev.* **1997**, *97*, 1303.
- (224) Schalley, C. A.; Springer, A. In *Mass Spectrometry and Gas-Phase Chemistry of Non-Covalent Complexes*; Desiderio, D.; Nibbering, N., Eds.; Wiley & Sons, Inc.: New Jersey, 2009; pp. 9–60.
- (225) Wang, H.; Agnes, G. R. *Anal. Chem.* **1999**, *71*, 3785.
- (226) Leize, E.; Jaffrezic, A.; Dorsselaer, A. Van. *J. Mass Spectrom.* **1996**, *31*, 537.
- (227) Gatlin, C. L.; Turecke, F. *Anal. Chem.* **1994**, *66*, 712.
- (228) Fenn, J. B. *J. Am. Soc. Mass Spectrom.* **1993**, *4*, 524.
- (229) Schug, K.; Frycak, P.; Maier, N. M.; Lindner, W. *Anal. Chem.* **2005**, *77*, 3660.
- (230) Carlin, T. J.; Freiser, B. S. *Anal. Chem.* **1983**, *55*, 571.
- (231) Cody, R. B.; Freiser, B. S. *Anal. Chem.* **1982**, *54*, 1431.
- (232) Emary, W. B.; Kaiser, R. E.; Kenttiimaa, H. I.; Cooks, R. G. *J. Am. Soc. Mass Spectrom.* **1990**, *1*, 308.
- (233) Pyatkivskyy, Y.; Ryzhov, V. *Rapid Commun. Mass Spectrom.* **2008**, *22*, 1288.
- (234) Zhang, J.; Brodbelt, J. S. *J. Am. Chem. Soc.* **2004**, *126*, 5906.
- (235) March, R. E.; Todd, J. *Practical Aspects of Trapped Ion Mass Spectrometry, Volume 5: Applications of Trapping Devices*; 2009; p. 566.
- (236) Liere, P.; March, R. E.; Blasco, T.; Tabet, J.-C. *Int. J. Mass Spectrom. Ion Process.* **1996**, *153*, 101.
- (237) Lovejoy, E. R. *Int. J. Mass Spectrom.* **1999**, *190*, 231.
- (238) Gronert, S.; Depuy, C. H.; Bierbaum, V. M. *J. Am. Chem. Soc.* **1991**, *113*, 4009.
- (239) Dedoublement, P. A. R.; Emplgi, C.; Spectrographle, D. E. L. A. *Tetrahedron Lett.* **1961**, *19*, 2707.
- (240) Reetz, M. T.; Becker, M. H.; Klein, H.; Stöckigt, D. *Angew. Chemie Int. Ed.* **1999**, *38*, 1758.
- (241) Schrader, W.; Eipper, A.; Pugh, D. J.; Reetz, M. T. *Can. J. Chem.* **2002**, *80*, 626.
- (242) Chen, B. C.; Sih, C. J. *Angew. Chemie., Int. Ed. Engl.* **1989**, *28*, 695.

- (243) Gordes, D.; Thurow, K. *J. Assoc. Lab. Autom.* **2006**, *11*, 128.
- (244) Guo, J.; Wu, J.; Siuzdak, G.; Finn, M. G. *Angew. Chemie., Int. Ed. Engl.* **1999**, *38*, 1755.
- (245) Tsukamoto, M.; Kagan, H. B. *Adv. Synth. Catal.* **2002**, *344*, 453.
- (246) Wu, L.; Andy Tao, W.; Cooks, R. G. *J. Mass Spectrom.* **2003**, *38*, 386.
- (247) Müller, C. A.; Markert, C.; Teichert, A. M.; Pfaltz, A. *Chem. Commun. (Camb)*. **2009**, 1607.
- (248) Ebner, C.; Müller, C. a; Markert, C.; Pfaltz, A. *J. Am. Chem. Soc.* **2011**, *133*, 4710.
- (249) Teichert, A.; Pfaltz, A. *Angew. Chem. Int. Ed. Engl.* **2008**, *47*, 3360.
- (250) Linker, T. *Angew. Chemie., Int. Ed. Engl.* **1997**, 2060.
- (251) Fagin, A. E.; Wang, G.; Lau, M. C.; Gronert, S. *Org. Lett.* **2008**, *10*, 1771.
- (252) Li, Z.; Tang, Z. H.; Hu, X. X.; Xia, C. G. *Chem. Eur. J.* **2005**, *11*, 1210.
- (253) Pellissier, H. *Tetrahedron* **2008**, *64*, 7041.
- (254) K, A. K. *Int. J. Pharm. Pharm. Sci.* **2013**, *5*, 1.
- (255) Davies, H. M. L. *Tetrahedron* **1993**, *49*, 5203.
- (256) Simmons, H., H.; Smith, R., D. *J. Am. Chem. Soc.* **1958**, *1556*, 5323.
- (257) Merlic, C. A.; Zechmean, A. L. *Synthesis (Stuttg)*. **2003**, *8*, 1137.
- (258) Kirmse, W. *Angew. Chem. Int. Ed. Engl.* **2003**, *42*, 1088.
- (259) Aratani, T. *Pure Appl. Chem.* **1985**, *57*, 1839.
- (260) Muller, D.; Umbricht, G.; Weber, B.; Pfaltz, A. *Helv. Chim. Acta* **1991**, *74*, 232.
- (261) Krupanidhi, S.; Sreekumar, A.; Sanjeevi, C. B. *Indian J. Med. Res.* **2008**, *128*, 448.
- (262) Festa, R.; Thiele, D. *Curr. Biol.* **2011**, *21*, R877.
- (263) Uauy, R.; Olivares, M.; Gonzalez, M. *Am. J. Clin. Nutr.* **1998**, *67*, 952S.

- (264) Caughey, W. S.; Zhao, X.; Mochizuki, M.; Yoshikawa, S. *J. Biol. Chem.* **1995**, *270*, 4270.
- (265) Tainer, J.; Getzoff, E.; Richardson, D. *Nature* **1983**, *306*, 284.
- (266) Audi, G.; Bersillon, O.; Blachot, J.; Wapstra, A. H. *Nucl. Phys. A* **2003**, *729*, 3.
- (267) Cotton, A.; Wilkinson, G. *Advanced Inorganic Chemistry*; 5th ed.; John Wiley & Sons: New York, 1988; p. 757.
- (268) Holloway, C. E.; Melnik, M. *Rev. Inorg. Chem.* **1995**, *15*, 147.
- (269) Conry, R. Copper: Inorganic & Coordination Chemistry. *Encyclopedia of Inorganic Chemistry*, 2006.
- (270) Yoshikai, N.; Nakamura, E. *Chem. Rev.* **2012**, *112*, 2339.
- (271) Suzuki, A. *Tetrahedron Lett.* **1979**, *20*, 3437.
- (272) Stille, B. J. K. *Angew. Chemie., Int. Ed. Engl.* **1986**, *25*, 508.
- (273) Ullmann, F.; Bielecki, J. *Chem. Ber.* **1901**, *34*, 2174.
- (274) Goldberg, I. *Berichte der Dtsch. Chem. Gesellschaft* **1906**, *39*, 1691.
- (275) Kolb, H. C.; Finn, M. G.; Sharpless, K. B. *Angew. Chem. Int. Ed. Engl.* **2001**, *40*, 2004.
- (276) Huisgen, R. *Proc. Chem. Soc.* **1961**, 357.
- (277) Hagihara, N.; Tohda, Y.; Sonogashira, K. *Tetrahedron Lett.* **1975**, *16*, 4467.
- (278) Pfaltz, A. *Helv. Chim. Acta* **1988**, *71*, 1553.
- (279) Rasmussen, T.; Jensen, J. F.; Ostergaard, N.; Tanner, D.; Ziegler, T.; Norrby, P.-O. *Chem.--Eur. J.* **2002**, *8*, 177.
- (280) Aldajaei, J. Determination of the factors that affect the gas-phase reactivity of metal-centered cyclopropanation catalysts and examination of the properties of their reaction, VCU, 2014, pp. 1–135.
- (281) Fraile, J. M.; García, J. I.; Martínez-Merino, V.; Mayoral, J. a; Salvatella, L. *J. Am. Chem. Soc.* **2001**, *123*, 7616.
- (282) Salomon, R. G.; Kochi, J. K. *J. Am. Chem. Soc.* **1973**, *559*, 3300.

- (283) Gupta, A. D.; Bhuniya, D.; Singh, V. K. *Tetrahedron* **1994**, *50*, 13725.
- (284) Moser, W. R. *J. Am. Chem. Soc.* **1968**, *1171*, 1135.
- (285) Pfaltz, A. *Chimia (Aarau)*. **1990**, *44*, 202.
- (286) Diaz-Requejo, M.; Belderrain, T. R.; Trofimenko, S.; Perez, P. *J. Am. Chem. Soc.* **2001**, *12*, 3167.
- (287) Fraile, J. M.; García, J. I.; Mayoral, J. A. In *Selective Nanocatalysts and Nanoscience*; Wiley, 2011; pp. 1–49.
- (288) Cross, L. C.; Klyne, W. *Pure Appl. Chem.* **1976**, *45*, 11.
- (289) Li, Z.; Quan, R. W.; Jacobsen, E. N. *J. Am. Chem. Soc.* **1995**, *117*, 5889.
- (290) Li, Z.; Conser, K. R.; Jacobsen, E. N. *J. Am. Chem. Soc.* **1993**, *115*, 5326.
- (291) Pfaltz, A.; Drury, W. J. *Proc. Natl. Acad. Sci. U. S. A.* **2004**, *101*, 5723.
- (292) Ers, L.; Daly, A. M.; Dalton, C. T.; Renehan, M. F.; Gilheany, D. G. *Tetrahedron Lett.* **1999**, *40*, 3617.
- (293) Holbach, M.; Zheng, X.; Burd, C.; Jones, C. W.; Weck, M. *J. Org. Chem.* **2006**, *71*, 2903.
- (294) Kleij, A. W. *Eur. J. Inorg. Chem.* **2009**, *2009*, 193.
- (295) Aldajaei, J. T.; Gronert, S. *Int. J. Mass Spectrom.* **2012**, *316-318*, 68.
- (296) Gronert, S.; Fagin, A. E.; Wong, L. *J. Am. Chem. Soc.* **2007**, *129*, 5330.
- (297) Gronert, S.; Pratt, L. M.; Mogali, S. **2001**, 3081.
- (298) Fagin, A. E.; Wang, G.; Lau, M. C.; Gronert, S. *Org. Lett.* **2008**, *10*, 1771.
- (299) Jacobsen, H.; Cavallo, L. *Chem.--Eur. J.* **2001**, 800.

## Appendix

### 8.1 – (1*S*, 2*S*)-diaminocyclohexane-based di-imines

Mass Spectrometer tune conditions

Tune file: benzaldehydes 090313.LCQTune

Infusion rate – 1  $\mu\text{l}/\text{min}$

Positive Ion Mode

Source type – ESI

Spray Voltage (kV) – 5

Spray current ( $\mu\text{A}$ ) – 0.1

Capillary heat ( $^{\circ}\text{C}$ ) – 165

Probe position – 1

Sheath flow (arb) – 20

Capillary (V) – 120

Octapole 1 offset (V) – -3.75

Octapole 2 offset (V) – -8.5

Tube lens offset (V) – 55

Trap offset (V) – -10

Multiplier – -1310

$\mu\text{scan}$  – 10

AGC – Off

Ion Gauge –  $2.69 \times 10^{-5}$  torr

Tune file – benzaldehydes 090313.LCQTune

Isolate 353.2 m/z

isolation window 5.0 m/z

Fragmentation energy – 35%

Activation time – 50 msec

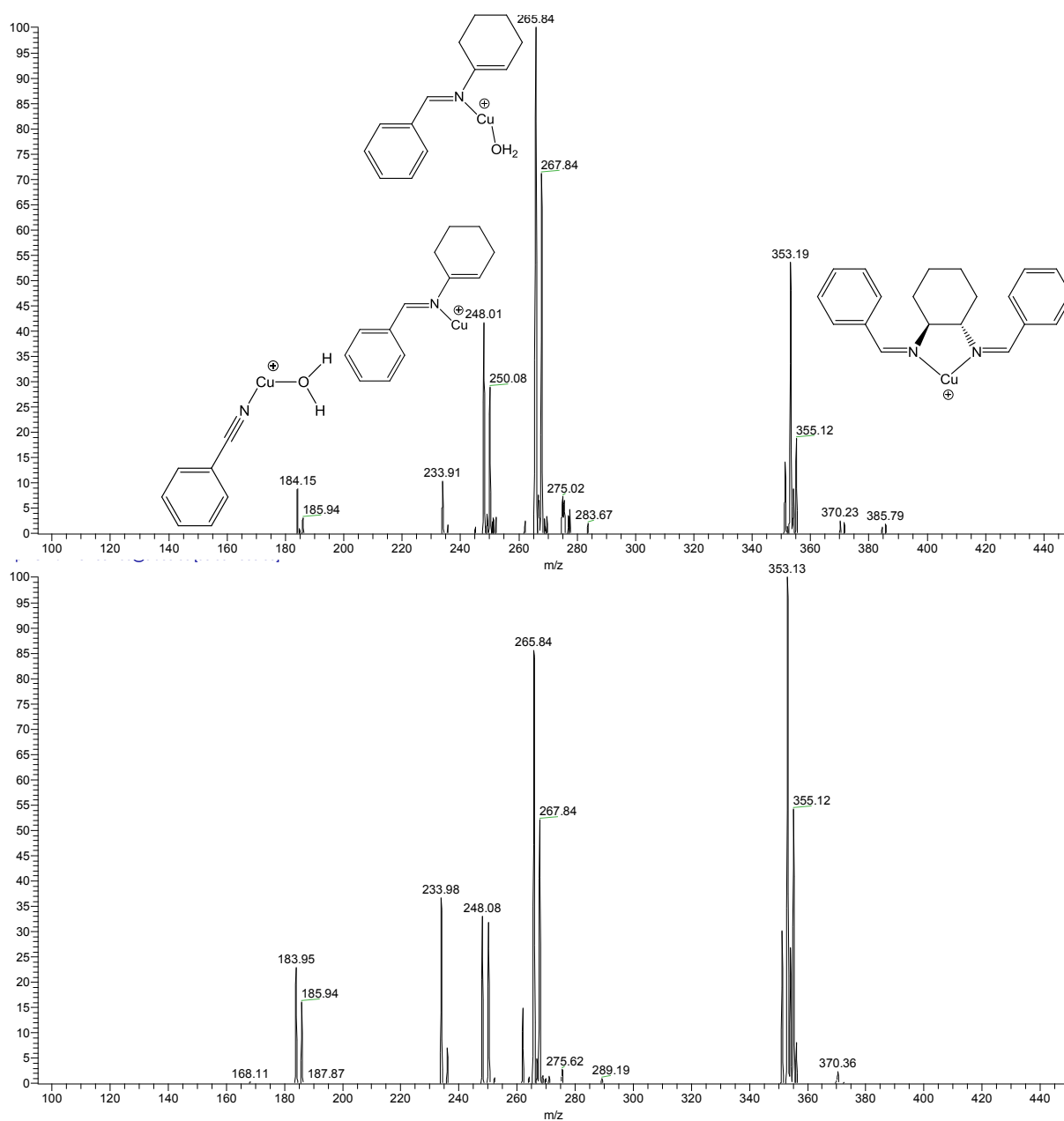


**Figure 146.** Catalyst 3a in mixture of catalysts 3 b-d-g (top) and as single solution (bottom).



Tune file – benzaldehydes 090313.LCQTune

Isolate – 425.1 m/z

Isolation width – 5.0 m/z

Fragmentation energy – 35%

Activation time – 50 msec

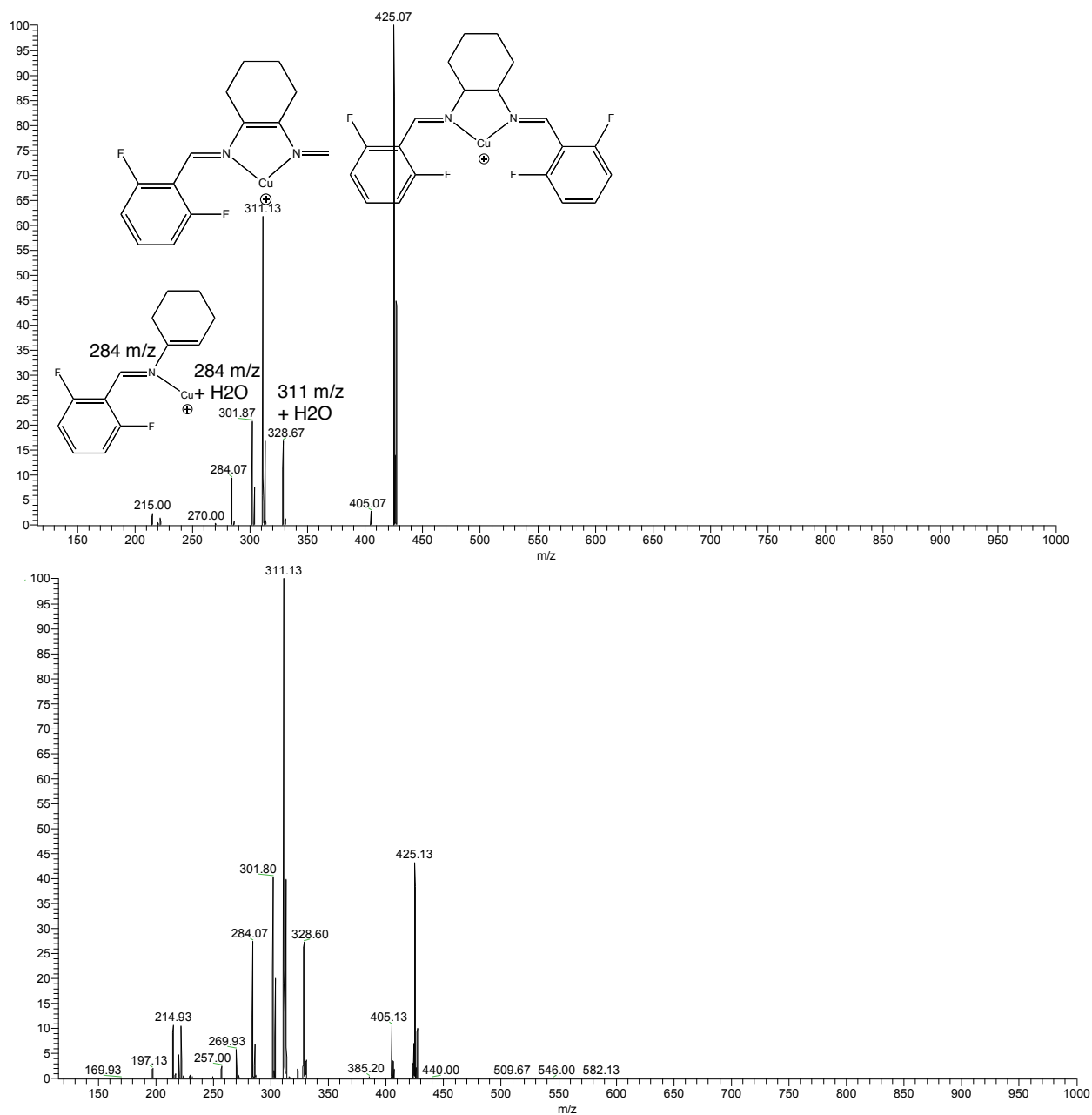


**Figure 147.** Catalyst 3b in mixture of catalysts 3 a, c, & d-g (top) and as single solution (bottom).

Tune file – benzaldehydes 090313.LCQTune  
 Isolate 437.2 m/z (top) and 439.2 m/z (bottom)  
 Isolation width 5.0 m/z (top) and 1.3 m/z (bottom)  
 Fragmentation energy – 45%  
 Activation time – 50 msec

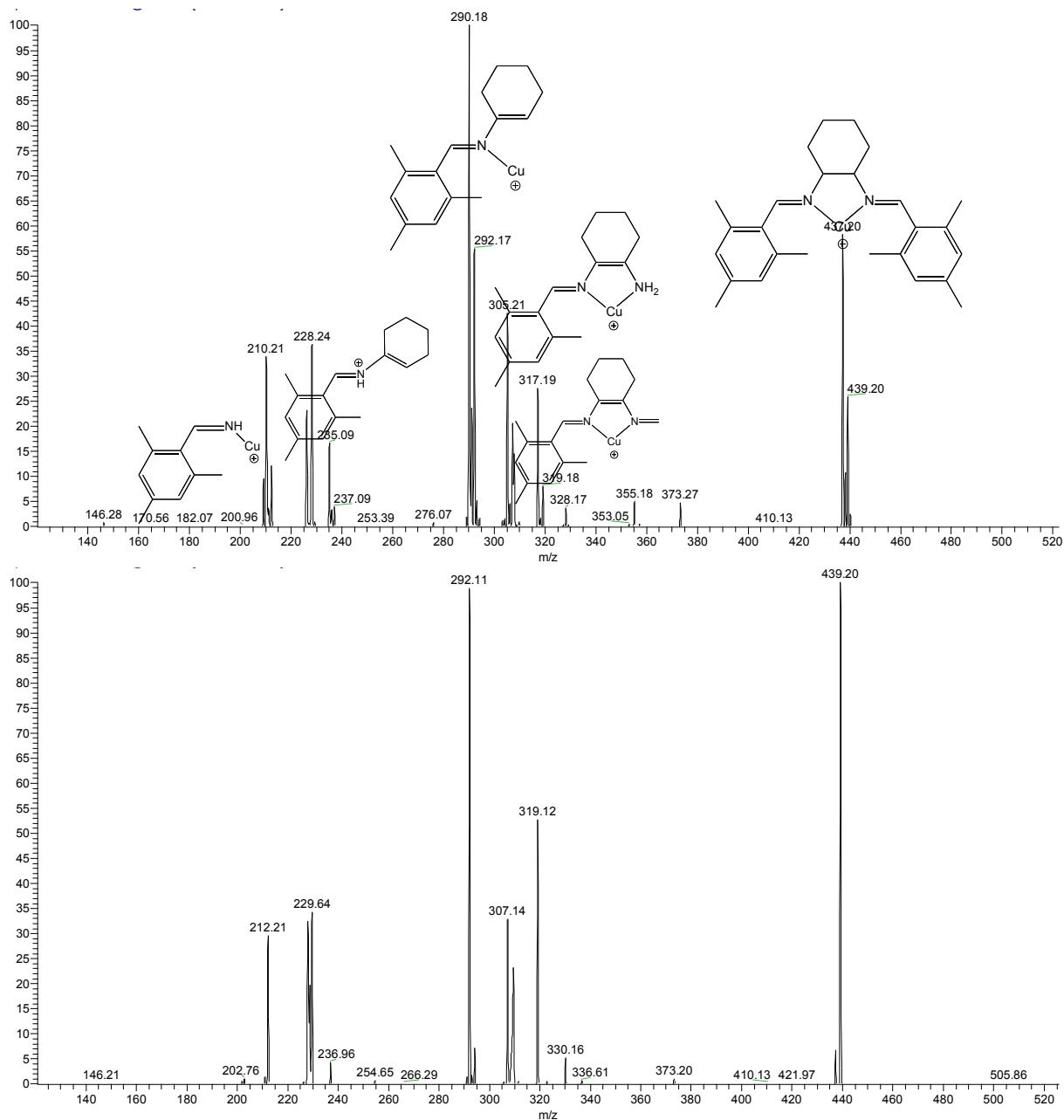


**Figure 148.** Catalyst 3c in mixture of catalysts 3 a, b, & d-g (top) and as single solution (bottom).

Tune file – benzaldehydes 090313.LCQTune

Isolate 577.4 m/z (top)

Isolation width 5.0 m/z (top)

Fragmentation energy – 40%

Activation time – 50 msec

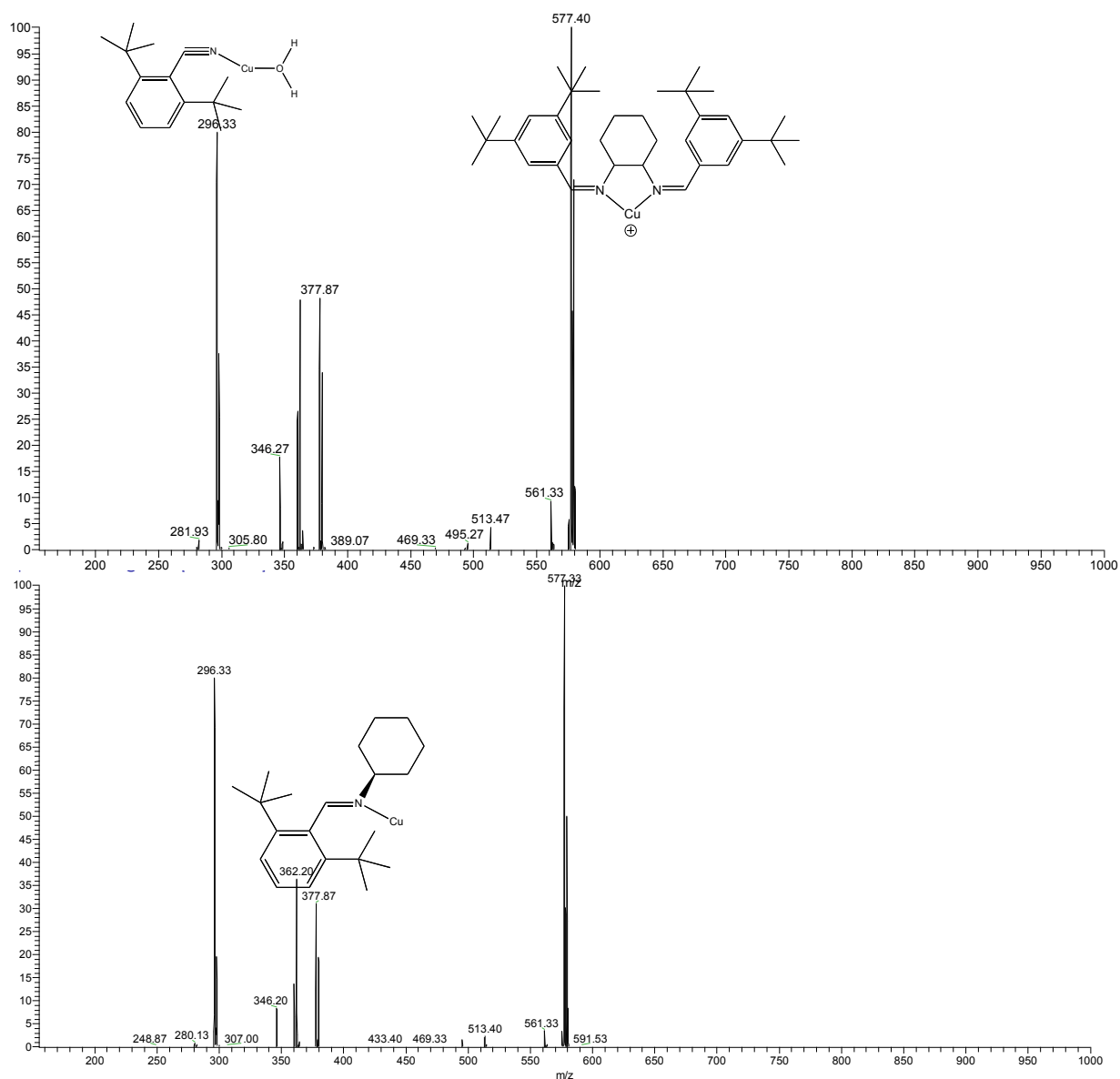


**Figure 149.** Catalyst 3d in mixture of catalysts 3 a – c, and e-g (top) and as single solution (bottom).

Tune file – benzaldehydes 090313.LCQTune  
 Isolate 491.0 m/z (top), weak signal (bottom)  
 Isolation width 5.0 m/z (top)  
 Fragmentation energy – 40%  
 Activation time – 50 msec

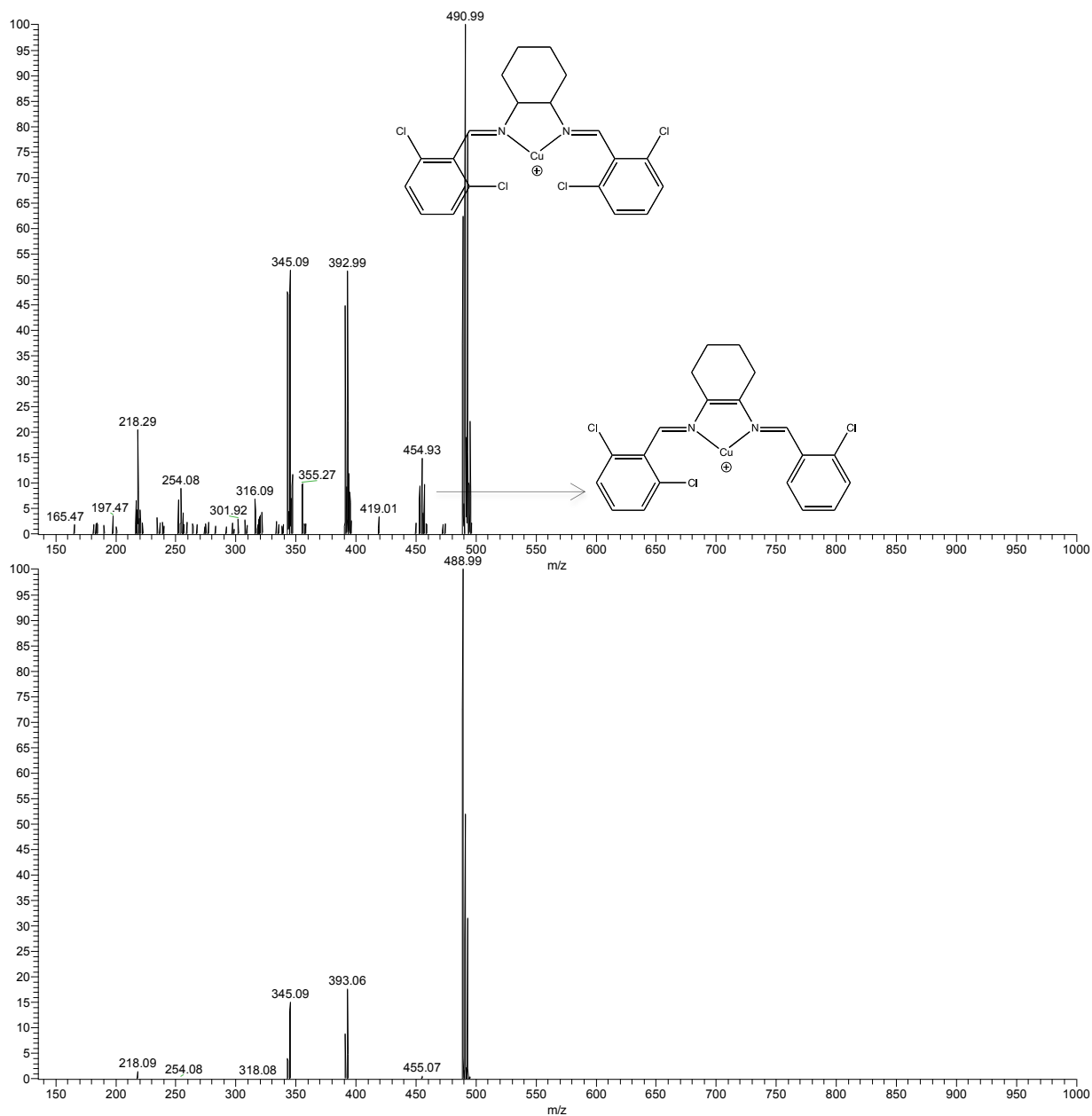


**Figure 150.** Catalyst 3e in mixture of catalysts 3 a – d, f, and g (top) and as single solution (bottom).

Tune file – benzaldehydes 090313.LCQTune  
 Isolate 473.2 m/z (top)  
 Isolation width 5.0 m/z (top)  
 Fragmentation energy – 35%  
 Activation time – 50 msec

Tune file – benzaldehydes 090313.LCQTune

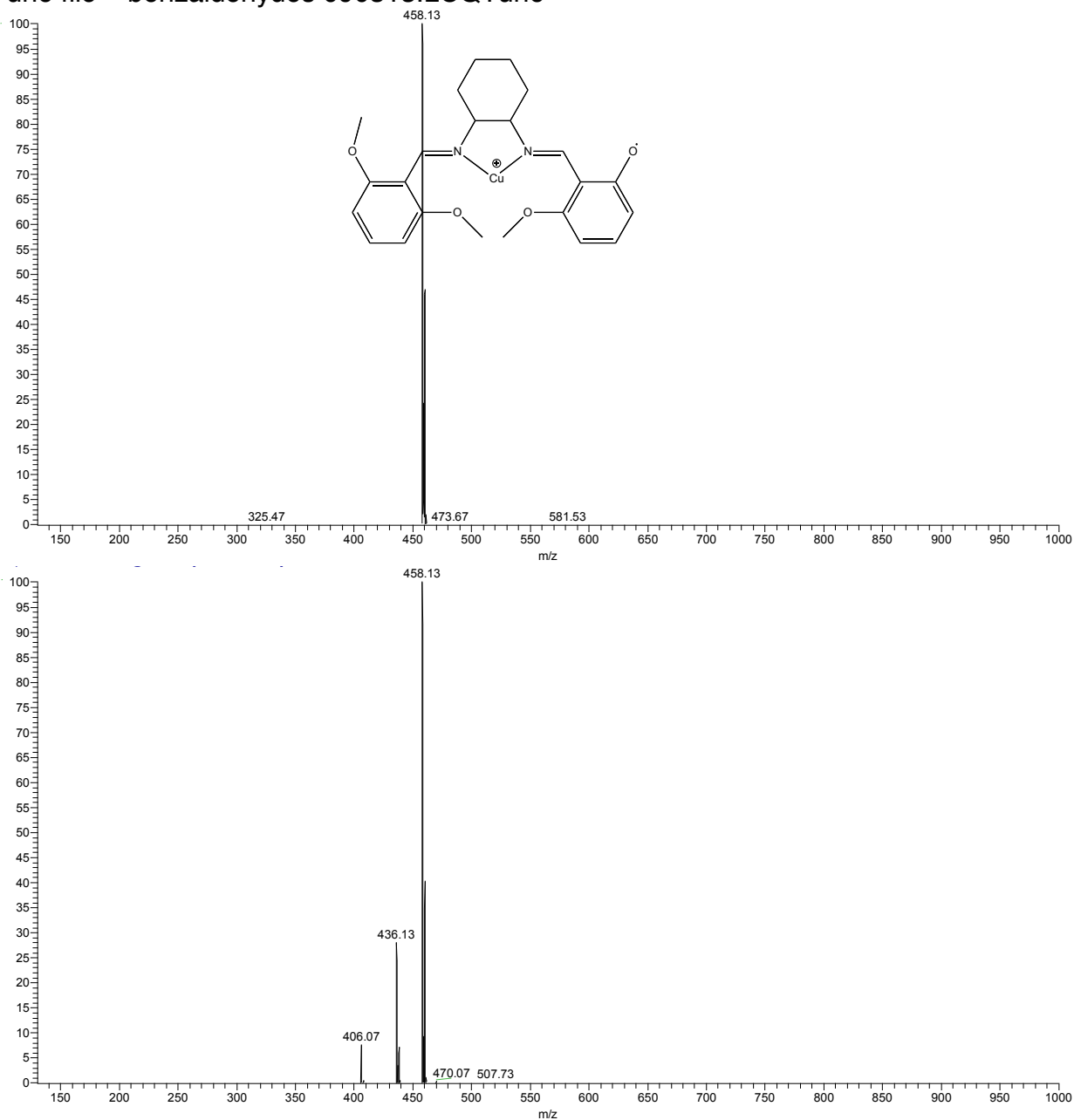


**Figure 151.** Catalyst 3f in mixture of catalysts 3a – e, and g (top) and as single solution (bottom).

Isolate 546.9 m/z (top)  
 Isolation width 5.0 m/z (top)  
 Fragmentation energy – 35%  
 Activation time – 50 msec

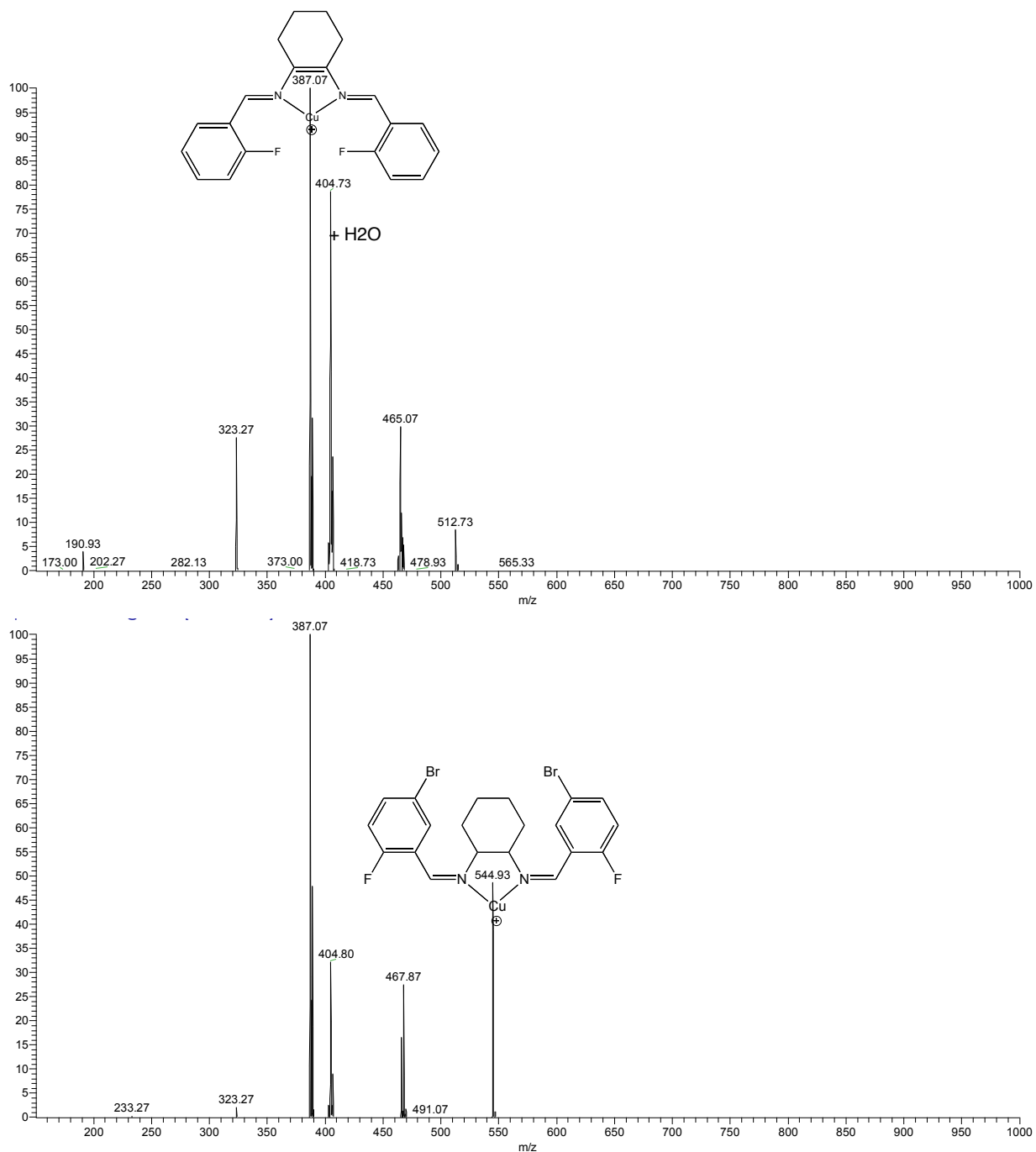


**Figure 152.** Catalyst 3g in mixture of catalysts 3 a – f (top) and as single solution (bottom).

## 8.2 – BINAM-based Di-imines

Mass Spectrometer tune conditions for BINAM-based di-imines

Tune file: BINAM Benz.LCQTune

Infusion rate – 1  $\mu\text{l}/\text{min}$

Positive Ion Mode

Source type – ESI

Spray Voltage (kV) – 4.5

Spray current ( $\mu\text{A}$ ) – 0.1

Capillary heat ( $^{\circ}\text{C}$ ) – 160

Probe position – 1

Sheath flow (arb) – 10

Capillary (V) – 37

Octapole 1 offset (V) – -4.5

Octapole 2 offset (V) – -8.5

Tube lens offset (V) – 55

Trap offset (V) – -10

Multiplier – -1310

$\mu\text{scan}$  – 10

AGC – Off

Ion Gauge –  $2.69 \times 10^{-5}$  torr

Tune file – BINAM Benz  
 Isolate 525.2 m/z (top)  
 Isolation width 1.7 m/z (top)  
 Fragmentation energy – 35%  
 Activation time – 50 msec

## 8.2 – 1,1'-binaphthyl-2,2'-diamine (BINAM)

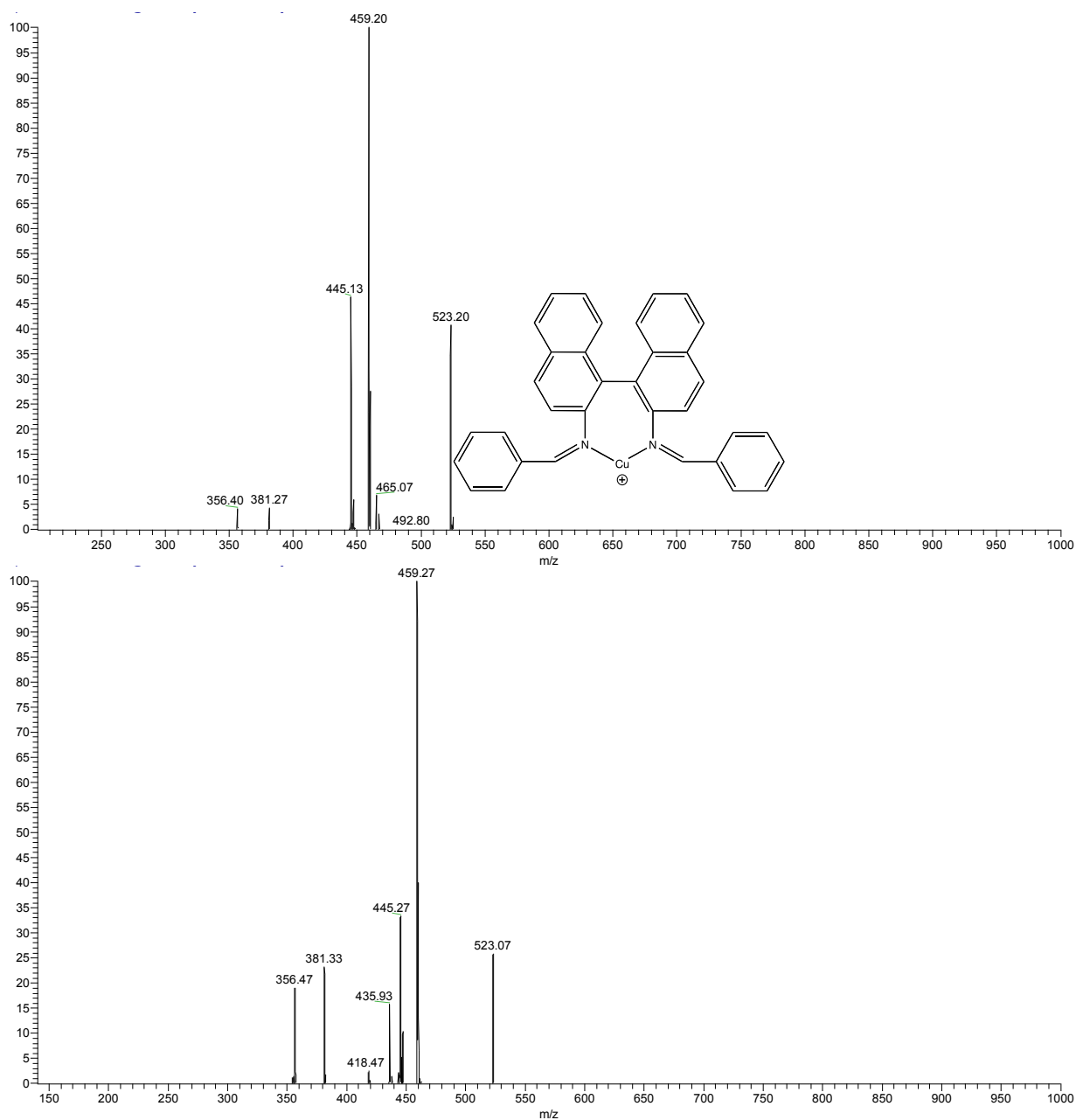


**Figure 153.** Catalyst 5a in a mixture of catalysts 5b-d (top) and single solution (bottom).



Tune file – BINAM Benz  
 Isolate 597.1 m/z (top)  
 Isolation width 1.5 m/z (top)  
 Fragmentation energy – 35%  
 Activation time – 50 msec

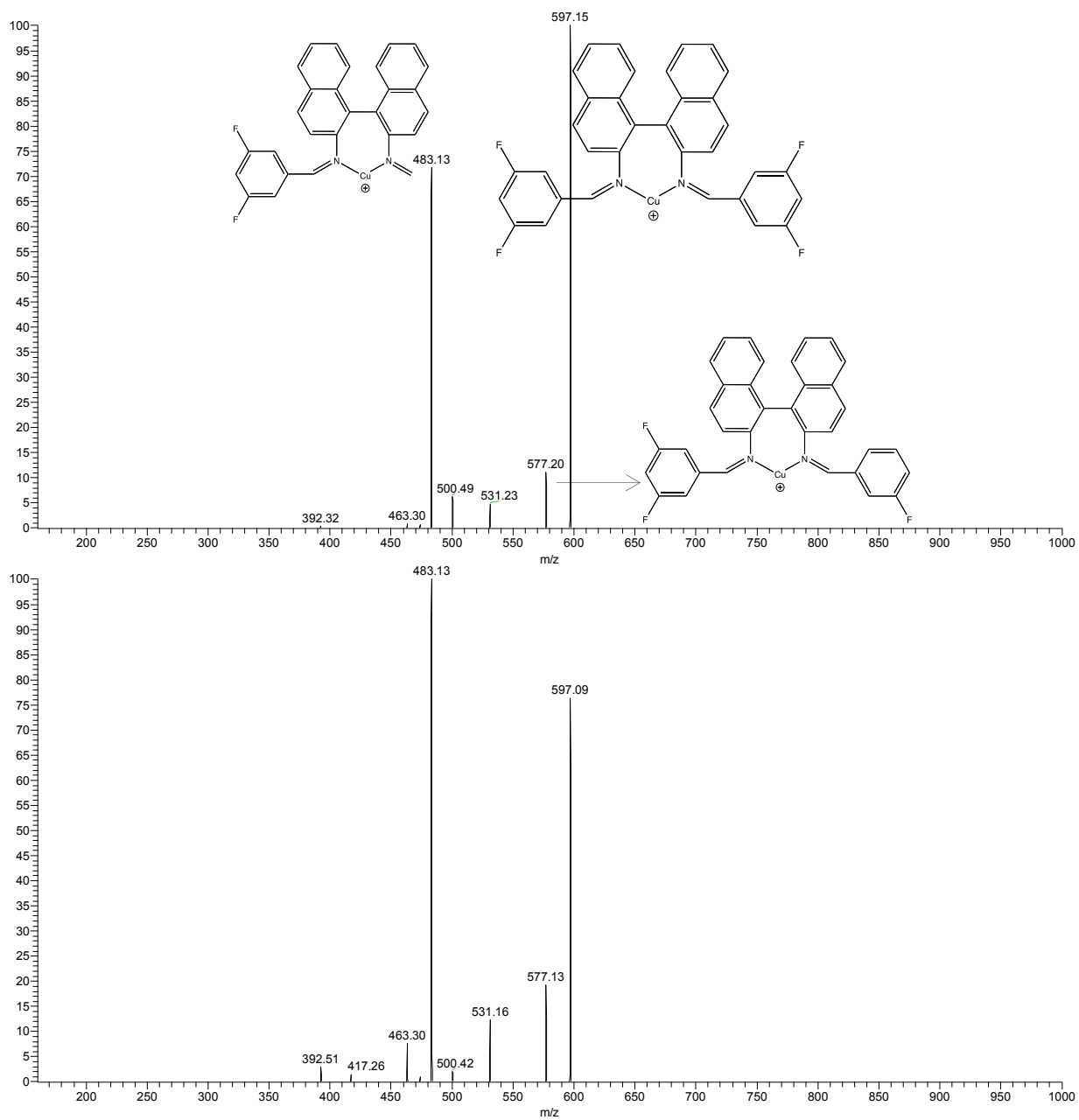


**Figure 154.** Catalyst 5b in a mixture of catalysts 5a, c, and d (top) and single solution (bottom).

Tune file – BINAM Benz  
 Isolate 609.2 m/z (top)  
 Isolation width 1.5 m/z (top)  
 Fragmentation energy – 35%  
 Activation time – 50 msec

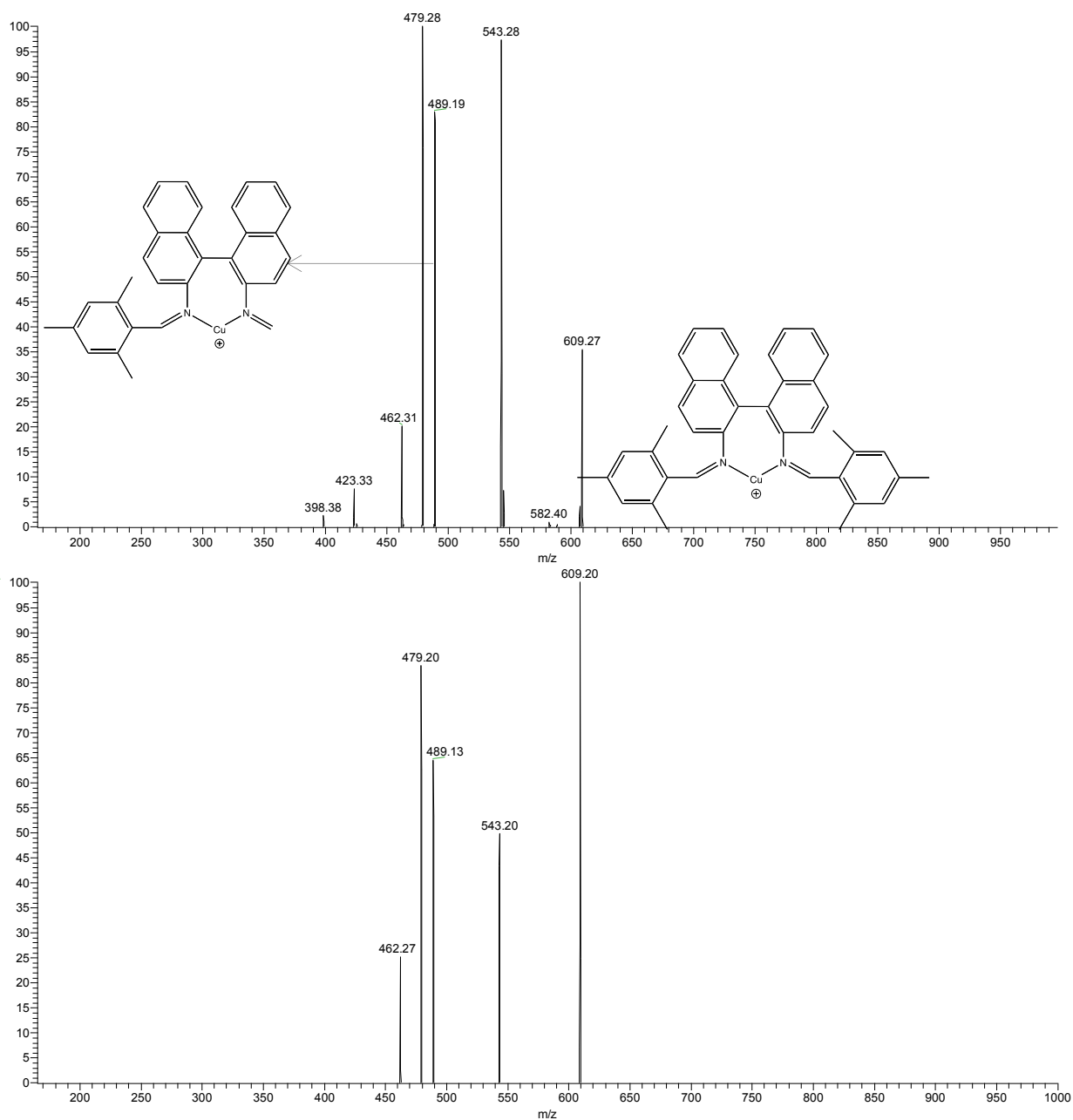


**Figure 155.** Catalyst 5c in a mixture of catalysts 5a, b, and d (top) and single solution (bottom).

Tune file – BINAM Benz  
Isolate 747.3 m/z (top)  
Isolation width 1.5 m/z (top)  
Fragmentation energy – 35%  
Activation time – 50 msec

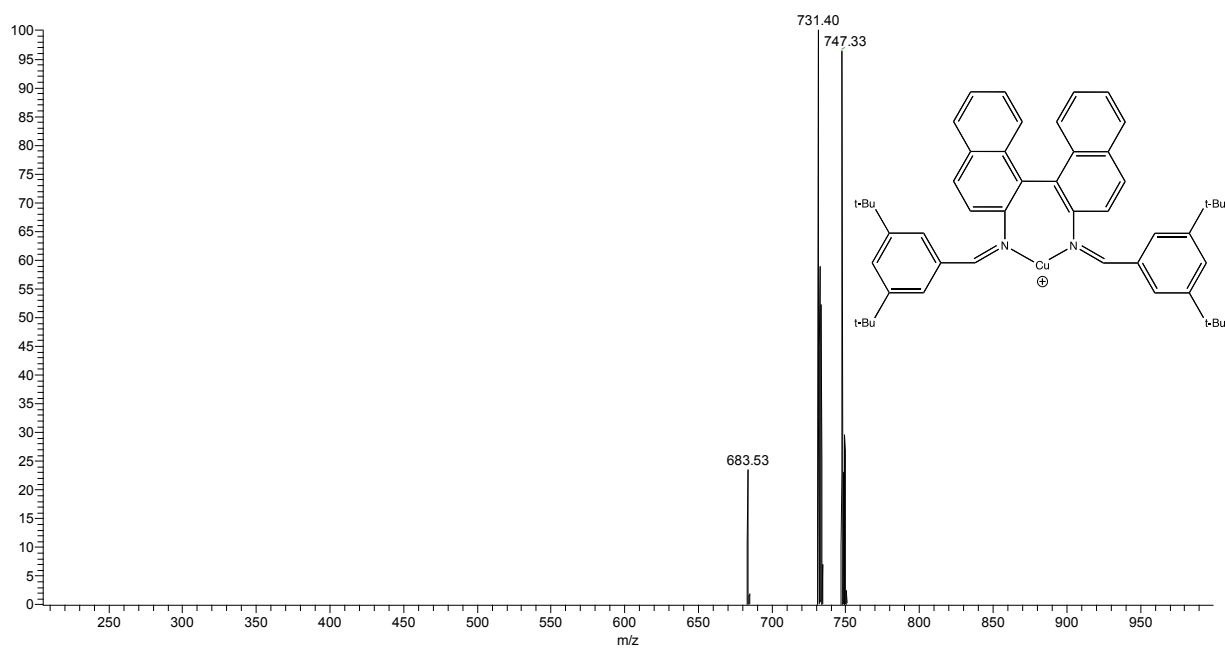


**Figure 156.** Catalyst 3d in mixture of catalysts a-c. No spectra was recorded for the single catalyst solution.

### 8.3 – Diphenylethylene-based di-imines

Mass Spectrometer tune conditions for Diphenyl-based di-imines

Tune file: BINAM Benz.LCQTune

Infusion rate – 1  $\mu\text{l}/\text{min}$

Positive Ion Mode

Source type – ESI

Spray Voltage (kV) – 5

Spray current ( $\mu\text{A}$ ) – 0.1

Capillary heat ( $^{\circ}\text{C}$ ) – 165

Probe position – 1

Sheath flow (arb) – 10

Capillary (V) – 60

Octapole 1 offset (V) – -5.0

Octapole 2 offset (V) – -8.0

Tube lens offset (V) – 25

Trap offset (V) – -10

Multiplier – -1310

$\mu\text{scan}$  – 10

AGC – Off

Ion Gauge –  $2.69 \times 10^{-5}$  torr

## 8.4 – Bis-Oxazolines

Mass Spectrometer tune conditions for Bisoxazolines

Tune file: BINAM Benz.LCQTune

Infusion rate – 1  $\mu\text{l}/\text{min}$   
Positive Ion Mode  
Source type – ESI  
Spray Voltage (kV) – 3.5  
Spray current ( $\mu\text{A}$ ) – 0.1  
Capillary heat ( $^{\circ}\text{C}$ ) – 150  
Probe position – 1  
Sheath flow (arb) – 10  
Capillary (V) – 50  
Octapole 1 offset (V) – -6.5  
Octapole 2 offset (V) – -9.5  
Tube lens offset (V) – 55  
Trap offset (V) – -10  
Multiplier – -1310  
 $\mu\text{scan}$  – 10  
AGC – Off  
Ion Gauge –  $2.69 \times 10^{-5}$  torr

## 8.5 – NMR

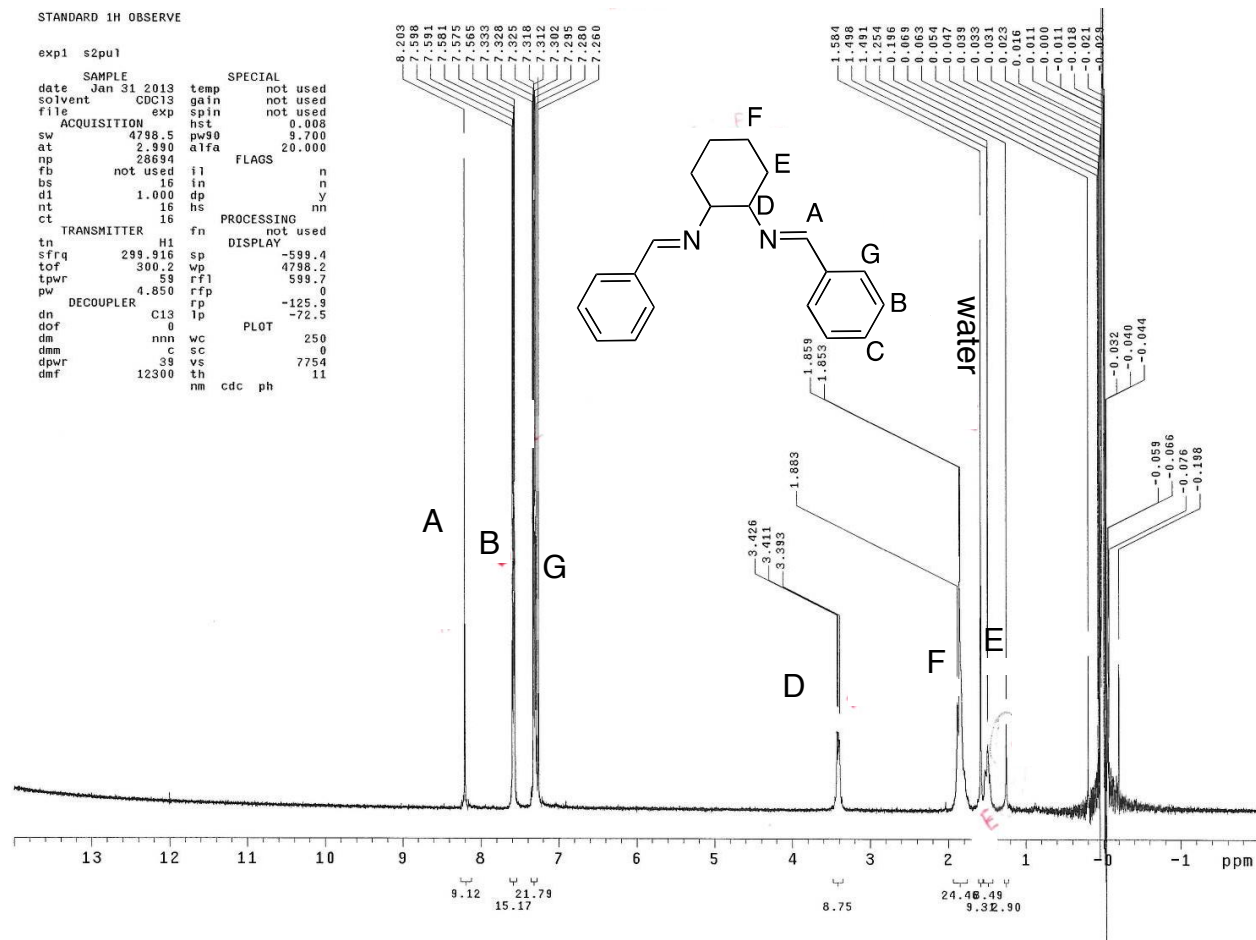
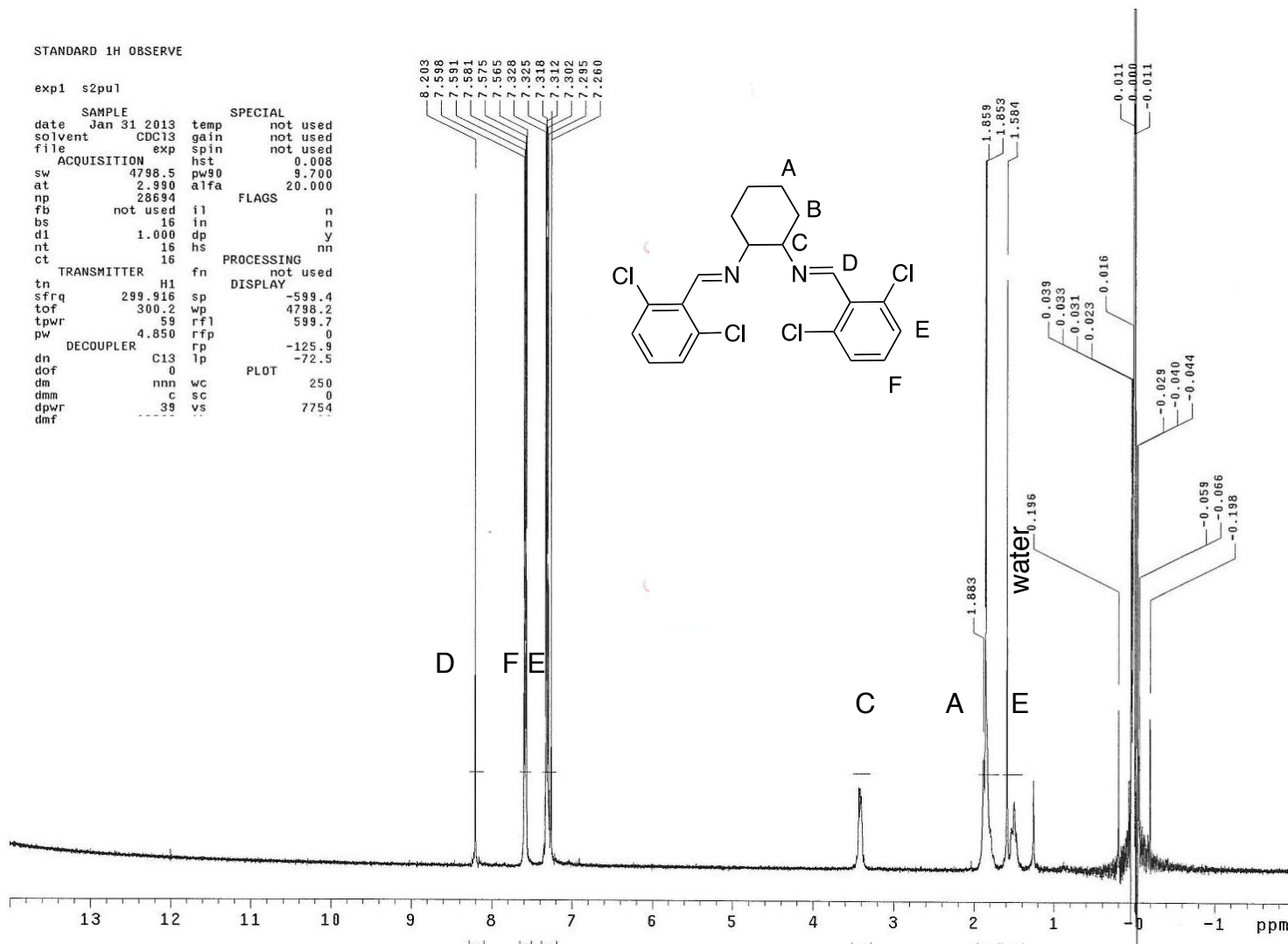


Figure 157. Proton NMR Catalyst 3a

(1S,2S)-N,N dibenzylidenecyclohexane-1,2-diamine

$^1\text{H}$  NMR (300MHz, CHLOROFORM- $d$ )  $\delta$  = 8.20 (s, 2 H), 7.58 (dd,  $J$  = 2.1, 5.6 Hz, 4 H), 7.31 (dd,  $J$  = 2.1, 4.7 Hz, 6 H), 3.41 (dd,  $J$  = 4.7, 5.9 Hz, 2 H), 1.92 - 1.81 (m, 6 H), 1.50 (d,  $J$  = 10.3 Hz, 2 H)



**Figure 158.** Proton NMR of catalyst 3e.

(1S,2S)-N,N-bis(2,6-dichlorobenzylidene)cyclohexane-1,2-diamine

$^1\text{H}$  NMR (300MHz,  $\text{CHLOROFORM-d}$ )  $\delta$  = 8.46 (s, 2 H), 7.29 (d,  $J$  = 1.2 Hz, 2 H), 7.26 (br. s, 2 H), 7.20 - 7.12 (m, 2 H), 3.74 - 3.51 (m, 2 H), 2.01 - 1.73 (m, 6 H), 1.55 - 1.45 (m, 2 H).

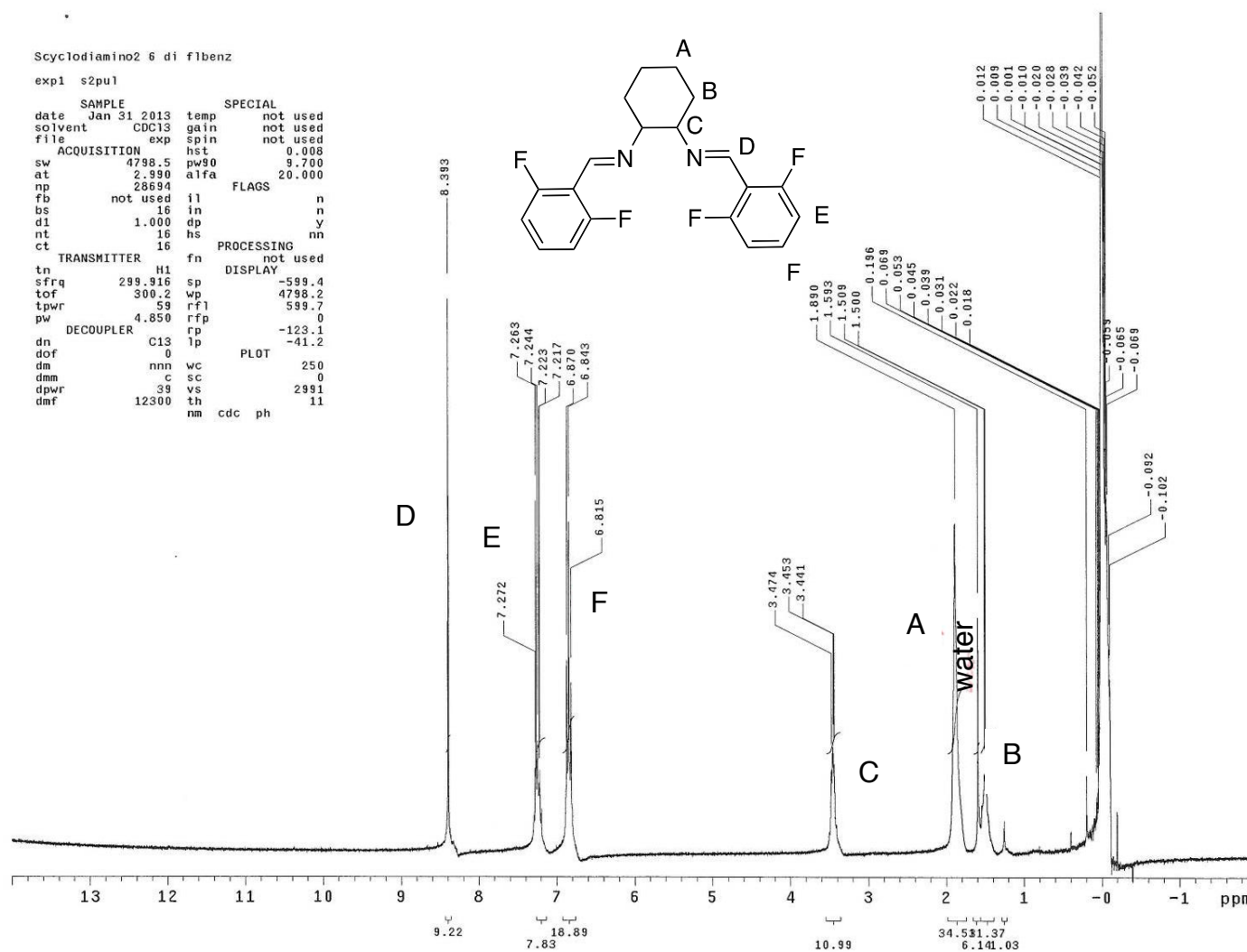


**Figure 159.** Proton NMR of catalyst 3b.

(1S,2S)-N,N-bis(2,6-difluorobenzylidene)cyclohexane-1,2-diamine

$^1\text{H}$  NMR (300MHz, CHLOROFORM- $d$ )  $\delta$  = 8.39 (s, 2 H), 7.33 - 7.14 (m, 3 H), 6.84 (t,  $J$  = 8.2 Hz, 3 H), 3.63 - 3.34 (m, 2 H), 1.89 (br. s., 6 H), 1.50 (br. s., 2 H).



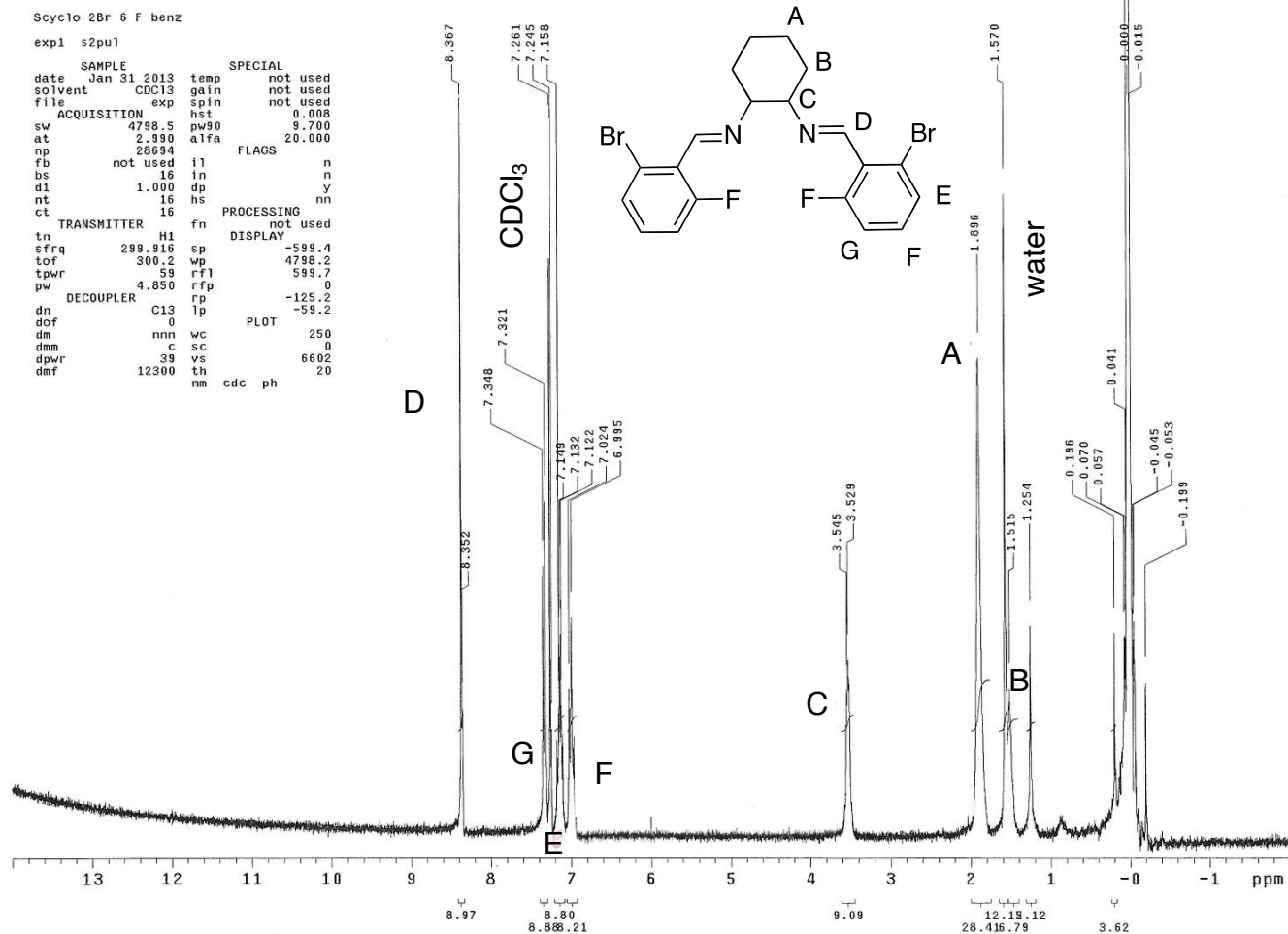


**Figure 160.** Proton NMR catalyst 3g.

(1S,2S)-N,N-bis(2-bromo-6-fluorobenzylidene)cyclohexane-1,2-diamine

$^1\text{H}$  NMR (300MHz,  $\text{CHCl}_3$ -d)  $\delta$  = 8.37 (s, 2 H), 7.33 (d,  $J$  = 7.9 Hz, 2 H), 7.14 (dt,  $J$  = 5.3, 8.1 Hz, 2 H), 7.05 - 6.95 (m, 2 H), 3.59 - 3.48 (m, 2 H), 1.90 (br. s., 6 H), 1.51 (br. s., 1 H), 1.25 (s, 1 H).

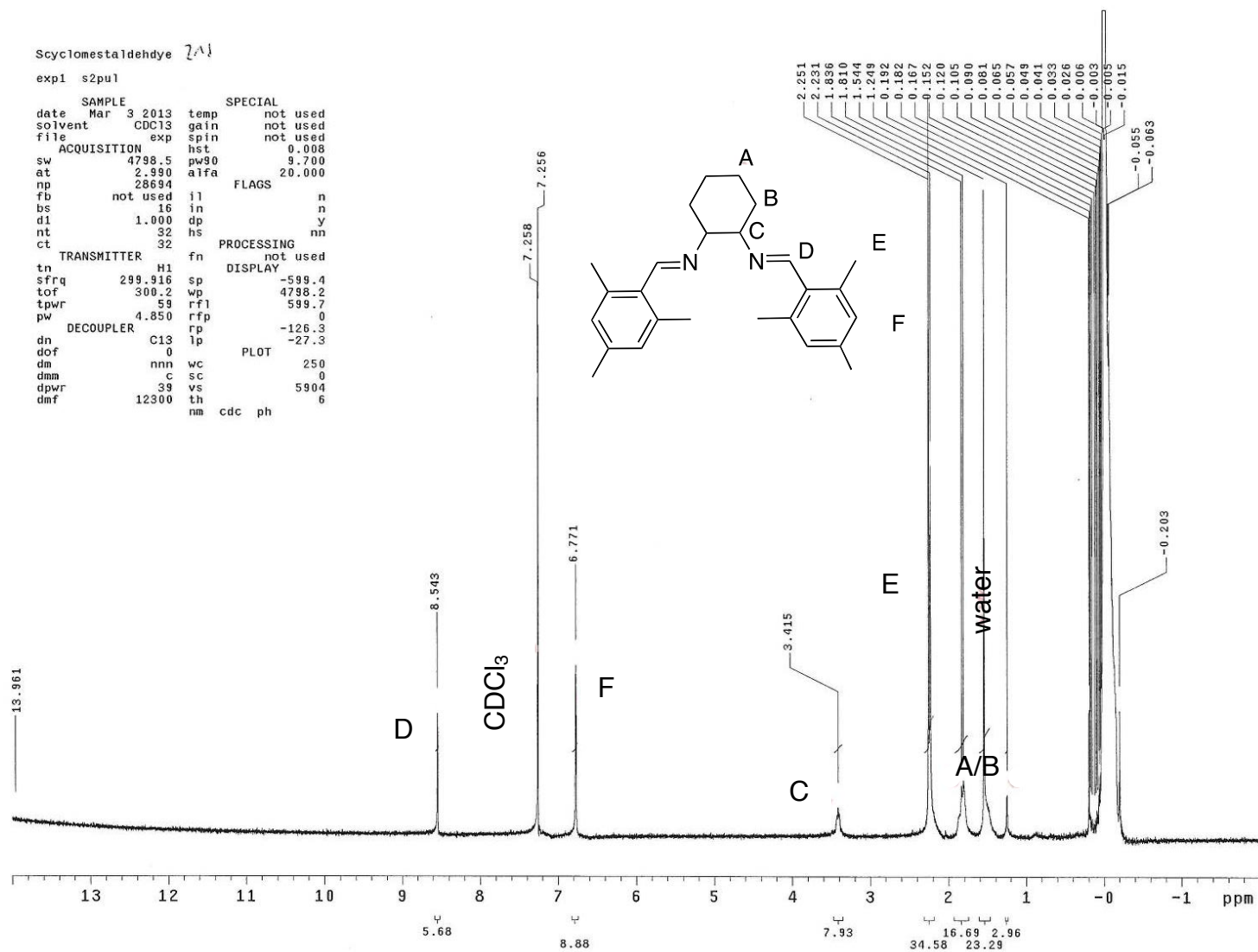


**Figure 161.** Proton NMR catalyst 3c.

(1S,2S)-N,N-bis(2,4,6-trimethylbenzylidene)cyclohexane-1,2-diamine

$^1\text{H}$  NMR (300MHz, CHLOROFORM-d)  $\delta$  = 8.54 (s, 2 H), 6.77 (s, 2 H), 3.49 - 3.37 (m, 2 H), 2.32 - 2.17 (m, 18 H), 1.82 (s, 8 H), 1.25 (s, 2 H).

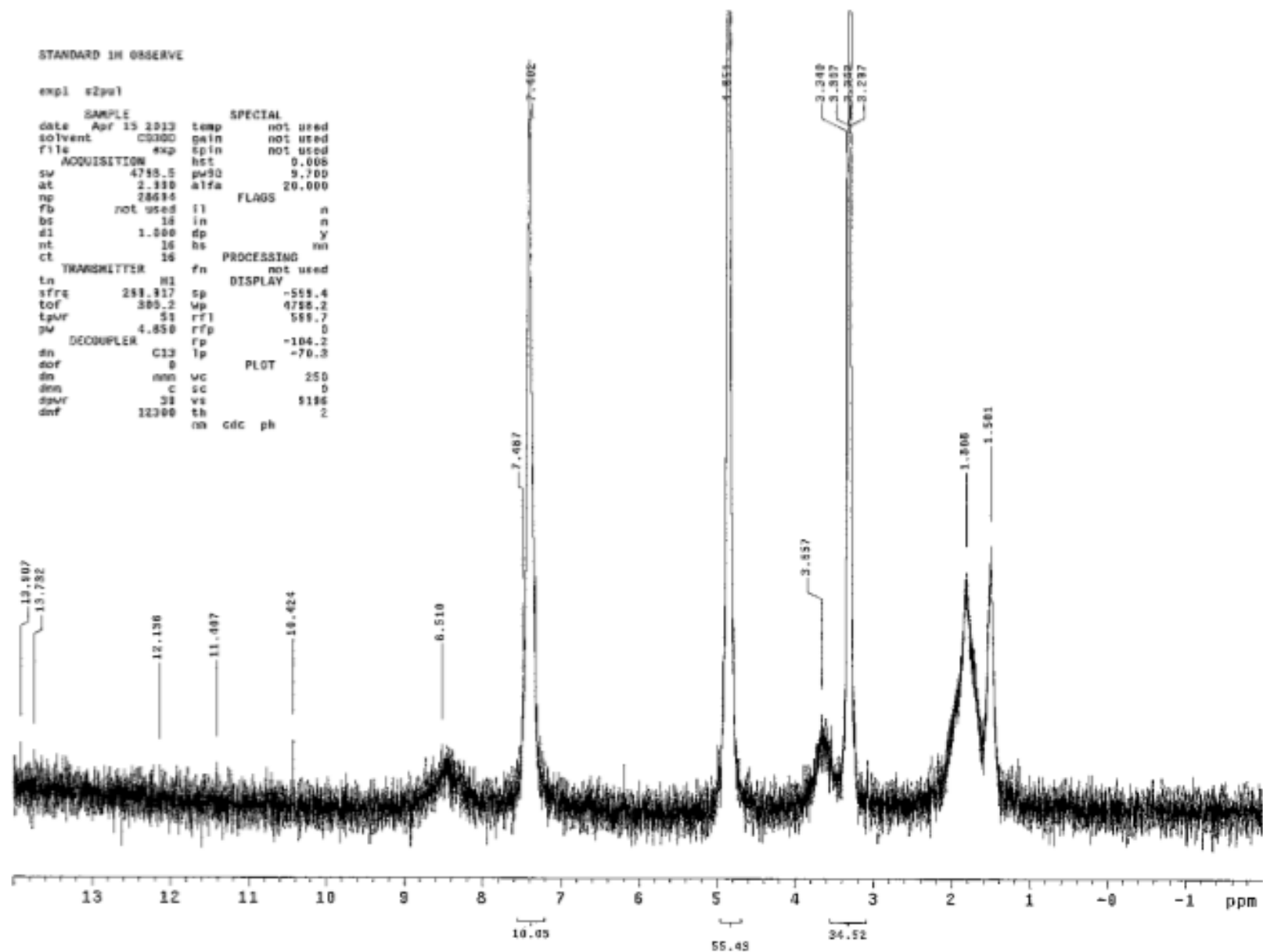


**Figure 162.** Proton NMR of Catalyst 3e with Cu(I) trifluoromethanesulfonate. Indicates oxidation of Cu (I) to Cu(II) which is paramagnetic and hence the lack /broadness of NMR peaks.

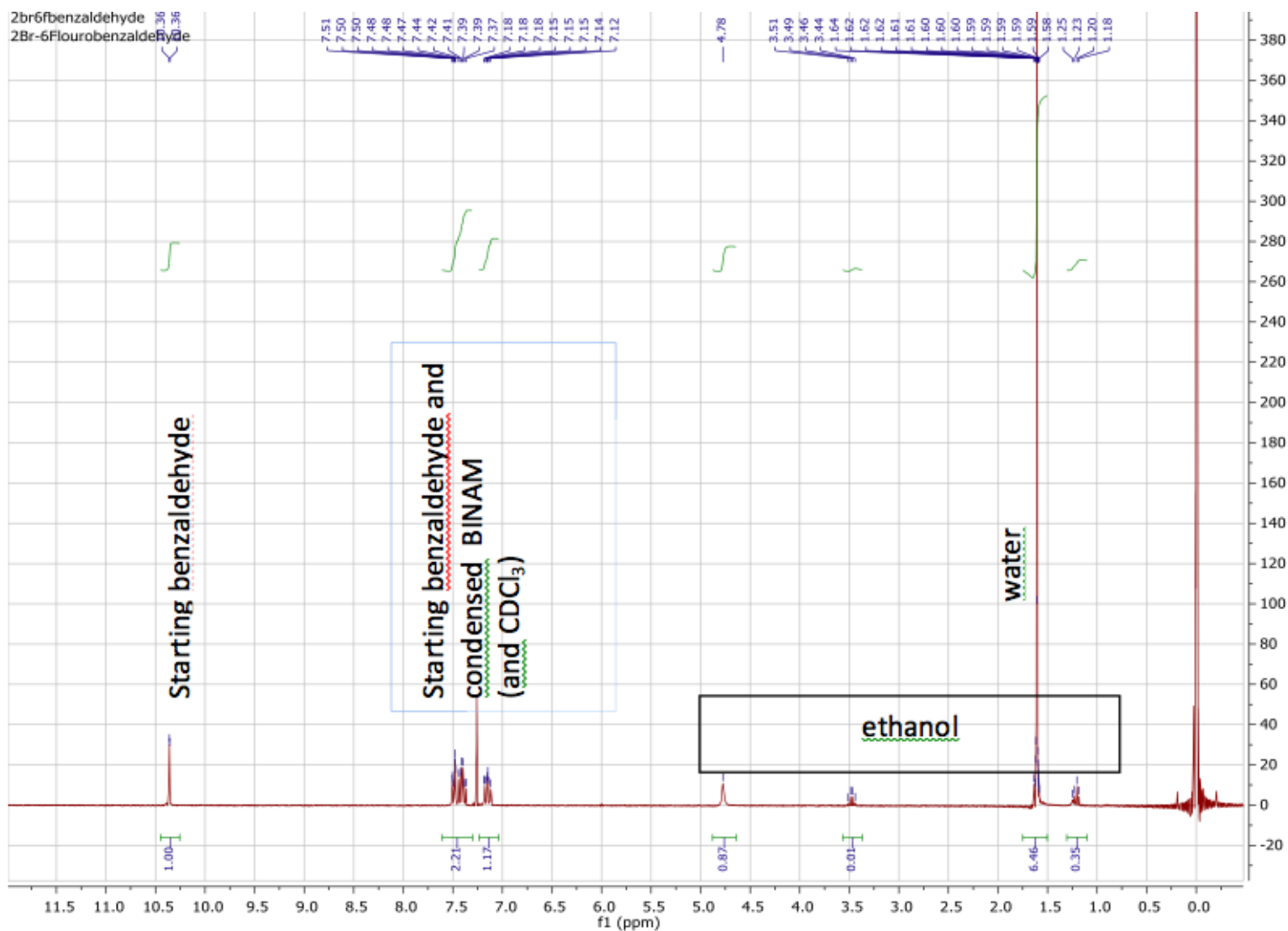


**Figure 163.** Proton NMR of catalyst 5i.

(1S,2S)-N,N-bis(2-bromo-6-fluorobenzylidene)cyclohexane-1,2-diamine

<sup>1</sup>H NMR (300MHz, CHLOROFORM-d)  $\delta$  = 8.37 (s, 2 H), 7.33 (d,  $J$  = 7.9 Hz, 2 H), 7.14 (dt,  $J$  = 5.3, 8.1 Hz, 2 H), 7.05 - 6.95 (m, 2 H), 3.59 - 3.48 (m, 2 H), 1.90 (br. s., 5 H), 1.51 (br. s., 1 H), 1.25 (s, 1 H).

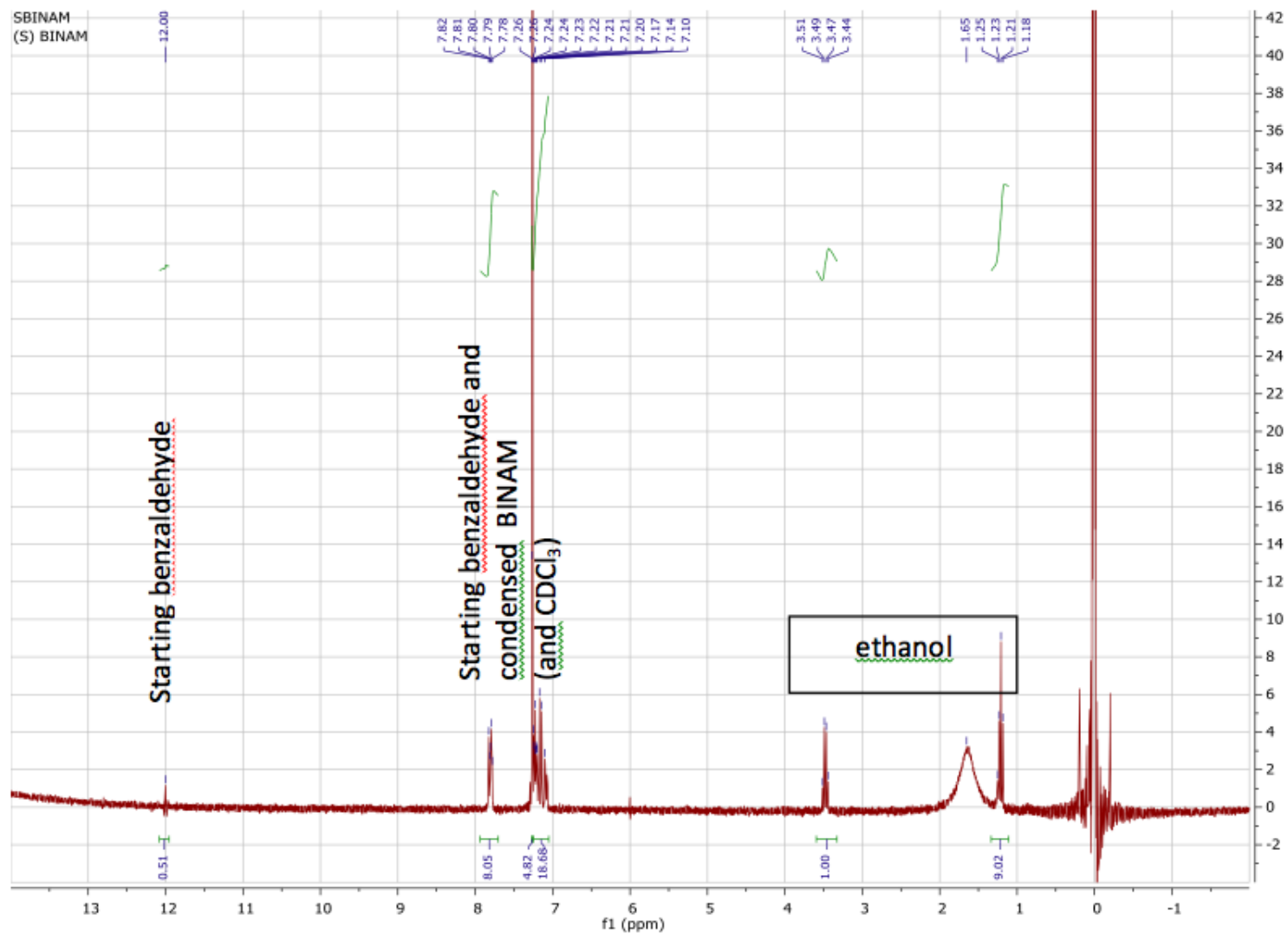


**Figure 164.** Proton NMR of catalyst 5a.

(S)-N2,N2'-dibenzylidene-[1,1'-binaphthalene]-2,2'-diamine

<sup>1</sup>H NMR (300MHz, CHLOROFORM-d) □ = 7.86 - 7.74 (m, 5 H), 7.31 - 7.03 (m, 19 H), 3.48 (q, *J* = 7.0 Hz, 2 H), 1.63 (br. s., 5 H), 1.21 (t, *J* = 7.0 Hz, 3 H).

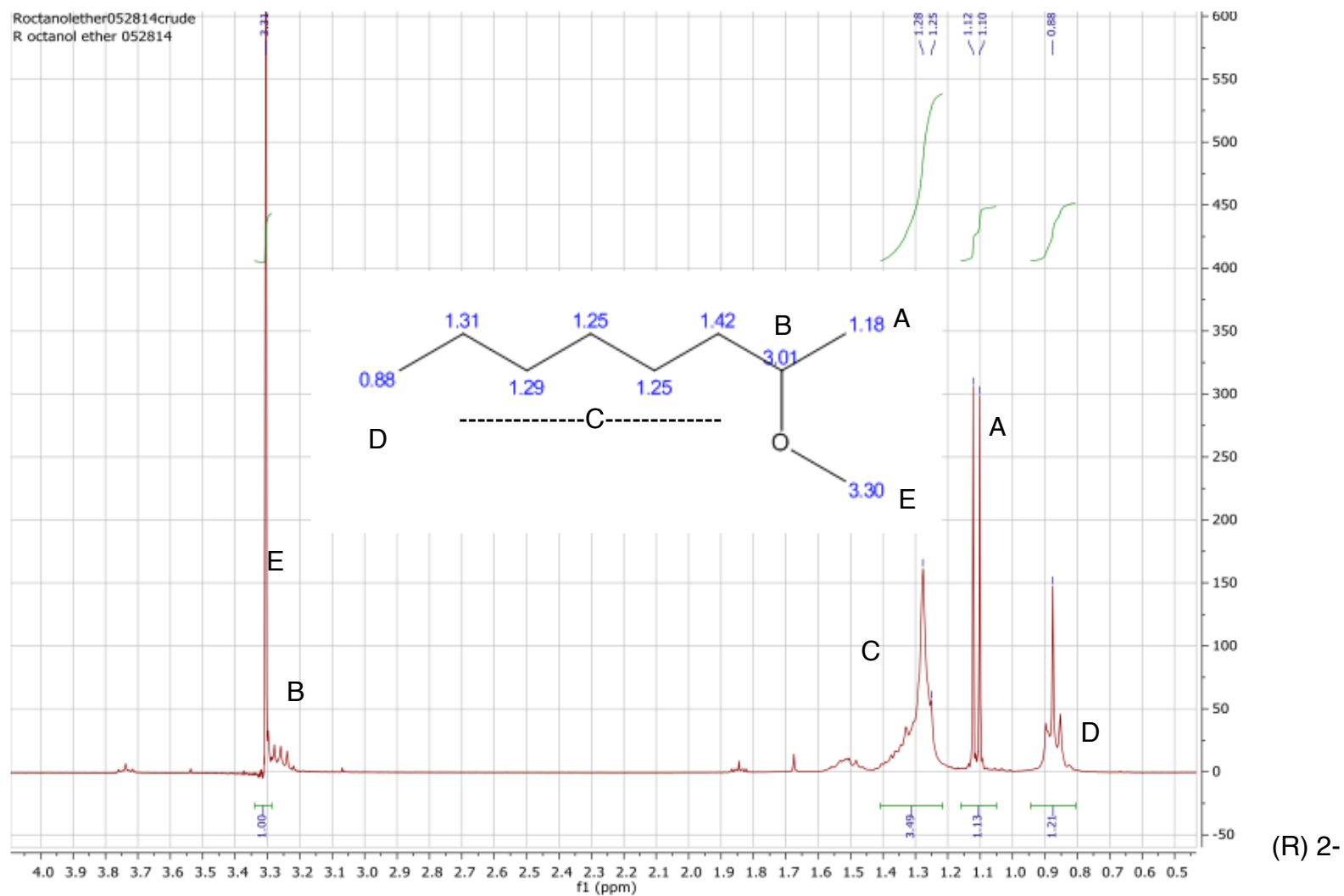
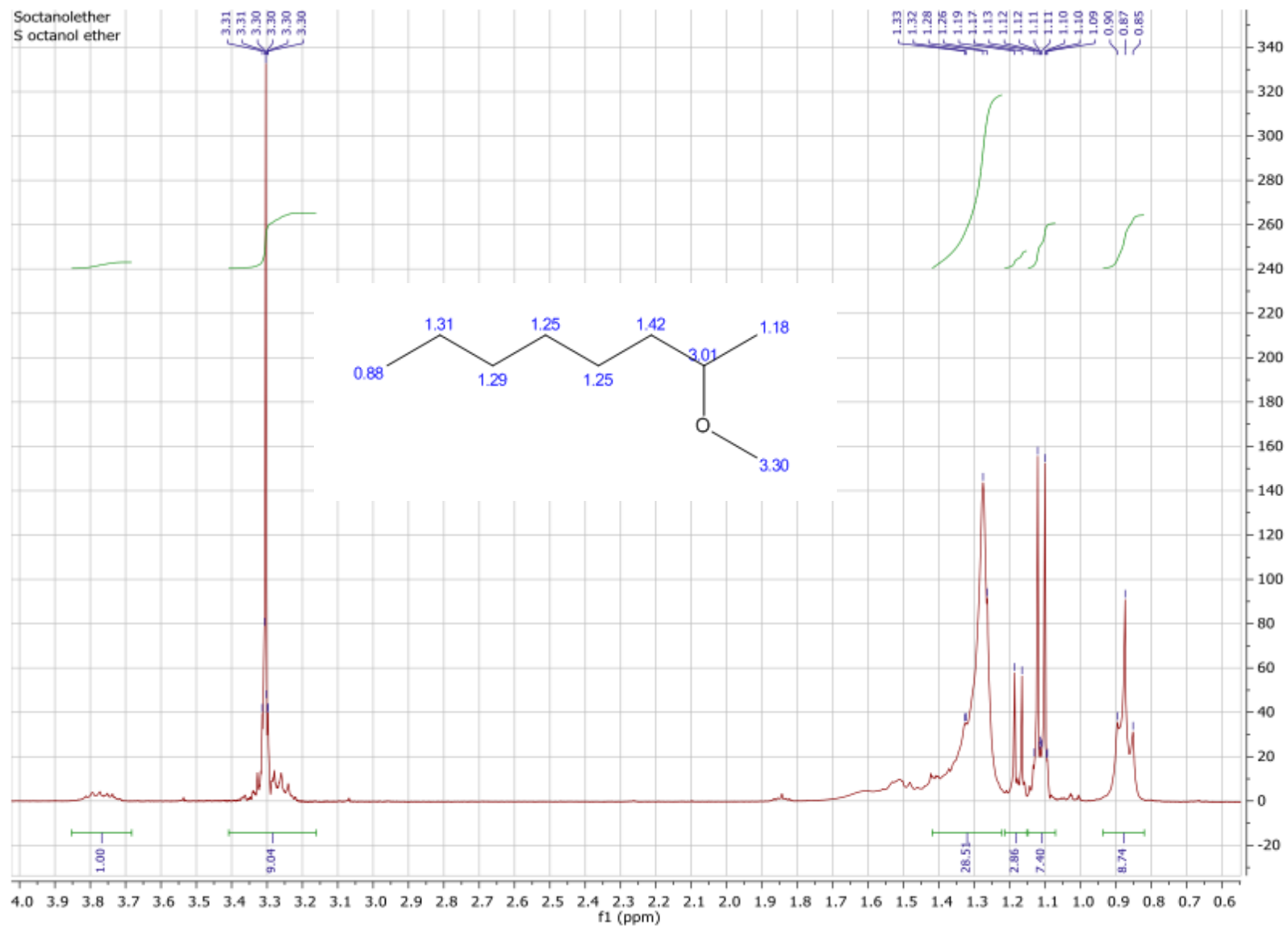


**Figure 165.** Expanded proton NMR of (R) 2-methoxyoctane.

methoxyoctane

<sup>1</sup>H NMR (300 MHz, Chloroform-*d*)  $\delta$  3.35 – 3.16 (m, 4H), 1.43 – 1.22 (m, 10H), 1.15 – 1.08 (m, 3H), 0.86 (q,  $J$  = 8.0, 7.3 Hz, 3H).



(S) 2-

**Figure 166.** Expanded proton NMR of (S) 2-methoxyoctane.

methoxyoctane

$^1\text{H}$  NMR (300 MHz, Chloroform- $d$ )  $\delta$  3.42 – 3.18 (m, 4H), 1.35 – 1.22 (m, 10H), 1.15 – 1.08 (m, 3H), 0.92 – 0.83 (m, 3H).

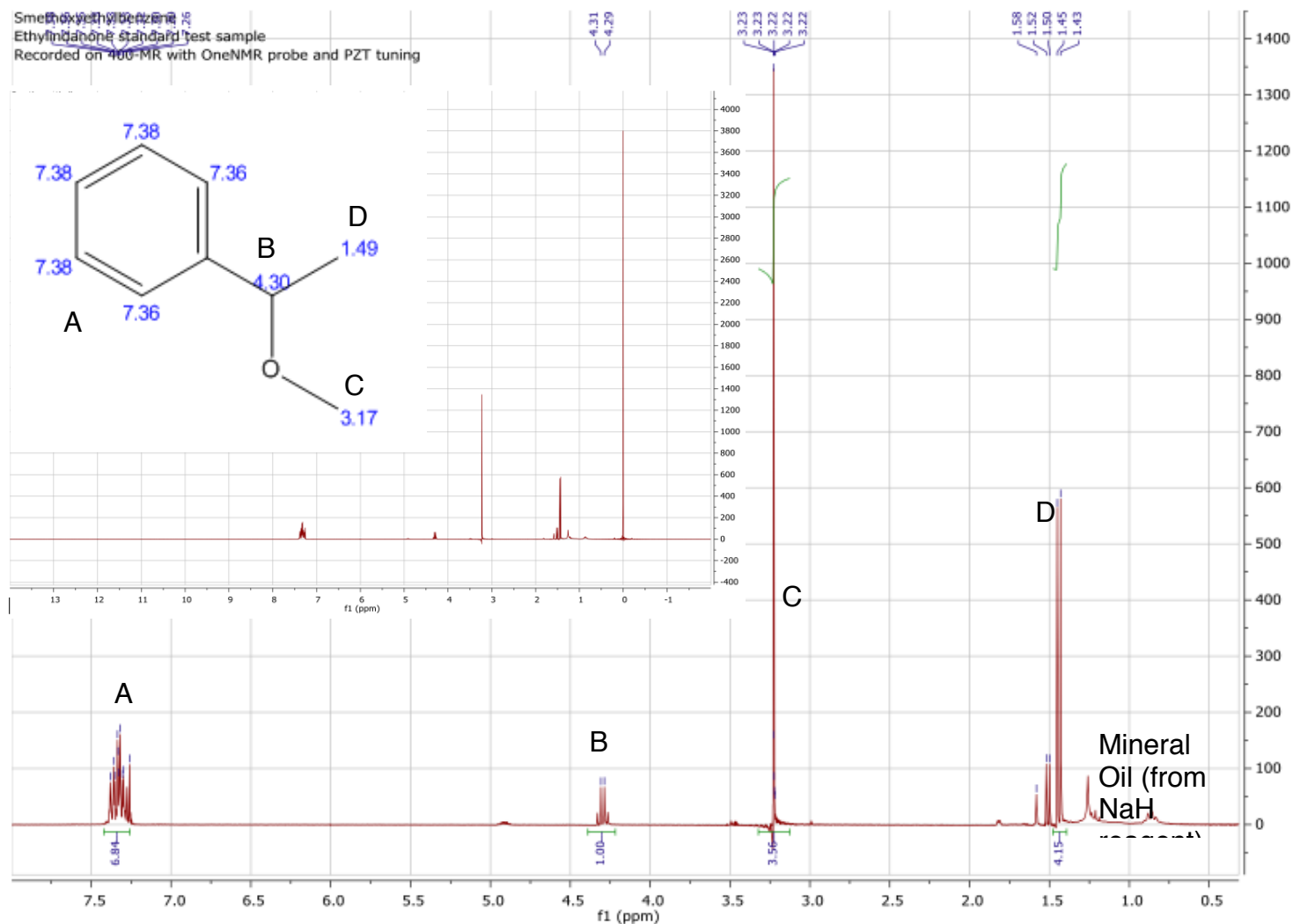


**Figure 167.** Proton NMR of (S)-2-methoxyethylbenzene.

(S) 1-methoxyethylbenzene

$^1\text{H}$  NMR (300 MHz, Chloroform-*d*)  $\delta$  7.38 (t,  $J$  = 1.5 Hz, 1H), 7.36 (q,  $J$  = 1.2 Hz, 1H), 7.34 – 7.31 (m, 2H), 7.30 (q,  $J$  = 1.5 Hz, 1H), 4.30 (q,  $J$  = 6.5 Hz, 1H), 3.27 – 3.19 (m, 3H), 1.46 – 1.41 (m, 3H).



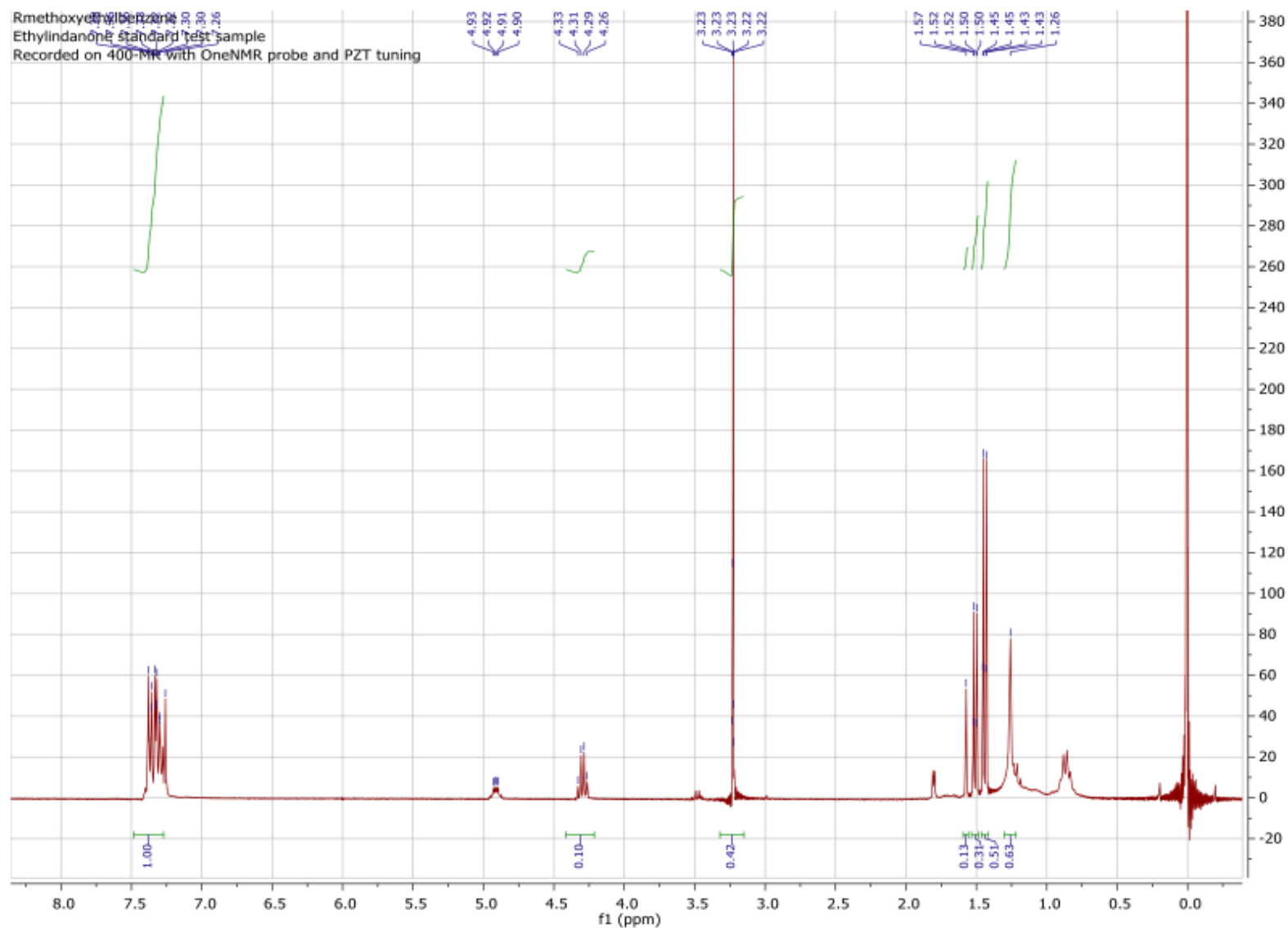


**Figure 168.** Expanded proton NMR (R)-2-methoxyethylbenzene.

(R) 1-methoxyethylbenzene

$^1\text{H}$  NMR (300 MHz, Chloroform- $d$ )  $\delta$  7.38 (d,  $J$  = 1.3 Hz, 1H), 7.37 – 7.35 (m, 1H), 7.35 – 7.32 (m, 2H), 7.30 (p,  $J$  = 2.1 Hz, 1H), 4.30 (q,  $J$  = 6.5 Hz, 1H), 3.28 – 3.19 (m, 3H), 1.47 – 1.40 (m, 3H).

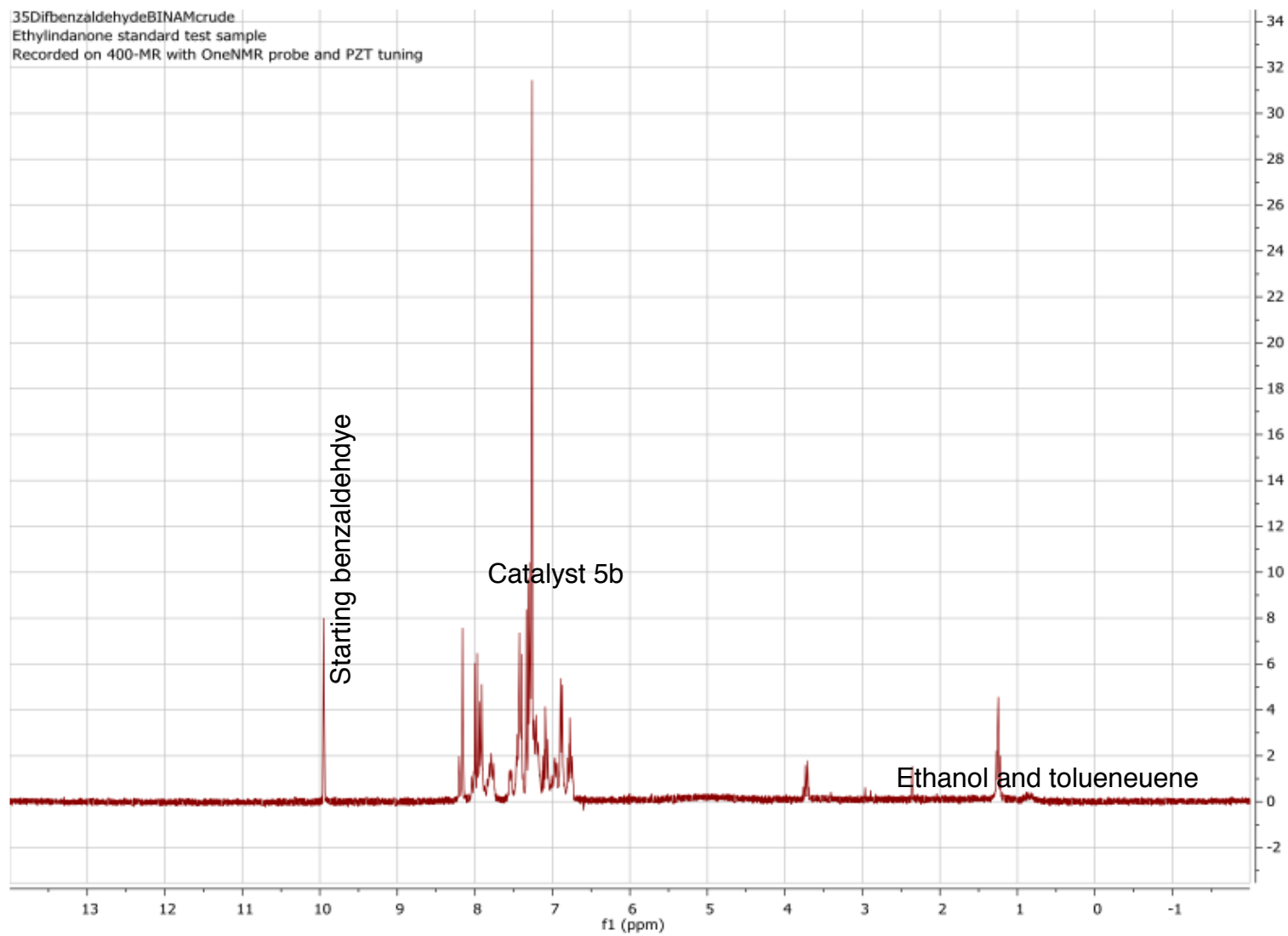


**Figure 169.** Proton NMR of catalyst 5b.

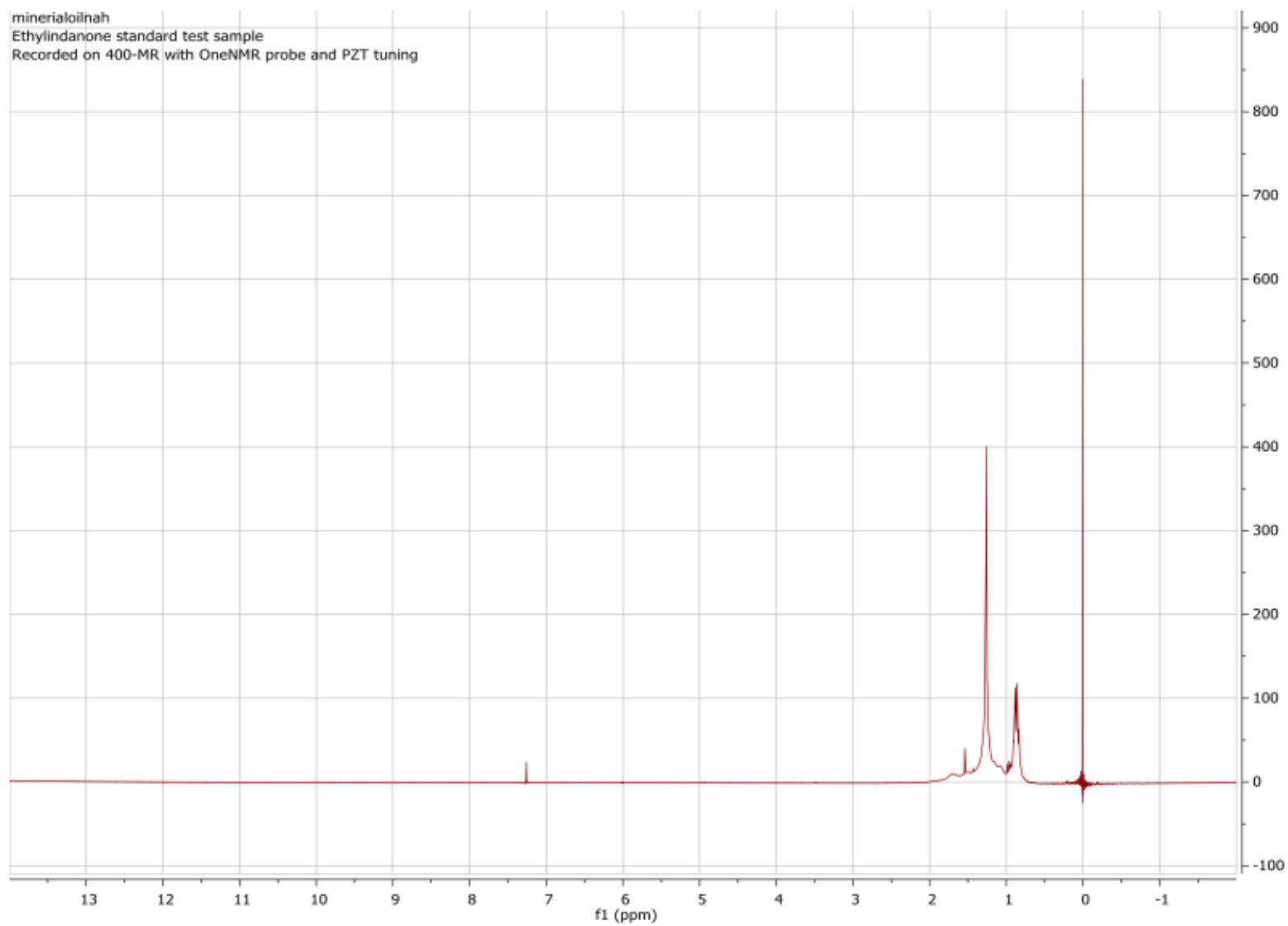


**Figure 170.** Extracted mineral oil from NaH.

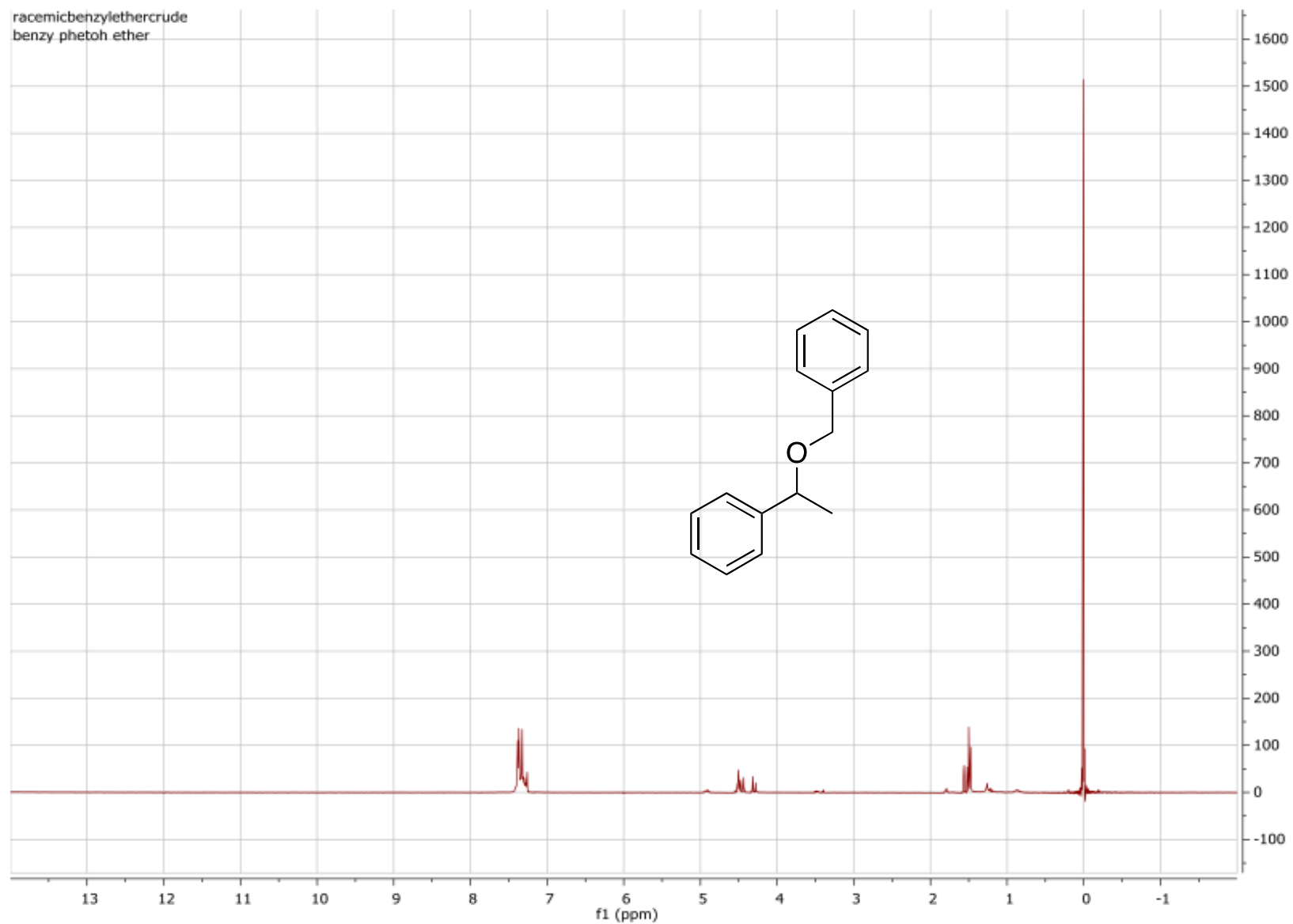


**Figure 171.** Proton NMR of racemic [1-(Benzyloxy)ethyl]benzene (too big to coordinate).

## 8.6 – Synthesis of catalysts

### 8.6.1 – *Meso*-1,2-diphenylethylenediamine

General procedure: weigh diamine into a 25 or 50 mL round bottom flask (RBF) and add solvent. Add benzaldehyde, stir and heat to reflux. Material was crystallized and/or recrystallized, washed with cold methanol, and dried in an oven at 105 °C overnight.

#### DiPhenyl Benzaldehyde (catalyst 4a)

Add 100.63 mg *meso*-1,2-diphenylethylenediamine, 10 mL ethanol (anhydrous 200 proof), 125  $\mu$ L benzaldehyde, and 10 mL toluene to a 50 mL RBF. Reflux for 1 hour. Distill until approximately 10 mL is left and let crystallize. Cool in ice bath, filter, wash with 10 mL cold methanol and dry in oven at 105 °C overnight. Yield 80%.

#### Mesitaldehyde diphenyl (catalyst 4c)

Add 100.6 mg of *meso*-1,2-diphenylethylenediamine, 4.5 mL of toluene, 5.5 mL ethanol (anhydrous, 200 proof), and 140  $\mu$ L mesitaldehyde to a 50 mL RBF. Reflux for 1 hour. Distill until approximately 5 mL left. Allow to crystallize. Filter and wash with cold methanol. Recrystallize in 5.5 mL toluene. Filter and wash with 10 mL cold methanol. Dry in oven at 105 °C overnight. Yield 51%.

#### 2,6-DiCl diphenyl (catalyst 4e)

Add 100 mg *meso*-1,2-diphenylethylenediamine, 175 mg of 2,6-dichlorobenzaldehyde, 5 mL toluene, 5 mL anhydrous ethanol (200 proof), into 25 mL RBF. Reflux for 1hr,

filter and recrystallize in 10 mL of anhydrous ethanol and 5 mL of toluene. Filter, wash with 10 mL cold methanol, and dry at 105 °C overnight. Yield 74%.

#### 3,5-di-*tert*-butyl benzaldehyde (catalyst 4d)

Add 104.32 mg of *meso*-1,2-diphenylethylenediamine, 223 mg of di-*tert*-butyl benzaldehyde, 4 mL of toluene into a 50 mL RBF. Reflux for 1 hour. Let cool to allow for crystallization. Filter and wash with cold 10 mL methanol. Dry at 105 °C overnight. Yield 47%.

#### 3,5-di-*tert*-butyl benzaldehyde (catalyst 4d)

Weigh 101 mg of *meso*-1,2-diphenylethylenediamine and 219.9 mg of 3,5-di-*tert*-butylbenzaldehyde into a 50 mL RBF. Add 125 mg 4Å molecular sieves (MS). Stir overnight. Filter and wash with 10 mL cold methanol. Dry at 105 °C overnight. Yield 24%.

#### 2,6-dimethoxy (catalyst 4f)

Add 100.03 mg of *meso*-1,2-diphenylethylenediamine, 160.94 mg of 2,6-dimethoxybenzaldehyde, 3 mL of toluene, 2.5 mL of anhydrous ethanol into a 25 mL RBF. Reflux for 1 hr. Let cool to crystallize, then filter and wash with 7 mL of cold methanol. Evaporate solvent with rotary evaporator. Dry at 105 °C overnight. Yield 42%.

#### 2Br,6F (catalyst 4g)

Add 100.3 mg *meso*-1,2-diphenylethylenediamine, 198.92 mg of 2-bromo,6-fluorbenzaldehyde, 7 mL of toluene, and 3 mL of anhydrous ethanol into a 25 mL RBF. Reflux for 1 hour. Allow to cool to crystallize, and then filter and wash with 5 mL cold methanol. Dry at 105 °C overnight.

#### 2,6-DiF (catalyst 4b)

Weigh 100.1 mg of *meso*-1,2-diphenylethylenediamine and pipet 104  $\mu\text{L}$  of 2,6-difluorobenzaldehyde into a 25 mL RBF. Add 3 mL of toluene, and 3 mL of anhydrous ethanol. Allow to reflux for 1 hour. Allow to cool to crystallize, then filter and wash with 7 mL of cold methanol. Dry at 105 °C overnight.

#### Imidazole-2-carboxaldehyde (catalyst 4h)

Weigh 99.6 mg of *meso*-1,2-diphenylethylenediamine and 91.64 mg of 2-imidazolecarboxaldehyde into a 50 mL RBF. Add 10 mL toluene and reflux for 1 hour, cool, and filter. Wash with 15 mL cold methanol. Recrystallize in approximately 7 mL toluene and 2 mL heptane. Filter and dry overnight at 105 °C. Yield 28%.

#### *Meso*-3,5-DiF (catalyst 4i)

Add 103 mg of *meso*-1,2-diphenylethylenediamine, 149.35 mg 3,5-difluorobenzaldehyde, 4 mL methanol, and 5 mL toluene into a 25 mL RBF. Reflux for 1 hour with 4 Å MS. Cool and filter, and wash with 7 mL cold methanol. Yield 71%.

### 8.6.2 – BINAM-based Di-imines

General procedure: Weigh BINAM into a 25 or 50 mL RBF. Add solvent, then benzaldehyde. Add stir bar and 4 Å MS. Allow to stir for 24-36 hours. Filter solution and use the rotary evaporator to remove solvent. Recrystallize with petroleum ether and hexanes. Store in solvent to prevent oxidation.

Benzaldehyde (catalyst 5a)

Add 100 mg of (S) BINAM and 77 µL of benzaldehyde, 5 mL of toluene, 5 mL of anhydrous ethanol, and 150 mg of 4 Å MS. Allow to stir for 1 day. Remove solvent via rotary evaporation, and recrystallize with petroleum ether and hexanes (50/50 v/v). Filter and wash with 10 mL of cold methanol. Redissolve in methanol. Yield 39%.

Mesitaldehyde (catalyst 5b)

Weigh 99.78 mg of (S) BINAM and 110 µL of mesitaldehyde into a 25 mL RBF. Add 4 mL of anhydrous ethanol, 5 mL of toluene, and 150 mg of 4 Å MS. Stir overnight. Proceed as in general procedure. Yield 45%.

2,6-DiF (catalyst 5e)

Add 100.33 mg of (S) BINAM, 83 µL of 2,6-difluorobenzaldehyde to a 50 mL RBF. Add 5mL of toluene, 4mL of anhydrous ethanol, and 100 mg of 4 Å MS. Stir overnight. Remove solvent with rotary evaporator. and redissolve in methanol. Yield 20%.



#### 3,5-di-*tert*-butyl benzaldehyde (catalyst 5d)

Weigh 99.72 mg of (S) BINAM and 166 mg of di-*tert*-butylbenzaldehyde to a 25 mL RBF. Add 5 mL of toluene, 4 mL of anhydrous ethanol, and 125 mg of 4 Å MS. Stir overnight. Remove solvent via rotary evaporator and redissolve in methanol. Yield 50%.

#### 3,5-difluoro (catalyst 5b)

Add 99.34 mg of (S) BINAM, 4 mL each toluene and anhydrous ethanol, 100  $\mu$  3,5-difluorobenzaldehyde, 200 mg 4 Å MS to a 50 mL RBF. Remove solvent with rotary evaporator and redissolve in methanol. Yield 38%.

#### 3,5-DiCl (catalyst 5e)

Add 99.5 mg of (S) BINAM, 190.65 mg 3,5-dichlorobenzaldehyde. Add 4 mL each of toluene and anhydrous ethanol, to a 25 mL RBF. Add 250 mg of 4 Å MS and stir overnight. Remove solvent (rotary evaporator) and redissolve in methanol. Yield 22%.

#### 3,5-di-*tert*-butyl (catalyst 5d)

Add 99.8 mg of (S) BINAM, 147.97 mg 3,5-di-*tert*-butylbenzaldehyde, 3 mL toluene, 4 mL ethanol, and 170 mg Å MS. Add additional 2 mL toluene and 2 mL of anhydrous ethanol. Heat to reflux for 4 hours. Allow to cool and then filter. Wash with 15 mL of cold methanol. Redissolve in methanol. Yield 43%.

2,6-DiCl (catalyst 5g)

Add 104.5 mg of (S) BINAM, 145 mg of 2,6-dichlorobenzaldehyde, 255 mg of 4 Å MS, and 3 mL each of toluene and anhydrous ethanol to a 50 mL RBF. Stir overnight and remove solvent via rotary evaporation. Redissolve in methanol.

2,6-dimethoxy (catalyst 5f)

Add 50.8 mg of (S) BINAM, 66 mg of 2,6-dimethoxybenzaldehyde, 3 mL each of toluene and anhydrous ethanol, and 200 mg of 4 Å MS into 50 mL RBF. Stir over weekend, and remove solvent. Redissolve in methanol.

2Br,6F (catalyst 5i)

Weigh 99.89 mg of (S) BINAM and 165.2 mg of 2-bromo,6-fluorobenzaldehyde into a 50 mL RBF. Add 4 mL each of toluene and anhydrous ethanol, and 200 mg of 4 Å MS. Stir for 48 hours. Remove solvent. Redissolve in methanol. Yield 33%.

3,5 DiCl (catalyst 5h)

Add 99.17 mg of (S) BINAM, 139 mg 3,5-dichlorobenzaldehyde, 4 mL each of toluene and anhydrous ethanol, and 150 mg of 4 Å MS to a 50 mL RBF. Stir for 48 hours. Remove solvent. Redissolve in methanol. Yield 27%.

### (R) BINAM diamines

#### Benzaldehyde (catalyst 5a)

Weigh 100.8 mg of (R) BINAM into a 25 mL RBF. Add 8 mL toluene and 73  $\mu$ L benzaldehyde. Add 100 mg of 4 Å MS and stir overnight. Remove solvent and redissolve in methanol.

#### Mesitaldehyde (catalyst 5c)

Weigh 99.88 mg of (R) BINAM into a 50 mL RBF. Add 8 mL of toluene, 110  $\mu$ L of mesitaldehyde, and 125 mg of 4 Å MS. Stir overnight. Remove solvent and redissolve in methanol.

#### 3,5-DiF (catalyst 5b)

Weigh 99.4 mg of (R) BINAM into a 50 mL RBF. Add 10 mL of toluene, 110  $\mu$ L 3,5-difluorobenzaldehyde, and 100 mg 4 Å MS. Monitor reaction via TLC. Add 30  $\mu$ L additional 3,5-difluorobenzaldehyde after 6 hours. Add additional 125 mg of 4 Å MS. Stir overnight and remove solvent.

#### 2,6-DiF (catalyst 5e)

Add 99.9 mg of (R) BINAM, 86.5  $\mu$ L of 2,6-difluorobenzaldehyde, 4 mL each toluene and anhydrous ethanol, and 250 mg of 4 Å MS into 50 mL RBF. Stir overnight and remove solvent. Redissolve in methanol.

### 8.6.3 – 1,2-diaminocyclohexane-based Ligands

General procedure: Weigh diamine into a 25 or 50 mL RBF. Add solvent(s) and benzaldehyde. Procedure A - add molecular sieves (MS) and stir for specified time. Filter and wash with cold methanol. Recrystallize with methanol or ethanol. Cool, filter and wash with cold methanol. Allow to dry overnight at 105 °C. Procedure B - heat to reflux for specified time. Allow to cool and crystallize.

#### 8.6.3.1 – *trans*-(1S, 2S)-diaminocyclohexane di-imines

3,5-DiF (catalyst 3i)

Add 103 mg of *trans*-(1S, 2S)-diaminocyclohexane (diamine) into a 25 mL RBF. Add 7 mL of ethanol and 300  $\mu$ L of 3,5-difluorobenzaldehyde, and 125 mg of 4 Å MS. Follow procedure A in general procedure. Stir overnight. Recrystallize in methanol. Yield 66%.

Benzaldehyde (catalyst 3a)

Add 100.17 mg of diamine, 170  $\mu$ L of benzaldehyde, and 5 mL of anhydrous ethanol, to a 50 mL RBF and reflux for 1 hour. Follow procedure B in general procedure. Product crystallized as it cooled. Yield 85%.

Mesitaldehyde (catalyst 3c)

Weigh 104.74 mg of diamine into a 50 mL RBF. Add 125  $\mu$ L of mesitaldehyde and 6 mL of anhydrous ethanol. Reflux for 1 hour. Follow procedure B in general procedure. Yield 74%.

2, 6-dichlorobenzaldehyde (catalyst 3e)

Add 103.22 mg of diamine, 348.89 mg of 2,6-dichlorobenzaldehyde, and 5 mL of anhydrous ethanol into 25 mL RBF. Heat to reflux for 1 hour. Isolate via procedure B. Yield 63%.

2-bromo,6-fluorobenzaldehyde (catalyst 3g)

Weigh 101.31 mg of diamine and 446.39 mg of 2-bromo-6-fluorobenzaldehyde into a 25 mL RBF. Add 5 mL of anhydrous ethanol. Reflux for 1 hour. Follow procedure B in general procedure. Yield 83%.

2,6-dimethoxybenzaldehyde (catalyst 3f)

Add 100.3 mg of diamine, 347 mg of 2,6-diethoxybenzaldehyde, and 5 mL of anhydrous ethanol to a 25 mL RBF. Reflux for 1 hour. Follow procedure B in general procedure. Yield 49%.

Imidazole-2-carboxaldehyde (catalyst 3h)

Add 100 mg of diamine, 187.21 mg imiadazole-2-carboxaldehyde, 170 mg of 4Å MS, and 10 mL of anhydrous ethanol to a 25 mL RBF and stir for 3 days. Follow procedure A in general procedure. Yield 20%.

2,6-difluorobenzaldehyde (catalyst 3b)

Add 101.1 mg of diamine and 95  $\mu$ L of 2,6-difluorobenzaldehyde to a 50 mL RBF. Add 7 mL of anhydrous ethanol and heat to reflux. Follow procedure B in general procedure. Yield 78%.

3,5-di-*tert*-butyl benzaldehyde (catalyst 3d)

Add 100.65 mg of diamine, 228.5 mg of 3,5-di-*tert*-butylbenzaldehyde, 10 mL of anhydrous ethanol, and 150 mg of 4 Å MS to a 50 mL RBF. Stir over weekend. Follow procedure B in general procedure.

*Trans*-(1R, 2R)-diaminocyclohexane

2,6-difluorobenzaldehyde (catalyst 3b)

Add 100.4 mg of diamine, 92  $\mu$ L of 2,6-difluorobenzaldehyde, 5 mL of anhydrous ethanol, and 200 mg of 4 Å MS to a 50 mL RBF. Follow procedure A in general procedure.

3,5-di-*tert*-butylbenzaldehyde (catalyst 3d)

Weigh 102.0 mg of diamine and 370.4 mg of 3,5-di-*tert*-butylbenzaldehyde into a 50 mL RBF. Add 6 mL of anhydrous ethanol and 260 mg of 4 Å MS. Stir for 48 hours. Follow procedure A in general procedure. Yield 67%.

Benzaldehyde (catalyst 3a)

Add 100.5 mg of diamine, 170  $\mu$ L of benzaldehyde, and 10 mL of anhydrous ethanol to a 50 mL RBF. Heat to reflux for 1 hour. Follow procedure B in general procedure. Yield 77%.

Mesitaldehyde (catalyst 3c)

Weigh 101.3 mg of diamine into a 50 mL RBF. Add 125  $\mu$ L of mesitaldehyde and 6 mL of anhydrous ethanol. Reflux for 1 hour. Follow procedure B in general procedure.

## 8.7 – Synthesis of Ethers

General procedure: Add anhydrous THF to a RBF, previously flame-dried and flushed with nitrogen. Place under ice bath to cool. Add NaH and stir for 10 minutes. Add the chiral alcohol drop-wise, not exceeding 10 °C during the addition and stir for 30 minutes. Add the alkylating reagent drop-wise, not exceeding 30 °C during the addition. Stir at room temperature for 1 hour and quench remaining NaH with methanol. Extract twice with 10 mL water and 10 mL diethyl ether. Combine organic layers and dry with either sodium sulfate or magnesium sulfate. Decant and evaporate the solvent. Store in amber vial.

(S)-1-methoxyethylbenzene

Add 10 mL anhydrous THF and 401.0 mg NaH (60%), at 10 °C under N<sub>2</sub> to a 50 mL RBF. Add 1.2 mL (S)-phenylethanol drop-wise, not exceeding 8 °C in the process. Add 600 µL of MeI, not exceeding 25 °C. Follow general procedure. Yield 84%.

#### (R)-1-methoxyethylbenzene

Add 10 mL of anhydrous THF and 400.1 mg NaH, at 10 °C under N<sub>2</sub>, to a 50 mL RBF. Add 1.2 mL (R)-phenylethanol drop-wise, not exceeding 10 °C in the process. Add 600 µL of MeI, not exceeding 25 °C during the addition. Follow general procedure. Yield 86%.

#### 1-methoxyethylbenzene with n-butyl lithium as base

Add 7 mL anhydrous hexane and 4 mL n-butyl lithium to a 50 mL RBF, previously flame-dried. Add 1-phenylethanol (1.2 mL), not exceeding 12 °C during the addition. Allow to stir for 30 minutes. Add 0.8 mL of methyl iodide over 30 minutes, not exceeding 25 °C during the addition. Follow extraction procedure in general procedure.

#### [1-(Benzyloxy)ethyl]benzene

Add 10 mL anhydrous THF and 400.1 mg NaH (60%) to a 50 mL RBF. Add 1.2 mL of (R) phenylethanol. Let mixture stir for 20 minutes with ice bath at ~10 °C. Add 950 µL of benzylbromide and stir for 3 hours at room temperature. Quench with methanol and follow general procedure to extract. Yield 84%.

#### (R)-1-methoxyethylbenzene



Add 440 mg of 60% NaH to anhydrous THF (10 mL) in a 50 mL RBF. Stir for 30 minutes under ice bath at 10 °C. Add 1.2 mL of (R) phenylethanol . Slowly add 630 µL of MeI. Stir 3 hours at room temperature. Quench reaction with methanol and follow general procedure. Yield 89%.

#### $d_8$ -methoxyethylbenzene

Add 450 mg of 60% NaH to anhydrous THF (10 mL) in a 50 mL RBF. Add 1 mL of  $d_5$ -ring phenylethanol and stir for 30 minutes with ice bath. Add 800 µL of  $d_3$ -MeI. Stir for 1 hour, quench with methanol, and follow general procedure to extract. Yield 81%.

#### (R)-2-methoxyoctane

Add 334 mg of 60% NaH into 10 mL of anhydrous THF in a 50 mL RBF. Add 1 mL (R)- 2-octanol and 800 µL of MeI. Stir at room temperature for 4 hours. Add methanol to quench reaction followed by 10 mL of water and 10 mL of diethyl ether to extract. Wash with 1N KOH (repeat extraction). Combine the aqueous layers and the organic layers. Follow general procedure to dry and isolate product. Yield 88%.

## 8.6 - Chiral GC Analysis of Ethers

Column –  $\beta$ -DEX 120 dimensions: 30 m x 0.25 mm

GC Instrument conditions:

Initial oven temperature (°C): 6

Hold time (min): 1:00

Ramp 1 rate (°C/min): 2.5

Temperature 2 (°C): 220

Hold Time (min): 5:00

Maximum Temperature (°C): 230

Pre-Run Timeout (min): 5:00

Equilibration Time (min): 1:00

Oven run Time (min): 70

Inlet Temperature (°C): 220

Split Flow (mL/min): 50

Split Ratio: 50

Constant Flow

Flow Rate (mL/min): 1.0

Gas Saver: Enabled

Gas Saver Flow (mL/min): 20

Time (min): 0.2

Detector temperature (°C): 220

Ignition Threshold (pA): 0.5

Detector gases

Air: On

H2: On

Make-up: On

Sample Volume ( $\mu$ L): 2

Plunger Strokes: 1

Viscous Sample: No

Sampling Depth in Vial: Bottom

Pre-Injection Solvent: A

Cycles: 2

Sample Rinses: 1

Post Injection Solvent: A

Cycles: 2

Injection Depth: Minimum

(*R*)-1-methoxyethylbenzene

Compound	Retention Time (min)	Area Percent
( <i>R</i> )-1-methoxyethylbenzene	18.272	85.35
( <i>R</i> )-1-Phenylethanol	30.237	14.13
Unknown	53.4	0.35

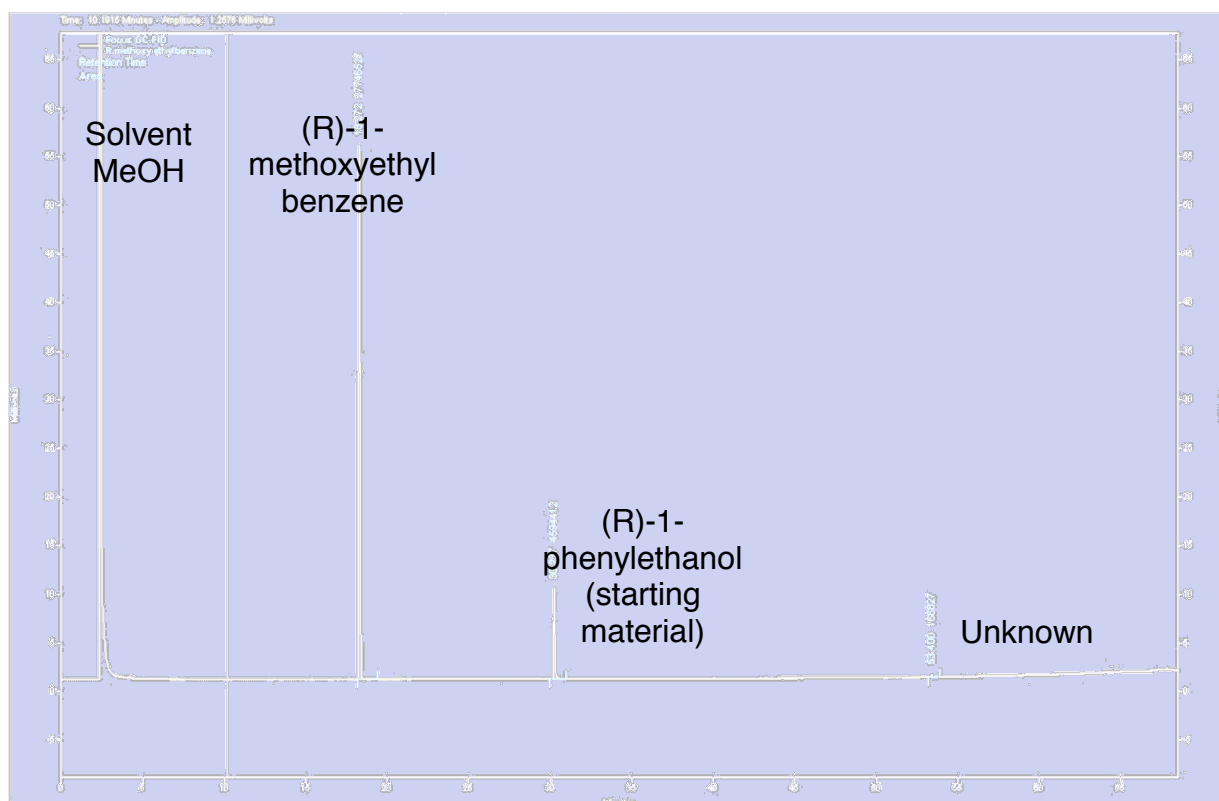


**Figure 172.** (*R*)-1-methoxyethylbenzene chiral GC analysis.

(S)-1-methoxyethylbenzene

Compound	Retention Time (min)	Area Percent
(S)-1-methoxyethylbenzene	18.379	82.12
(S)-1-Phenylethanol	30.815	12.08
Unknown	53.4	5.80

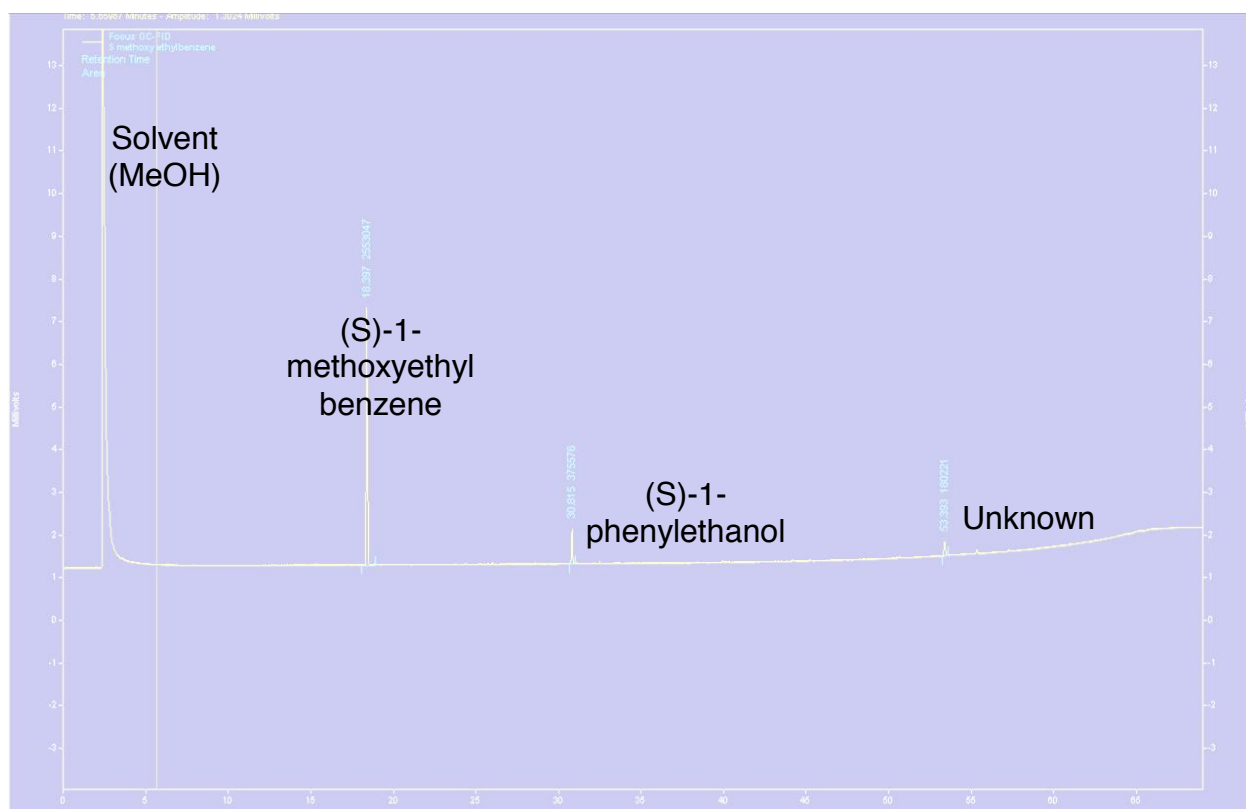
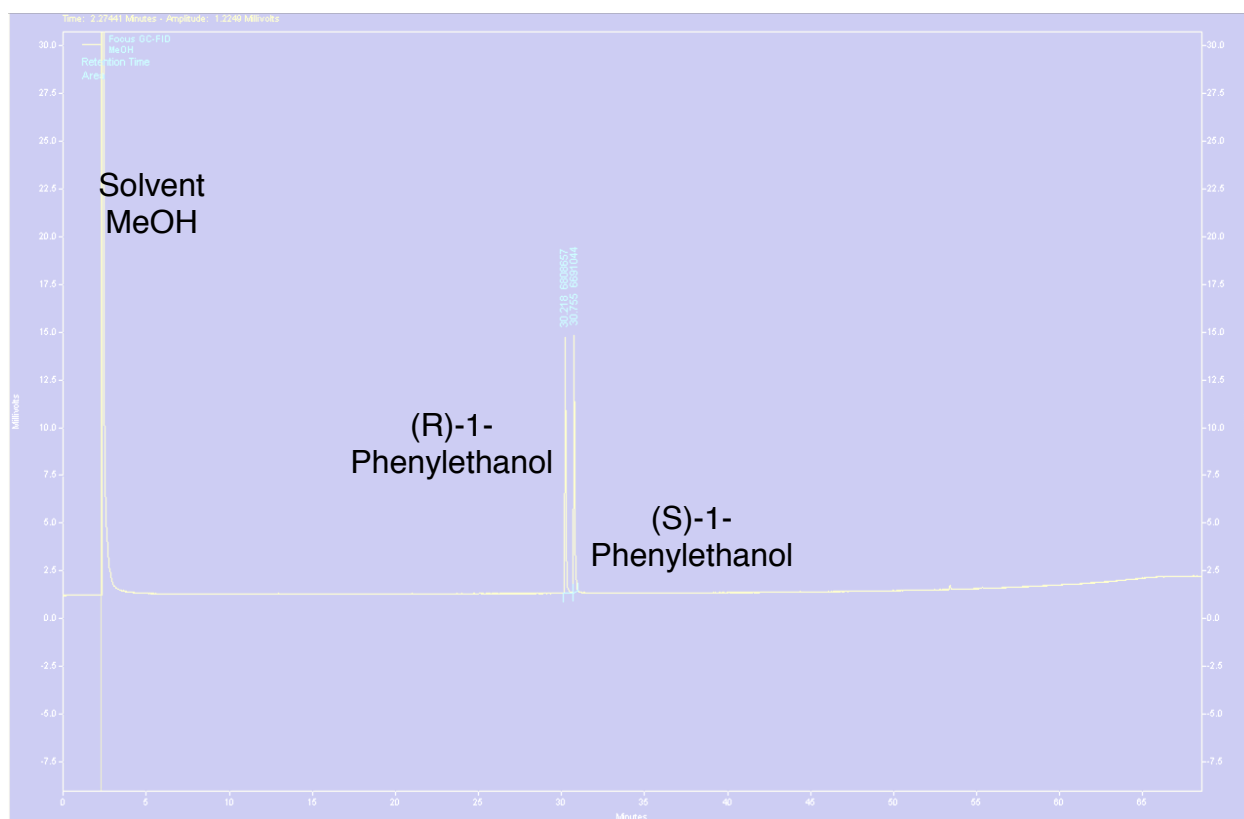


Figure 173. (S)-1-methoxyethylbenzene chiral GC analysis.

# Racemic Phenylethanol

Compound	Retention Time (min)	Area Percent
(R)-1-Phenylethanol	30.218	50.44
(S)-1-Phenylethanol	30.755	49.56



**Figure 174.** Racemic phenylethanol GC analysis.

(S)-2-methoxyoctane

Compound	Retention Time (min)	Area Percent
Unknown 1	5.45	2.52
(S)-2-Methoxyoctane	25.73	95.38
Unknown 2	77.93	1.51
Unknown 3	78.90	0.58

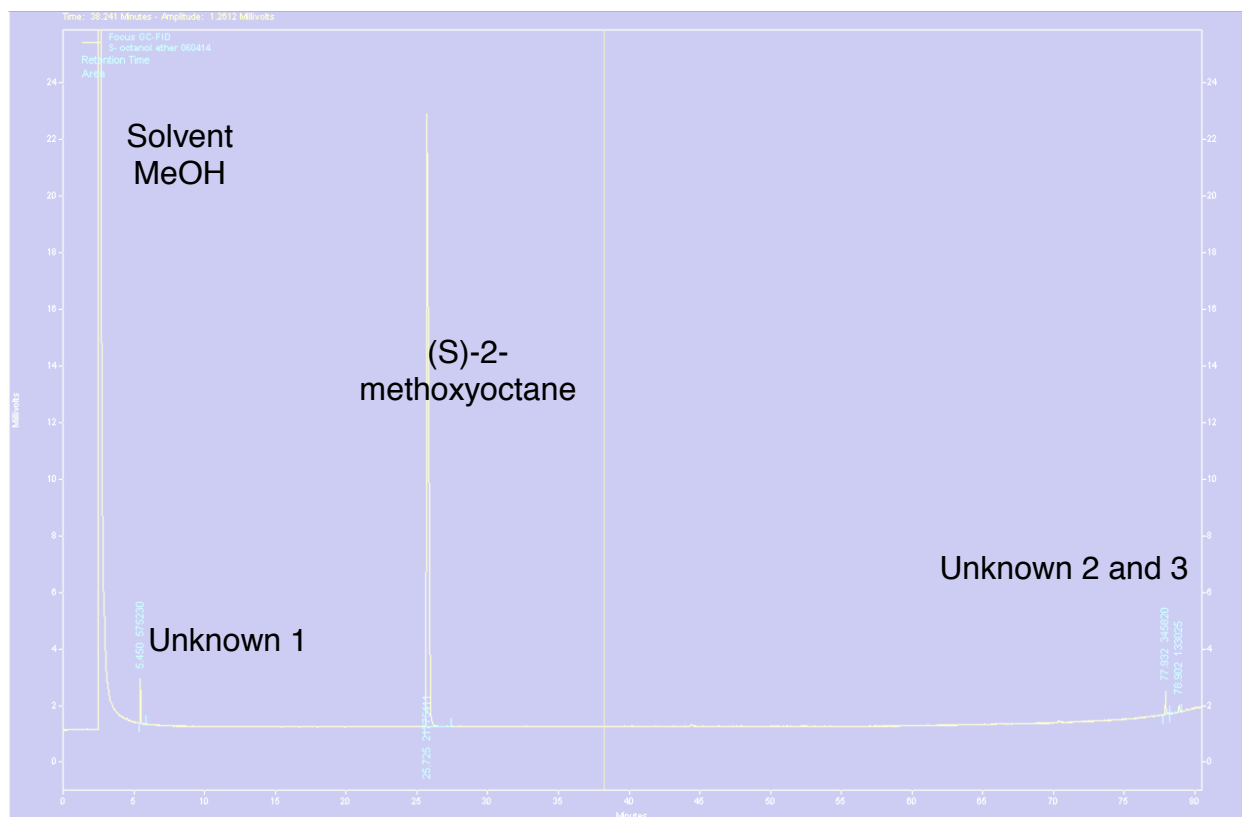
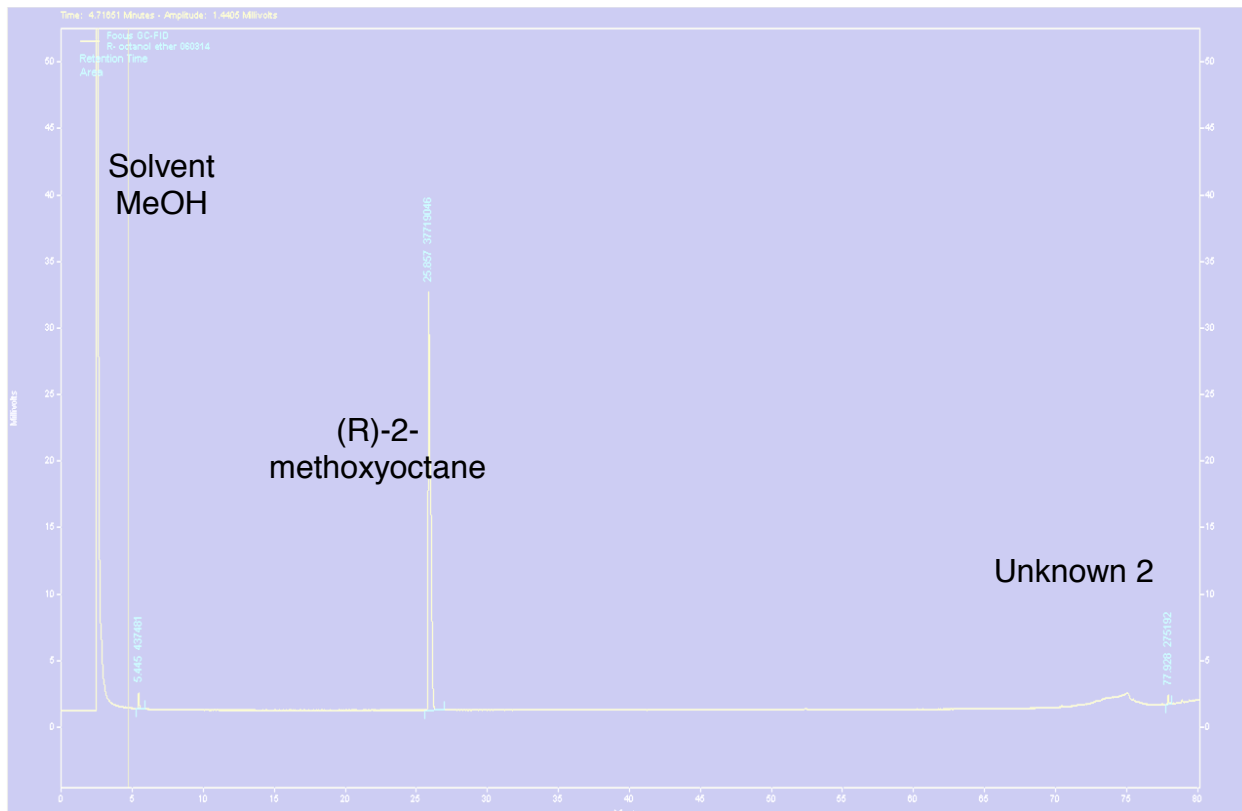


Figure 175. (S)-2-methoxyoctane chiral GC analysis.

(*R*)-2-methoxyoctane

Compound	Retention Time (min)	Area Percent
Unknown 1	5.45	1.14
( <i>R</i> )-2-Methoxyoctane	25.86	98.15
Unknown 2	77.93	0.72



**Figure 176.** (*R*)-2-methoxyoctane chiral GC analysis.

(*R*)-2-octanol (for retention time)

Compound	Retention Time (min)	Area Percent
MeOH	2.57	92.54
( <i>R</i> )-2-Octanol	43.54	7.38

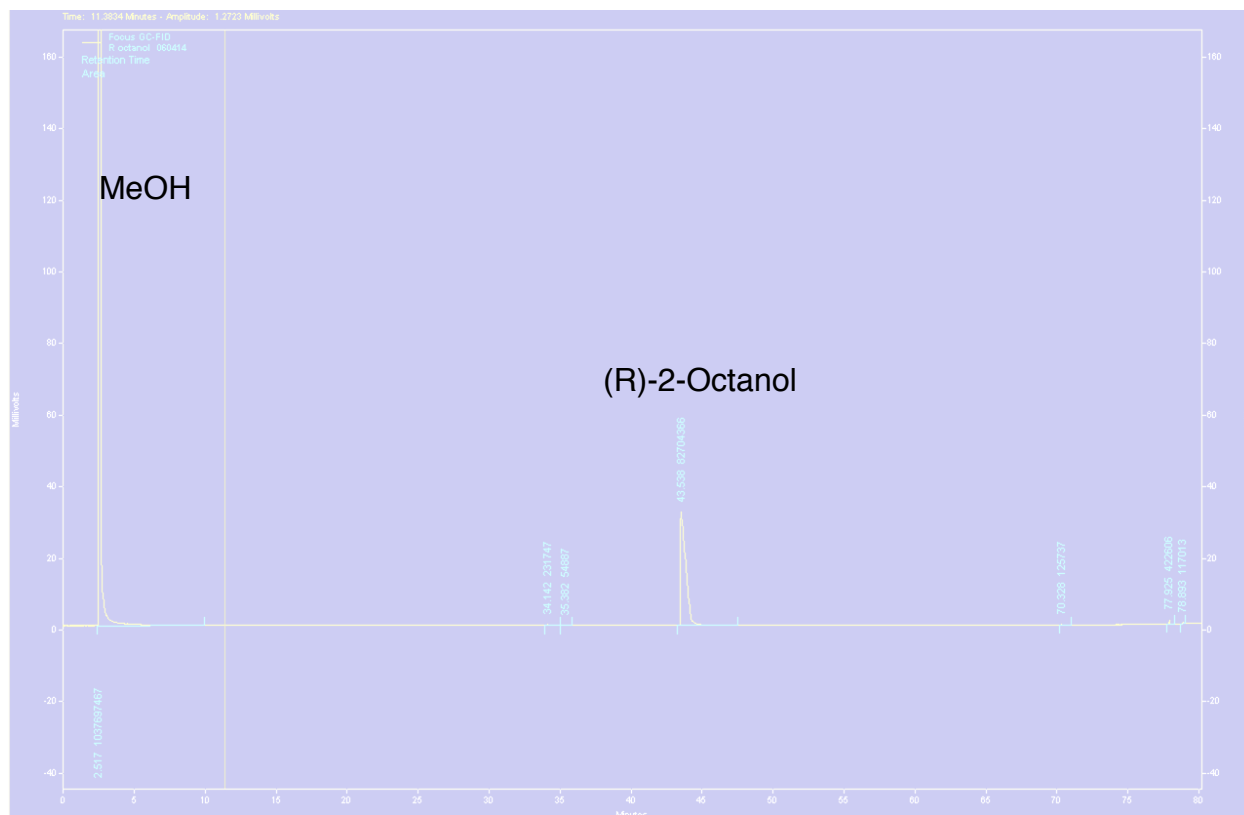


**Figure 177.** (*R*)-2-octanol chiral GC analysis.



(S)-2-octanol (for retention time)

Compound	Retention Time (min)	Area Percent
(S)-2-Octanol	44.07	98.06

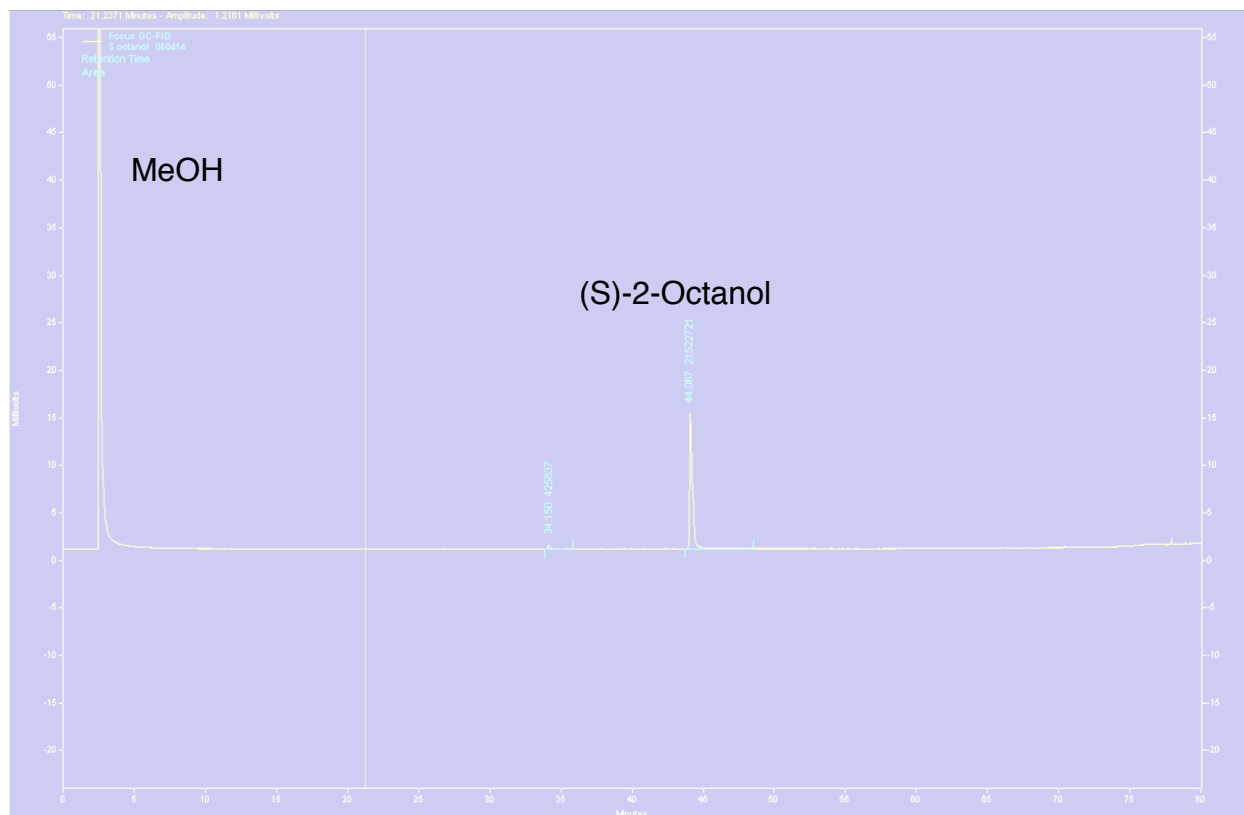


**Figure 178.** (S)-2-Octanol chiral GC analysis.

## **Vita**

### **Profile**

Ph.D. degree December 2014. More than eleven years' experience in the pharmaceutical industry. Rapidly promoted through the technical ranks of the Quality Control, Analytical Methods Development, and Process Chemistry Departments.

### **Education**

8/05 – 8/14 Ph.D. Analytical/Organic Chemistry Virginia Commonwealth University  
part/full-time Thesis: Exploring the asymmetric environment of various chiral catalysts using a modified ion-trap mass spectrometer: Towards the development of a rapid chiral catalyst screening method

08/95 – 05/98 B.S. in Chemistry and Biology Heidelberg College (now University)

08/91 – 05/95 A.S. in General Studies John Tyler Community College

### **Professional Experience**

8/14 – present Gilead Sciences Edmonton Canada

**Research Scientist II**, Analytical Method Development

*Lead team of scientists to develop and validate analytical methods for the analysis of small molecule API's. Project leader for qualification of analytical methods at new CMO to supply Solvaldi® to European market.*

01/12 – 8/14

Virginia Commonwealth University

Richmond, VA

**Teaching Assistant**, Organic Chemistry Labs

*Supervise labs of 24 undergraduate students while they perform experiments required of the two-credit course.*

- Monitor the students' safety and progress of the weekly experiment during the course of the lab.

04/09 – 03/11

Boehringer Ingelheim Chemicals Inc. (BICI)

Petersburg, VA

**Senior Scientist**, Process Chemistry

*Responsible for disseminating and adding to the chemical/manufacturing knowledge base of Active Pharmaceutical Ingredients (APIs) via synthetic or analytical lab work, plant investigations, and/or as a member of a multidisciplinary team to ensure the safe, efficient production of quality products and customer satisfaction.*

- Developed, optimized, and scaled-up a transfer-hydrogenation process, which saved over \$300,000 and allowed the company to meet its customer obligations in a timely manner.
- Monitored production bays and technicians during critical transfers/steps. Authored and reviewed: batch records for technicians to follow; process risk

analysis reports that detailed each step of the process and the corresponding safety hazards; investigation and technical reports; SOPs and training manuals.

- Integral member of multiple cross-functional Six Sigma teams that stabilized numerous chemical and production processes using root cause analysis, design of experiments, and statistical analysis.

02/02 – 04/09

Boehringer Ingelheim Chemicals Inc. (BICI)

Petersburg, VA

**Senior Analytical Chemist I, II, and III, Analytical Method Development**

*Support Company and departments with analytical services to improve product quality and efficiency. Lead Analytical Chemist for the Company's most important projects.*

*Developed critical analytical procedure that allowed the site's most important project to move forward to completion.*

- Led team of multi-departmental chemists in investigation of newly found impurity. Resulted in testing 157 lots of material over three-day weekend under full current Good Manufacturing Practices (cGMP) conditions.
- Lead analytical chemist for multiple high-priority projects. Developed and validated a UV spectroscopy method that correlated the products final color to its pre-isolation solution color. This allowed the plant to know, with a high degree of confidence, when passing material would be obtained, saving time and money.
- Developed, validated, and transferred new, robust analytical methods. Wrote specifications and test methods for products/intermediates/starting materials for use by the Quality Control Department. Analyzed, reported and presented data

and recommendations to upper management that dictated the course of the project(s) and disposition of products.

- Researched, recommended, and implemented new technologies to the site that would save time and money. Championed newer chromatography systems that shortened run times by 80%.

11/99 – 02/02

Boehringer Ingelheim Chemicals Inc. (BICI)

Petersburg, VA

**Analytical Chemist I, II, and III, Quality Control**

*Ensure consumer safety and product quality of APIs, intermediates, and raw materials by testing products in accordance to internal specifications, SOPs, and cGMP guidelines. Brought the lab into cGMP compliance by writing instrument logbooks, instituting daily and weekly performance qualifications, and SOPs for maintenance and use.*

- Released materials (including schedule II controlled substances) in adherence to all regulatory requirements.
- Developed and validated new gas chromatography methods with internal standards to replace problematic ones resulting in increased efficiency, reliability, turnaround time, and decreased out-of-specification investigations.
- Wrote and revised in-process specifications and test methods to make clearer, resulting in increased efficiency, decreased plant downtime, and increased QC employee morale.

- Developed, wrote and implemented current logbook system for all instruments in preparation for regulatory audit. Received positive comments from regulatory agency on the logbook system.

11/98 – 10/99

BFGoodrich

Brecksville, OH

**Assistant Research Scientist**, Advanced Technology Group

*Perform quality testing of drug coating for drug-delivery project.*

- Analyzed capsules using microscopy for drug delivery system. Co-developed a capsule cutting device for analysis of the capsule coating.

**Technical experience:** Organic Synthesis; Spectroscopy - Mass Spectrometry (single and triple quad, ion-trap, TOF), NMR 1D and 2D (COSY, NOESY, HMBC, HMQC), IR (Infrared Microscopy), UV/Vis; Chromatography –reverse and normal phase, prep, and chiral (Waters, Agilent, Perkin Elmer and associated software), UPLC, GC (Headspace), Capillary Electrophoresis; Thermal Analysis – RCOne, DSC and TGA; Titrimetry – acid/base, potentiometric, precipitation, complexometric; Particle Size Analysis; Optical Microscopy, SEM (Scanning Electron Microscopy); Gravimetric Analysis; TOC; cGMP Regulations.

### **Posters/Publications**

Tetrahedron (Ref TET-D-14-01968)

Pending

Richmond, VA

*A mass spectrometric method for rapidly assaying the chiral selectivities of the copper salts of C<sub>2</sub>-symmetric ligands*

Virginia Commonwealth University                      Oct. 2013                      Richmond, VA

*Chiral Selectivity of Copper (I) Di-Imine Catalysts in the Gas-Phase*

American Society for Mass Spectrometry (ASMS) Annual Conference Meeting

June 2013      Minneapolis, MN

*Chiral Selectivity of Copper (I) Di-Imine Catalysts in the Gas-Phase*

Virginia Commonwealth University                      Oct. 2012                      Richmond, VA

*Chiral Selectivity of Copper (I) Bis-Oxazolines in the Gas-Phase*

ASMS Annual Conference Meeting                      May 2012                      Vancouver, BC

*Chiral Selectivity of Copper (I) Bis-Oxazolines in the Gas-Phase*

Southeast Regional Meeting of the American Chemical Society (SERMACS)

Oct. 2011      Richmond, VA

*Chiral Bis-Oxazoline Catalysts and Their Stereoselective Binding to Various Functional Groups in the Gas-Phase*

**Miscellaneous**

01/12                      Private Tutor/Owner ChemWise Tutors                      Richmond, VA

- Tutor advanced high school students in Chemistry and Organic Chemistry to pre-professional students

12/06                      Leadership Development Program

BICI

- Identified future leaders of the company for the program